

แคทไอออนิกฟีนิลซีนเอไอนิลซีนแบบกิ่งละลายน้ำที่เป็นตัวตรวจวัดการเกิดอันตรกิริยาเชิง
ซูปรามอเลกุล

นางสาววราทิพย์ ศิริพรนพคุณ

วิทยานิพนธ์นี้เป็นส่วนหนึ่งของการศึกษาตามหลักสูตรปริญญาวิทยาศาสตรดุษฎีบัณฑิต
สาขาวิชาเคมี ภาควิชาเคมี
คณะวิทยาศาสตร์ จุฬาลงกรณ์มหาวิทยาลัย
ปีการศึกษา 2554
ลิขสิทธิ์ของจุฬาลงกรณ์มหาวิทยาลัย

บทคัดย่อและแฟ้มข้อมูลฉบับเต็มของวิทยานิพนธ์ตั้งแต่ปีการศึกษา 2554 ที่ให้บริการในคลังปัญญาจุฬาฯ (CUIR)
เป็นแฟ้มข้อมูลของนิสิตเจ้าของวิทยานิพนธ์ที่ส่งผ่านทางบัณฑิตวิทยาลัย

The abstract and full text of theses from the academic year 2011 in Chulalongkorn University Intellectual Repository (CUIR)
are the thesis authors' files submitted through the Graduate School.

WATER-SOLUBLE CATIONIC BRANCHED PHENYLENE-ETHYNYLENE AS
FLUORESCENT PROBES FOR SUPRAMOLECULAR INTERACTION

Miss Warathip Siripornnoppakhun

A Dissertation Submitted in Partial Fulfillment of the Requirements
for the Degree of Doctor of Philosophy Program in Chemistry

Department of Chemistry

Faculty of Science

Chulalongkorn University

Academic Year 2011

Copyright of Chulalongkorn University

Thesis Title WATER-SOLUBLE CATIONIC BRANCHED PHENYLENE-
ETHYNYLENE AS FLUORESCENT PROBES FOR
SUPRAMOLECULAR INTERACTION
By Miss Warathip Siripornnoppakhun
Field of Study Chemistry
Thesis Advisor Associate Professor Mongkol Sukwattanasinitt, Ph.D.
Thesis Co-advisor Assistant Professor Paitoon Rashatasakhon, Ph.D.

Accepted by the Faculty of Science, Chulalongkorn University in Partial
Fulfillment of the Requirements for the Doctoral Degree

..... Dean of the Faculty of Science
(Professor Supot Hannongbua, Dr.rer.nat.)

THESIS COMMITTEE

..... Chairman
(Professor Sophon Roengsumran, Ph.D.)

..... Thesis Advisor
(Associate Professor Mongkol Sukwattanasinitt, Ph.D.)

..... Thesis Co-advisor
(Assistant Professor Paitoon Rashatasakhon, Ph.D.)

..... Examiner
(Associate Professor Tirayut Vilaivan, D. Phil.)

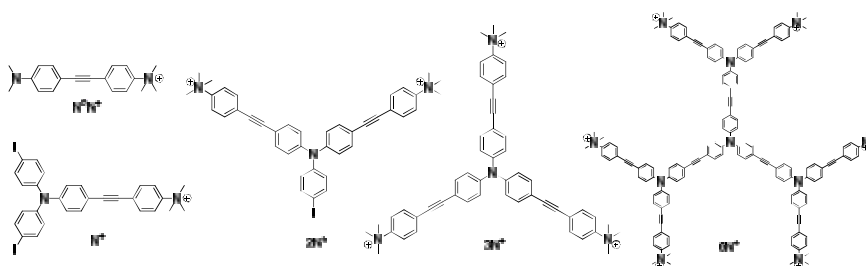
..... Examiner
(Assistant Professor Patchanita Thamyongkit, Dr. rer. nat.)

..... Examiner
(Professor Thawatchai Tuntulani, Ph.D.)

..... External Examiner
(Assistant Professor Tienthong Thongpanchang, Ph.D.)

วราทิพย์ ศิริพรนพคุณ : แคทไอออนิกพีนิลลีนเอไทนิลลีนแบบกิ่งละลายน้ำที่เป็นตัวตรวจวัด การเกิดอันตรกิริยาเชิงซูปราโมเลกุล. (WATER-SOLUBLE CATIONIC BRANCHED PHENYLENE-ETHYNYLENE AS FLUORESCENT PROBES FOR SUPRAMOLECULAR INTERACTION) อ. ที่ปรึกษาวิทยานิพนธ์หลัก : รศ. ดร.มงคล สุขวัฒน์สินิทธิ, อ. ที่ปรึกษาวิทยานิพนธ์ร่วม : ผศ. ดร.ไพฑูรย์ รัชตะสาคร, 149 หน้า.

แอมฟิฟิลิกฟลูออโรฟอร์ 5 ตัว (N^0N^+ , N^+ , $2N^+$, $3N^+$ and $6N^+$) ซึ่งมีหน่วยให้แสงฟลูออเรสเซนซ์เป็นพีนิลลีนเอไทนิลลีนได้ถูกนำมาใช้เป็นฟลูออเรสเซนซ์โพรบสำหรับการตรวจสอบการเปลี่ยนแปลงสัญญาณฟลูออเรสเซนซ์ในสิ่งแวดล้อมที่จำกัดระดับนาโนเมตรของดีเอ็นเอ โปรตีนซีรัมน้ำเลือดวัว สารลดแรงตึงผิวและไซโคลเด็กซ์ทริน ในระบบตัวทำละลายน้ำ โมเลกุล เป็นตัวอย่างของโพรบที่ตอบสนองวงไวที่สุดต่อตัววิเคราะห์ทั้งหมด ตัวอย่างเช่นการขยายสัญญาณฟลูออเรสเซนซ์ของ $3N^+$ อย่างมากด้วยแกมมาไซโคลเด็กซ์ทรินเนื่องมาจากการเกิดอินคลูชันคอมเพล็กซ์ที่เสถียรที่อัตราส่วน 1:1 ($K_b = 3.0 \times 10^4 \text{ M}^{-1}$) การค้นพบเกี่ยวกับการขยายสัญญาณฟลูออเรสเซนซ์ของ $3N^+$ โดยการจับกันด้วยแรงทางประจุกับดีเอ็นเอสายเดี่ยวนำไปสู่การออกแบบระบบการตรวจวัดที่มีความเลือกจำเพาะและความไวต่อไอออนของโพแทสเซียมด้วยสัญญาณฟลูออเรสเซนซ์โดยใช้แอปตาเมอริได้ การตอบสนองของสัญญาณฟลูออเรสเซนซ์ที่สูงต่อโปรตีนซีรัมน้ำเลือดวัวชี้ให้เห็นถึงการป้องกันการเกิดกระบวนการระงับสัญญาณด้วยตัวเองได้อย่างมีประสิทธิภาพซึ่งอาจจะเป็นเพราะปฏิสัมพันธ์ทั้งแบบไฮโดรโฟบิกและไฮโดรฟิลิก ($K_b = 6.7 \times 10^5 \text{ M}^{-1}$) นอกจากนี้ $3N^+$ ยังได้ถูกนำมาใช้เป็นฟลูออเรสเซนซ์โพรบซึ่งเหนี่ยวนำให้เกิดไมเซลล์เพื่อตรวจหาค่า CMC ของสารลดแรงตึงผิวได้อีกด้วย ในกรณีของ $6N^+$ นั้น การขยายสัญญาณฟลูออเรสเซนซ์เกิดขึ้นเฉพาะกับโปรตีนซีรัมน้ำเลือดวัวและสารลดแรงตึงผิวเท่านั้น การเกิดปฏิสัมพันธ์กับดีเอ็นเอสายเดี่ยวสามารถพิสูจน์ได้ด้วยสัญญาณ FRET ซึ่งมีประโยชน์สำหรับการตรวจวัดลำดับเบสของดีเอ็นเอ



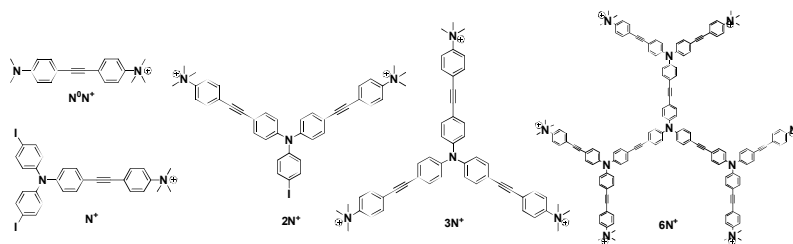
ภาควิชา.....เคมี..... ลายมือชื่อนิสิต.....
 สาขาวิชา.....เคมี..... ลายมือชื่อ อ.ที่ปรึกษาวิทยานิพนธ์หลัก.....
 ปีการศึกษา.....2554..... ลายมือชื่อ อ.ที่ปรึกษาวิทยานิพนธ์ร่วม.....

4873848823 : MAJOR CHEMISTRY

KEYWORDS : CYCLODEXTRIN/ DENDRIMER/ DNA/ FLUORESCENCE/
HOST-GUEST CHEMISTRY

WARATHIP SIRIPORNNOPPAKHUN : WATER-SOLUBLE CATIONIC
BRANCHED PHENYLENE-ETHYNYLENE AS FLUORESCENT
PROBES FOR SUPRAMOLECULAR INTERACTION. ADVISOR :
ASSOC.PROF. MONGKOL SUKWATTANASINITT, Ph.D.,
CO-ADVISOR : ASSIST.PROF. PAITON RASHATASAKHON, Ph.D.,
149 pp.

Five amphiphilic fluorophores (N^0N^+ , N^+ , $2N^+$, $3N^+$ and $6N^+$) with phenylene-ethynylene fluorogenic units are employed as the fluorescent probes for investigation of fluorescence responses in nano-confined environments of DNAs, BSA protein, surfactants and cyclodextrins in aqueous media. $3N^+$ represents one of the most responsive probes to all analytes. For example, the strong fluorescence enhancement of $3N^+$ by γ -cyclodextrin is due to a 1:1 stable inclusion complexation ($K_b = 3.0 \times 10^4 M^{-1}$). The discovery of fluorescence enhancement of $3N^+$ via charge interaction with ssDNA chain leads to the design of selective and sensitive potassium ion fluorescence aptasensing system. Strong fluorescence response to BSA protein suggest effective self-quenching prevention probably via both hydrophobic and hydrophilic interaction ($K_b = 6.7 \times 10^5 M^{-1}$). $3N^+$ is also used as a fluorescence micellization probe to determine CMC of surfactants. In the case of $6N^+$, the fluorescence enhancement becomes apparent only for BSA protein and surfactants. The interaction with ssDNA is proven by FRET signals which are useful for DNA sequence detection.



Department : Chemistry Student's Signature

Field of Study : Chemistry Advisor's Signature

Academic Year : 2011 Co-advisor's Signature

ACKNOWLEDGEMENTS

I wish to express my deep gratitude to my advisor, Associate Professor Dr. Mongkol Sukwattanasinitt, and my co-advisor, Assistant Professor Dr. Paitoon Rashatasakhon for his generous assistance, invaluable guidance and encouragement throughout the course of this research.

I would like to express my sincere appreciation to my supervisor in University of Massachusetts Amherst, Professor Dr. Sankaran Thayumanavan for his suggestion, generousness, and especially for giving me a chance to have a wonderful experience in America.

I would like to gratefully acknowledge the committees, Professor Dr. Sophon Roengsumran, Associate Professor Dr. Tirayut Vilaivan, Professor Dr. Thawatchai Tuntulani, Assistant Professor Dr. Patchanita Thamyongkit and Assistant Professor Tienthong Thongpanchang for their comments, guidance and extending cooperation over my presentation. I would like to thank Dr. Gamolwan Tumcharern from National Nanotechnology Center (NANOTEC) for AFM data, Dr. Anawat Ajawachom and Assistant Professor Dr. Sumrit Wacharasindhu for his attention and suggestion during our group meeting.

My appreciation is also given to many people in our research group; Dr. Anupat Potisatiyuenyong, Dr. Arisa Jaiyu, Dr. Chantana Sae-Lim, Dr. Nakorn Niamnont for their helpful suggestions and guidances; Mr. Akachai Krumsri, Ms. Kunnigar Vongnam, Ms. Wannapa Yuanboonlim, Ms. Suricha Pumtang, my greatest colleagues; and everyone in MAPS research group for a great friendships and encouragement.

I would like to thank Royal Golden Jubilee Ph.D. program (Grant No financially supported this Work, PHD/0050/2549), the Thailand Research Fund for financial support and also thank Center of excellent on Petrochemicals and Materials Technology, and the National Research University of CHE and the Ratchadaphiseksomphot Endowment Fund (AM1006A) and Center of Excellence on Petrochemical and Materials Technology for student scholarship.

Finally, I would like to express my thankfulness to my beloved parents who always stand by my side during both of my pleasant and hard time.

CONTENTS

	Page
ABSTRACT (THAI).....	iv
ABSTRACT (ENGLISH).....	v
ACKNOWLEDGEMENTS.....	vi
CONTENTS.....	vii
LIST OF TABLES.....	x
LIST OF FIGURES.....	xi
LIST OF SCHEMES.....	xvii
LIST OF ABBREVIATIONS.....	xviii
CHAPTER	
I INTRODUCTION.....	1
1.1 Overview.....	1
1.2 Supramolecular chemistry.....	3
1.3 Cyclodextrins.....	4
1.4 Deoxyribonucleic acid (DNA).....	6
1.5 Protein structures.....	10
1.6 Surfactants.....	11
1.7 Fluorescence.....	13
1.8 Literature surveys.....	15
1.9 Objectives.....	19
II EXPERIMENTAL.....	21
2.1 Materials and chemicals.....	21
2.2 Analytical instruments.....	21
2.3 Synthesis of 3N⁺	22
2.3.1 Preparation of TI₃	22
2.3.2 Preparation of IAMe₂	22
2.3.3 Preparation of SiEAMe₂	23
2.3.4 Preparation of EAMe₂	24
2.3.5 Preparation of 3N⁰	24
2.3.6 Preparation of 3N⁺	25
2.4 Synthesis of 6N⁺	26

CHAPTER	Page
2.4.1 Preparation of TI(EAMe₂)₂	26
2.4.2 Preparation of T(SiET)₃	27
2.4.3 Preparation of T(ET)₃	27
2.4.4 Preparation of T(ET(EAMe₂)₂)₃	28
2.4.5 Preparation of 6N⁺	29
2.5 Synthesis of multi-branches cationic phenylene-ethynylene fluorophores.....	29
2.5.1 Preparation of 2N⁰	29
2.5.2 Preparation of N⁰N⁺	30
2.5.3 Preparation of N⁺	30
2.5.4 Preparation of 2N⁺	31
2.6 Photophysical properties study.....	31
2.6.1 UV-visible spectroscopy.....	31
2.6.2 Fluorescence spectroscopy.....	32
2.6.3 Fluorescence quantum yields.....	32
2.6.4 Fluorescence spectra with various conditions.....	33
2.6.5 The computational chemistry for structure simulation.....	33
2.7 Supramolecular interaction of fluorophores study.....	33
2.7.1 General procedure for photophysical responses study.....	33
2.7.2 Interaction with cyclodextrins.....	34
2.7.3 Interaction with DNA.....	35
2.7.4 Interaction with BSA proteins.....	37
2.7.5 Interaction with surfactants and CMC determination.....	37
III RESULTS AND DISCUSSION.....	39
3.1 Synthesis and characterization of 3N⁺	39
3.2 Synthesis and characterization of 6N⁺	41

CHAPTER	Page
3.3 Synthesis and characterization of the multi-branched cationic fluorophores	44
3.4 Photophysical properties of the cationic fluorophores	50
3.4.1 Electronic absorption and emission spectra.....	50
3.4.2 Molar absorptivities and quantum yields.....	51
3.4.3 Electronic structure based on computational chemistry.....	52
3.4.4 Emission spectra with various conditions.....	54
3.5 Supramolecular interaction of the fluorophores with cyclodextrins	57
3.6 Supramolecular interaction of 3N^+ and 6N^+ with DNA.....	69
3.7 Supramolecular interaction of 3N^+ with BSA protein.....	79
3.8 Supramolecular interaction of 3N^+ and 6N^+ with surfactants.....	82
3.8.1 Fluorogenic responses with anionic surfactants	83
3.8.2 Fluorogenic responses with nonionic surfactants	86
3.8.3 Fluorogenic responses with cationic surfactants	87
3.8.4 Determination of critical micelle concentration (CMC).....	88
3.9 Comparison of supramolecular interactions of 3N^+ with various analytes	91
IV CONCLUSION	93
REFERENCES	94
APPENDIX.....	118
VITAE.....	149

LIST OF TABLES

Table		Page
1.1	Cyclodextrins properties.....	4
2.1	List of all ssDNA sequences.....	36
3.1	Photophysical properties of the polycationic fluorophores	52
3.2	Structures and CMC values of various types of surfactants	83
3.3	The CMC of surfactants determined by 3N⁺ and 6N⁺ probes	90
3.4	Summary of absorption changes, fluorogenic responses and possible interactions of 3N⁺ with various analytes.....	92

LIST OF FIGURES

Figure	Page
1.1 Structure of cyclodextrins	5
1.2 Chemical formula of a single chain of DNA and diagram of DNA double helix.....	6
1.3 Chemical structures of DNA bases	7
1.4 Watson-Crick base pairing.....	7
1.5 3D structures of double helical DNA	8
1.6 Three binding modes of double-stranded DNA with small molecules.....	9
1.7 Levels of protein structure illustrated by the catabolite activator protein ..	11
1.8 Plots of physical properties as a function of surfactant concentration.....	12
1.9 Jablonski diagram	14
1.10 Electron-transfer fluorescence quenching and Förster resonance energy transfer	15
1.11 Amplification of fluorescence quenching sensitivity	15
1.12 Structures of cationic conjugated polymers.....	16
1.13 Structure of the octupolar fluorophore.....	16
1.14 Structure of dendritic fluorescent probe and the cysteine sensing based on ICT switch on.....	17
1.15 Fluorescence quenching by Hg ²⁺ ions of the first generation dendritic compound in the presence of Triton X-100	17
1.16 Structures of various charged dendritic phenylene-ethynylene fluorophores, fluorescence response array, and PCA analysis for protein discrimination	18
1.17 Structure of the target fluorophores	20
3.1 ¹ H-NMR spectra of TI ₃ , EAMe ₂ , compound 1 and 3N ⁺	40
3.2 ESI MS data of 3N ⁺	41
3.3 ¹ H-NMR spectra of T(ET) ₃ , TI(EAMe) ₂ , compound 2 and 6N ⁺	43
3.4 ESI MS data of 6N ⁺	44
3.5 ¹ H-NMR spectra of IAMe ₂ , EAMe ₂ , 2N ⁰ , and N⁰N ⁺	45

Figure	Page
3.6	ESI MS data of N^0N^+ 46
3.7	^1H -NMR spectra of $\text{TI}(\text{EAMe}_2)_2$, $\text{TI}_2(\text{EAMe}_2)$, N^+ , and 2N^+ 48
3.8	ESI MS data of N^+ 49
3.9	ESI MS data of 2N^+ 50
3.10	Absorption spectra and emission spectra of N^0N^+ , N^+ , 2N^+ , 3N^+ and 6N^+ 51
3.11	AM1 structure of 3N^+ 53
3.12	HOMO and LUMO structure of 3N^+ 54
3.13	Emission intensity of 3N^+ and 6N^+ in various pH 55
3.14	Emission intensity of 3N^+ in various buffers 55
3.15	Chemical structures of Tris, MOPS and PIPES 56
3.16	Emission intensity of 3N^+ with various concentration of NaCl 57
3.17	Emission spectra and absorption spectra of 3N^+ in the presence of α -, β -, and γ -CyD 58
3.18	^1H -NMR spectra in D_2O of 3N^+ in the presence of α -, β -, and γ -CyD 60
3.19	Job's Plot of 3N^+ with β -, and γ -CyD 61
3.20	Circular dichroism spectra of 3N^+ in the presence of α -, β -, and γ -CyD ... 62
3.21	Benesi-Hilderbrand plot of 3N^+ with β -, and γ -CyD 63
3.22	Structural parameters of 3N^+ and CyDs 63
3.23	Fluorescence spectra of 3C^- in the presences of α -, β -, and γ -CyD 64
3.24	Fluorescence spectra of 2N^+ , N^+ and N^0N^+ in the presences of α -, β -, and γ -CyD 65
3.25	CD spectra of N^0N^+ , N^+ and 2N^+ in the presences of α -, β -, and γ -CyD... 65
3.26	^1H -NMR spectra in D_2O of 2N^+ in the presence of α -, β -, and γ -CyD 66
3.27	MM2 models of $2\text{N}^+/\gamma$ -CyD and $3\text{N}^+/\gamma$ -CyD complexes 67
3.28	^1H -NMR spectra in D_2O of 2N^+ in the presence of α -, β -, and γ -CyD 68
3.29	Histogram of the fluorophores (3C^- , N^0N^+ , N^+ , 2N^+ , and 3N^+) with the presence of α -, β -, and γ -CyD 69
3.30	Fluorescence spectra of 3N^+ in the presence of DNA 70

Figure	Page
3.31 Fluorescence spectra and absorption spectra of $3\mathbf{N}^+$ in the presence of ssDNA	71
3.32 Fluorescence spectra and wavelength shifting at maximum emission and fluorescence intensity of $3\mathbf{N}^+$ with various concentrations of dsDNA	72
3.33 Normalized emission intensity and Maximum wavelength shifting of $3\mathbf{N}^+$ in the presence of various ssDNA chain lengths	73
3.34 CD spectra of $3\mathbf{N}^+$ in the presence of dsDNA	73
3.35 Fluorescence spectra of $3\mathbf{N}^+$ in the present of mercury aptamer and $\text{Hg}(\text{OAc})_2$	74
3.36 Fluorescence spectra and Absorption spectra of $6\mathbf{N}^+$ in the presence of dsDNA	75
3.37 Absorption spectra and Emission spectra of $3\mathbf{N}^+$, $6\mathbf{N}^+$ and SyBrGreen II.....	76
3.38 Emission spectra of $3\mathbf{N}^+$ in the presence of ssDNA and SyBrGreenII	77
3.39 Emission spectra of $6\mathbf{N}^+$ in the presence of ssDNA and SyBrGreenII	78
3.40 Emission spectra of $6\mathbf{N}^+$ in the present of various ssDNA chain lengths...	79
3.41 Fluorescence spectra and absorption spectra of $3\mathbf{N}^+$ in the present of BSA.....	80
3.42 CD spectra of $3\mathbf{N}^+$ in the presence of BSA.....	81
3.43 Fluorescence spectra and wavelength shifting at maximum emission and fluorescence intensity of $3\mathbf{N}^+$ with various concentrations of BSA....	82
3.44 Fluorescence spectra of $3\mathbf{N}^+$ with various concentrations of anionic surfactants	84
3.45 Fluorescence spectra of $6\mathbf{N}^+$ with various concentrations of SDS	85
3.46 Fluorescence spectra of $3\mathbf{N}^+$ with various concentrations of nonionic surfactants	86
3.47 Fluorescence spectra of $6\mathbf{N}^+$ with various concentrations of Triton X-100	87

Figure	Page
3.48	Fluorescence spectra of $3\mathbf{N}^+$ with various concentrations of cationic surfactants 88
3.49	Fluorescence spectra of $6\mathbf{N}^+$ with various concentrations of DTAB 88
3.50	The CMC determination of Triton X-100 by $3\mathbf{N}^+$ 89
A.1	^1H NMR of \mathbf{TI}_3 119
A.2	^{13}C NMR of \mathbf{TI}_3 119
A.3	^1H NMR of \mathbf{IAME}_2 120
A.4	^{13}C NMR of \mathbf{IAME}_2 120
A.5	^1H NMR of \mathbf{SiEAME}_2 121
A.6	^{13}C NMR of \mathbf{SiEAME}_2 121
A.7	^1H NMR of \mathbf{EAME}_2 122
A.8	^{13}C NMR of \mathbf{EAME}_2 122
A.9	^1H NMR of $3\mathbf{N}^0$ 123
A.10	^{13}C NMR of $3\mathbf{N}^0$ 124
A.11	^1H NMR of $3\mathbf{N}^+$ 125
A.12	^{13}C NMR of $3\mathbf{N}^+$ 126
A.13	^1H NMR of $\mathbf{TI(EAME}_2)_2$ 127
A.14	^{13}C NMR of $\mathbf{TI(EAME}_2)_2$ 127
A.15	^1H NMR of $\mathbf{T(SiET)}_3$ 128
A.16	^{13}C NMR of $\mathbf{T(SiET)}_3$ 128
A.17	^1H NMR of $\mathbf{T(ET)}_3$ 129
A.18	^{13}C NMR of $\mathbf{T(ET)}_3$ 129
A.19	^1H NMR of $6\mathbf{N}^0$ 130
A.20	^{13}C NMR of $6\mathbf{N}^0$ 131
A.21	^1H NMR of $6\mathbf{N}^+$ 132
A.22	^1H NMR of $2\mathbf{N}^0$ 132
A.23	^{13}C NMR of $2\mathbf{N}^0$ 133
A.24	^1H NMR of $\mathbf{N}^0\mathbf{N}^+$ 133
A.25	^{13}C NMR of $\mathbf{N}^0\mathbf{N}^+$ 134
A.26	^1H NMR of \mathbf{N}^+ 134

Figure	Page
A.27 ^{13}C NMR of N^+	135
A.28 ^1H NMR of 2N^+	135
A.29 ^{13}C NMR of 2N^+	136
A.30 ESI MS data of 3N^+	136
A.31 ESI MS/MS data of 3N^+	137
A.32 ESI MS data of 6N^+	137
A.33 ESI MS/MS data of 6N^+	138
A.34 ESI MS data of N^+	138
A.35 ESI MS/MS data of N^+	139
A.36 ESI MS data of 2N^+	139
A.37 ESI MS/MS data of 2N^+	140
A.38 Linear graph plot for the fluorescence quantum yield of quinine sulfate standard, N^+ , 2N^+ , 3N^+ and 6N^+	140
A.39 Histogram showed the emission intensity of 3N^+ with various concentration of NaCl, NaBr, NaI and AgNO_3	141
A.40 ^1H -NMR spectra of cyclodextrins.....	142
A.41 Benesi-Hilderbrand's plot for 1:1 complexes of 3N^+ /dsDNA.....	143
A.42 Fluorescence spectra of 3N^+ with various concentrations of sodium triphosphate pentabasic and PVS.....	143
A.43 Fluorescence spectra and absorption spectra of 6N^+ in the presence of BSA.....	143
A.44 Benesi-Hilderbrand's plot for 1:1 complexes of 3N^+ /BSA	144
A.45 Normalized absorption spectra of 3N^+ in the presence of analytes	144
A.46 Wavelength shifting of 3N^+ with various concentrations of analytes.....	145
A.47 Fluorescence spectra of 3N^+ with various concentrations of analytes.....	145
A.48 CD spectra of 3N^+ in the presence of BSA, γ -CyD and DNA with alternated mixing steps	146
A.49 Fluorescence spectra of 3N^+ and SDS mixtures in the presence of dsDNA	146
A.50 AFM images on the mica surface of 3N^+ , 3N^+ / β -CyD, and 3N^+ / γ -CyD ...	147

Figure	Page
A.51 AFM images on the mica surface of 2N^+ , $2\text{N}^+/\beta\text{-CyD}$, and $2\text{N}^+/\gamma\text{-CyD}$...	147
A.52 AFM images on the mica surface of β - and γ -CyD	148

LIST OF SCHEMES

Scheme	Page
3.1 Synthesis of the $3\mathbf{N}^+$	39
3.2 Synthesis of $6\mathbf{N}^+$	42
3.3 Synthesis of the $\mathbf{N}^0\mathbf{N}^+$	44
3.4 Synthesis of the $2\mathbf{N}^+$ and \mathbf{N}^+	47
3.5 Purposed interactions of $3\mathbf{N}^+$ with anionic surfactant.....	85

LIST OF ABBREVIATIONS

Ar	aromatic
calcd	calculated
^{13}C NMR	carbon-13 nuclear magnetic resonance
CDCl_3	deuterated chloroform
CD_3CN	deuterated acetonitrile
$\text{DMSO-}d_6$	deuterated dimethyl sulfoxide
CD_3OH	deuterated methanol
D_2O	deuterated oxide
DMSO	dimethylsulfoxide
d	doublet (NMR)
dd	doublet of doublet (NMR)
ESI MS	electrospray ionization mass spectrometry
equiv	equivalent (s)
g	gram (s)
^1H NMR	proton nuclear magnetic resonance
Hz	Hertz
hr	hour (s)
<i>J</i>	coupling constant
mg	milligram (s)
mL	milliliter (s)
mmol	millimole (s)
<i>m/z</i>	mass per charge
m	multiplet (NMR)
M.W.	molecular weight
M	molar
MHz	megaHertz
rt	room temperature
s	second (time)
s	singlet (NMR)

THF	tetrahydrofuran
TLC	thin layer chromatography
UV	ultraviolet
Å	Angstrom
α	alpha
β	beta
δ	chemical shift
°C	degree Celsius
γ	gamma
λ	wavelength
μL	microliter (s)
μM	micromolar (s)
% yield	percentage yield
Φ	quantum yield

CHAPTER I

INTRODUCTION

1.1 Overview

During the past few decades, we have witnessed rapid progress in sensor and biosensor applications based on fluorescent compounds. Success of the fluorescent sensors relies largely on their sensitive signal transduction via various energy and electron related processes upon fluorophore-analyte interactions. Direct detection of double stranded deoxyribonucleic acids (DNAs) by organic dyes consisting of rigid planar fused aromatic rings is based mainly on fluorescence enhancement via DNA-dye intercalation [1-4]. Protein sensing has been achieved via varieties of intermolecular interactions ranging from hydrophobic, hydrogen bonding, dipole-dipole and electrostatic forces [5-6]. The host-guest chemistry of a well-defined structure such as cyclodextrins (CyDs) are widely applied in sensing and controlled release applications via inclusion complexes [7-15]. These supramolecular interactions have been attributed to changes of electron energy levels, self-aggregation, energy and electron transfers. Characterization of the supramolecular interaction affecting the fluorescence signals of the fluorophore is thus fundamentally important for development of efficient fluorescence sensing system.

Recently, water-soluble conjugated polyelectrolytes (CPs) present a useful platform for the development of highly sensitive fluorescence-based sensors for chemical [16-18] and biological detections [19-24]. Especially, cationic conjugated polymers (CCPs) have been effectively utilized for DNA sensing [25-32] including labeled-free system [33-35]. Despite the applications of CPs show higher sensitivity, due to amplification effect, than that of the corresponding small conjugated molecules with similar structures [36-41]. The conformation of linear CCPs are very complex that their 3-D molecular structures are highly unpredictable. The nature of fluorescence responses associated to their molecular and supramolecular structures thus cannot be easily drawn [42-43]. The difficulty in controlling molecular weight distribution of linear CPs is another concern in obtaining reproducible responses for

practical uses [44]. It is thus interesting to investigate an alternative class of structurally well-defined cationic fluorophores possessing the beneficial features of CPs i.e. multiple charges and fluorogenic units.

Dendrimers, which are hyperbranched architectural macromolecules, can be constructed with exactly controlled structures and globular shape by the stepwise synthetic approach [45]. Compare to their linear analogues, the dendrimers can display a high density of functional groups [46-48] and chromophores [49-51] within the same molecular radius. The rigid spherical dendrimers have been applied for modeling or studying of photophysical properties [52-54]. Because its excellent fluorescence and high quantum efficiency, phenyleneethynylene fluorophores have been successfully exploited as fluorescent signal transducer for various chemical and biological sensing systems [55-59]. Recently, a new series of water-soluble fluorescent dendritic phenylene-ethynylene with ionic peripheries were synthesized and used as fluorescence sensors for metal ions and biological agents [60-63]. The water soluble compounds with phenylene-ethynylene fluorogenic units are also interesting probes for studying the supramolecular interactions of their strong fluorescence responses to the nano-confined environments and more predictable geometries [64-65].

Surfactant molecules and micellar solutions are also known to be used in a wide variety of fields such as organic reactions, catalysis, polymerization and controlled drug delivery [66-70]. Many literature reports revealed that the presence of surfactants in solution can lead to the changes of photoproperties (i.e. band shift and quantum yield enhancement and have been applied in increasing sensitivity and selectivity in DNA detection [66-81]. Moreover, the collisional probability and solvation dynamics of water in the nano-confined micellar systems are considerably slowed down leading to changes in their physical and chemical properties of the probes in aqueous systems [82-85]. As mentioned earlier, it is thus important to investigate the supramolecular binding events of the water soluble phenylene-ethynylene fluorophores with various types of nano-confined environments mainly via fluorescence spectroscopic data in aqueous media that should also be helpful in host-guest pairs for applications such as controlled release system.

1.2 Supramolecular chemistry

Supramolecular chemistry has been defined as the chemistry of a non-covalent bond between a host and guest molecules as expressed by Jean-Marie Lehn [86]. Modern supramolecular chemistry can be categorized into two main systems; host-guest chemistry and self assembly [87]. The host is termed as a larger molecule that can enclose another smaller one called guest via non-covalent interactions such as hydrogen bonding, electrostatic forces, dative bonding, van der Waals forces and crystal close packing, metal-to-ligand binding, π - π stacking interactions and closed shell interactions where their host-guest relationships associate with binding sites [88]. The host-guest aggregate is held together in the binding site which is a region of the host or guest that interact with the correct size, geometry and chemical nature of the other species. While self-assembly is termed that the two or more components joining to form a larger, non-covalently bound aggregate with the spontaneous and reversible association resulting to the most thermodynamically stable aggregate structure under the prevailing condition system. This equilibrium process is responsible for the structure and complexity of many biological systems and molecular devices [89-90]. A variety of not only two-dimensional but also three-dimensional morphologies can be formed by a cooperative interaction and balancing between three classes of distinctive forces; an attractive driving force and a repulsive opposition force are responsible for nondirectional self-assembly while a functional force including such as hydrogen bond, coordination bond and steric repulsion acts uniquely to be directly responsible for directionality [91]. Furthermore, supramolecular chemistry is very useful for the development of molecular devices and nanotechnology, biological recognition and biomimetic chemistry, pharmaceuticals and medicinal systems, catalysis design approaches, green chemistry applications and radioactive waste treatments [92-95]. Therefore, the study of non-covalent interactions to understand the relationship between supramolecular chemical principles and the biological influences often provides the inspiration behind supramolecular phenomenon researches in the chemistry of life.

1.3 Cyclodextrins

One of the most important compounds using in the host-guest chemistry is cyclodextrins (CyDs) that are a group of cyclic oligosaccharides produced enzymatically by *Bacillus macerans* [92-93]. Some physiochemical properties of cyclodextrins (α -, β -, and γ -CyD) that contain six, seven and eight glucose entities respectively were compared as shown in Table 1.1. The inner cavity diameter of CyD increases in proportion to the glucosyl units but the depth remain the same height [96-99]. However, the inclusion complex formation is mainly disciplined by the guest thickness compared to their internal diameter, guest thicker than the minimum diameter do not penetrate to the CyD cavity to form a stable axial inclusion complex with its hydrophobic part [100].

Table 1.1 Cyclodextrins properties [96-100].

Property	α -CyD	β -CyD	γ -CyD
Number of glucopyranose units	6	7	8
Molecular Weight (g/mol)	972	1135	1297
Outer diameter (Å)	14.6	15.4	17.5
Minimum internal diameter (Å)	4.4	5.8	7.4
Height of torus (Å)	7.9	7.9	7.9
Cavity volume (Å ³)	174	262	427
$[\alpha]_D$ at 25°C	+150±0.5	+162.5±0.5	+177.4±0.5
Water molecule in cavity	6	11	17

Cyclodextrin structures are shaped like cones with the secondary hydroxyl groups of the C2 and C3 positions extending from the wider rim and the primary groups of the C6 position extending from the narrow rim due to chair formation of the glucopyranose units as shown in Figure 1.1. While H5 hydrogen of glucosyl units located at a CyD bottleneck of toroidal shape refer to the minimum internal diameter. Therefore, the toroidal shape contained hydrophobic internal cavity and hydrophilic external surface which a high electron density inside CyD cavity can activate electrons of the guest molecule [101].

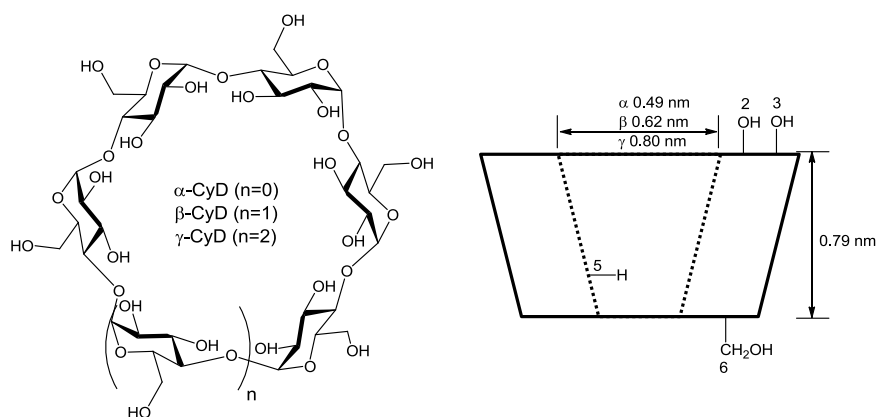


Figure 1.1 Structure of cyclodextrins

Inclusion complexes with various guest molecules of CyDs upon the supramolecular size and shape and also the environments that correspond to the guest which penetrate into cyclodextrin cavity have been effectively proved by various methods. Various characterization techniques can be used to determine the interactions between CyDs and guest molecules; for example, ^1H NMR [102-106], mass spectrometry [107], electrophoresis, [108] UV-vis absorption spectroscopy [109], fluorescence spectroscopy [110-114], x-ray crystallography [115-118] and computational chemistry. [119] In addition, a binding constant (K_b) of molecular interaction of host-guest types for stoichiometric 1: 1 inclusion complex ratio was derived from a linear plot corresponding to Benesi-Hilderbrand equation [120-126]:

$$\frac{1}{I - I_0} = \frac{1}{I_1 - I_0} + \frac{1}{(I_1 - I_0)K_b} \frac{1}{[\text{CyD}]}$$

Where that I_0 corresponds to the initial fluorescence intensity of free guest (blank solution), I_1 is the intensity of the guest/CyD complex and I is the observed fluorescence intensity of the mixtures. The ground state association constant (K_b) for 1: 1 complex formation was derived from a linear graph plotting $\frac{1}{I - I_0}$ against $\frac{1}{[\text{CyD}]}$ as equal to $K_b = \frac{Y\text{-intercept}}{\text{gradient}}$ since $\frac{1}{I_1 - I_0}$ is the intercept on the Y axis and $\frac{1}{(I_1 - I_0)K_b}$ is a gradient of the linear fit as followed the equation.

Due to their complexation ability, low cytotoxicity effects, the capable modified material properties, cyclodextrins are widely use in different application areas such as industrial products, technologies and analytical methods, drug carrier,

food and flavors, cosmetics, packing, textiles, separation processes, environment protection and fermentation and catalysis [127-130].

1.4 Deoxyribonucleic acid (DNA)

Deoxyribonucleic acid (DNA) is a nucleic acid that is a central molecule in the transmission, expression, and conservation of genetic information. The main role of DNA molecules is as the carrier of genetic information that its blueprints set contains the genetic instructions needed to construct other essential components of cells such as proteins and ribonucleic acid (RNA) molecules used in the development and functioning of all known living organisms [131]. DNA structure was elucidated as a double helix that consists of two long polymers of simple units called nucleotides, with backbones containing sugar and phosphate groups joined by ester bonds (Figure 1.2) and these two nucleic acid strands run in opposite directions to each other called anti-parallel [132-133].

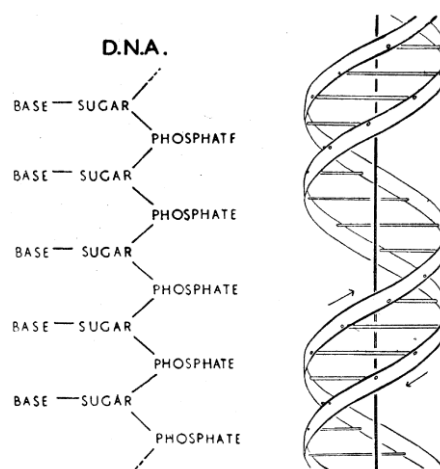


Figure 1.2 (*left*) chemical formula of a single chain of DNA and (*right*) Diagram of DNA double helix that the two ribbons represent the two phosphate-sugar chains, and the horizontal rods the pair of bases holding the chain together. The vertical line marks the fiber axis [133].

All nucleotides repeating unit consists of three components: a phosphate group, a pentose sugar that is 2-deoxy-D-ribose and one of four nitrogen heterocyclic bases that are monocyclic pyrimidines or bicyclic purines. The major purines: adenine (A) and guanine (G) and the major pyrimidines: cytosine (C) and thymine (T) are found in DNA bases (Figure 1.3) [134].

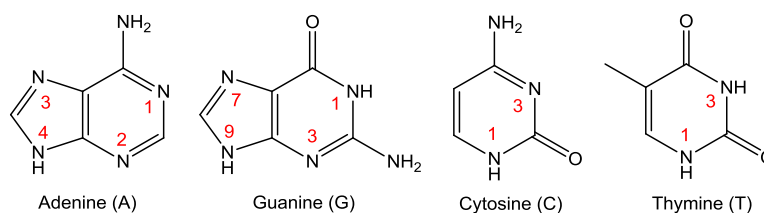


Figure 1.3 Chemical structures of DNA bases

According to first discovered by James D. Watson and Francis Crick, the DNA structure of right-handed double helix B-form has 10 base pairs per complete turn, and the paired bases are almost exactly perpendicular to and stacked over the helix axis with each the helical rise $\sim 3.4 \text{ \AA}$ [135] and a helical pitch of 34 \AA . In DNA double helix, the two chains are held together with hydrogen bond between the bases that there are two hydrogen bonds in an A•T pair and three in a C•G pair as the dominant pattern of Watson-Crick base pairing shown in Figure 1.4. Major groove, which possesses a wider gap between the strands in the helix, is $\sim 12 \text{ \AA}$ wide while the width of the minor groove is $\sim 6 \text{ \AA}$ [136].

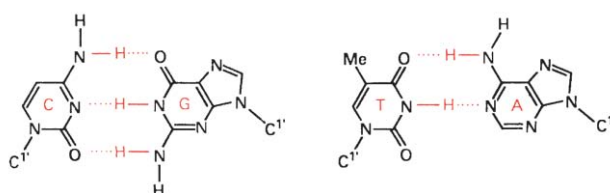


Figure 1.4 Watson-Crick bases pairing for C•G (*left*) and T•A (*right*) [134].

Moreover, not only B-DNA double helix or duplex but also alternate conformations such as A-form and Z-form in functional organism and higher-order structure such as a triple helix or triplex, a guanine quadruplex, and a Holliday junction structure are found upon their environmental conditions (Figure 1.5).

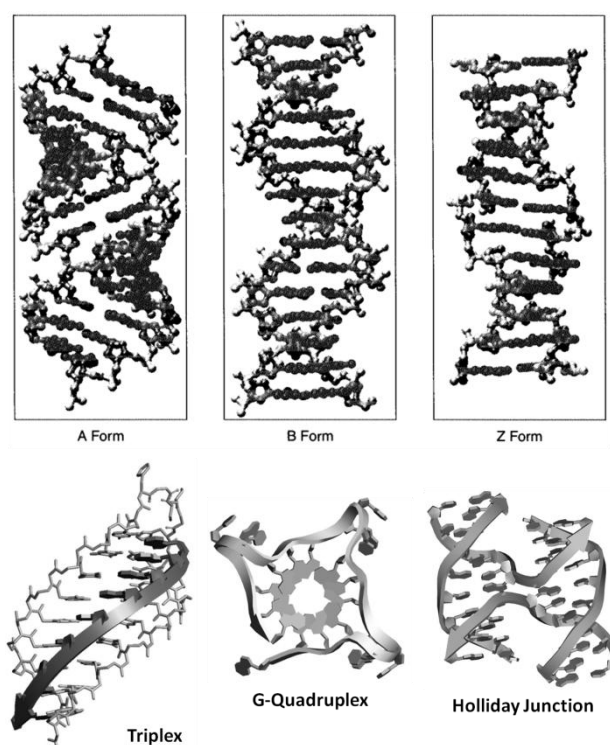


Figure 1.5 (*top*) 3D structures of double helical DNA; the A, B, and Z forms [131] and (*bottom*) crystal structures of the PNA-DNA triplex, the potassium form of the intermolecular quadruplex, and the Holliday junction [136].

The interaction of double-stranded DNA (dsDNA) with small molecules are mainly classified into three binding modes; outside-edge binding, intercalation, and groove binding (Figure 1.6) [134, 137]. Outside-edge binding relates to a ligand binding such as Na^+ , Mg^{2+} or polyamines that can interact non-specifically with the sugar-phosphate backbone through mainly electrostatic interactions. While intercalation is involved in a planar or near planar aromatic ring system such as ethidium, daunomycin, proflavin, actinomycin, or acridines that inserts in between two adjacent base pairs, perpendicular to the helical axis. Intercalators that can have an extended, electron-deficient, planar aromatic ring system generally form a platform of approximately the same size as a DNA base pair [138-143]. Also, groove binding is evolved into a bound ligand such as netropsin, or lexitropsins that fit its molecular contact direction with functional groups on the edges of the bases into the floor of grooves [144]. DNA conformation and stability has been effected by the outside-edge, electrostatic interactions of the positively charged counterions and DNA polyanion association. However, an electrostatic potential, hydrogen-bonding characteristics,

steric effects, and hydration have also influenced to groove binding interactions between groove binder and the major or minor DNA grooves.

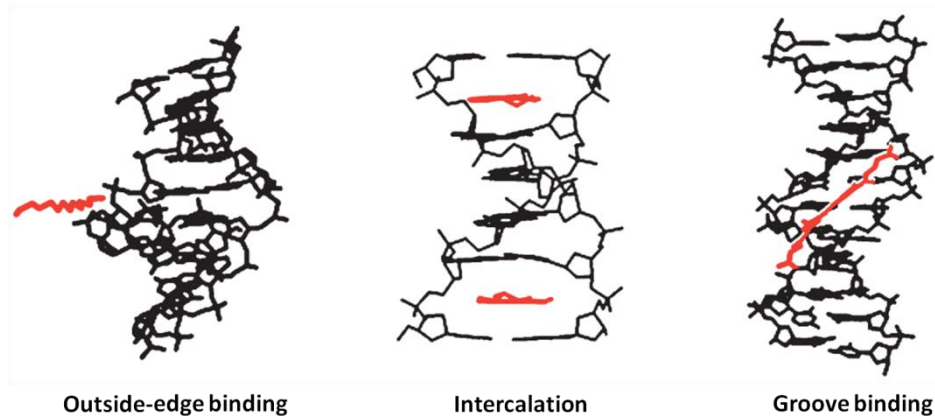


Figure 1.6 Three binding modes of double-stranded DNA with small molecules; outside-edge binding, intercalation, and groove binding [134].

Triplex DNA can be formed when a single-stranded oligonucleotide (ODN) or a short single stranded DNA (ssDNA) fragment specifically recognizes the major groove and forms hydrogen bonds with the base pairs of the duplex DNA that given a number of different conformations. Therefore, the intermolecular triplex-forming oligonucleotides have been a versatile and powerful tool for an antigene therapy due to their specificity of base-base interactions. For the reason of low stability under physiological conditions, high cation concentrations are required or an intercalating ligand is used to stabilize the triplex DNA [134, 136]. In addition, polyelectrolyte/hybridized nucleic acid triplex are effectively applied to use for DNA detection via fluorescence methods [25-28, 32, 35, 81]. Another higher-order structure, G-quadruplex that four guanine bases can form self-associate cyclic, planar tetrameric structures known as G-tetrads have high potential in structure/sequence-specific agents for human treatment diseases [134]. Specific sequence of single-stranded G-rich aptamers, which are artificial nucleic acid ligands that can be generated against amino acids, drugs, proteins and other molecules, can be formed G-quadruplex with target molecules such as K^+ [146-147], neomycin B [148], hemin [149-150] and ochratoxin A [151] leading to useful *in vitro* diagnostic assays [152-154]. In addition, the other single-stranded forms such as hairpin and beacon has been also exhibited high-throughput approaches for many recently applications and researches [33, 155-163].

1.5 Protein structures

Proteins are the major functional molecules of life that are products of evolution including duplications or deletions and mutations by changing the nucleotide sequences of genes.

Due to their useful properties, we can employ the protein as therapeutic agents, catalysts, and materials. Protein with mutations that cause detrimental changes in structure and/or function may result in a disease, as a consequence, many diseases such as muscular dystrophy, Creutzfeld-Jakob disease or other transmissible encephalopathies, amyloidosis, and cancers result from protein structure change, a loss of physical function or mutations. Moreover, enzymes and receptors that are a protein analogue can usually be drug targets, restore function or destroy infectious agents or cancers. Therefore, the prediction of protein structures and protein activity assays are ultimate goal to be able to design and synthesize novel catalysts, materials, or drugs that will eradicate diseases and minimize illness [164-165].

Proteins are unbranched polymers consisting of 20 different amino acids connected by peptide bonds. The sequence of the different amino acids in a protein, which is directly determined by the sequence of nucleotides in the gene encoding, is called its *primary structure* that it is usually given starting with the N-terminal and ending with the C-terminal amino acids due to the addition order of amino acids during protein synthesis. *Secondary structure* refers to the local conformation of amino acids in the protein main-chain that is stabilized by hydrogen-bonding interactions between amino- (N-H) and keto- (C=O) groups of the peptide bonds. These groups holding partial positive and negative charges can form hydrogen bonds with only a relatively small energy to give two major forms that are alpha helices and beta sheets. The combinations of alpha and/or beta recurring substructures or folds may form a *supersecondary structure* or *motifs*. In a globular form, *tertiary structure* refers to the three-dimensional structure of a single protein molecule which elements of its secondary structure are arranged in space. The protein folds are determined by ionic interactions between charged amino acid R-groups, by non-specific hydrophobic interactions (hydrophobic residues are buried inside while hydrophilic part can interact with water), by hydrogen and van der Waals forces and rarely by disulfide (S-S) bonds between cysteine residues. Many proteins are formed by association of the

folded chains of more than one polypeptides resulting to a larger assembly called *quaternary structure*. The quaternary structure is stabilized by the same interactions that are non-covalent bonds and disulfide bonds as the tertiary structure (Figure 1.7) [164, 166-169].

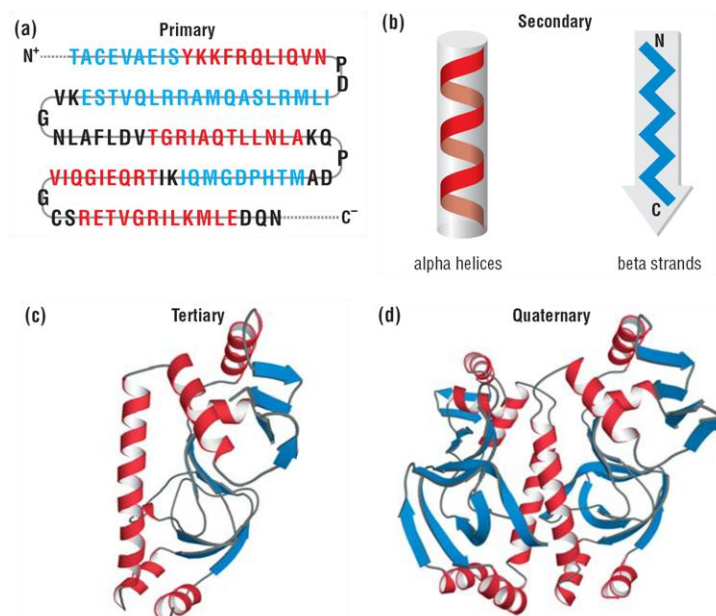


Figure 1.7 Levels of protein structure illustrated by the catabolite activator protein; (a) primary-, (b) secondary-, (c) tertiary- and (d) quaternary structures [167]

In addition, the determination methods of three-dimensional structure of protein can be achieved by x-ray crystallography, x-ray and neutron diffraction, NMR spectroscopy, optical spectroscopy, mass spectrometry, electrophoresis, cryo-electron microscopy and immunochemical analysis. [165-173]

1.6 Surfactants

Surface active agents or surfactants are amphiphilic molecules containing a hydrophilic head or polar moiety, which is readily soluble in water, and a hydrophobic tail or nonpolar moiety, which is generally insoluble in water [174]. There are four primary groups of the surfactant classification based on the nature of the hydrophilic head; anionic, cationic, nonionic, and zwitterionic [175-176]. In addition, the hydrophobic tail is usually a long hydrocarbon chain even though a halogenated, oxygenated or siloxane chains can be used [177]. Surfactant molecules and micellar solutions are known to be used in a wide variety of fields that are

detergents and cleaners, cosmetics and personal care products, pharmaceuticals, petroleum recovery processes, high-tech areas, medicine and biochemical research, plant protection and pest control, foods and packaging, paper and cellulose products, paints and coating products, plastics and composite materials, metal processing, textiles and fibers, leather and furs, oilfield chemicals, mining and flotation, and chemical and industrial applications [175, 178]. One of the most important parameters for surfactant characterization is the critical micelle concentration (CMC) which surfactant aggregates or micelles are spontaneously formed at this concentration. The physico-chemical properties of self-assembled structures that differ from surfactant molecules show an abrupt change at and above CMC as illustrated in Figure 1.8.

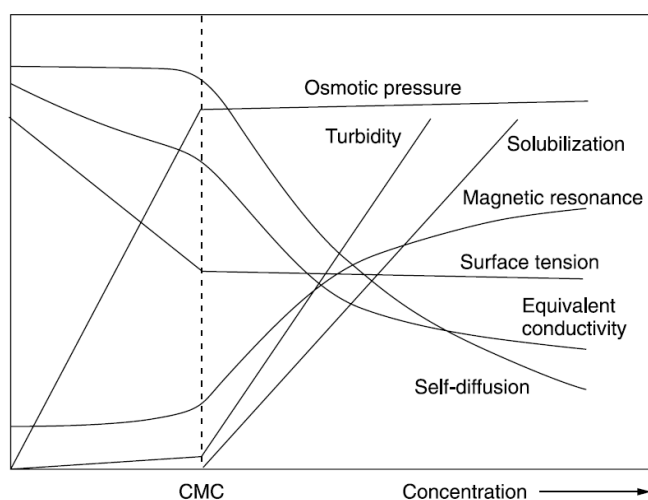


Figure 1.8 Plots of physical properties as a function of surfactant concentration [176].

Therefore, CMC have now been determined by several methods, for examples; conductivity [179-181], osmometry [182], surface tension [183-187], nuclear magnetic resonance (NMR) spectroscopy [188], UV-Vis [189-190] and fluorescence spectroscopy [69, 191-194], X-ray diffraction (XRD), electron spin resonance (ESR), small-angle neutron scattering (SANS), light scattering, and calorimetry. Moreover, one of effective surfactant detections is achieved by fluorometric method [195-196]. Also, in the mixed micellar system including polyelectrolyte-surfactant complexes [71-72, 197-201] and fluorescence dye-surfactant aggregate [53] have been studied to discover supramolecular formation, and cyclodextrin-surfactant complex [73] or even deoxyribonucleic acid (DNA) systems [77-79, 202-203] has been utmost interested in by recently researchers for biological application approaches.

1.7 Fluorescence

Fluorescence is an emission of light from the excited state by a substance that has absorbed light or other electromagnetic radiation returning to the ground state. The fluorescent processes that occur between the absorption and emission of light are usually described by the Jablonski diagram (Figure 1.9) [204]. Molecules that can absorb photons relating to the electronic, vibrational, and rotational energy levels, is allowed to reach an excited state after absorption within 10^{-15} s and thus absorbed photons induces excitation. Following light absorption, a fluorophore, molecule can give the fluorescence, is usually excited to some higher vibrational level of either S1 or S2 and form an excited fluorophore, and then rapidly relaxes to the lowest level of S1 within 10^{-12} s or less by internal conversion. The fluorescence signal is observed when the excited fluorophore relaxes to ground singlet electronic state (S_0) via photon emission that the fluorescence lifetime goes from 10^{-9} to 10^{-12} s. Molecules can also undergo a spin conversion of its S1 state to the first triplet state T1 called intersystem crossing and then emit the phosphorescence by transition from T1 to the singlet ground state. From the diagram, phenomenon that the fluorescence naturally occurs at the lower energies or longer wavelength than the absorption is observed as called as the Stokes shift. This phenomenon can be caused by energy losses between excitation and emission which are the rapid decay to the lowest vibrational level of S1, or thermalization of the excess vibrational energy from the decay of fluorophores to higher vibrational levels of S_0 , and also occurred by solvent effects, excited-state reactions, complex formation, and/or energy transfer. [31]

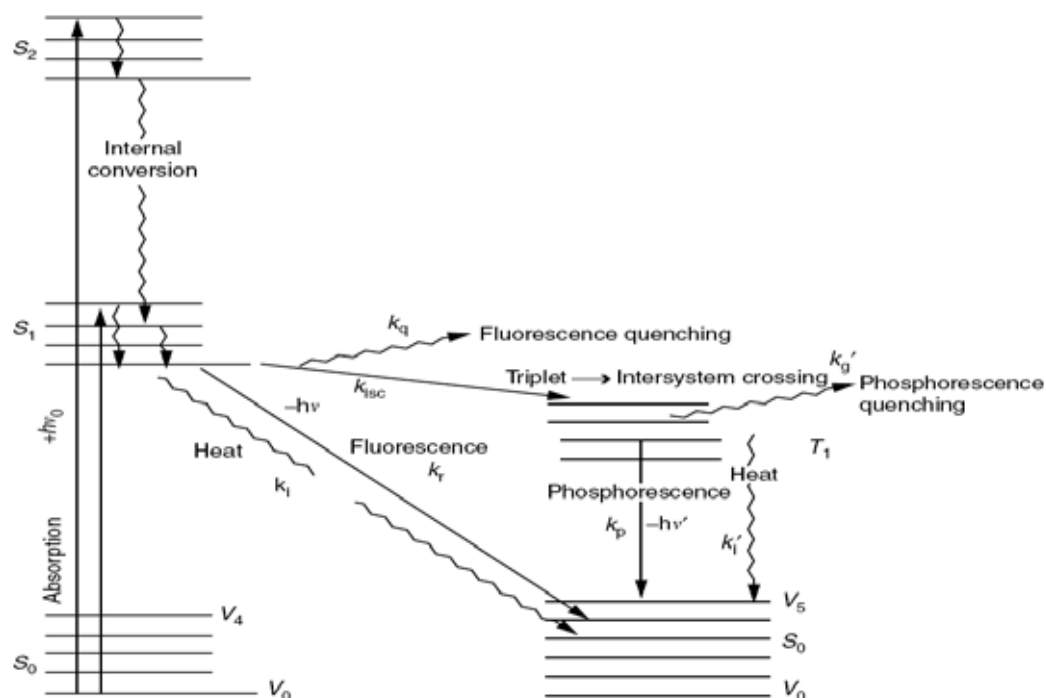


Figure 1.9 Jablonski diagram [204]

Any processes that can decrease the fluorescence intensity of a given substance are referred to as quenching, caused by different mechanisms such as excited state reactions, energy transfer, complex-formation, excimer formation, and collisional quenching. The molecules that can cause fluorescence quenching are called quenchers. For example, photoinduced electron transfer (PET) can occur whenever a lone electron pair is located in an orbital of the fluorophore itself or an adjacent molecule and this orbital energy lies between those of the HOMO and LUMO. The transfer of an electron between the fluorophore and the quencher provides nonradiative deactivation of the excited state, leading to quenching [206]. In contrast, fluorescence resonance energy transfer (FRET) is a dynamic quenching mechanism that occurs whenever the emission spectrum of a fluorophore donor overlaps with the absorption spectrum of an acceptor (Figure 1.10). FRET is influenced by factors such as the donor-acceptor distance, the extent of spectral overlap between the donor emission and acceptor absorption, and the relative orientation of the donor and acceptor dipole moments [207-208]. These quenching processes are useful for sensing applications in the form of “turn-off” mode.

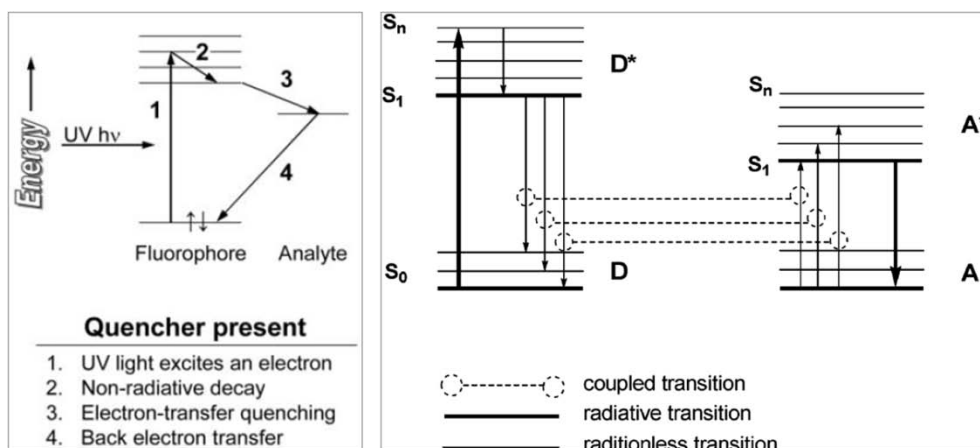


Figure 1.10 (left) Electron-transfer fluorescence quenching and (right) Fröster resonance energy transfer [206-207]

Moreover, the reduction of self-quenching via degregation of π - π stacking, the decreasing of intramolecular charged transfer (ICT), or the increasing of molecular rigidity via geometrical lock, and/or deleting any quenching factors can effectively present fluorescence enhancement that be helpful in many sensing in the term of “turn-on” mode. [205]

1.8 Literature surveys

In 1999, Chen [19] et al. showed that water-soluble polyanionic CP (poly(2-methoxy-5-propyloxy)sulfonate phenylenevinylene, **MPS-PPV**) gave a greater fluorescence quenching than million-fold amplification of the sensitivity relative to that of corresponding small conjugated molecules with similar structure (Figure 1.11). Also, this fluorescent polymer exhibited a much greater quenching than that of the micelle system and sensitive and selectively applied for biological sensing.

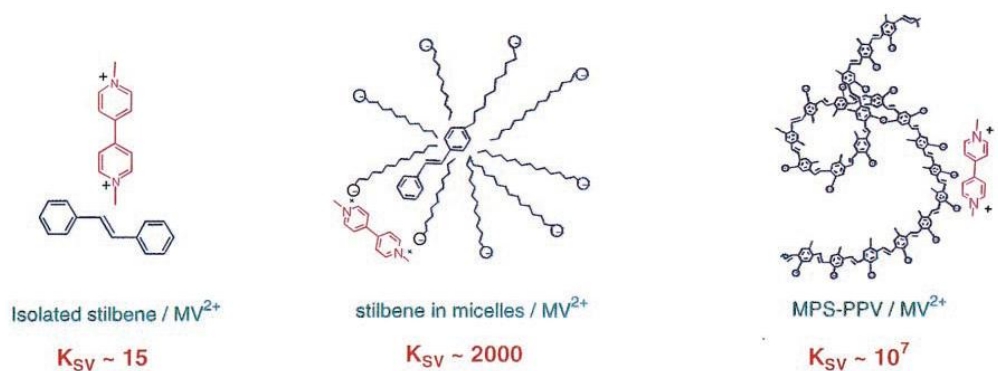


Figure 1.11 Amplification of fluorescence quenching sensitivity [19]

Recently, many researchers have reported that water-soluble cationic conjugated polymers (CCPs) such as poly(bis(fluorenyl)benzene) [25, 28], polythiophene [26, 32] and polyphenyleneethynylene [26] were effectively used for DNA sensors (Figure 1.12).

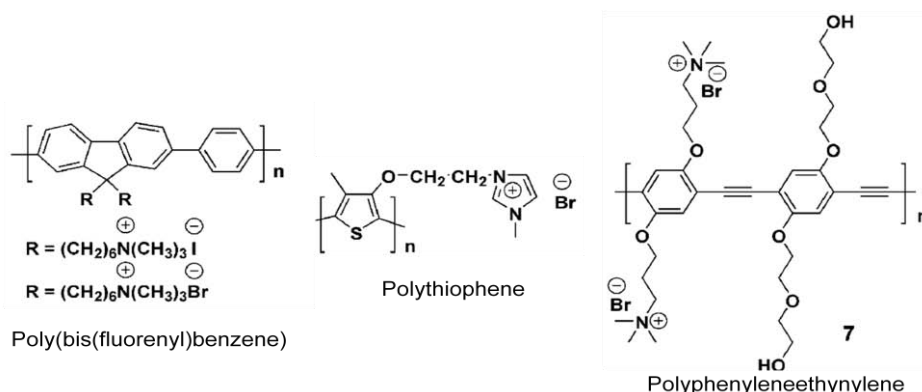


Figure 1.12 Structures of cationic conjugated polymers [26]

In 2004, Porrès [209] et al. exhibited that the octupolar fluorophore containing a triphenylamine core with strong acceptor peripheral groups via phenylene-ethynylene linkers gave high fluorescence quantum yield ($\Phi = 0.72$) (Figure 1.13).

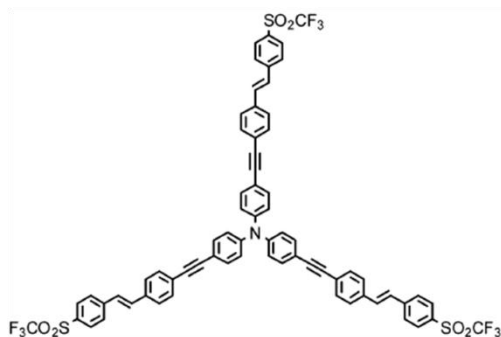


Figure 1.13 Structure of the octupolar fluorophore [209]

In 2009 Zhang [59] et al. synthesized a dendritic fluorescent probe exhibiting strong two-photon absorption and efficient intramolecular charge transfer (ICT) for cysteine (Cys) and homocysteine (Hcy) with a turn-on mode in polar solvent (DMSO). This is the first report that exhibits both greatly enhanced emission intensity and large peak shift. This work should be a general guideline for the design of novel multisignal one- and two-photon turn-on probes, based on ICT switch on/off, with various sensing applications due to the potential reactivity of aldehyde toward other nucleophiles (Figure 1.14).

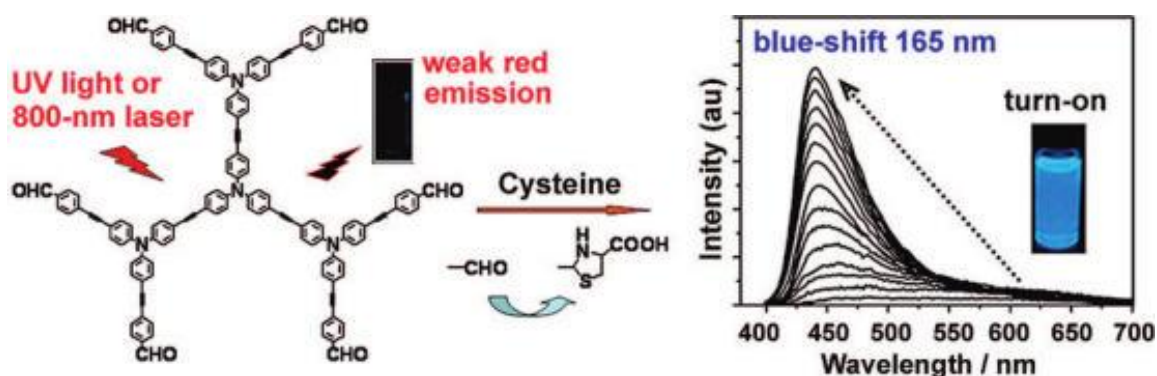


Figure 1.14 Structure of dendritic fluorescent probe (*left*) and the cysteine (Cys) sensing based on ICT switch on (*right*). [59]

In 2009, Niamnont [60] and co-workers successfully synthesized a series of water-soluble fluorescent dendritic compounds composed of phenylene-ethynylene repeating units and anionic carboxylate or cationic ammonium peripheral groups. These fluorophores can be dissolved in aqueous media. The first generation fluorescent dendrimer containing nine phenylene-ethynylene units and six carboxylate peripheral groups exhibited a highly selective fluorescence quenching by Hg^{2+} ions. The Stern-Volmer quenching constant (K_{sv}) was $33,700 \text{ M}^{-1}$ with wide linear Hg^{2+} concentration of the fluorescence responses (2-80 μM) in aqueous media in the presence of Triton X-100 surfactant (Figure 1.15).

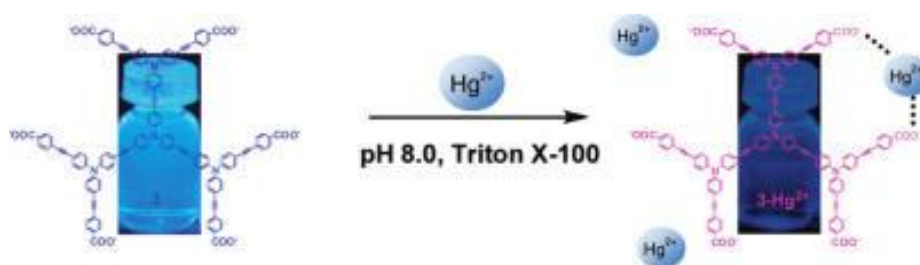


Figure 1.15 Fluorescence quenching by Hg^{2+} ions of the first generation dendritic compound in the presence of Triton X-100. [60]

In 2010, Niamnont [62] et al. developed the fluorescent sensor array for the protein discrimination by various charged dendritic phenylene-ethynylene fluorophores in phosphate buffer saline pH 7.4. The data set of fluorescent intensities can be statistically sorted into eight clusters corresponding to each protein by principal component analysis (PCA). Factorial discriminant analysis (FDA) cross-

validation is applied to locate the optimum detection wavelength and reduce the number of sensing elements from nine to two with 100% discriminating accuracy (Figure 1.16). The results highlighted the benefits of the charge variation in the development of high performance protein sensing arrays and the method described should be generally practical for the development of electronic tongue for protein related food analysis and medical diagnosis.

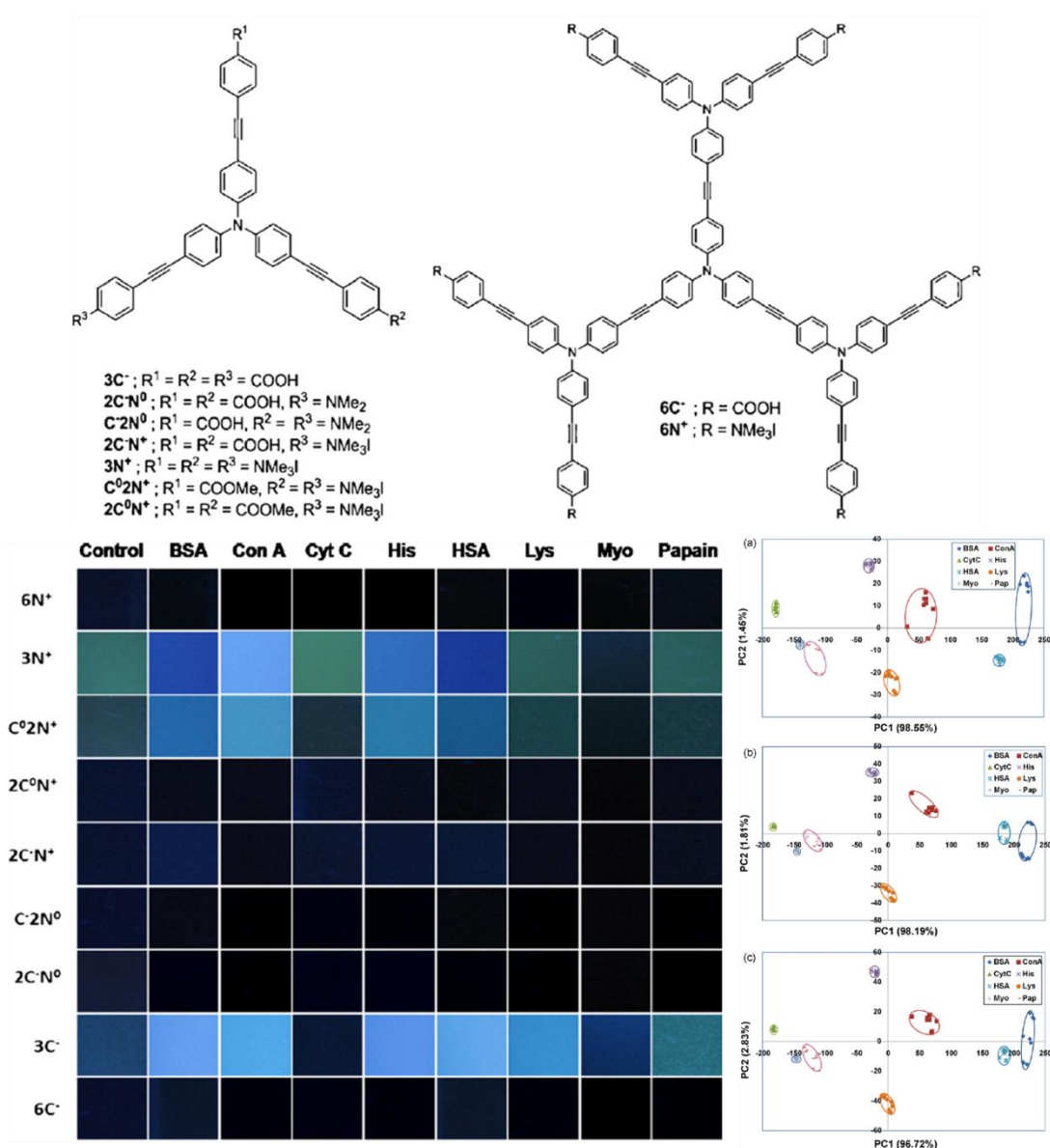


Figure 1.16 Structures of various charged dendritic phenylene-ethynylene fluorophores, fluorescence response array, and PCA analysis for protein discrimination. [62]

From the literatures, it is thus summarized that the phenylene-ethynylene fluorescent polyelectrolytes showed interesting fluorescence responses for chemical and biological sensing applications.

1.9 Objectives

The aim of this work focuses on the synthesis of water soluble dendritic fluorophores composed of phenyleneethynylene repeating units and cationic ammonium peripheral groups (Figure 1.17) to study of their fluorescence responses in various analytes. The application of these fluorophores as supramolecular sensors in aqueous media will also be explored.

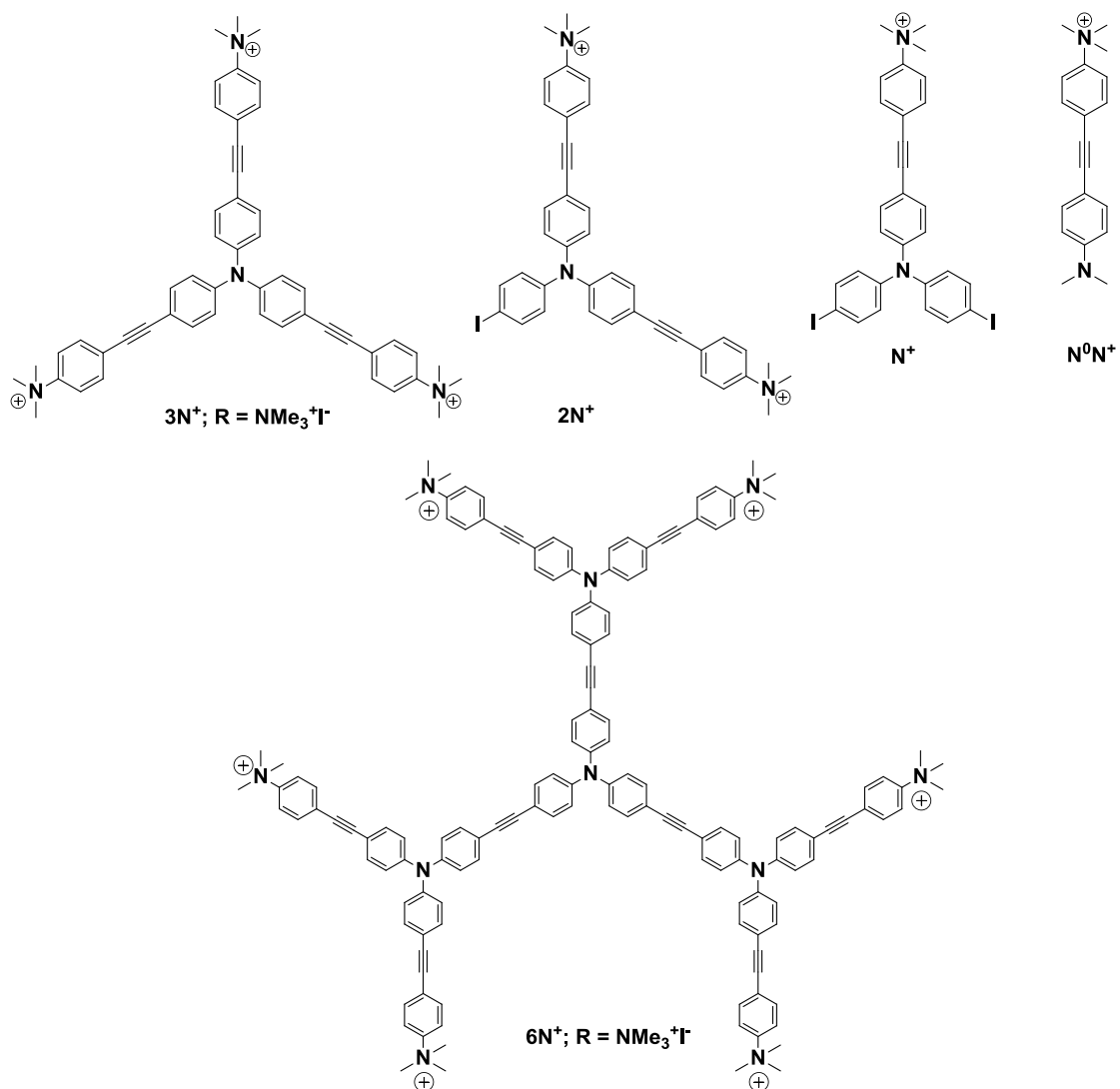


Figure 1.17 Structure of the target fluorophores

CHAPTER II

EXPERIMENTAL

2.1 Materials and chemicals

All reagents were purchased from Sigma-Aldrich (Switzerland), Fluka[®] (Switzerland) and Merck[®] (Germany). For general reactions, solvents such as hexane, methanol and toluene were reagent grade stored over molecular sieves. Diethyl ether and methanol used for reactions was reagent grade. All column chromatography were operated using silica gel 60 (70-230 mesh), Merck[®]. Thin layer chromatography (TLC) was performed on silica gel plates (Merck F₂₄₅). Solvents such as methylene chloride and hexane used for extraction and chromatography were commercial grade and distilled before use. Deionized water was used in all experiments unless specified otherwise. All reactions were carried out under positive pressure of N₂ filled in rubber balloon. Cyclodextrins, bovine serum albumin (BSA), surfactants, buffers and salts were purchased from Sigma-Aldrich (Switzerland), the oligonucleotides (ODNs) were purchased from Biodesign (Thailand) and were used without further purification. Potassium poly(vinyl)sulfate (PVSK) was purchased from Wako (Japan).

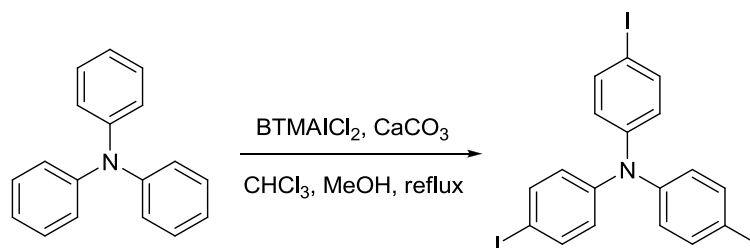
2.2 Analytical instruments

The products were characterized by Micromass Quattro micro TM API electrospray ionization mass spectrometer (Waters, USA). ¹H-NMR and ¹³C-NMR spectra were recorded on Varian Mercury 400 MHz NMR spectrometer (Varian, USA) and 100 MHz on Bruker 400 MHz NMR spectrometer using CDCl₃, MeOH-*d*₄, Acetone-*d*₆, CD₃CN and D₂O. The UV-Visible spectra were obtained from Varian Cary 50 UV-Vis spectrophotometer (Varian, USA) and Cary 100 Bio UV-Visible spectrophotometer (Varian, USA) using MilliQ water, the solution of sodium phosphate buffer (PB 10 mM) and sodium chloride (NaCl 100 mM) as a solvent. Fluorescence emission spectra were acquired by using Perkin Elmer precisely LS 45 Luminescence Spectrometer (PerkinElmer, UK) and a Varian Cary Eclipse spectrofluorometer (Varian, USA) for photophysical property study. Circular

dichroism spectra were recorded on JASCO CD spectrometer (JASCO, Japan). AFM images were taken on a SPA 400 Atomic Forced Microscope (Seiko, Japan).

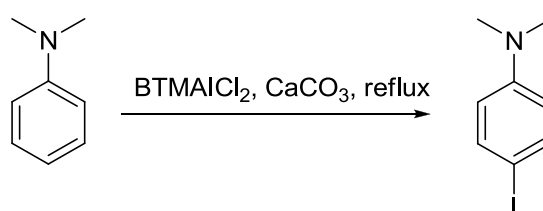
2.3 Synthesis of the zero generation dendrimer (3N⁺)

2.3.1 Preparation of 4, 4', 4''-triiodotriphenylamine, TI₃



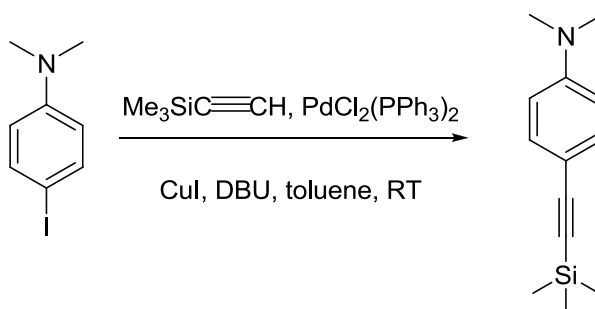
In a 500 mL round-bottomed flask equipped with a magnetic stirring bar, a mixture of triphenylamine (7.37 g, 30 mmol), chloroform (CHCl₃) (100 mL) and methanol (MeOH) (50 mL) was stirred under N₂ atmosphere. Benzyltrimethylammonium chloriodate (BTMAICl₂) (34.50 g, 99 mmol) and calcium carbonate (CaCO₃) (18.44 g, 0.18 mol) were added with vigorously stirrer. The reaction mixture was refluxed for 3 days, 20% NaHSO₃ solution was added to the mixture until the mixture became the light green. The mixture was filtered and the filtrate was separated. The aqueous layer was extracted with methylene chloride (CH₂Cl₂) (2×50 mL). The combined organic layer was washed with water (2×100 mL) and dried over anhydrous magnesium sulfate (MgSO₄) and evaporated by a rotary evaporator. The residue was crystallized from CH₂Cl₂/MeOH yielding the desired product as a white solid (15.2465 g, 81% yield). ¹H NMR (400 MHz, CDCl₃) δ ppm 7.53 (d, *J* = 8.44 Hz, 6 H), 6.81 (d, *J* = 8.49 Hz, 6 H), ¹³C NMR (400 MHz, CDCl₃) δ ppm 146.49, 138.39, 125.98, 86.52.

2.3.2 Preparation of 4-iodo-*N,N'*-dimethylaniline, IAME₂



In a 500 mL round-bottomed flask equipped with a magnetic stirring bar, a mixture of *N, N'*-dimethylaniline (6.64 g, 55 mmol), CaCO₃ (15.2367 g, 0.15 mmol) and CH₂Cl₂ (50 mL) was stirred under N₂ atmosphere. The solution of BTMAICl₂ (18.32 g, 53 mmol), CH₂Cl₂ (80 mL) and MeOH (100 mL) was dropwisely added by addition funnel. After 24 hours, 20% NaHSO₃ solution was added to the mixture until the mixture became the deep purple. The mixture was filtered and the filtrate was separated. The aqueous layer was extracted with methylene chloride (CH₂Cl₂) (2×50 mL). The combined organic layer was washed with water (2×100 mL) and dried over anhydrous magnesium sulfate (MgSO₄) and evaporated by a rotary evaporator. The residue was crystallized from CH₂Cl₂/MeOH yielding the desired product as a white solid (11.95 g, 92% yield). ¹H NMR (400 MHz, CDCl₃) δ ppm 7.46 (d, *J* = 9.00 Hz, 4 H), 6.49 (d, *J* = 8.93 Hz, 4 H), 2.92 (s, 6 H), ¹³C NMR (400 MHz, CDCl₃) δ ppm 149.98, 137.52, 114.69, 77.40, 40.33.

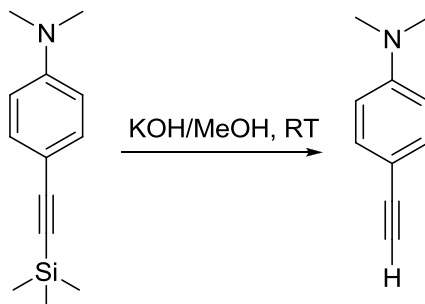
2.3.3 Preparation of 4-trimethylsilylethynyl *N, N'*-dimethylsilane, SiEAMe₂



In a 250 mL round-bottomed flask equipped with a magnetic stirring bar, a mixture of **IAMe₂** (4.9759 g, 20 mmol), bis(triphenylphosphine)palladium (II) chloride (PdCl₂(PPh₃)₂) (0.034 g, 48 μmol), copper(I)iodide (CuI) (0.0257 g, 0.13 mmol), and toluene (30 mL) was stirred under N₂ atmosphere. 1,8-diazacycloundec-7-ene (DBU) (3.6093 g, 24 mmol) and then trimethylsilylacetylene (2.3380 g, 24 mmol) was slowly added to this stirred solution. After 2 hours, the mixture was filtered and washed by toluene. The filtrate was collected and then evaporated by a rotary evaporator. The residue was purified by short column chromatography using hexane as an eluent yielding the desired product as a light yellow solid (3.97 g, 91% yield). ¹H NMR (400 MHz, CDCl₃) δ ppm 7.34 (d, *J* = 8.98 Hz, 2 H), 6.59 (d, *J* =

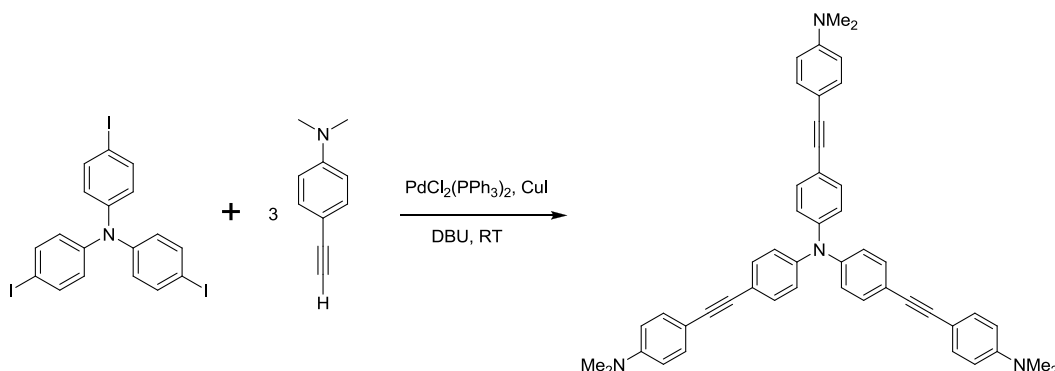
8.91 Hz, 2 H), 2.97 (s, 6 H), 0.24 (s, 9 H), ^{13}C NMR (400 MHz, CDCl_3) δ ppm 150.17, 133.09, 111.57, 109.87, 106.55, 91.14, 40.14, 0.21.

2.3.4 Preparation of 4-ethynyl *N,N'*-dimethylaniline, **EAMe₂**



In a 100 mL round-bottomed flask equipped with a magnetic stirring bar, a mixture of **SiEAMe₂** (2.2394 g, 10 mmol), MeOH (30 mL) and saturated potassium hydroxide (KOH) (0.3 mL) was stirred under N_2 atmosphere. After 6 hours, saturated ammonium chloride (NH_4Cl) (45 mL) and CH_2Cl_2 (30 mL) was added into the mixture. The organic layer was separated and the aqueous layer was extracted with hexane (2×30 mL). The combined organic layer was washed with water (2×100 mL) and dried over anhydrous magnesium sulfate (MgSO_4) and evaporated by a rotary evaporator to obtain a yellow solid (1.46 g, 98% yield). ^1H NMR (400 MHz, CDCl_3) δ ppm 7.38 (d, $J = 8.85$ Hz, 2 H), 6.62 (d, $J = 8.83$ Hz, 2 H), 2.98 (s, 7 H), ^{13}C NMR (400 MHz, CDCl_3) δ ppm 150.32, 133.14, 111.62, 108.66, 84.82, 74.75, 40.12.

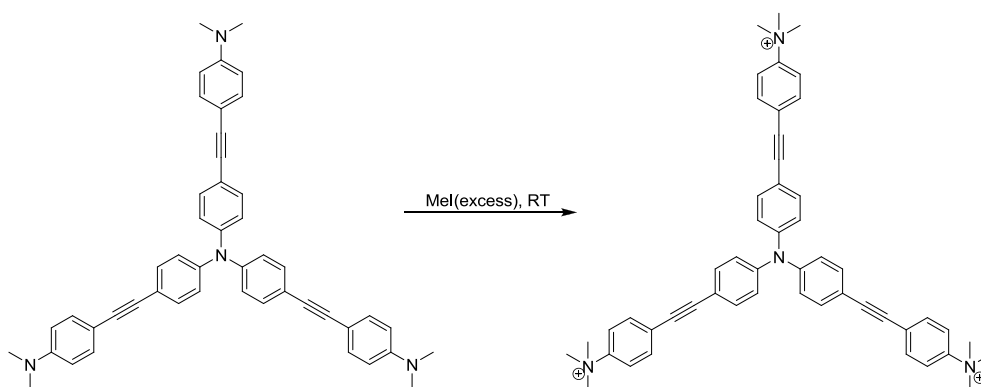
2.3.5 Preparation of 4, 4', 4''-tris-(4-dimethylaminophenylethynyl)triphenyl amine, **3N⁰**



In a 500 mL round-bottomed flask equipped with a magnetic stirring bar, a mixture of **TI₃** (1.0257 g, 1.6 mmol), $\text{PdCl}_2(\text{PPh}_3)_2$ (0.1194 g, 0.17 mmol), CuI

(0.0267 g, 0.14 mmol), and toluene (10 mL) was stirred and bubbled with Ar gas for 15 minutes. **EAMe₂** (0.7979 g, 5.5 mmol) was quickly charged into the stirred solution and then DBU (0.8 mL, 5.3 mmol) was added dropwisely into the mixture. After 6 hours, MeOH (40 mL) was added and was then filtrated to obtained the yellow solid (0.6333 g, 57% yield). ¹H NMR (400 MHz, *CDCl*₃) δ ppm 7.39 (dd, *J* = 2.82, 8.64 Hz, 12 H), 7.04 (d, *J* = 8.49 Hz, 6 H), 6.67 (d, *J* = 8.34 Hz, 6 H), 2.99 (s, 18 H), ¹³C NMR (400 MHz, *CDCl*₃) δ ppm 149.98, 146.18, 132.60, 132.35, 123.92, 118.60, 111.85, 110.26, 90.27, 87.20, 40.23.

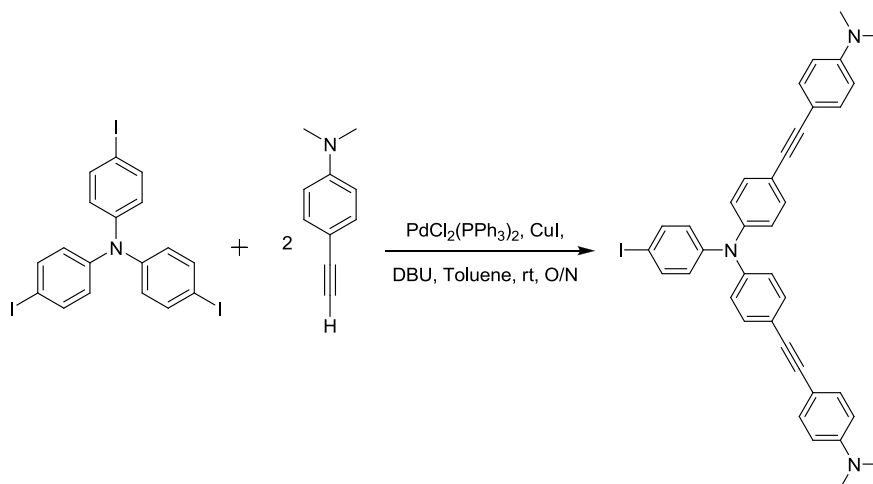
2.3.6 Preparation of 4, 4', 4''-tris-(4-trimethylaminophenylethynyl) triphenylamine triiodide, 3N⁺



A mixture of 4, 4', 4''-tris-(4-dimethylaminophenylethynyl)triphenylamine (0.5051 g, 0.75 mmol), methyl iodide (MeI) (0.50 mL), and acetonitrile (7 mL) was charged into the sealed-tube. After the mixture was stirred at 90°C for overnight, ethylacetate (EtOAc) (10 mL) was added and the precipitation was washed by diethyl ether to obtain a yellow solid (0.7108 g, 86% yield). ¹H NMR (400 MHz, *MeOH-d*₄) δ ppm 7.91 (d, *J* = 9.14 Hz, 6 H), 7.72 (d, *J* = 8.88 Hz, 6 H), 7.48 (d, *J* = 8.40 Hz, 6 H), 7.09 (d, *J* = 8.55 Hz, 6 H), 3.66 (s, 27 H), ¹³C NMR (400 MHz, *MeOH-d*₄) δ ppm 148.65, 147.66, 134.31, 134.25, 127.31, 125.44, 121.74, 118.62, 93.00, 87.94, 57.86. ESI MS/MS *m/z* Calcd for C₅₁H₅₁N₄³⁺, 239.80 Found: 240.

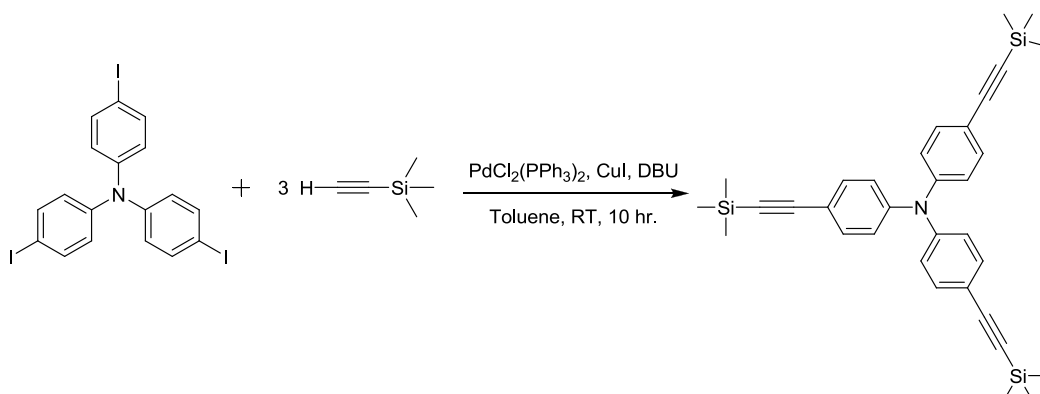
2.4 Synthesis of the first generation dendrimer (6N⁺)

2.4.1 Preparation of 4-iodo-4',4''-bis(4-dimethylaminophenylethynyl) triphenylamine, TI(EAME₂)₂



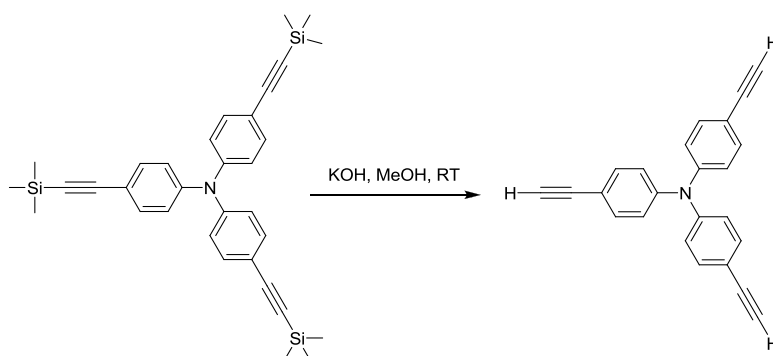
In a 250 mL 2-necked round-bottomed flask equipped with a magnetic stirring bar, a mixture of **TI**₃ (2.0248 g, 3.3 mmol), PdCl₂(PPh₃)₂ (0.1492 g, 0.21 mmol), CuI (0.0567 g, 0.30 mmol), and toluene (80 mL) was stirred and bubbled with Ar gas for 15 minutes. The solution of **EAMe**₂ (1.0988 g, 8 mmol) and toluene (50 mL) was slowly added by addition funnel while DBU (1.10 mL, 7.4 mmol) was drop wisely added into the mixture. After stirred overnight, the mixture was filtered and washed by toluene. The filtrate was collected and then evaporated by a rotary evaporator. The residue was purified by column chromatography using hexane: EtOAc (6: 1) as an eluent yielding the desired product as a yellow solid (0.5952 g, 28% yield). ¹H NMR (400 MHz, CDCl₃) δ ppm 7.54 (d, *J* = 8.23 Hz, 2 H), 7.39 (t, *J* = 7.24, 7.24 Hz, 8 H), 7.01 (d, *J* = 8.40 Hz, 4 H), 6.86 (d, *J* = 8.74 Hz, 2 H), 6.66 (d, *J* = 8.23 Hz, 4 H), 2.99 (s, 12 H), ¹³C NMR (400 MHz, CDCl₃) δ ppm 149.96, 146.00, 138.28, 133.60, 132.58, 132.37, 126.26, 123.78, 118.72, 111.81, 110.11, 90.35, 87.08, 86.21, 40.22.

2.4.2 Preparation of tris(4-((trimethylsilyl)ethynyl)phenyl)amine, T(SiET)₃



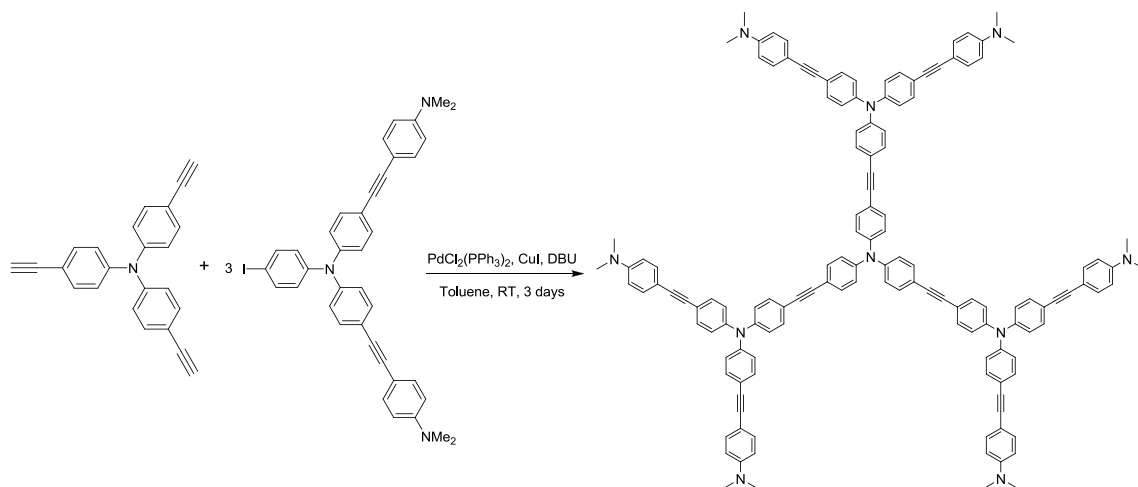
In a 100 mL round-bottomed flask equipped with a magnetic stirring bar, a mixture of **TI**₃ (0.1967 g, 0.32 mmol), PdCl₂(PPh₃)₂ (0.0241 g, 34 μmol), CuI (0.0066 g, 35 μmol), and toluene (20 mL) was stirred under Ar atmosphere and then bubbled Ar gas into the solution for 15 minutes. Trimethylsilylacetylene (0.20 mL, 1.4 mmol) and DBU (0.20 mL, 1.3 mmol) were slowly added to this stirred solution. After 10 hours, saturated NH₄Cl (30 mL) and hexane (30 mL) was added into the mixture. The organic layer was separated and the aqueous layer was extracted with CH₂Cl₂ (2×50 mL). The combined organic layer was washed with water (2×50 mL) and dried over anhydrous sodium sulfate (Na₂SO₄) and evaporated by a rotary evaporator. The residue was purified by short column chromatography using hexane as an eluent yielding the desired product as a light yellow solid (0.1431 g, 85% yield). ¹H NMR (400 MHz, CDCl₃) δ ppm 7.34 (d, *J* = 8.74 Hz, 6 H), 6.95 (d, *J* = 8.73 Hz, 6 H), 0.24 (s, 27 H), ¹³C NMR (400 MHz, CDCl₃) δ ppm 146.74, 133.14, 123.78, 117.73, 104.81, 93.93, 0.00.

2.4.3 Preparation of tris(4-ethynylphenyl)amine, T(ET)₃



In a 100 mL round-bottomed flask equipped with a magnetic stirring bar, a mixture of **T(SiET)**₃ (0.1431 g, 0.27 mmol), MeOH (10 mL) and saturated KOH (0.02 mL) was stirred under N₂ atmosphere. After stirred overnight, saturated NH₄Cl (10 mL) and hexane (10 mL) was added into the mixture. The organic layer was separated and the aqueous layer was extracted with CH₂Cl₂ (2×20 mL). The combined organic layer was washed with water (2×50 mL) and dried over anhydrous Na₂SO₄ and evaporated by rotary. The residue was purified by short column chromatography using hexane as an eluent yielding the desired product as a yellow solid (0.0783 g, 92% yield). ¹H NMR (400 MHz, CDCl₃) δ ppm 7.38 (d, *J* = 8.43 Hz, 2 H), 7.01 (d, *J* = 8.40 Hz, 2 H), 3.06 (s, 1 H), ¹³C NMR (400 MHz, CDCl₃) δ ppm 146.99, 133.34, 123.90, 116.80, 83.37, 76.97.

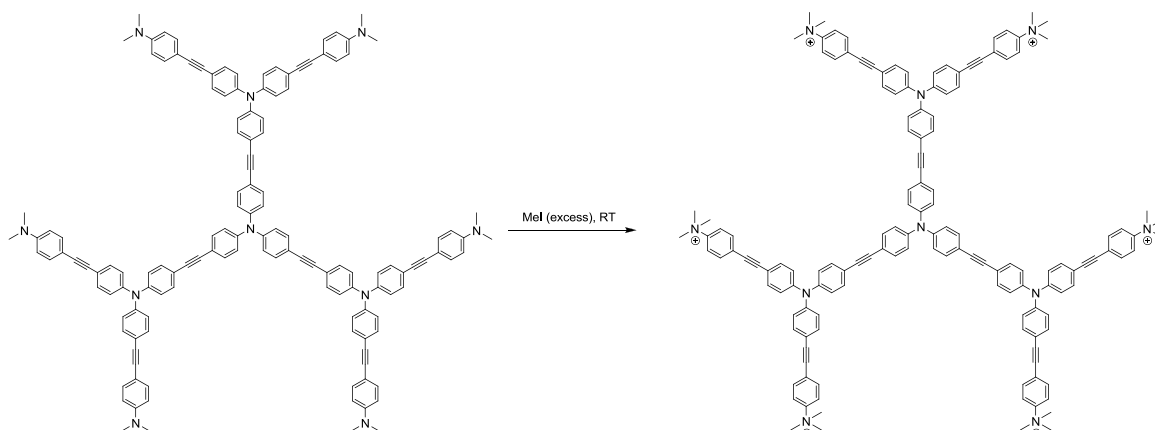
2.4.4 Preparation of 4, 4', 4''-tri-((bis-(4, 4''-dimethylaminophenylethynyl)phenylamino)phenylethynyl)phenylamine, **T(ET(EAMe₂))₃**



In a 100 mL 2-necked round-bottomed flask equipped with a magnetic stirring bar, a mixture of **TI(EAMe₂)₂** (0.1789 g, 27 mmol), PdCl₂(PPh₃)₂ (0.0091 g, 13 μmol), CuI (0.0026 g, 14 mmol), and toluene (20 mL) was stirred under N₂ atmosphere and then bubbled N₂ gas into the solution for 15 minutes. The solution of **T(ET)**₃ (0.0262 g, 83 μmol) and toluene (20 mL) was slowly added by addition funnel while and DBU (0.04 mL, 27 mmol) were slowly added to this stirred solution. After 3 days, the mixture was filtered and washed by toluene. The filtrate was collected and then concentrated by rotary evaporator. The concentrated residue was

added drop wisely into MeOH and then the precipitated was filtered. The precipitation was purified by column chromatography using 100%hexane to 100%CH₂Cl₂ as gradient eluent. The obtained solid was recrystallized from CH₂Cl₂/MeOH yielding the desired product as a yellow solid (0.1209 g, 77% yield). ¹H NMR (400 MHz, CDCl₃) δ ppm 7.40 (d, *J* = 8.59 Hz, 36 H), 7.05 (d, *J* = 8.31 Hz, 24 H), 6.66 (dd, *J* = 0.64, 8.47 Hz, 12 H), 2.99 (s, 36 H), ¹³C NMR (400 MHz, CDCl₃) δ ppm 150.08, 146.11, 132.68, 132.64, 132.43, 130.44, 130.15, 127.60, 124.16, 124.10, 124.04, 123.63, 118.97, 111.91, 110.32, 100.01, 90.43, 87.18, 77.20, 40.23.

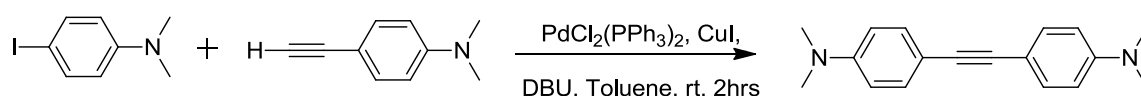
2.4.5 Preparation of 4, 4', 4''-tri-((bis-(4, 4''-trimethylaminophenylethynyl) phenyl amino)phenylethynyl)phenylamine, 6N⁺



A mixture of **T(ET(EAMe₂)₂)₃** (0.0552 g, 29 μmol) and methyl iodide (1 mL) was charged into the sealed-tube. After the mixture was stirred at room temperature for 30 minute, diethyl ether was added and the mixture was filtered to obtain the yellow solid (0.0487 g, 61% yield). ¹H NMR (400 MHz, MeOH-*d*₄) δ ppm 7.91 (d, *J* = 8.2 Hz, 2H), 7.73 (d, *J* = 8.4 Hz, 2H), 7.56 – 7.36 (m, 4H), 7.09 (d, *J* = 7.0 Hz, 2H), 3.66 (s, 12H). ESI MS/MS *m/z* Calcd for C₁₄₄H₁₂₆N₆⁶⁺, 332.50 Found: 332.

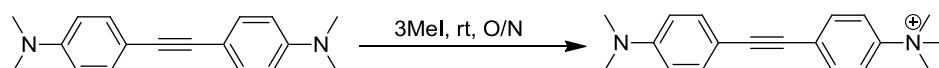
2.5 Synthesis of multi-branches cationic phenylene-ethynylene fluorophores

2.5.1 Preparation of 2N⁰



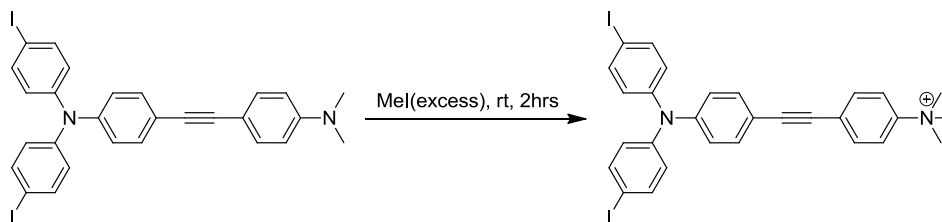
In a 100 mL round-bottomed flask equipped with a magnetic stirring bar, a mixture of **IAMe₂** (4.9927 g, 20 mmol), PdCl₂(PPh₃)₂ (0.4865 g, 0.69 mmol), CuI (0.1021 g, 0.54 mmol), and toluene (50 mL) was stirred and bubbled with Ar gas for 15 minutes. **EAMe₂** (2.1793 g, 15 mmol) and DBU (3 mL, 20 mmol) were slowly added to this stirred solution. After 2 hours, the mixture was concentrated by rotary evaporator. The residue was purified by column chromatography using 50%hexane/CH₂Cl₂ as an eluent yielding the desired product as a green-brown solid (2.810 g, 71% yield). ¹H NMR (400 MHz, CDCl₃) δ ppm 7.38 (d, *J* = 8.7 Hz, 2H), 6.66 (d, *J* = 8.5 Hz, 2H), 2.98 (s, 6H). ¹³C NMR (101 MHz, CDCl₃) δ ppm 149.86, 132.53, 112.12, 111.37, 88.24, 77.48, 76.84, 40.43.

2.5.2 Preparation of N⁰N⁺



A mixture of **2N⁰** (0.3000 g, 1.14 mmol) and methyl iodide (MeI) (0.2 mL) was charged into a sealed-tube. After the mixture was stirred at room temperature for overnight, diethyl ether was added and the mixture was filtered to obtain the light brown solid (0.0650 g, 14% yield). ¹H NMR (400 MHz, DMSO) δ 7.97 (d, *J* = 8.6 Hz, 2H), 7.72 (d, *J* = 8.7 Hz, 2H), 7.39 (d, *J* = 8.5 Hz, 2H), 6.73 (d, *J* = 8.6 Hz, 2H), 3.60 (s, 9H), 2.97 (s, 6H). ¹³C NMR (101 MHz, DMSO) δ 150.47, 146.02, 132.76, 132.07, 125.26, 121.07, 111.87, 107.43, 93.50, 85.70, 56.37, 30.77. ESI MS/MS *m/z* Calcd for C₁₉H₂₃N₂⁺, 279.19 Found: 278.670.

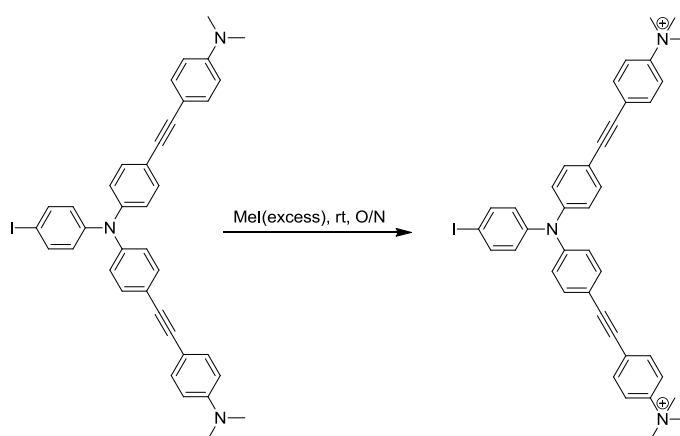
2.5.3 Preparation of N⁺



A mixture of **TI₂(EAMe₂)** (a mono-substituted byproduct of **3N⁰** reaction) (0.1039 g, 0.16 mmol), methyl iodide (MeI) (2 mL), and acetonitrile (1 mL) was charged into a sealed-tube. After the mixture was stirred at room temperature for 2

hours, diethyl ether was added and the mixture was filtered to obtain the light pink solid (0.0242 g, 19% yield). ^1H NMR (400 MHz, CD_3CN) δ 7.80 – 7.68 (m, 4H), 7.64 (d, J = 8.7 Hz, 4H), 7.44 (d, J = 8.6 Hz, 2H), 7.03 (d, J = 8.5 Hz, 2H), 6.88 (d, J = 8.6 Hz, 4H), 3.53 (s, 9H). ^{13}C NMR (101 MHz, CD_3OD) δ 160.67, 147.89, 139.89, 134.28, 134.11, 127.89, 124.04, 121.59, 111.17, 93.20, 87.96, 57.64. ESI MS/MS m/z Calcd for $\text{C}_{29}\text{H}_{25}\text{I}_2\text{N}_2^+$, 655.01 Found: 654.760.

2.5.4 Preparation of 2N^+



A mixture of $\text{TI}(\text{EAMe}_2)_2$ (0.2059 g, 0.31 mmol), methyl iodide (MeI) (2 mL), and acetonitrile (1 mL) was charged into a sealed-tube. After the mixture was stirred at room temperature for overnight, diethyl ether was added and the mixture was filtered to obtain the green-yellow solid (0.2576 g, 87% yield). ^1H NMR (400 MHz, CD_3CN) δ 7.75 (d, J = 9.1 Hz, 4H), 7.69 (d, J = 9.1 Hz, 4H), 7.63 (d, J = 8.6 Hz, 2H), 7.44 (d, J = 8.5 Hz, 4H), 7.04 (d, J = 8.5 Hz, 4H), 6.88 (d, J = 8.6 Hz, 2H), 3.51 (s, 18H). ^{13}C NMR (101 MHz, DMSO) δ 146.86, 146.65, 145.68, 138.67, 133.15, 132.56, 127.51, 124.36, 123.41, 121.23, 115.90, 91.50, 89.11, 87.28, 56.38. ESI MS/MS m/z Calcd for $\text{C}_{40}\text{H}_{38}\text{IN}_3^{2+}$, 343.605 Found: 343.301.

2.6 Photophysical properties study

2.6.1 UV-visible spectroscopy

The stock solutions of N^0N^+ , N^+ , 2N^+ and 3N^+ (1 mM) and 6N^+ (~ 100 μM) in MilliQ water were prepared and then were diluted to 5.0 μM with pH 7 sodium phosphate buffer ($\text{Na}_2\text{HPO}_4:\text{NaH}_2\text{PO}_4$ (1:1) 10 mM) and NaCl (100 mM). The

absorption spectra of $\mathbf{N^0N^+}$, $\mathbf{N^+}$, $\mathbf{2N^+}$, $\mathbf{3N^+}$ and $\mathbf{6N^+}$ were recorded from 200 nm to 500 nm at ambient temperature.

2.6.2 Fluorescence spectroscopy

The stock solutions of $\mathbf{N^0N^+}$, $\mathbf{N^+}$, $\mathbf{2N^+}$, $\mathbf{3N^+}$ and $\mathbf{6N^+}$ were diluted to 5.0 μM with pH 7 sodium phosphate buffer (10 mM) and NaCl (100 mM). The emission spectra of $\mathbf{N^0N^+}$ were recorded from 350 nm to 700 nm at ambient temperature using an excitation wavelength at 328 nm. The emission spectra of $\mathbf{N^+}$, $\mathbf{2N^+}$, $\mathbf{3N^+}$ and $\mathbf{6N^+}$ were recorded from 390 nm to 700 nm at ambient temperature using an excitation wavelength at 368, 368, 370 and 376 nm, respectively.

2.6.3 Fluorescence quantum yields

The fluorescence quantum yield measurement of $\mathbf{N^0N^+}$, $\mathbf{N^+}$, $\mathbf{2N^+}$, $\mathbf{3N^+}$ and $\mathbf{6N^+}$ was performed in MilliQ by using quinine sulfate in 0.1 M H_2SO_4 ($\Phi = 0.54$) as a reference. The UV-Visible absorption spectra of five analytical samples and five reference samples at varied concentrations were recorded. The maximum absorbance of all samples should never exceed 0.1. The fluorescence emission spectra of the same solutions using appropriate excitation wavelengths selected were recorded based on the absorption maximum wavelength (λ_{max}) of each compound. Graphs of integrated fluorescence intensities were plotted against the absorbance at the respective excitation wavelengths. Each plot should be a straight line with 0 interception and gradient m .

In addition, the fluorescence quantum yield (Φ_{F}) was obtained from plotting of integrated fluorescence intensity vs absorbance represented into the following equation:

$$\Phi_{\text{X}} = \Phi_{\text{ST}} \left(\frac{\text{Grad}_{\text{X}}}{\text{Grad}_{\text{ST}}} \right) \left(\frac{\eta_{\text{X}}^2}{\eta_{\text{ST}}^2} \right)$$

The subscripts Φ_{ST} denote the fluorescence quantum yield of a standard reference which used quinine sulfate in 0.1 M H_2SO_4 ($\Phi = 0.54$) and Φ_{X} is the fluorescence quantum yield of sample and η is the refractive index of the solvent.

2.6.4 Fluorescence spectra with various conditions

For the effect of pH study, the stock solutions of 3N^+ and 6N^+ were diluted to $5.0\ \mu\text{M}$ with varied pH ranging from 5 to 11 of sodium phosphate buffer (10 mM) containing sodium chloride (150 mM).

For the effect of buffer media study, sodium phosphate, (3-(*N*-morpholino)propane sulfonic acid (**MOPS**), tris- (hydroxymethyl)aminomethane (**Tris**) and piperazine-*N,N'*-bis(2-ethanesulfonic acid (**PIPES**) buffer pH 7 were prepared at 10 mM. The stock solutions of 3N^+ were diluted to $5.0\ \mu\text{M}$ with 10 mM buffers.

For the effect of salts concentration study, all salt stock solutions of sodium chloride, sodium bromide, sodium iodide and silver nitrate were prepared at 1 M in MilliQ water. The stock solutions of 3N^+ were diluted to $5.0\ \mu\text{M}$ and salts stock solutions were varied from 0 to 500 mM with the addition of the desired volumes into the fluorophore solutions.

The emission spectrum of 3N^+ was recorded from 390 nm to 700 nm and of 6N^+ was recorded from 390 nm to 600 nm at ambient temperature using an excitation wavelength at 370 nm and 376 nm, respectively. The stock solutions of the fluorophore in each condition were prepared to the designated concentrations and allowed to stand at room temperature ($\sim 30\ ^\circ\text{C}$) overnight, unless specified otherwise, before the measurement. The final volumes of the mixtures were adjusted to 2 mL.

2.6.5 The computational chemistry for structure simulation

The structure of 3N^+ was drawn and simulated in the AM1 and GS., DFT, B3LYP; 6-31G mode by using the GuassView program. MM2 calculation was applied by ChemBio3D Ultra 12.0 program.

2.7 Study of supramolecular interaction of fluorophores study

2.7.1 General procedure for photophysical responses study

The absorption spectra of 3N^+ and 6N^+ with the presence of analytes (cyclodextrins, DNA and bovine serum albumin) were recorded from 200 nm to 450 nm at $25\ ^\circ\text{C}$. The emission spectrum of 3N^+ was recorded from 390 nm to 700 nm and of 6N^+ was recorded from 390 nm to 600 nm at ambient temperature using an

excitation wavelength at 370 nm and 376 nm, respectively. The stock solutions of the fluorophore and analyte were mixed and diluted to the designated concentrations with pH 7 sodium phosphate buffer (10 mM) containing NaCl (100 mM) and allow to stand for at room temperature (~30 °C) overnight, unless specified otherwise, before the measurement. The final volumes of the mixtures were adjusted to 2 mL.

For the CD measurement, the solution of diluted polycationic fluorophores ($[N^0N^+, N^+, 2N^+$ and $3N^+] = 10 \mu\text{M}$) from the stock solutions (1 mM) in sodium phosphate buffer (10 mM) and sodium chloride (100 mM) were prepared. The CD spectra were recorded from 200 nm to 500 nm at 20 °C. The stock solutions of analytes were prepared in pH 7 sodium phosphate buffer (10 mM) containing NaCl (100 mM) at 1 mM. Concentrations of all analytes (cyclodextrins, DNA and BSA protein) were adjusted to 10 μM with the addition of the desired volumes into the fluorophore solutions. The final volumes of the mixtures were adjusted to 1.5 mL. The stock solutions of the fluorophore and analytes were mixed and diluted to the designated concentrations with pH 7 sodium phosphate buffer (10 mM) containing NaCl (100 mM) and allow standing for 2 minutes at 20 °C before the measurement.

2.7.2 Interactions with cyclodextrins

The solution of diluted polycationic fluorophores (5 μM of N^0N^+ , N^+ , $2N^+$, $3N^+$ and $6N^+$) from the stock solution in pH 7 sodium phosphate buffer (10 mM) and sodium chloride (100 mM) were prepared. The photophysical properties were studied for α -, β -, and γ -cyclodextrins. The stock solutions of cyclodextrins were prepared in pH 7 sodium phosphate buffer (10 mM) at 1 mM. Concentrations of all stock cyclodextrins were adjusted to 20 μM or were varied from 0 to 1 mM with the addition of the desired volumes into the fluorophore solutions.

Job's plot for an inclusion complex with β -CyD and γ -CyD was obtained from plotting fluorescence intensity against a mole fraction of two components ($[\text{CyD}]/\{[3N^+]+[\text{CyD}]\}$). The total molar concentration of each mixture was fixed at 5 μM and molar ratio of $[3N^+]: [\text{CyD}]$ components were varied from 10: 0 to 0: 10 ratios. The emission spectrum of $3N^+$ was recorded using an excitation wavelength at 368 nm.

With the screening of selectively fluorogenic responses, the different fluorescence enhancements ($F/F_0 - 1$) toward each CyD presences were plotted where F and F_0 are the maximum fluorescence intensity of the fluorophores with the presence of and with the absence of CyDs, respectively.

For the ^1H NMR study, the mixture of fluorophores and CyDs were prepared in D_2O at room temperature. The final concentrations are $[\text{N}^0\text{N}^+] = 2.1 \text{ mM}$, $[\text{N}^+] = 2.0 \text{ mM}$, $[\text{2N}^+] = 2.1 \text{ mM}$, $[\text{3N}^+] = 1.5 \text{ mM}$, $[\text{CyDs}] = 6 \text{ mM}$ or 8 mM (fluorophore: CyD = 1:1) ^1H NMR spectra were recorded on 400 MHz NMR spectrometer at ambient temperature ($\sim 20 \text{ }^\circ\text{C}$).

2.7.3 Interactions with DNA

The solution of diluted polycationic fluorophores ($1 \text{ } \mu\text{M}$ for 3N^+ , and 1 or $5 \text{ } \mu\text{M}$ for 6N^+) from the stock solutions in sodium phosphate buffer (10 mM) and sodium chloride (100 mM) were prepared. All DNA stock solutions were prepared in MilliQ water at $100 \text{ } \mu\text{M}$. The concentrations of the DNA stock solutions were determined based on the absorbance at 260 nm using molar absorptivity provided by the vendor. For dsDNA, stock solutions of complimentary DNAs were mixed and allowed to stand for at least 30 minutes before stock solution of the fluorophore was added. Concentrations of all stock DNA were adjusted to $2.5 \text{ } \mu\text{M}$ or were varied from 0 to $2 \text{ } \mu\text{M}$ with the addition of the desired volumes into the fluorophore solutions.

For the effect of DNA chain length study, ssDNA chain length with random sequences were varied from 0 to 0 bases at the same charge concentration controlling by fixed A_{260} of the mixture at the same absorbance ($A_{260} = 0.05$). Sodium triphosphate pentabasic ($\text{Na}_5\text{O}_{10}\text{P}_5$) and potassium poly(vinyl)sulphate (PVSK) stock solutions were prepared in MilliQ water at 300 mM and 2.4 mM respectively. Concentrations of all stock $\text{Na}_5\text{O}_{10}\text{P}_5$ and PVSK were adjusted to vary from 0 to 300 mM and 0 to 2.4 mM , respectively, with the addition of the desired volumes into the fluorophore solutions. The stock solutions of 3N^+ and analytes were mixed and diluted to the designated concentrations with pH 7 sodium phosphate buffer (10 mM) containing NaCl (100 mM , for DNA mixtures) or with MilliQ water (for $\text{Na}_5\text{O}_{10}\text{P}_5$ and PVSK mixtures) and allow to stand at room temperature ($\sim 30 \text{ }^\circ\text{C}$) for 2 minutes before the measurement.

Table 2.1 List of all ssDNA sequences

Name	Length (bases)	Molecular Weight	GC content (%)	Base Sequences (5'→3')	Calculated T _M (°C)
B1	6	1791.3	33	5'GACATT3'	16
B1A	6	1791.3	33	5'AATGTC3'	16
B2	6	1775.3	17	5'AATATC3'	14
C1	8	2385.6	63	5'TATGCCCG3'	26
C1A	8	2434.6	63	5'CGGGCATA3'	26
P1	11	3316.2	45	5'GCATATGCCTA3'	32
P1A	11	3356.3	45	5'TAGGCATATGC3'	32
P2	11	3340.3	36	5'GCATATGCATA3'	30
P4	11	3357.2	64	5'GCGTATGCAGC3'	36
P4A	11	3317.2	64	5'GCTGCATACGC3'	36
A1	15	4544.1	27	5'AATTACGACATCATA3'	31
A'1	15	4597.1	27	5'TATGATGTCGTAATT3'	31
A2	15	4581.1	20	5'TATGAT GTCATAATT3'	28.3
P3	23	7034.6	65	5'CGTCGCCGGAGAAGGC ATCACCT3'	62.4
P3A	23	7089.7	61	5'AGGTGATGCCATATCCG GCGACG3'	60.6
P3B	23	7056.6	65	5'AGGTGATGCCTTCTCCG GCGACG3'	62.4
P5	23	7131.7	57	5'GATAGCCGGAGAAAGCA TGCAGC3'	58.8
D1	30	9241.1	57	5'CGTCGCCGGAGAAGGC ATCACCTATATAGG3'	65.7
D1A	30	9174.0	57	5'CCTATATAGGTGATGCCT TCTCCGGCGACG3'	65.7

2.7.4 Interaction with BSA proteins

The solution of diluted polycationic fluorophores (1 or 5 μM for 3N^+ , and 1 μM for 6N^+) from the stock solutions in sodium phosphate buffer (10 mM) and sodium chloride (100 mM) were prepared. The stock solutions of BSA were prepared in pH 7 sodium phosphate buffer (10 mM) at 2 mM. Concentrations of all stock BSA were adjusted to 5 μM or were varied from 0 to 100 μM with the addition of the desired volumes into the fluorophore solutions. The stock solutions of the fluorophore and analyte were mixed and diluted to the designated concentrations with pH 7 sodium phosphate buffer (10 mM) containing NaCl (100 mM) and allow to stand for at 20 °C overnight (for absorption change and fluorogenic responses) or allow to stand for at room temperature (~ 30 °C) 2 minutes (for fluorogenic response 3N^+ with various concentrations of BSA) before the measurement.

2.7.5 Interaction with surfactants and CMC determination

The solution of diluted polycationic fluorophores (1 μM for 3N^+ and 0.1, 0.5 or 1 μM for 6N^+) from the stock solution in MilliQ water was prepared. The photophysical properties were studied for 9 surfactants such as anionic, cationic and non-ionic surfactants. The stock surfactants were prepared in MilliQ water at 100 mM. The final concentrations of all surfactants were varied from 0 to 100 mM by added the stock solutions with the desired volume of surfactants as well as the fluorophores solution was diluted to the final concentration. The stock solutions of the fluorophore and analyte were mixed and diluted to the designated concentrations with MilliQ water and allow to stand for at room temperature (~ 30 °C) 2 minutes before the measurement.

The CMC value of each surfactants were obtained from the inflection points of the fitted sigmoidal curve in the graph that plot an emission intensity at maximum wavelength of the fluorophores probe against log of surfactant concentration as followed Boltzman equation:

$$y = (A_1 - A_2) / \{ [1 + \exp[-(x - x_0) / x]] \} + A_2$$

Where y corresponds to the maximum emission intensity. The variable x is the log of total surfactant concentration, x_0 is the center of the sigmoid, x is the slope

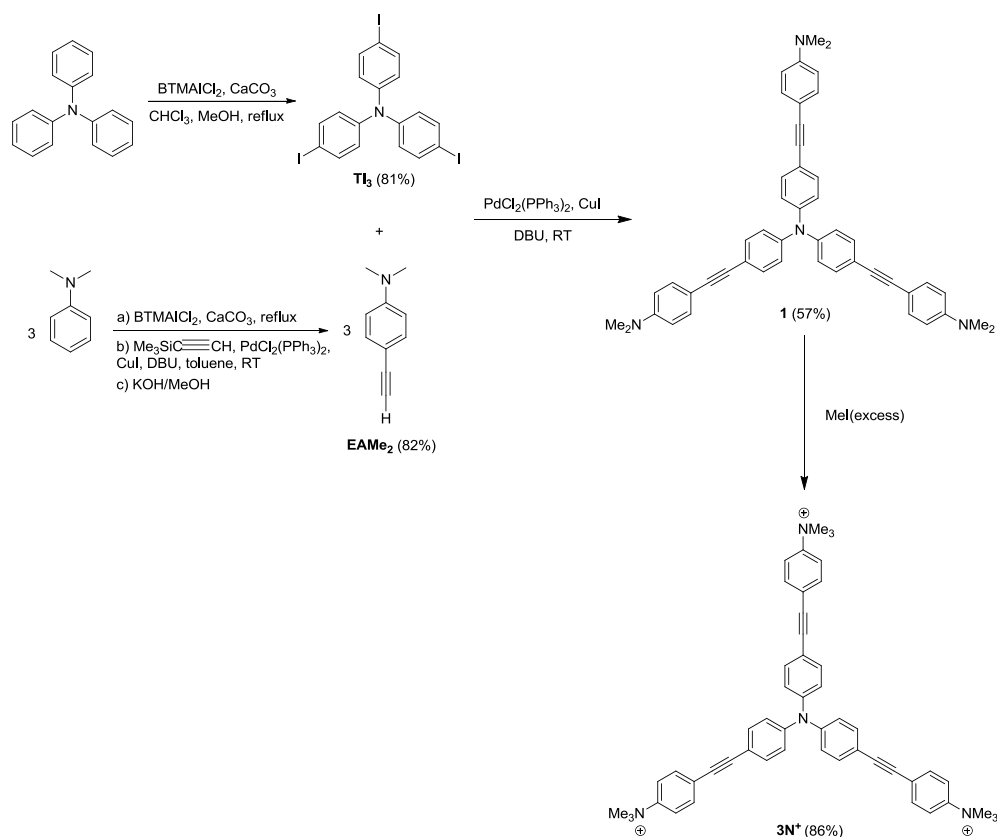
factor, and A_1 and A_2 are the upper limit of the fluorescence intensity and the background fluorescence at zero surfactant concentration. Then CMC were derived from that break point as equal to $x_0 - 2\Delta x$.

CHAPTER III

RESULTS AND DISCUSSION

3.1 Synthesis and characterization of the tricationic fluorophore ($3N^+$)

4, 4', 4''-triiodotriphenylamine core (TI_3) was prepared by triple iodination of benzyltrimethyl-ammonium iododichloride ($BTMAICl_2$) in basic condition (Scheme 3.1). The periphery amine, 4-ethynyl *N,N'*-dimethylaniline ($EAMe_2$) was synthesized by triple iodination of *N,N'*-dimethylaniline then Sonogashira cross-coupling with trimethylsilylacetylene. After that desilylation was affected using potassium hydroxide in methanol. The triple branched amine compound or 4,4',4''-tris-(4-dimethylaminophenylethynyl)triphenylamine (**1**) was obtained by the Pd-catalyzed Sonogashira cross-coupling of the reactive core TI_3 with the periphery amine $EAMe_2$ at room temperature. After methylation of compound **1** by using an excess of methyl iodide (MeI), the tricationic fluorophore ($3N^+$) was obtained.



Scheme 3.1 synthesis of the tricationic fluorophore ($3N^+$)

$^1\text{H-NMR}$ spectra of **TI**₃, **EAMe**₂, compound **1** and **3N**⁺ are shown in Figure 3.1. All signals can be assigned to all protons in each corresponding structure. Initially, 4,4',4''-triiodotriphenylamine core showed two doublet signals at 6.8 and 7.5 ppm corresponding to its aromatic protons. 4-ethynyl *N,N'*-dimethylaniline also revealed two doublet signals at 6.6 and 7.3 ppm corresponding to its aromatic protons, and one singlet signal at 3.0 ppm corresponding to its methyl- and ethynyl-protons. Then **TI**₃ coupled with **EAMe**₂ by using Sonogashira reaction, triple branches amine **1** showed a signal of methyl amine protons as a singlet at 3.0 ppm and two doublet signals at 6.7, 7.0 ppm and one doublet of doublet signal at 7.4 ppm corresponding to the aromatic protons moiety. The methylation product (**3N**⁺) which is insoluble in chloroform appeared four separated doublet signals at 7.1, 7.4, 7.7 and 7.9 ppm corresponding to its aromatic protons and one singlet signal of the methyl ammonium protons at 3.7 ppm in MeOH-*d*₄.

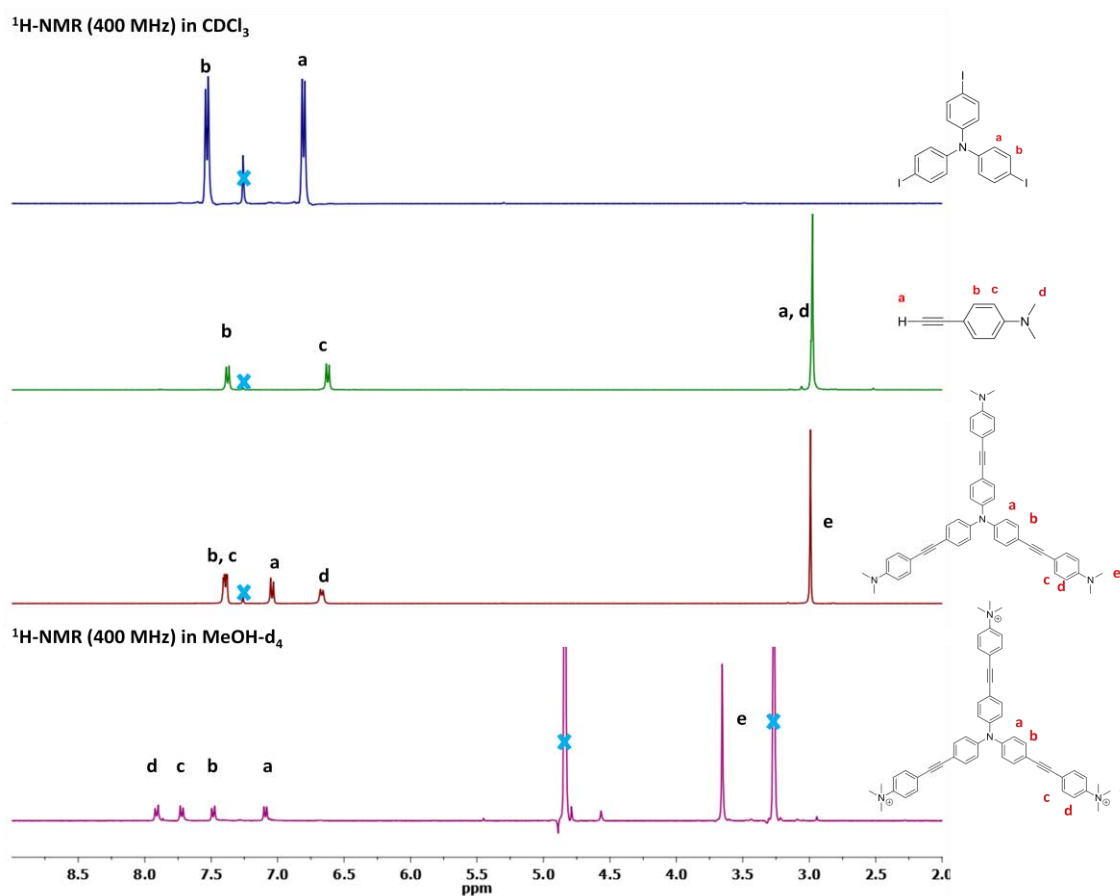


Figure 3.1 $^1\text{H-NMR}$ spectra of **TI**₃, **EAMe**₂, compound **1** and **3N**⁺

The structure characterizations of the tricationic fluorophore were confirmed by ESI-MS/MS spectra that showed the molecular ion peaks corresponding to its molecular weights (Figure 3.2). Quasi molecular peak was showed at 240 m/z that matched with 3N^+ molecular ion ($[\text{M}]^{3+}$).

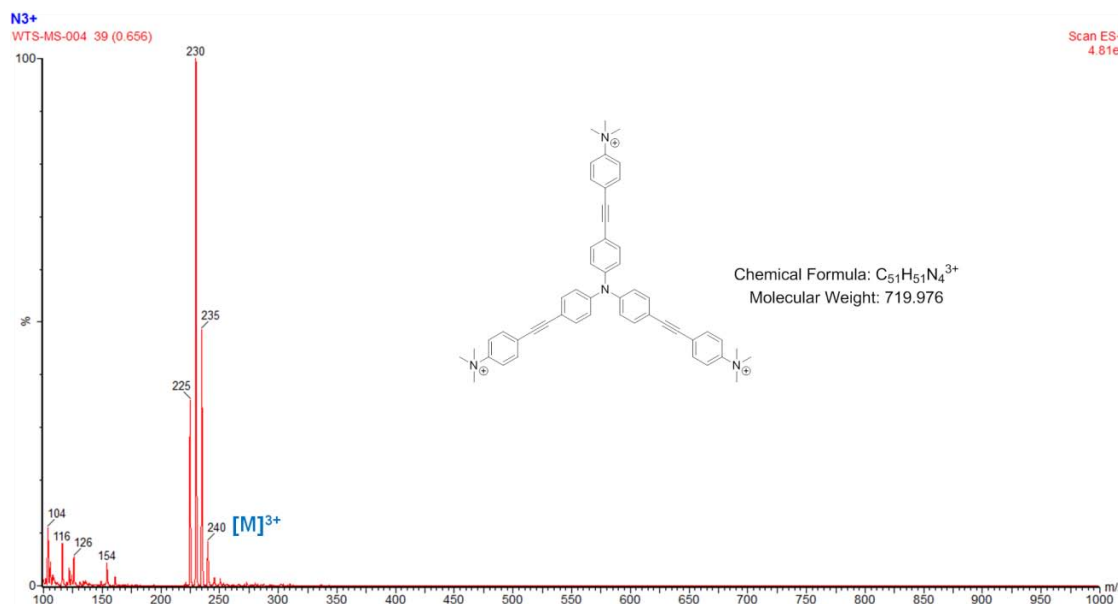
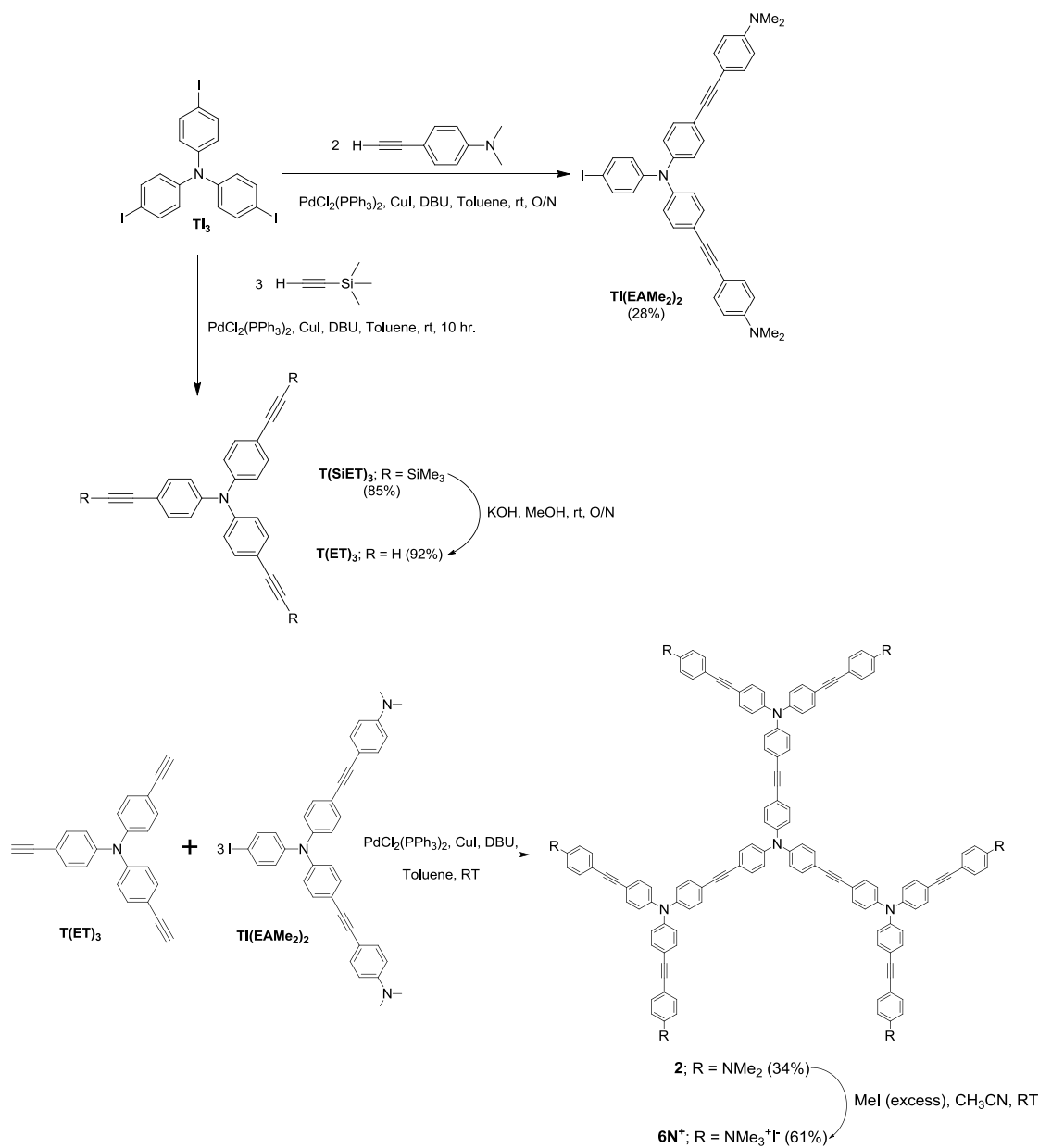


Figure 3.2 ESI MS data of 3N^+

3.2 Synthesis and characterization of the dendritic hexacationic fluorophore (6N^+)

TI_3 was coupled with 4-ethynyl *N,N'*-dimethylaniline to get a iodo-dendron ($\text{TI}(\text{EAMe}_2)_2$) and was also coupled with trimethylsilylacetylene followed by base-catalyzed desilylation to provide core ($\text{T}(\text{ET})_3$) in a good yield (Scheme 3.2). Next, polyamine compound **2** was synthesized by Sonogashira cross-coupling of triethynyltriphenylamine core $\text{T}(\text{ET})_3$ with the iodo-dendron, and the dendritic hexacationic fluorophore (6N^+) was obtained by methylation of **2** with an excess amount of MeI.



Scheme 3.2 Synthesis of the dendritic hexacationic fluorophore (**6N⁺**)

¹H-NMR spectra of **T(ET)₃**, **TI(EAMe₂)₂**, compound **2** and **6N⁺** are shown in Figure 3.3. All signals can be assigned to all protons in each corresponding structure. Tris(4-ethynylphenyl)amine core showed two doublet signals at 7.0 and 7.3 ppm corresponding to its aromatic protons and one singlet signal at 3.0 ppm corresponding to a terminal alkyne proton.

While iodo-dendron **TI(EAMe₂)₂** appeared three doublet signals at 6.8, 7.0 and 7.5 ppm, one triplet signals at 7.4 ppm and a broad peak at 6.7 ppm corresponding to its aromatic protons of the mounted *p*-disubstituted ethynyl *N,N'*-dimethylaniline moiety onto iodo-triphenylamine core, and one singlet signal at 3.0 ppm corresponding to its methyl amine protons. Then **T(ET)₃** coupled with **TI(EAMe₂)₂** by using Sonogashira cross-coupling, polyamine compound **2** showed a signal of methyl amine protons as a singlet at 3.0 ppm and two doublet signals at 7.0, 7.4 ppm and one doublet of doublet signal at 6.6 ppm corresponding to its aromatic protons. The final product of methylation or **6N⁺** which is insoluble in chloroform presented four separated signals of aromatic protons as three doublets at 7.0, 7.7 and 7.8 ppm, one multiplet at 7.4 ppm, and one singlet signal of the methyl ammonium protons at 3.6 ppm in MeOH-*d*₄.

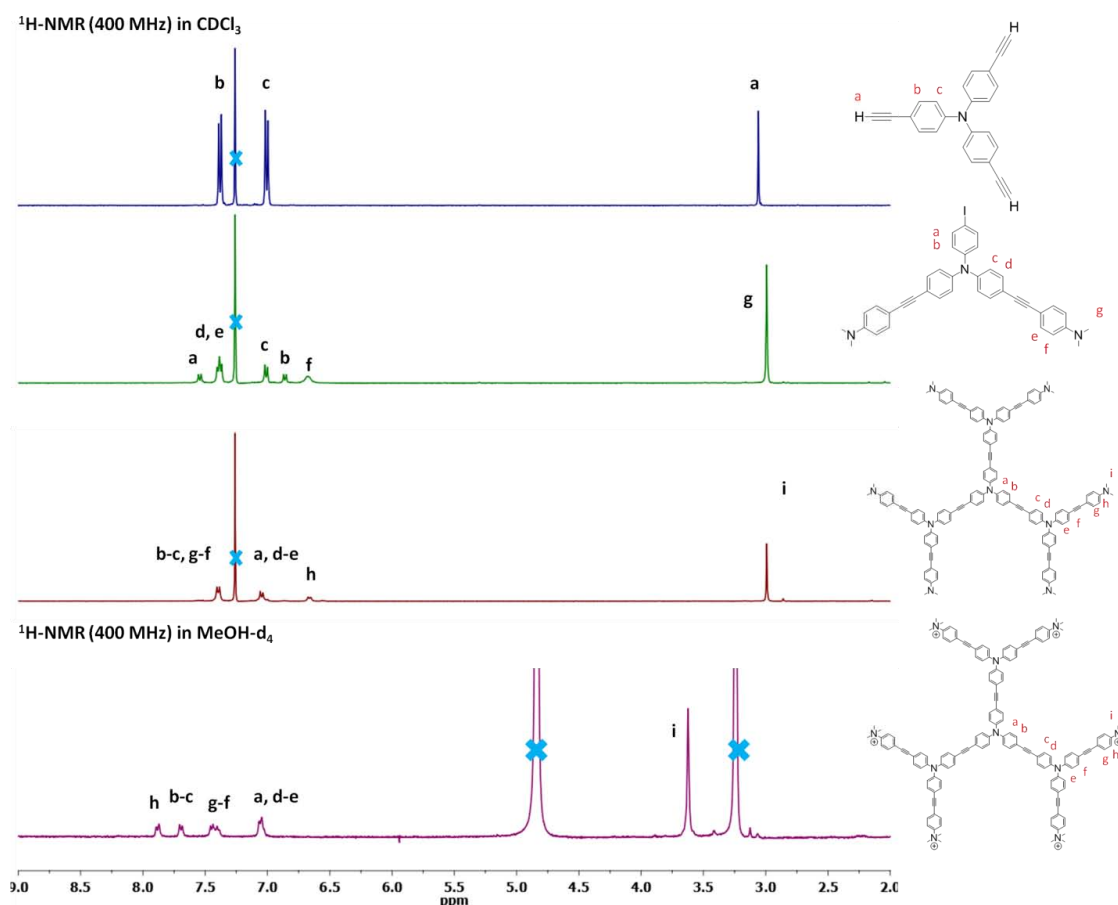


Figure 3.3 ¹H-NMR spectra of **T(ET)₃**, **TI(EAMe₂)₂**, compound **2** and **6N⁺**

The structure characterization of the dendritic hexacationic fluorophore ($6N^+$) was confirmed by ESI-MS/MS spectra that showed the molecular ion peak corresponding to its molecular weight (Figure 3.4). From the spectrum, there were three based-peaks at 332, 399 and 499 m/z that matched with its quasi molecular peak of molecular ion ($[M]^{6+}$), one proton loss from the molecular ion ($[M-H^+]^{5+}$) and two proton loss from the molecular ion ($[M-2H^+]^{4+}$), respectively.

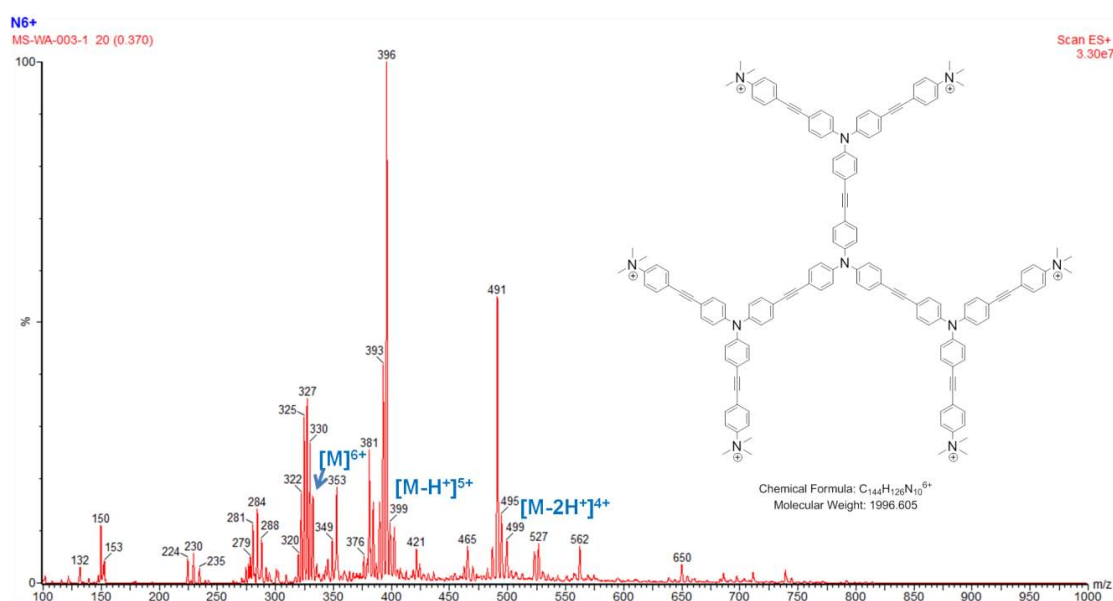
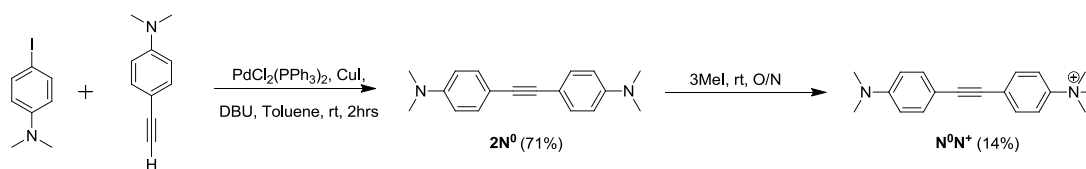


Figure 3.4 ESI MS data of $6N^+$

3.3 Synthesis and characterization of the multi-branched cationic fluorophores

4-iodo *N,N'*-dimethylaniline ($IAME_2$) was coupled with 4-ethynyl *N,N'*-dimethylaniline ($EAME_2$) to get 4,4'-(ethyne-1,2-diyl)bis(*N,N'*-dimethylaniline) ($2N^0$) then methylation by using 3 equivalents of methyl iodide to provide N^0N^+ with 14% yield (Scheme 3.3).



Scheme 3.3 Synthesis of the N^0N^+

1H -NMR spectra of $IAME_2$, $EAME_2$, $2N^0$ and N^0N^+ are shown in Figure 3.5. All signals can be assigned to all protons in each corresponding structure. $IAME_2$ showed two doublet signals at 6.5 and 7.5 ppm corresponding to its aromatic protons and one

singlet signal at 2.9 ppm corresponding to a methyl group. **EAMe₂** revealed two doublet signals at 6.6 and 7.4 ppm corresponding to its aromatic protons and one singlet signal at 2.9 ppm corresponding to a methyl group and terminal alkyne protons. After the coupling reaction, **2N⁰** displayed the similar ¹H NMR peaks as **EAMe₂** that showed two doublet signals at 6.7 and 7.4 ppm corresponding to its aromatic protons and one singlet signal at 3.0 ppm corresponding to a methyl group. Then the mono-methylation product (**N⁰N⁺**) exhibited four doublet signals at 6.7, 7.4, 7.7 and 8.0 ppm corresponding to its aromatic protons and two singlet signals at 3.0 and 3.6 ppm corresponding to the trimethyl ammonium protons.

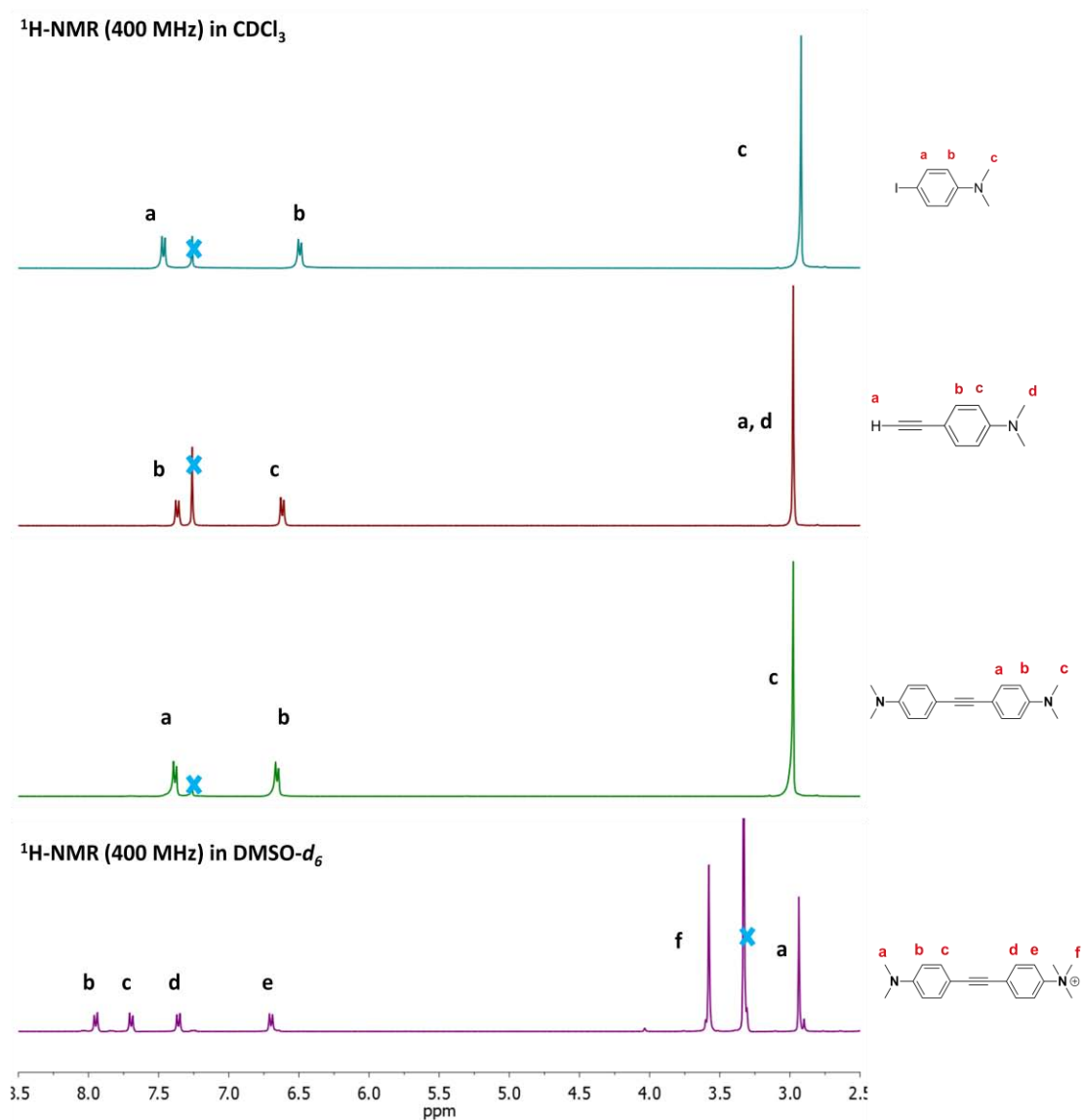


Figure 3.5 ¹H-NMR spectra of **IAMe₂**, **EAMe₂**, **2N⁰**, and **N⁰N⁺**

The structure characterization of the monocationic fluorophore (N^0N^+) was confirmed by ESI-MS/MS spectra that showed the molecular ion peak corresponding to its molecular weight (Figure 3.6). Quasi molecular peak was showed at 279 m/z that matched with N^0N^+ molecular ion ($[\text{M}]^+$).

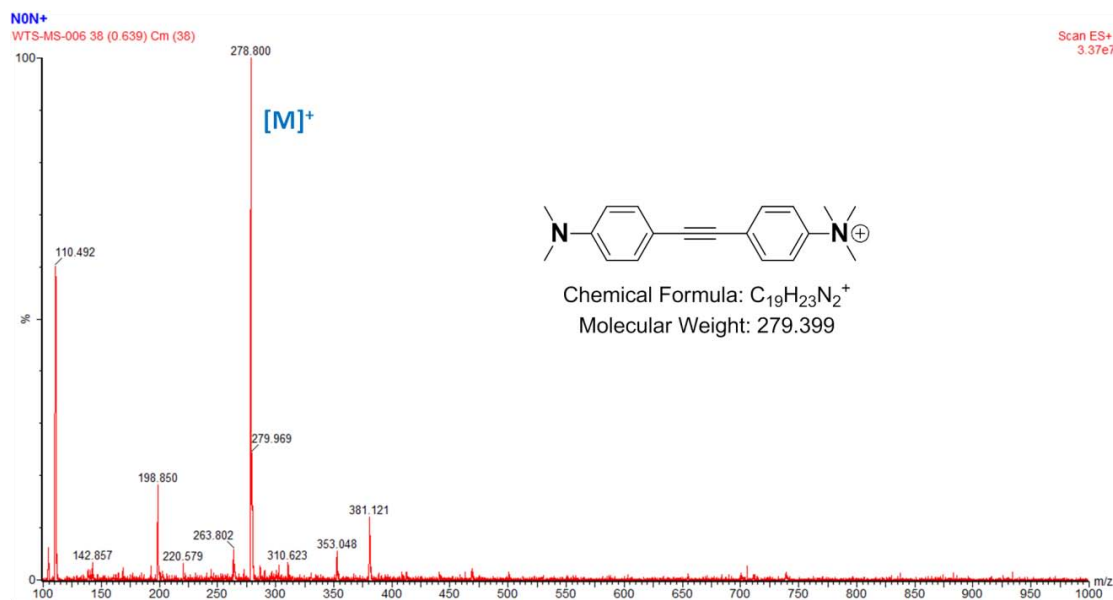
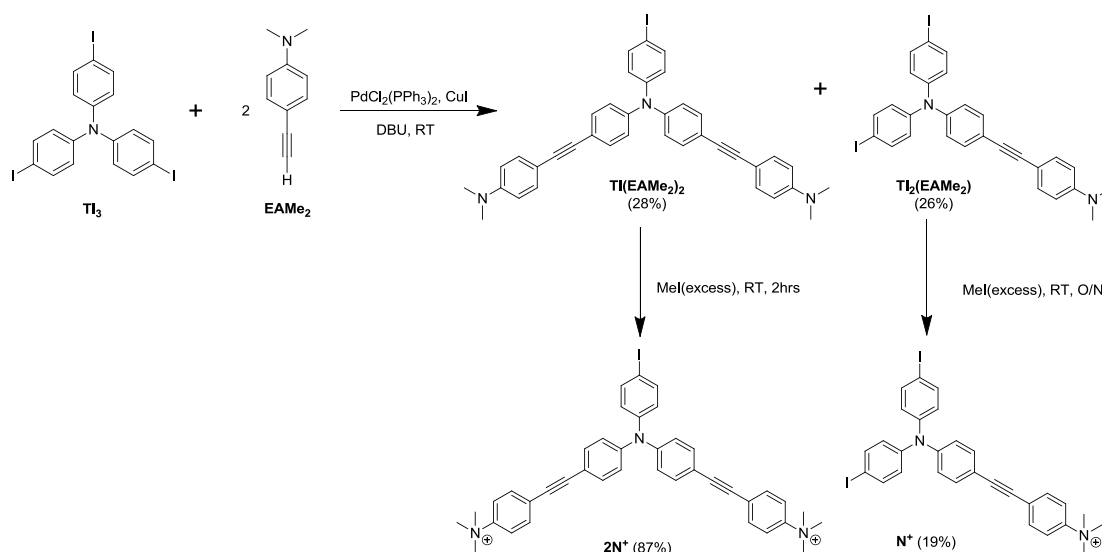


Figure 3.6 ESI MS data of N^0N^+

The disubstituted product ($\text{TI}(\text{EAMe}_2)_2$) was synthesized by the Pd-catalyzed Sonogashira cross-coupling of TI_3 with 2 equivalents of EAMe_2 at room temperature to obtain the expected product (28%) and mono-substituted byproduct ($\text{TI}_2(\text{EAMe}_2)$, 26%). After methylation of both compounds by using an excessive equivalent of MeI, positive charged fluorophores (2N^+ and N^+) were obtained (Scheme 3.4).



Scheme 3.4 Synthesis of the 2N^+ and N^+

^1H -NMR spectra of $\text{TI}_2(\text{EAMe}_2)$, $\text{TI}(\text{EAMe}_2)_2$, N^+ and 2N^+ are shown in Figure 3.7. All signals can be assigned to all protons in each corresponding structure. Initially, Monosubstituted product ($\text{TI}_2(\text{EAMe}_2)$) showed four doublet signals at 7.54, 6.98, 6.83 and 6.65 ppm and one doublet of doublet peak at 7.38 ppm corresponding to its aromatic protons and one singlet signal at 2.99 ppm corresponding to dimethyl protons as well as the disubstituted compound ($\text{TI}(\text{EAMe}_2)_2$) exhibited four doublet signals at 7.54, 7.01, 6.86 and 6.66 ppm and one doublet of doublet peak at 7.38 ppm corresponding to its aromatic protons and one singlet signal at 2.99 ppm corresponding to dimethyl protons.

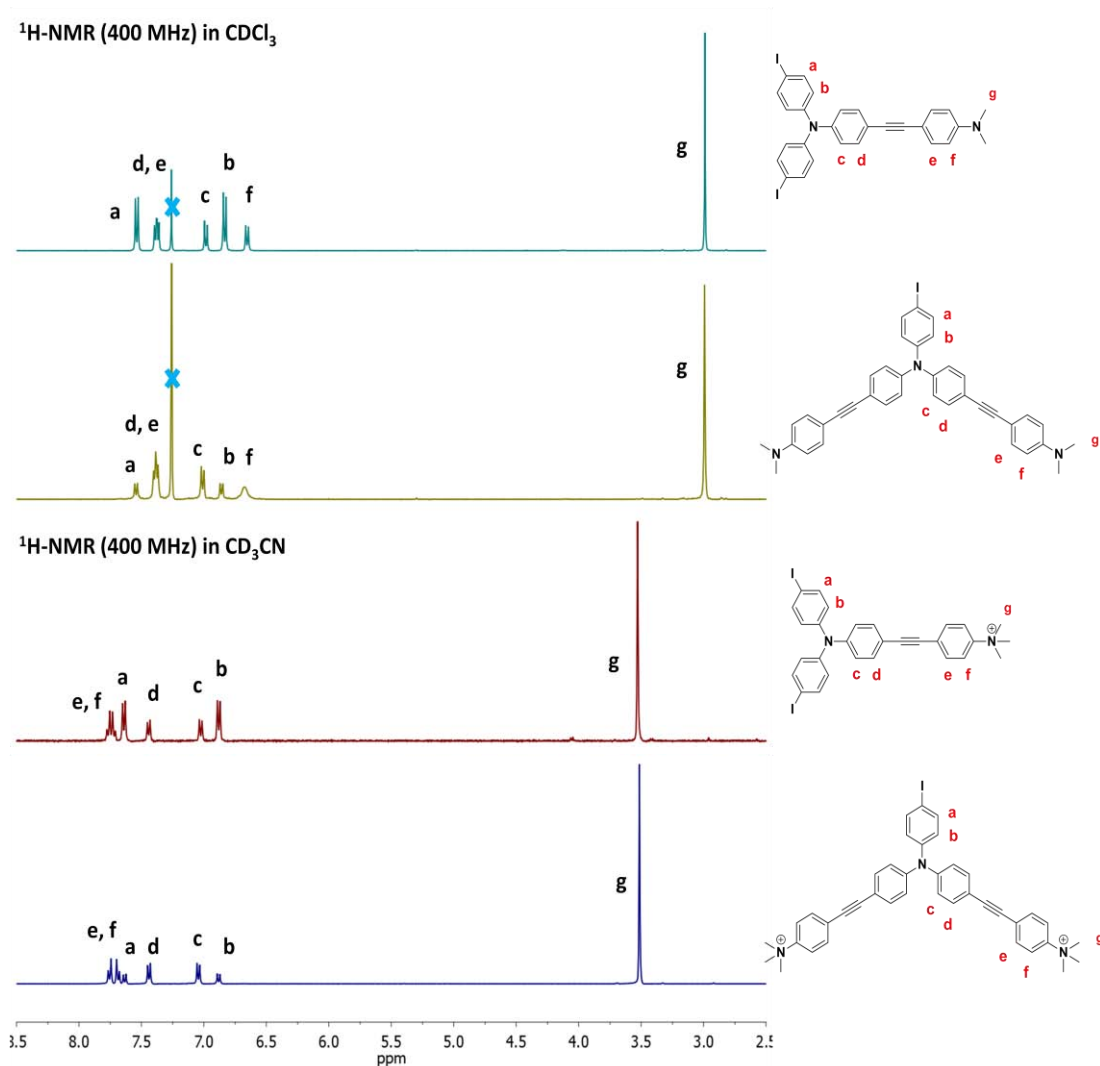


Figure 3.7 $^1\text{H-NMR}$ spectra of $\text{TI}(\text{EAME}_2)_2$, $\text{TI}_2(\text{EAME}_2)$, N^+ , and 2N^+

After the methylation, N^+ product displayed ^1H NMR peaks of four doublet signals at 7.64, 7.44, 7.03 and 6.88 ppm and one quartet signal at 7.75 ppm corresponding to its aromatic protons, and one singlet signal at 3.53 ppm corresponding to a trimethylammonium group. Similarly to N^+ , 2N^+ showed six doublet signals at 7.75, 7.69, 7.63, 7.44, 7.04 and 6.88 ppm corresponding to its aromatic protons, and one singlet signal at 3.51 ppm corresponding to its trimethylammonium protons.

The structure characterization of the monocationic fluorophore (\mathbf{N}^+) was confirmed by ESI-MS/MS spectra that showed the molecular ion peak corresponding to its molecular weight (Figure 3.8). A quasi molecular peak was showed at 655 m/z that matched with \mathbf{N}^+ molecular ion ($[\mathbf{M}]^+$).

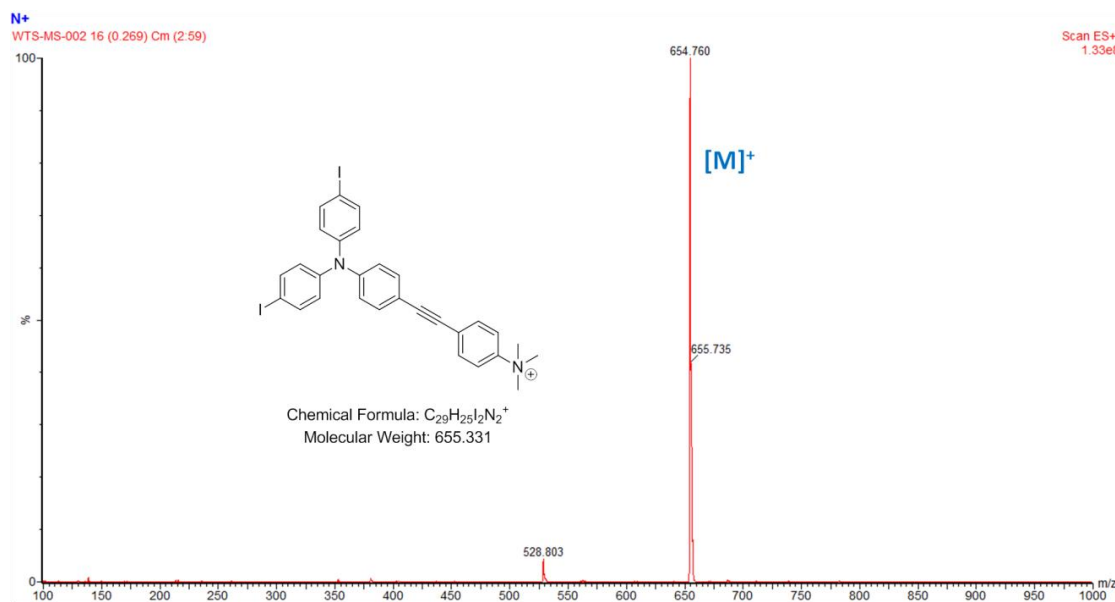


Figure 3.8 ESI MS data of \mathbf{N}^+

The structure characterization of the monocationic fluorophore ($2\mathbf{N}^+$) was confirmed by ESI-MS/MS spectra that showed the molecular ion peak corresponding to its molecular weight (Figure 3.9). Quasi molecular peak was showed at 343 m/z that matched with $2\mathbf{N}^+$ molecular ion ($[\mathbf{M}]^{2+}$).

X

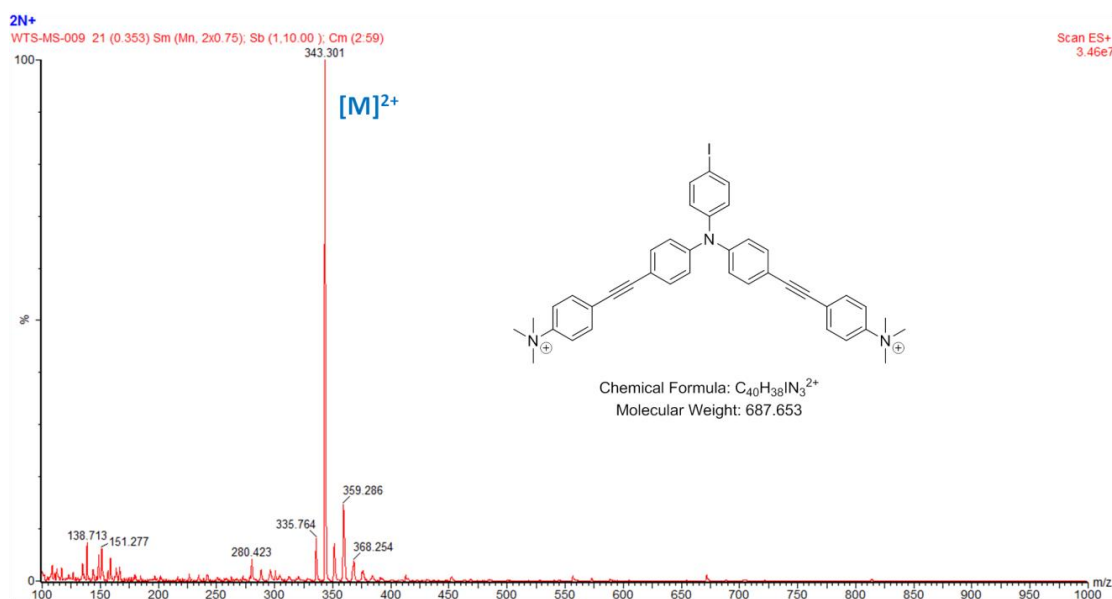


Figure 3.9 ESI MS data of $2N^+$

3.4 Photophysical properties of the cationic fluorophores

3.4.1 Electronic absorption and emission spectra

The photophysical properties of the cationic fluorophores (N^0N^+ , N^+ , $2N^+$, $3N^+$ and $6N^+$) were studied in aqueous solution. When the fluorophores (N^0N^+ , $2N^+$, and $3N^+$) that attached with one, two and three cationic branches, respectively, displayed their maximum absorption wavelength (λ_{max}) increasing with the number of its branches (330, 358 and 370 nm) as well as the emission wavelength (467, 488 and 497 nm). The N^+ solution that could only slightly dissolved in water; therefore, it was not compared to other fluorophores. $6N^+$ gave similar λ_{max} as $3N^+$ while the fluorophores exhibited a much shorter emission wavelength than $3N^+$ (Figure 3.10). This probably indicates that an electronic state of the higher multi-branched structure become an narrower energy band gap due to longer π -conjugated system while their rigidities of the molecules slightly increase since less Stoke's shift of bigger structure [31]. Increase of fluorophore units in the bigger structure ($6N^+$) cannot sufficiently effect its electronic ground state comparing to the smaller one ($3N^+$) because conformational rotation of $6N^+$ become a harder move than the smaller molecule as noticed from its less stoke's shift.

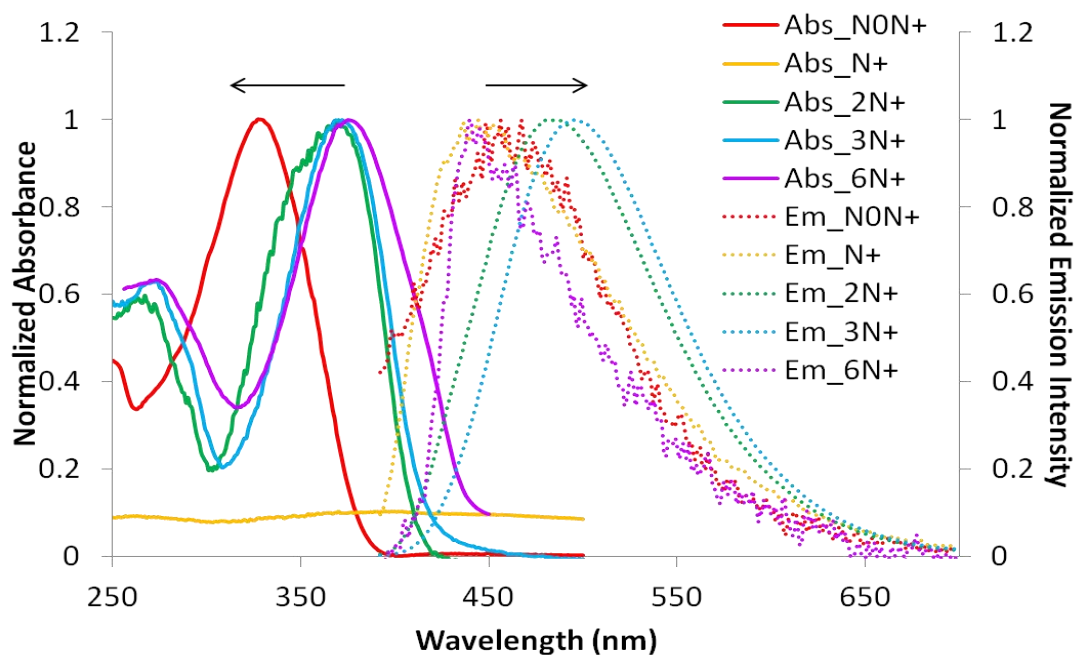












Figure 3.10 Absorption spectra (solid line), and Emission spectra (dot line) of N^0N^+ , N^+ , 2N^+ , 3N^+ and 6N^+ ($5 \mu\text{M}$) in sodium phosphate buffer pH 7 (10 mM) and NaCl (100 mM) upon excitation at 328, 368, 358, 370 and 376 nm, respectively

3.4.2 Molar absorptivities and quantum yields

The fluorescence quantum yield (Φ_F) of the fluorophores in Milli-Q water were 2%, 7%, 12% and 0.3% for N^+ , 2N^+ , 3N^+ and 6N^+ , respectively while that of N^0N^+ was very trace to be no detectable. Molar absorptivity (ϵ) of N^0N^+ , 2N^+ , 3N^+ were quite the same while N^+ gave lower ϵ but 6N^+ showed the highest value (Table 3.1). These results suggest that the bigger number of fluorophore units can absorb more photon as noticed in its high ϵ comparing to the other structures. Because iodide (I-) group onto the structures can quench its fluorescence intensity [31]; it is thus indicates that N^+ and 2N^+ gave lower Φ_F than 3N^+ due to iodide attached. However, there is highly aggregation in the case of the dendritic hexacationic fluorophore according to its larger hydrophobic inner part which induced fluorescence self-quenching because of its π - π stacking although.

Table 3.1 Photophysical properties of the polycationic fluorophores

Compounds	Absorption		Emission	
	λ_{\max} (nm)	$\log \epsilon$ ($M^{-1}cm^{-1}$)	λ_{\max} (nm)	$\% \Phi_F$
Quinine sulfate ^a	345	-	450	54
N⁰N⁺	330	4.2 	467	N.D. ^b 
N⁺	370	3.7 	443	2 
2N⁺	358	4.4 	488	7 
3N⁺	370	4.5 	497	12 
6N⁺	376	5.2 	442	0.3 

^a Reference standard^b Not detectable

3.4.3 Electronic structure based on computational chemistry

According to AM1 structure calculated by GuassView Program, the tricationic fluorophore displayed its branch width of 4.38 Å and a branch length (N_{core} to $N_{\text{periphery}}$) of ~ 12.6 Å as shown in Figure 3.11. The simulated structure showed that 3-D structure of **3N⁺** was a propeller-like structure that the triple branches represent its blades and the central atom represents its rotation center. Each branch was independently evidenced its fluorophore as phenylene-ethynylene unit and the longest length between their peripheries was around 26 Å.

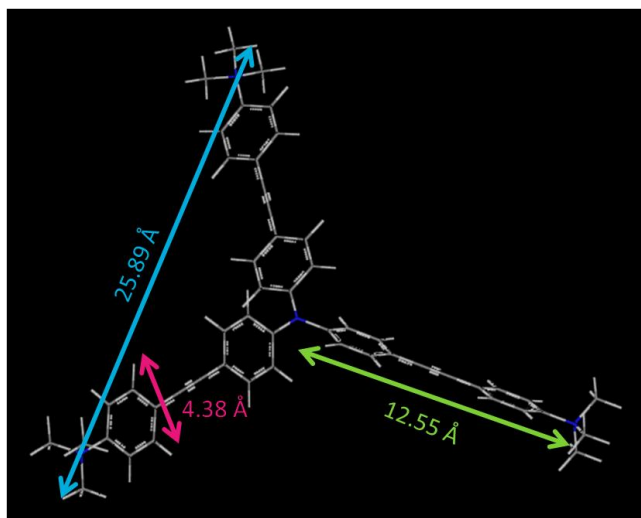


Figure 3.11 AM1 structure of $3N^+$

Moreover, the density functional theory (DFT) calculation for $3N^+$ structure showed that energy of the highest occupied molecular orbital (HOMO) level was equal to -9.41 eV and energy of the lowest unoccupied molecular orbital (LUMO) level was equal to -6.48 eV. Therefore, the energy difference (ΔE) or energy band gap was calculated to be 2.93 eV and then converted to be 423 nm ($\lambda = hc/E$) of wavelength which was corresponding to its observed absorption wavelength. The illustration of molecular orbital showed that an electron density clouded around its $3N^+$ core area at the HOMO state while the electron density shifted to around its branched tips at the LUMO state (Figure 3.12). These results suggest that an electronic ground state that donating molecule can stabilize around the periphery area will be induced to a lower HOMO energy level resulting to wider HOMO-LUMO gap. Also, the wavelength blue shift can be possibly caused by the LUMO energy level changing to higher state due to destabilized excited state [119] compared to its initial ground state structure.

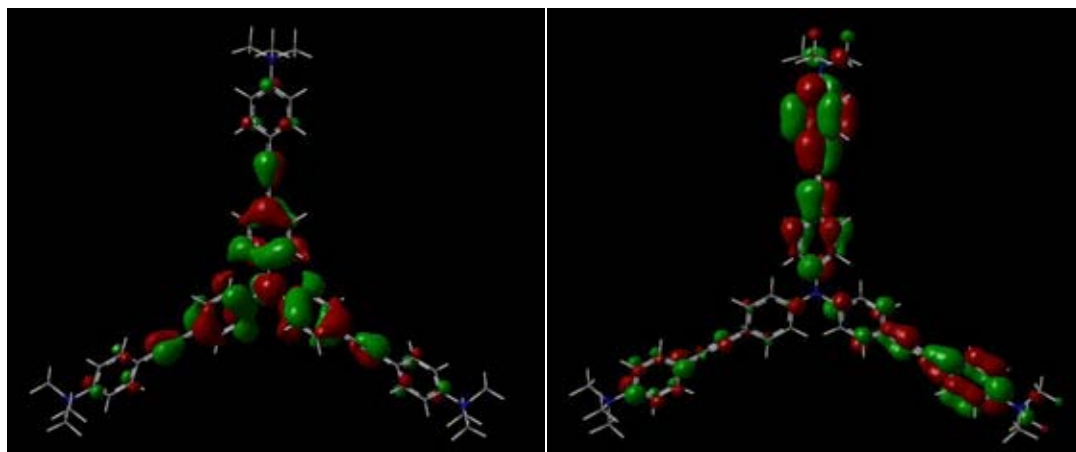


Figure 3.12 HOMO (*left*) and LUMO structure (*right*) of 3N^+ from DFT calculation with B3LYP/6-31G(d) level.

3.4.4 Emission spectra with various conditions

In aqueous solution containing sodium chloride and sodium phosphate buffer, the fluorescence intensity of both 3N^+ and 6N^+ displayed no significant difference in their various pH of buffer media ranging from 5 to 11 (Figure 3.13). This is unsurprising since the designed fluorophores carry permanent positive charges onto their peripheries, they should not be affected by pH changing. These pH conditions are an easy way to investigate and to understand their further supramolecular interactions without misleading results.

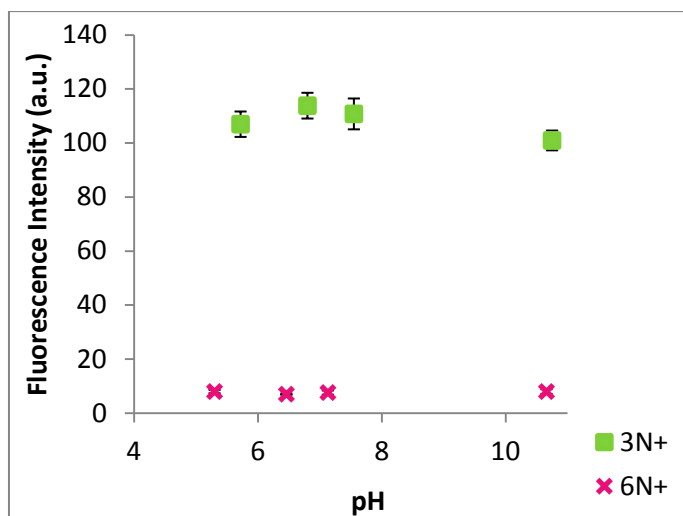


Figure 3.13 Emission intensity of 5 μM 3N^+ (■) and 5 μM 6N^+ (×) in sodium phosphate buffer with various pH (5 – 11) (10mM) and NaCl (150 mM) upon excitation at 370 and 376 nm, respectively.

Moreover, the different kinds of aqueous media buffers were studied with the same concentration and pH for the tricationic fluorophore, the results showed that the fluorescence intensity of 3N^+ in each buffer was not the same (Figure 3.14).

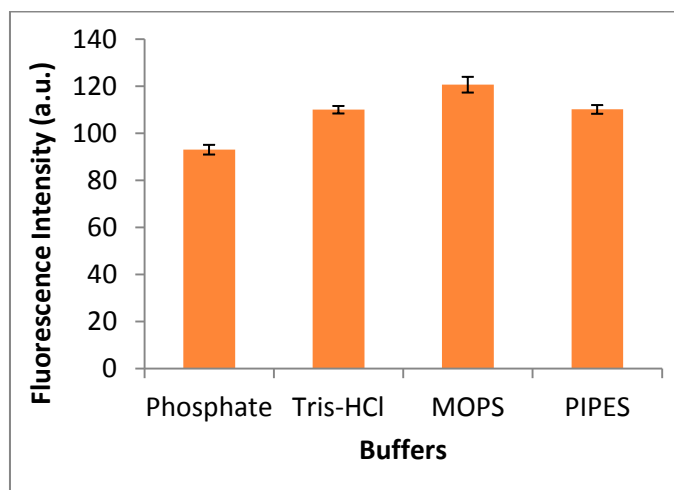


Figure 3.14 Emission intensity of 3N^+ 5 μM in buffer pH 7 (sodium phosphate, Tris-HCl, MOPS and PIPES, 10 mM) upon excitation at 370 nm.

According to buffer structures, fluorescent signal of each mixtures showed different intensity although pH of each media was controlled at around 7. With comparison of hydrophobic and hydrophilic ratio in their structure (**Figure 3.15**), 3-

(*N*-morpholino)propanesulfonic acid (**MOPS**) that gave the highest fluorescence intensity exhibited fewer larger hydrophobic ratio than tris-(hydroxymethyl)amino methane (**Tris**) and piperazine-*N,N'*-bis(2-ethanesulfonic acid) (**PIPES**) that showed lower fluorescence intensity while sodium phosphate buffer that presented the lowest fluorescence intensity hardly revealed the hydrophobic part. This indicated that the buffer structure with more hydrophobicity could discrete the molecular aggregation of **3N⁺** with higher potential because of the more structure like and directly affected to the fluorescent signal.

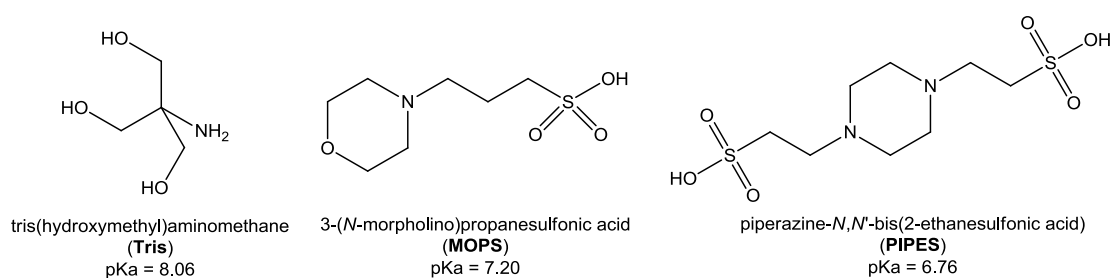


Figure 3.15 Chemical structures of Tris, MOPS and PIPES.

The concentration of sodium chloride salt was also varied from 0 to 500 mM and we found that the fluorescence intensity of **3N⁺** dropped since 200 mM of the NaCl concentration (**Figure 3.16**). At very high concentration of salt, the fluorophore molecule could be solvated by salt ions and the free solvent would decrease because it solvated the excess salt ions, then the more hydrophobic interaction between the fluorophores resulted the signal quenching as well as the salting out process would be observed.

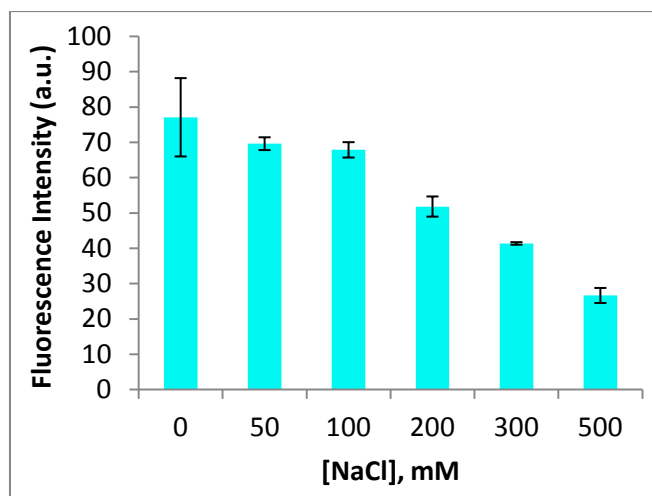


Figure 3.16 Emission intensity of 3N^+ $5\ \mu\text{M}$ in sodium phosphate buffer pH 7 (10 mM) with various concentration (0 – 500 mM) of NaCl upon excitation at 370 nm.

According to this information, buffer types and salt concentration affected directly to the fluorescence signal in any cases. Therefore, the further experiments would be not allowed to be held in the NaCl concentration up to 200 mM for avoiding misleading data and sodium phosphate buffer would be choose to control their pH solutions because we believed that there was not another factor from the buffer structure which could have shown a complicated relationing.

3.5 Supramolecular interaction of the fluorophores with cyclodextrins

We started our investigation by observing the changes of fluorescence signal of 3N^+ ($5\ \mu\text{M}$) upon the addition of α -, β - and γ -CyD ($20\ \mu\text{M}$). As shown in Figure 3.17, γ -CyD dramatically enhanced the emission signal of 3N^+ while β -CyD increased the signal only slightly but α -CyD did not create any changes of the spectrum at all. These results suggested that 3N^+ interacted strongly with γ -CyD and only weakly with β -CyD but has no interaction with α -CyD. It is also interesting to note that the signal enhancement goes hand-in-hand with blue shift which implies the interaction with γ -CyD may be involved either the changes of the π -conjugation length of the fluorophore or merely the reduction of its geometrical relaxation.

To identify the cause of this blue shift, the absorption spectra of 3N^+ in the absence and presence of CyDs were recorded. From the absorption spectra (Figure

3.17), only γ -CyD caused a slight blue shift of the maximum absorption wavelength (λ_{\max}) of the fluorophore from 370 to 364 nm. This shift (6 nm) was much smaller than the shift (58 nm) observed in the emission spectra that indicated only minor change of π -conjugation length of the fluorophore and the blue shift of its emission should be mainly contributed by restriction of the geometrical relaxation. Therefore, we hypothesized that only γ -CyD formed a stable inclusion complex with 3N^+ in the aqueous medium.

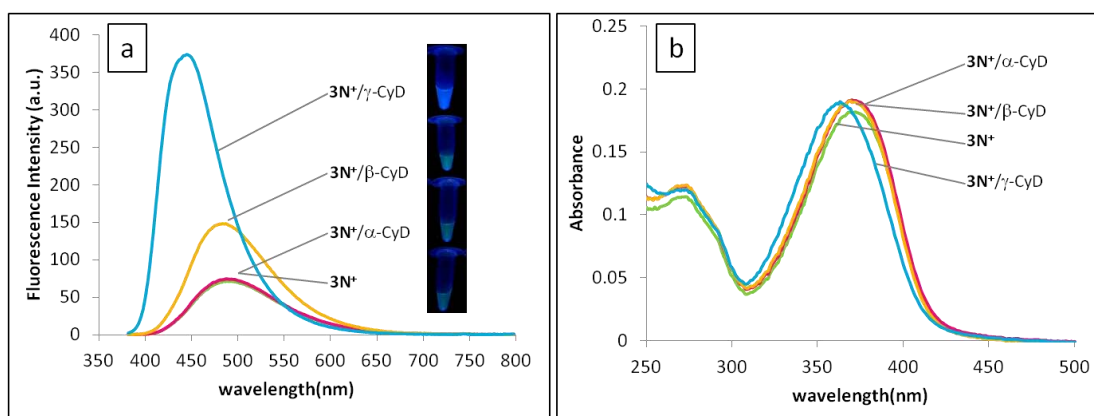


Figure 3.17 a) Emission spectra and b) absorption spectra of 3N^+ (5 μM) in the presence of α -, β -, and γ -cyclodextrins (20 μM), excited at 370 nm. Inset: the photographs of mixtures of 3N^+ with CyDs under black light irradiation.

To support the absorption and emission spectroscopy results, ^1H NMR spectra of 3N^+ and its mixture with each CyD, at 1:4 mole ratio, were compared. $3\text{N}^+/\alpha\text{-CyD}$ mixture gave sharper and slightly down field shifted ^1H NMR signals of 3N^+ indicating some interactions between 3N^+ and $\alpha\text{-CyD}$. This interaction was not observed in the form of fluorescence enhancement as noted earlier, which is likely due to a much lower concentration ($\sim 1/400$) used in the fluorescence experiment. Therefore, the interaction between 3N^+ and $\alpha\text{-CyD}$ is probably rather weak and very dynamic. For the mixture with $\beta\text{-CyD}$, all four aromatic signals of 3N^+ became even sharper and more down field shifted (Figure 3.18) that signified stronger dynamic interaction. In the case of $3\text{N}^+/\gamma\text{-CyD}$, the four aromatic signals of 3N^+ split into seven peaks which could be assigned into two sets of chemically unequivalent phenylene-ethynylene branches. One set consisted of the signals at 7.94, 7.71, 7.03 and 6.87

ppm (a, b, c and d) and another set contained the peaks at 7.83, 7.77 and 7.30 ppm (a', b', c' and d'). The peaks in the first set appeared with a similar pattern to the original peaks of 3N^+ while the second set of peaks showed up with a quite different pattern. These two sets of peaks indicate unsymmetrical interaction of the three phenylene-ethynylene branches of 3N^+ with γ -CyD. The 2:1 integration ratio between the first and second sets also signify that two phenylene-ethynylene branches of 3N^+ interact only weakly with γ -CyD while the other branch interacts quite strongly, probably via the stable inclusion complexation. As the mixture contained excess γ -CyD (4 equiv), the ^1H NMR spectrum also showed the original signals of γ -CyD noted specifically at 5.07 ppm for the anomeric protons (H1). Near this signal, another peak was also observed at a slightly more up field chemical shift (5.00 ppm) which could be reasonably assigned to the corresponding proton (H1') of γ -CyD complexing with 3N^+ . The integration ratio between eight protons of H1' (on γ -CyD) and two protons of a' (or b', c', d' on 3N^+) was about 4:1 giving another good evidence for 1:1 complexation between 3N^+ and γ -CyD. The 1:1 complex was also confirmed by the Job's plot of the fluorescence responses (Figure 3.19). In summary, the NMR data described here clearly support the hypothesis that the fluorescence enhancements of 3N^+ are involved stable inclusion complex with γ -CyD but fast dynamic interaction with β -CyD.

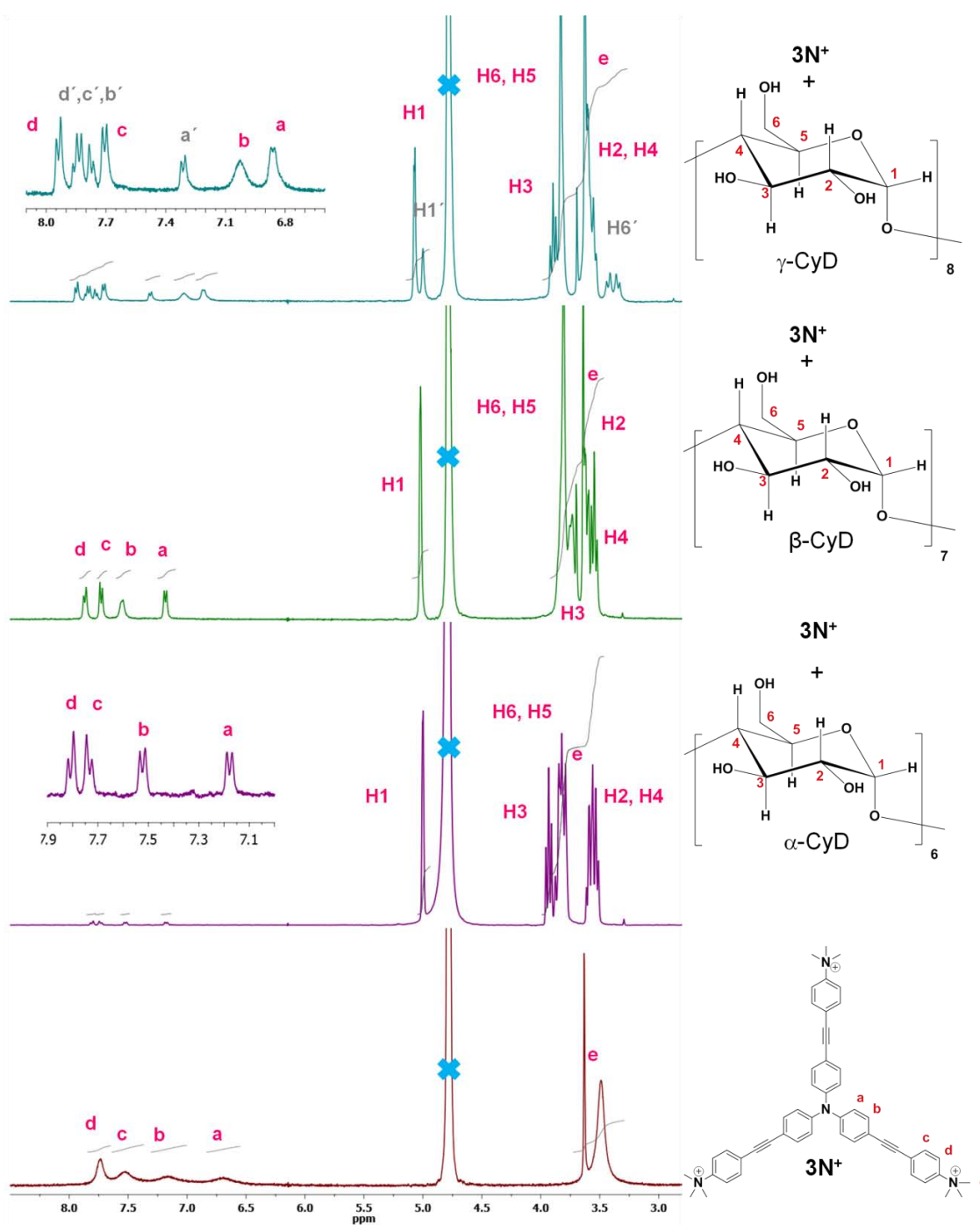


Figure 3.18 $^1\text{H-NMR}$ spectra in D_2O of 3N^+ in the presence of α -, β - and γ -CyD

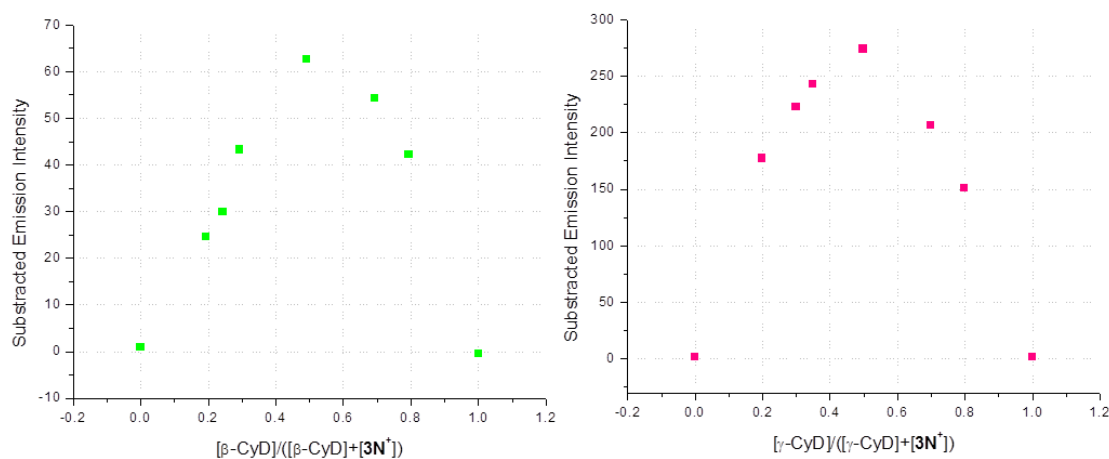


Figure 3.19 Job's Plot of 3N^+ with β -CyD (*left*) and γ -CyD (*right*) in phosphate buffer pH 7 (10 mM) in the presence of NaCl (150 mM).

To confirm the interaction modes, CD spectroscopy of the 3N^+ /CyD mixtures was studied. As an achiral compound, 3N^+ did not give any CD peaks in the range of 200-500 nm (Figure 3.20). In the presence of α - and β -CyD, the CD spectra of the mixtures remained structureless. However, γ -CyD showed strong induced CD signal of 3N^+ with at least four CD peaks. The CD peaks in the range of 300-400 nm corresponding to the π - π^* absorption of the phenylene-ethynylene conjugated system of 3N^+ (Figure 3.17). The cotton effect of CD signal in this range is a good evidence for the tight interaction between the fluorophore and chiral γ -CyD cavity.

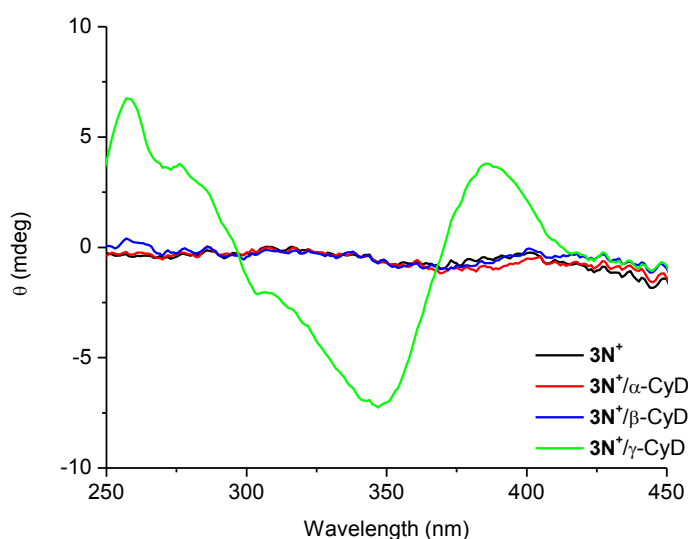


Figure 3.20 Circular dichroism (CD) spectra of 3N^+ ($10\ \mu\text{M}$) in the presence of α -, β -, and γ -cyclodextrins ($10\ \mu\text{M}$) in sodium phosphate buffer pH 7 ($10\ \text{mM}$) and NaCl ($100\ \text{mM}$) at $20\ ^\circ\text{C}$.

To determine the binding constant (K_b) between 3N^+ and CyD, we utilized Benesi-Hilderbrand's double reciprocal plot for a 1:1 complex which were 1.53×10^4 and 3.00×10^4 for β - and γ -CyD, respectively (Figure 3.21). It is important to point out here that 3N^+ give one of the highest 1:1 complexation constants with γ -CyD. [210-223] However, to our surprise, the binding constant for $3\text{N}^+/\beta$ -CyD was relatively high despite showing only moderate fluorescence enhancement and no clear CD signal change. This relatively high K_b with little effect on fluorescence and CD signals may be resulted from several weak interaction sites which is also quite dynamic as observed by ^1H NMR. In fact, we even doubt that the interaction between 3N^+ and β -CyD is involved any inclusion modes.

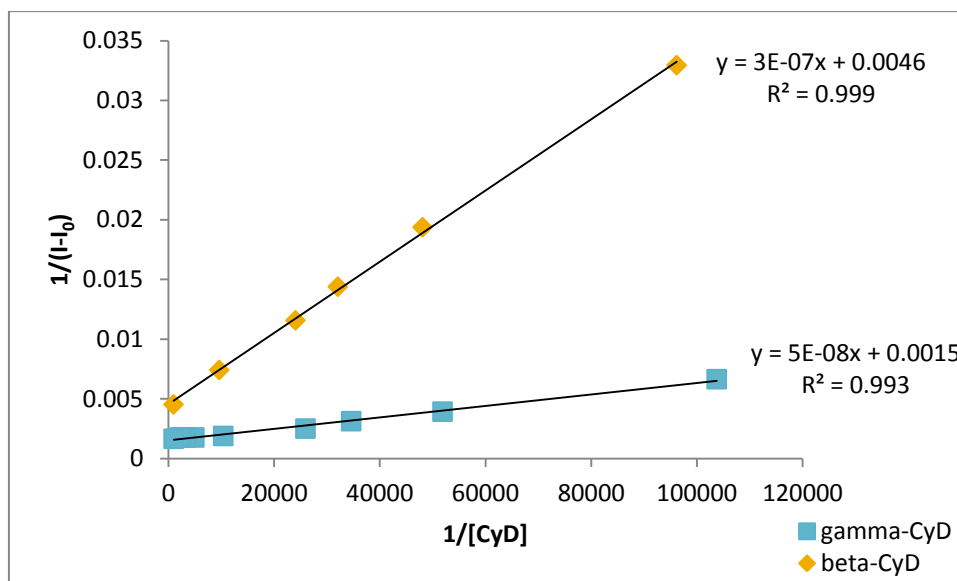


Figure 3.21 Benesi-Hilderbrand plot for 1:1 complexes of $3N^+$ (5 μ M) with β - and γ -CyD, excited at 370 nm.

From the size of the ammonium head group of $3N^+$ (4.4Å) and the minimum internal diameter of CyDs (α -: 4.4Å, β -: 5.8Å, γ -: 7.4Å), the head group should have no problem inserting into β - and γ -CyDs. However, all the spectroscopic results described above gave only clear evidences for the stable inclusion complex of $3N^+$ / γ -CyD (Figure 3.22). There thus remain stirring questions if other structural traits also contribute to this extraordinary strong complexation.

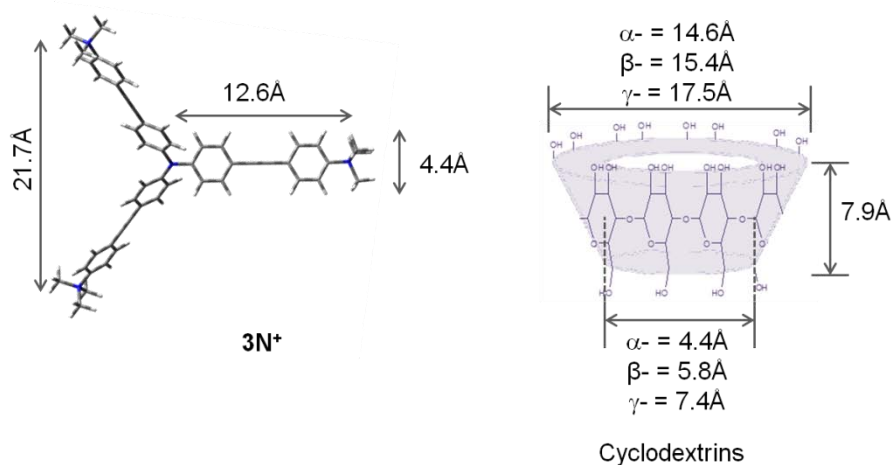


Figure 3.22 Structural parameters of $3N^+$ and CyDs .

To determine the structural parameters contributing to inclusion complexation, we investigated the fluorescence responses of three more fluorophores ($3C^-$, N^+ and $2N^+$) to CyDs in aqueous solution. For $3C^-$, a tricarboxylate anion analogue of $3N^+$, no significant fluorescence change was observed upon the addition of all CyDs (Figure 3.23) suggesting no interaction between this fluorophore and CyDs.

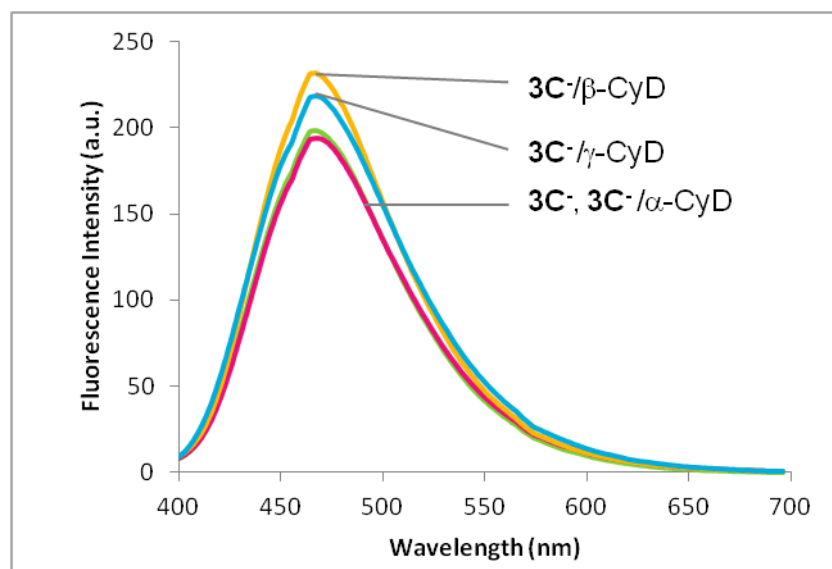


Figure 3.23. Fluorescence spectra of $3C^-$ (5 μ M) in the presences of α -, β -, and γ -cyclodextrins (CyD, 20 μ M) in sodium phosphate buffer pH 7 (10 mM) and NaCl (100 mM) upon excitation at 378 nm.

In the case of electrostatically positive fluorophores (N^+ and $2N^+$), each CyD induced different fluorescence changes (Figure 3.24). The responses of $2N^+$ were reasonably similar to $3N^+$ of which signals were strongly enhanced by γ -CyD, moderately enhanced by β -CyD but not enhanced by α -CyD. The results can again be rationalized as the formation of the inclusion complex of $2N^+$ with only γ -CyD. Surprisingly, N^+ which also contains the positively charged ammonium group did not show any fluorescence responses to γ -CyD. It however still gave a little fluorescence enhancement with the addition of β -CyD. Also, only $2N^+$ showed induced CD signal in the presence of γ -CyD (Figure 3.25). All the results described above gave strong evidences for the stable inclusion complex only in the case of $2N^+/\gamma$ -CyD pair.

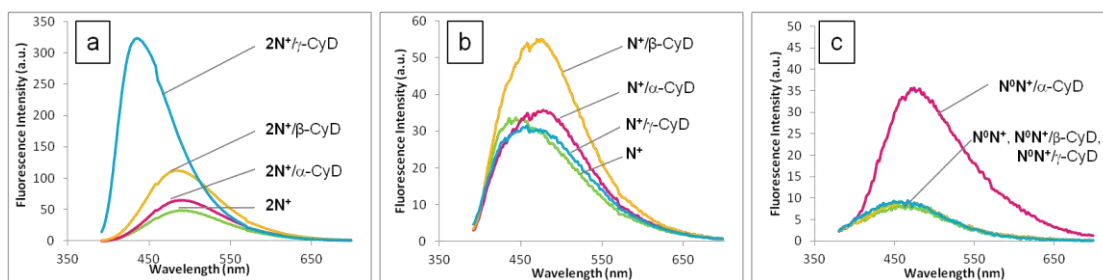


Figure 3.24 Fluorescence spectra of $2N^+$ ($5 \mu\text{M}$), N^+ ($5 \mu\text{M}$) and N^0N^+ ($5 \mu\text{M}$) in the presences of α -, β -, and γ -CyDs ($20 \mu\text{M}$) in sodium phosphate buffer pH 7 (10mM) and NaCl (100mM) upon excitation at 368nm .

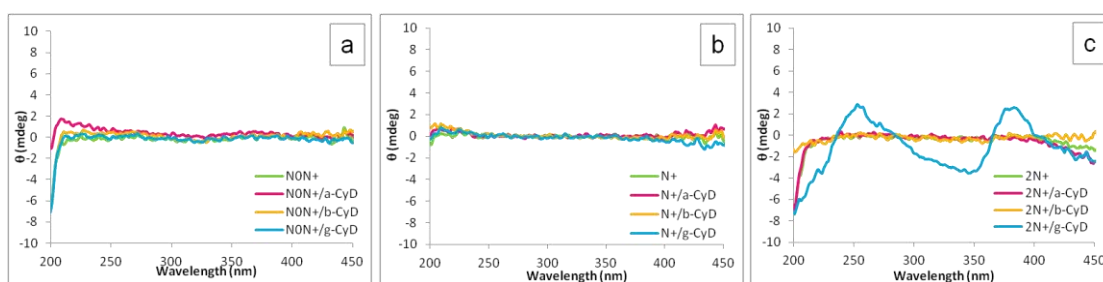


Figure 3.25 CD spectra of N^0N^+ ($5 \mu\text{M}$), N^+ ($10 \mu\text{M}$) and $2N^+$ ($10 \mu\text{M}$) in the presences of α -, β -, and γ -CyD ($10 \mu\text{M}$) in sodium phosphate buffer pH 7 (10mM) and NaCl (100mM) at 20°C .

To gain insight into the interactions of $2N^+$ and CyDs, ^1H NMR spectra of their mixtures in D_2O were acquired and we found that only γ -CyD induced significant signal shifts (Figure 3.26). There was again a new peak at 5.00ppm ($\text{H}1'$) corresponding to the anomeric $\text{H}1$ protons of the complexing γ -CyD. These results are quite similar to those observed for $3N^+$ that indicate the inclusion complex between $2N^+$ and γ -CyD. However, there was only one set of ^1H NMR signals for protons (a-f) in the case of $2N^+$ while there were two sets (a-d and a'-d') observed in the case of $3N^+$.

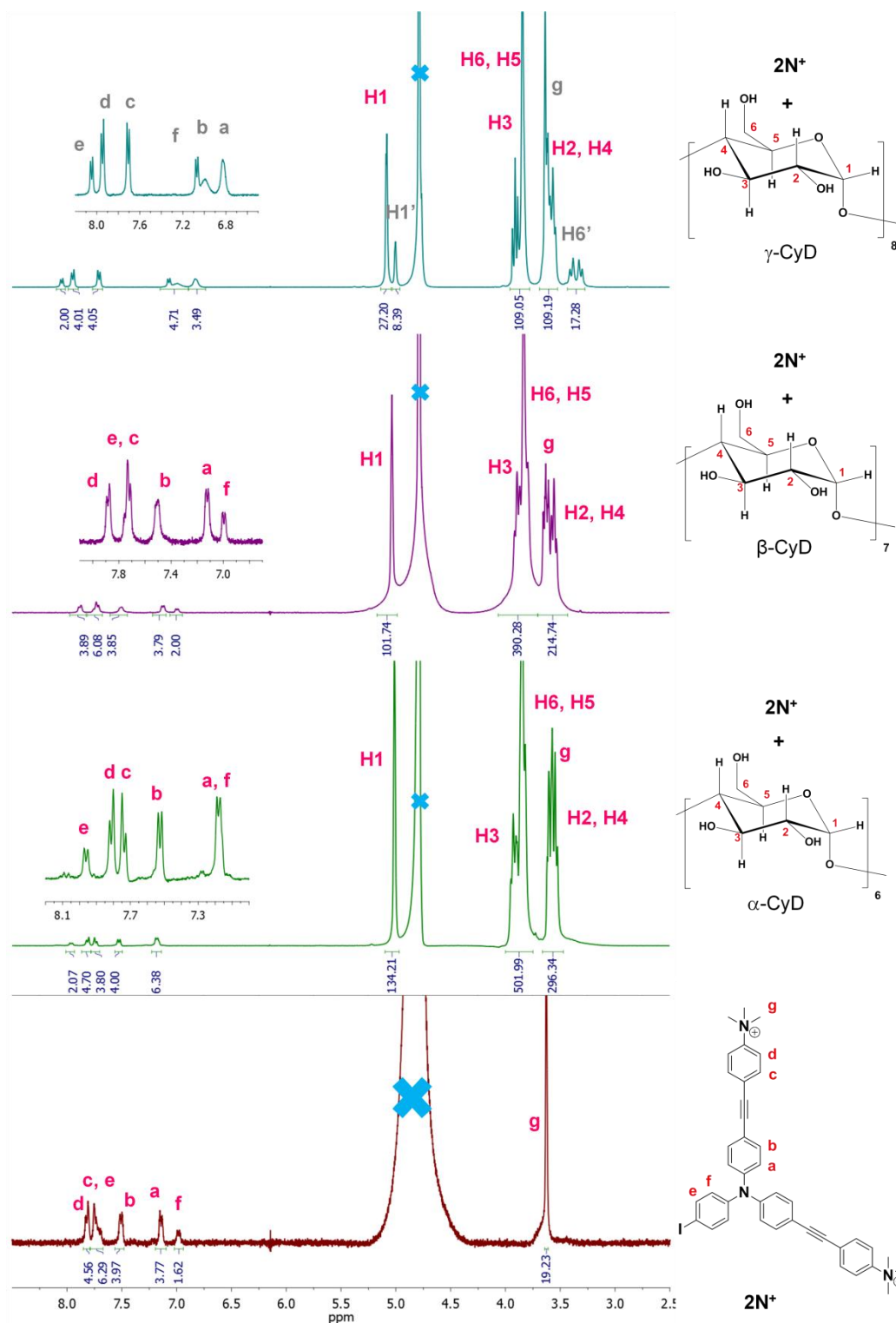


Figure 3.26 ^1H -NMR spectra in D_2O of 2N^+ in the presence of α -, β - and γ -CyD

The single set of ^1H NMR indicates that two phenylene-ethynylene branches are in the same environment which is only possible with the inclusion of γ -CyD at the

iodophenyl branch. This outcome is quite surprising and leads us to believe that the inclusion complexation is significantly contributed by the two strong electron withdrawing ammonium head groups. The MM2 geometrical optimization of the $2\text{N}^+/\gamma\text{-CyD}$ complex also reveals that the $\gamma\text{-CyD}$ is capable to include the entire triphenylamine core into its cavity and its hydrophilic wider rim is in the close proximity with the strongly polarized trimethylanilinium rings (Figure 3.27).

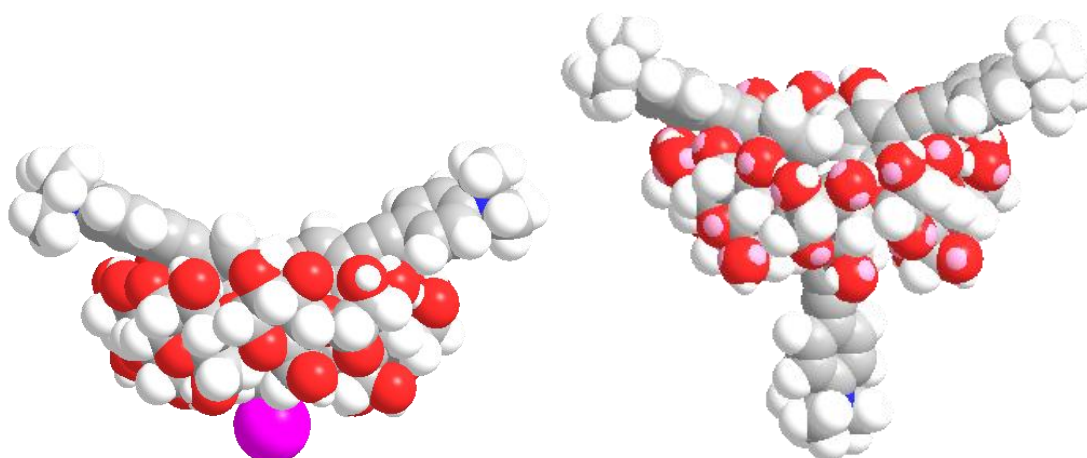


Figure 3.27 MM2 models of $2\text{N}^+/\gamma\text{-CyD}$ and $3\text{N}^+/\gamma\text{-CyD}$ complexes.

To reassure that two ammonium groups are necessary for inclusion complexation with $\gamma\text{-CyD}$, another fluorophore (N^0N^+) containing only one positive phenylene-ethynylene branch was investigated as a guest molecule. As expected, no fluorescence change of this compound in the presence of $\gamma\text{-CyD}$ (or $\beta\text{-CyD}$) confirming no stable inclusion complexation. However, to our surprise, the fluorescence signal was considerably enhanced in the presence of $\alpha\text{-CyD}$ (Figure 3.24c). The results suggested that only $\alpha\text{-CyD}$ strongly interacted with N^0N^+ , possibly via the inclusion complex. The ^1H NMR spectrum of $\text{N}^0\text{N}^+/\alpha\text{-CyD}$ mixture showed some shifts of the signals of aromatic protons and only one peak of anomeric protons around 5.02 ppm (Figure 3.28). This ^1H NMR observation is consistent with the formation of fast exchange complexation either in an inclusion or non-inclusion modes. However, the CD spectra of N^0N^+ and its mixture with $\alpha\text{-CyD}$ were essentially identical (Figure 3.25a) that did not support the formation of stable inclusion complex. We therefore would like to propose that the fluorescence

enhancement and ^1H NMR signal shift are caused by fast exchange complexation which is probably a non-inclusion one.

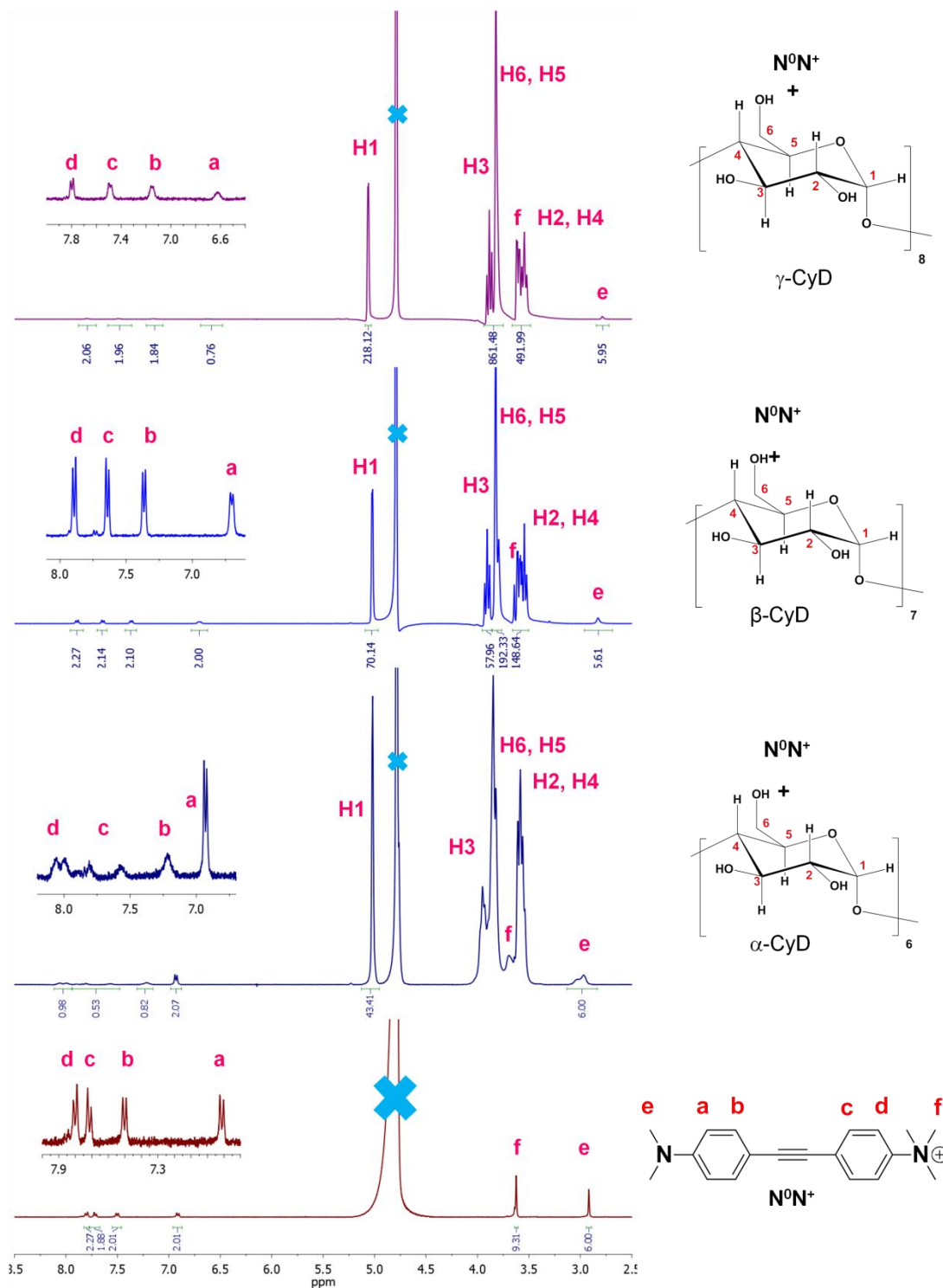


Figure 3.28 ^1H -NMR spectra in D_2O of 2N^+ in the presence of α -, β - and γ -CyD

The fluorescence responses of the fluorophores upon the interactions with CyDs can be summarized as a histogram plot in Figure 3.29. The fluorescence signals of $3N^+$ and $2N^+$ were enhanced strongly ($F/F_0 > 4$) by γ -CyD and moderately enhanced by β -CyD ($F/F_0 \sim 2$) while the signals of N^+ and N^0N^+ were enhanced exclusively by β -CyD and α -CyD, respectively. These differentiable fluorescence responses should be useful for simple identification of CyDs. The fluorescence responses of three selected fluorophores (N^0N^+ , N^+ and $3N^+$) showed easily distinguishable patterns for α -, β - and γ -CyD.

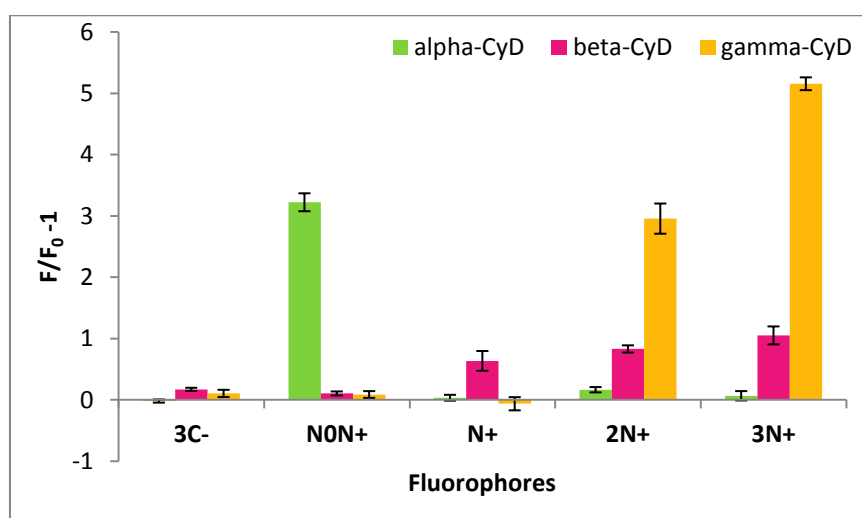


Figure 3.29 Histogram of the fluorophores ($3C^-$, N^0N^+ , N^+ , $2N^+$, and $3N^+$, 5 μ M) with the presence of α -, β -, and γ -CyDs (10 μ M) in sodium phosphate buffer pH 7 (10 mM) and NaCl (100 mM) upon excitation at 378, 328, 368, 368 and 370 nm, respectively.

3.6 Supramolecular interaction of $3N^+$ and $6N^+$ with DNA

We started our investigation by observing the changes of fluorescence signal of $3N^+$ (5 μ M) upon the addition of DNA (15 base pair chain length). As shown in Figure 3.30, complementary double strand DNA (dsDNA; AT and CG) dramatically enhanced the emission signal of $3N^+$ while single strand DNA (ssDNA; 2A and 2C) or non-complementary DNA (AC and GT) showed both fluorescence enhancement and quenching. These results suggest that $3N^+$ interacted with a definitely duplex structure of dsDNA differ from an unpredictable structure of ssDNA. According to the various fluorescence responses of $3N^+$ with the different type of ssDNA, we

hypothesized that the interaction of ssDNA with the fluorophore may be involved with the ability of encompassing of DNA chain onto the $3N^+$ surfaces. Due to the rigid structure of DNA duplexes that cannot arbitrarily move, dsDNA can probably only interact with $3N^+$ by a similar interaction for any dsDNAs that are the same chain length. It is also interesting to note that the signal enhancement goes hand-in-hand with blue shift which implies the interaction with DNA may be involved either the changes of the π -conjugation length of the fluorophore or merely the reduction of its geometrical relaxation.

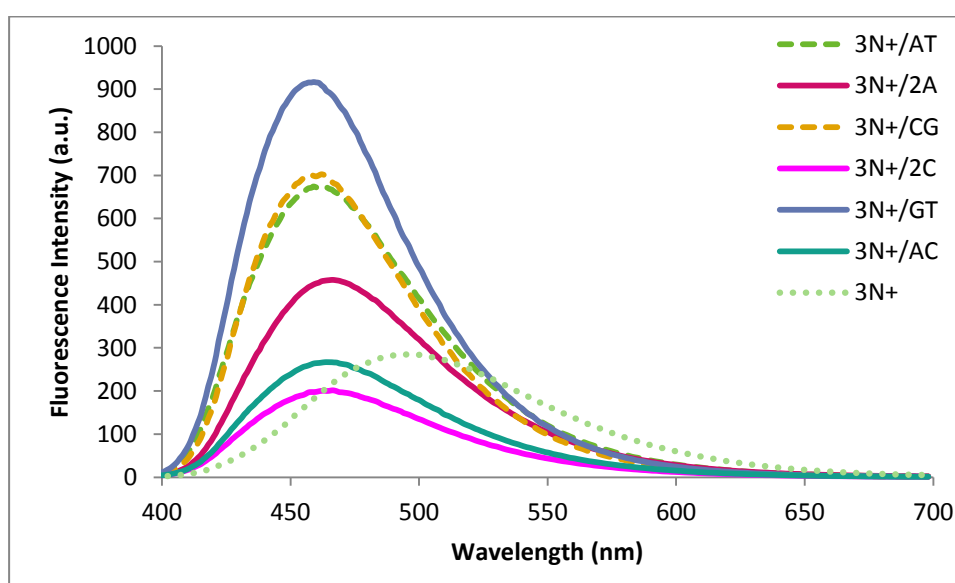


Figure 3.30 Fluorescence spectra of $3N^+$ ($5 \mu\text{M}$) in the presence of ssDNA (2A and 2C, $5 \mu\text{M}$), dsDNA (AT and CG, $5 \mu\text{M}$) and ncDNA (AC and GT, $5 \mu\text{M}$) in sodium phosphate buffer pH 7 (10 mM) and NaCl (100 mM) upon excitation at 370 nm. (A = $5' \text{AAAAAAAAAAAAAAAAA}3'$, C = $5' \text{CCCCCCCCCCCCCCC}3'$, T = $5' \text{TTTTTTTTTTTTTTT}3'$ and G = $5' \text{GGGGGGGGGGGGGGG}3'$)

To gain insight into the interaction, ssDNA which can form duplex structure due to its self-hybridization property were used to study the fluorescence responses as showed in Figure 3.31. Fluorescence signals of $3N^+$ were similarly enhanced in the presence of both ssDNA and dsDNA. This result suggests that both ssDNA and dsDNA probably bind to $3N^+$ with the same interactions and also indicate that the rigid structure of DNA duplex should bind with the fluorophore only a unique interaction especially from an intercalation. However, these DNAs induced $3N^+$

solution to show at longer maximum absorption wavelength. This is indicated that the energy band gap of the fluorophore is reduced by interaction with DNA. It is possible that destabilization of HOMO state is occurred by the conformational lock of 3N^+ structure with DNA chain and the propeller structure become more rigid while LUMO state may be stabilized by the DNA interaction if the excited state has required a high electron density from DNA charges.

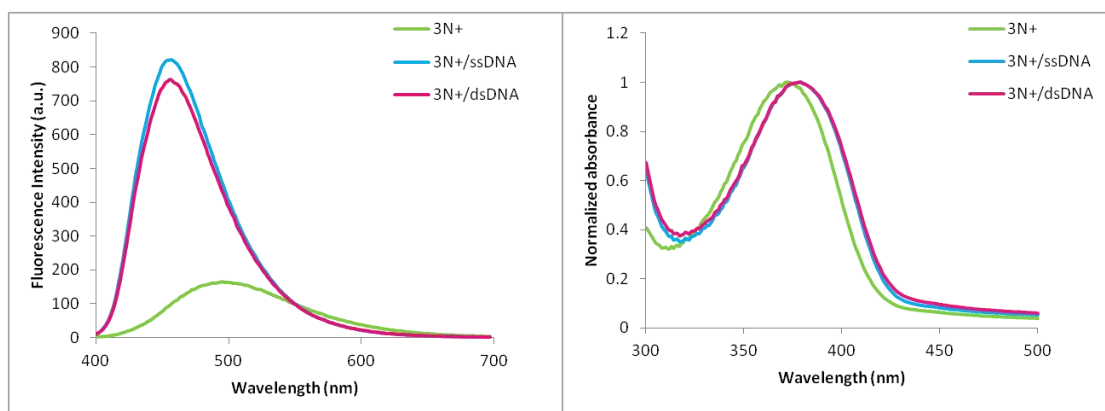


Figure 3.31 Fluorescence spectra (*left*) and absorption spectra (*right*) of 3N^+ ($5\ \mu\text{M}$) in the presence of ssDNA ($5'\text{GCATATGCCTA}3'$, $10\ \mu\text{M}$) and dsDNA ($5'\text{GCATATGCCTA}3' + 5'\text{TAGGCATATGC}3'$, $5\ \mu\text{M}$) in sodium phosphate buffer pH 7 ($10\ \text{mM}$) and NaCl ($100\ \text{mM}$) upon excitation at $370\ \text{nm}$.

In addition, the stoichiometric ratio of 3N^+ /dsDNA complex were studied by varied the concentration of dsDNA from 0 to $2\ \mu\text{M}$. 3N^+ mixtures showed fluorescence enhancement with increasing of DNA concentration (Figure 3.32). When the fluorescence intensity of mixtures was plot against the concentration ratio of 3N^+ /dsDNA as well as a maximum emission wavelength, graph showed that four times of fluorescent enhancement were saturated at about 1.0 ratio indicating $1:1$ complexation. From the Benesi-Hilderbrand's double reciprocal plot for $1:1$ complexes, the binding constant of 3N^+ /dsDNA was $1.55 \times 10^7\ \text{M}^{-1}$ (Figure A.41).

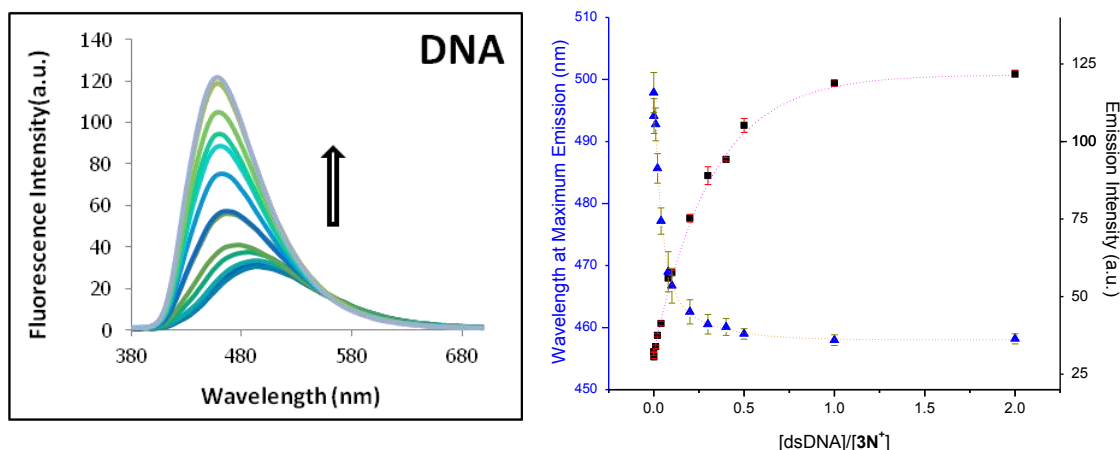


Figure 3.32 (left) Fluorescence spectra and (right) wavelength shifting at maximum emission (▲) and fluorescence intensity (■) of 3N^+ (1 μM) with various concentrations (0 – 2 μM) of dsDNA (5'GCATATGCCTA3' + 5'TAGGCATATGC3') in sodium phosphate buffer pH 7 (10 mM) and NaCl (100 mM) upon excitation at 370 nm.

To investigate the interaction between 3N^+ and ssDNA chain, we varied DNA chain length of random sequences from 0 to 30 bases controlling with the same charge concentration by fixed absorbance (A_{260}) at 0.05. Fluorescence signal of the mixtures were corrected by a factor of A_{260} . The plot of the fluorescence signal against length of DNA chain showed that fluorescence intensity was enhanced by increasing of DNA chain length and it was saturated at around 20 bases (Figure 3.33). This result suggests that the ssDNA may interact with 3N^+ via an encompassing of DNA chain around the fluorophore molecules supporting by AM1 calculation that a circle arc of 3N^+ which was calculated for whole three branches can possibly be fitting at 18 base lengths of ssDNA. After wrapping, 3N^+ molecules were discrete into less aggregation thus fluorescence self-quenching was reduced to lead the emission enhancement. A little change of CD signal of 3N^+ /DNA also confirms this interaction (Figure 3.34).

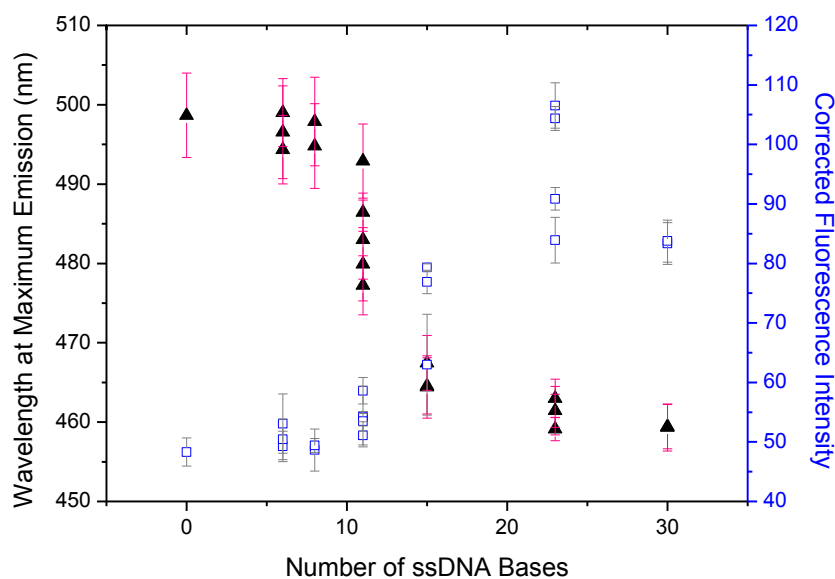


Figure 3.33 Normalized emission intensity (\square) and Maximum wavelength shifting (\blacktriangle) of $3N^+$ (1.0 μM) in the presence of various ssDNA chain lengths (0 to 30 bases and $A_{260} = 0.05$ of each ssDNA) in sodium phosphate buffer pH 7 (10 mM) and NaCl (100 mM) upon excitation at 370 nm.

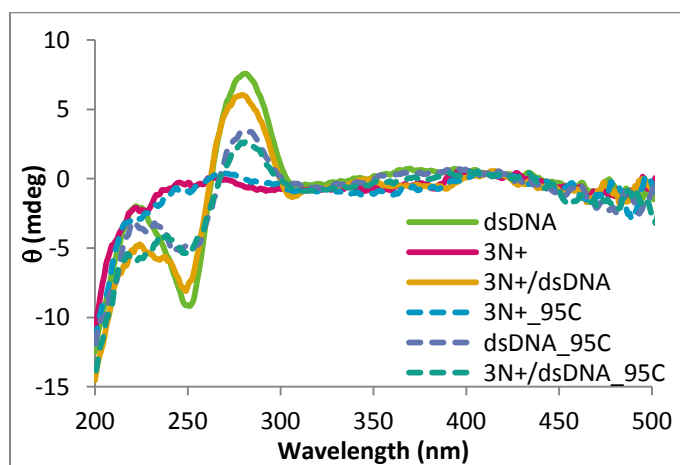


Figure 3.34 CD spectra of $3N^+$ (10 μM) in the presence of dsDNA (5'GCATATGCC TA3' + 5'TAGGCATATGC3', 10 μM) in sodium phosphate buffer pH 7 (10 mM) and NaCl (100 mM) at 20 and 90 $^{\circ}\text{C}$

From the investigation, we use $3N^+$ to apply for any chemical or biological sensing associated by the interaction with aptamer, which is a subtype of DNA that

can specifically interact with the target since our fluorophore can give highly fluorescence enhancement after binding with the DNA short chain. If the specific interaction of aptamer and target form stronger than that of 3N^+ , we should turn the fluorescence signal back to the original state as turn-off mode of the detection. To proof our hypothesis, aptamer that can specific bind with mercury (Apt-Hg) were used to test the detection principle in the aqueous media. The results showed that fluorescence enhancement of 3N^+ /Apt-Hg was nearly quenched into an initial fluorescence intensity while Hg^{2+} exhibited a little quenching (Figure 3.35). This preliminary result confirms that the interaction of 3N^+ and ssDNA is set up via electrostatic interaction and can be weakened by the specific target. It is thus bringing us up to apply for sensing of other target such as a rapid K^+ assays in the real urine samples as demonstrated in our recent publication. [64]

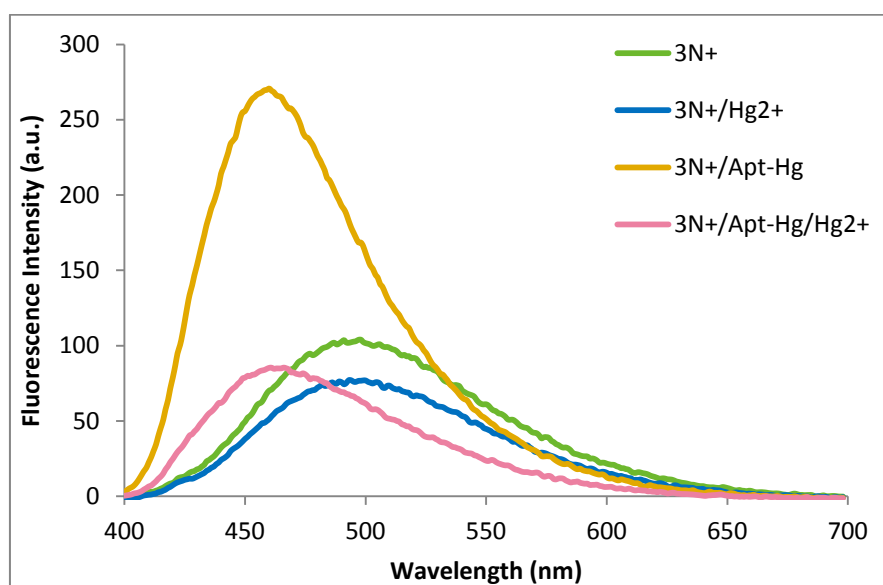


Figure 3.35 Fluorescence spectra of 3N^+ ($1\ \mu\text{M}$) in the presence of mercury aptamer (Apt-Hg = $5'\text{TGTGTTTGTGTTGGGTTGTTTGTGTT}3'$, $0.1\ \mu\text{M}$) and $\text{Hg}(\text{OAc})_2$ ($10\ \mu\text{M}$) in sodium phosphate buffer pH 7 ($10\ \text{mM}$) and NaCl ($100\ \text{mM}$) upon excitation at $370\ \text{nm}$.

To study the dendritic effect onto the DNA interaction, the spectroscopic data of 6N^+ was investigated in the presence of DNA. Surprisingly, absorption change and fluorescence responses of 6N^+ /DNA mixtures were not observed (Figure 3.36). According to their structures, the interaction between positive charge of 6N^+

peripheries and negative charge of DNA chain should be occurred, it is possible that their interaction cannot effectively conduct the signal change of the fluorophore.

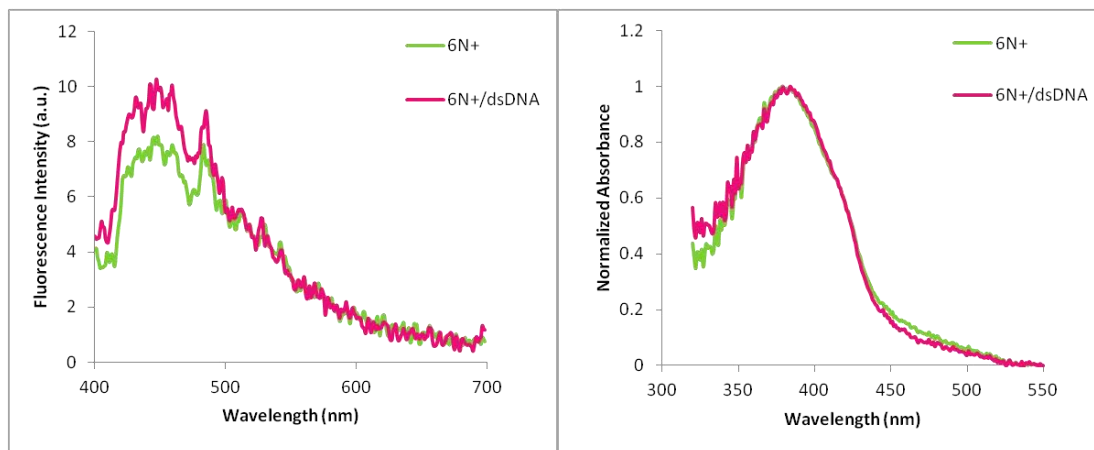


Figure 3.36 Fluorescence spectra (*left*) and Absorption spectra (*right*) of 6N^+ ($5\ \mu\text{M}$) in the presence of dsDNA ($5'\text{GCATATGCCTA}3' + 5'\text{TAGGCATATGC}3'$, $5\ \mu\text{M}$) in sodium phosphate buffer pH 7 (10 mM) and NaCl (100 mM) upon excitation at 376 nm.

Due to insignificantly change of fluorescence responses of 6N^+ /DNA, Förster resonance energy transfer (FRET), that requires spectral overlap between emission of donor and absorption of acceptor and closed distance of the donor-acceptor interaction at $10\text{--}100\text{\AA}$ approximately, was used to investigate the interaction. SyBrGreenII (SBGII), a commercial fluorescent dye that popularly use for detection RNA in electrophoretic gels, was candidate for our study. Spectral data of 3N^+ , 6N^+ and SBGII were shown in Figure 3.37. Both absorption and emission of SBGII was overlapped within an emission area of 3N^+ while spectral overlapping of 6N^+ emission and SBGII absorption did not overwhelm the emission of SBGII. Therefore, FRET phenomena that the energy transfer from the fluorophore donors to SBGII acceptor should be easily observed by the choice of 6N^+ .

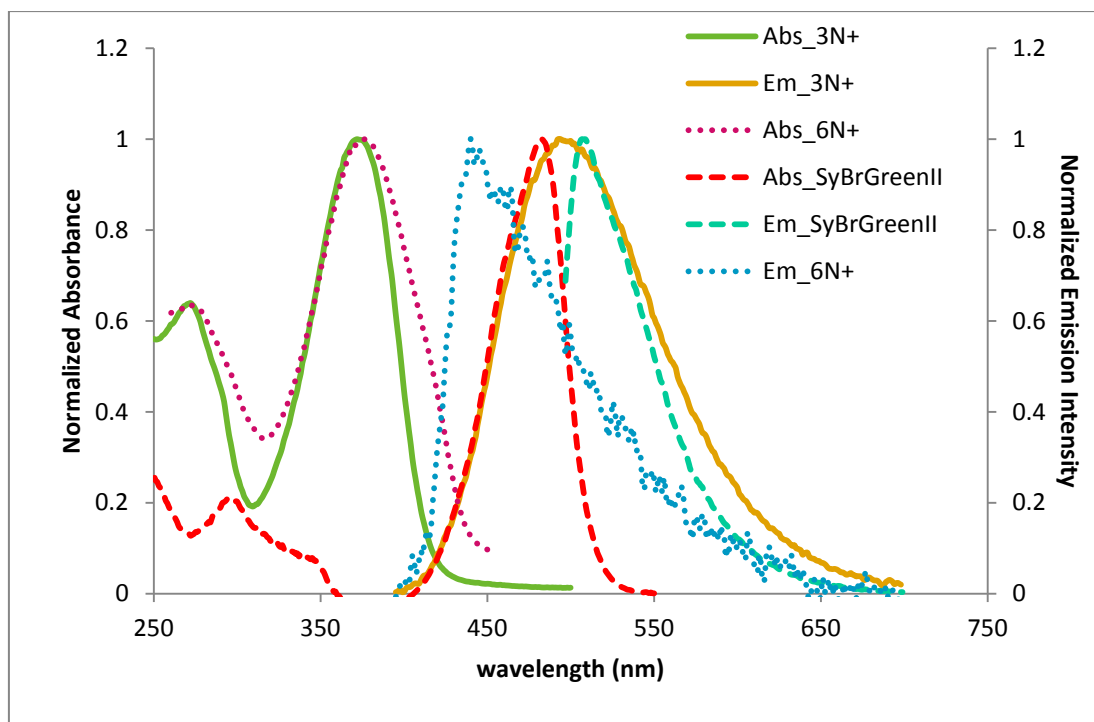


Figure 3.37 Absorption spectra and Emission spectra of 3N^+ (solid line, $5\ \mu\text{M}$), 6N^+ (dot line, $5\ \mu\text{M}$) and SyBrGreen II (dash line, diluted at 10000X) in sodium phosphate buffer pH 7 (10 mM) and NaCl (150 mM) upon excitation at 370, 376 and 390 nm, respectively.

However, FRET signal of 3N^+ /DNA in the presence of SBGII was studied as shown in Figure 3.38. From the spectral data, FRET phenomena of 3N^+ /DNA with SBGII was successfully occurred while an energy transfer from 3N^+ to SyBrGreenII was not obtained without the presence of ssDNA. In addition, fluorescence signal background of the DNA/SBGII mixture was not obtained at high intensity by excited at 3N^+ excitation wavelength. These results indicate that there are no interactions between SBGII and 3N^+ due to their positive charge repulsions while ssDNA interact with 3N^+ and also gather the SBGII molecules together resulting in a closed distance between fluorophore and acceptor dye to give FRET signals.

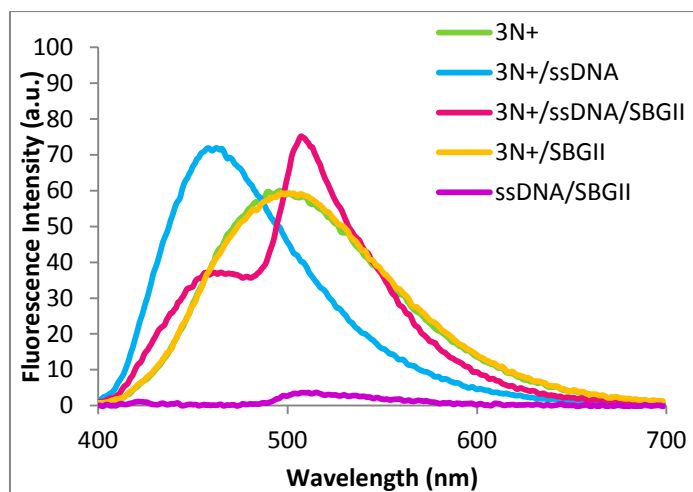


Figure 3.38 Emission spectra of 3N^+ ($1.0 \mu\text{M}$) in the presence of ssDNA ($5'\text{CCTATATAGGTGATGCCTTCTCCGGCGACG3}'$, $A_{260} = 0.05$) and SyBrGreenII (diluted at 10000X) in sodium phosphate buffer pH 7 (10 mM) and NaCl (150 mM) upon excitation at 370 nm.

To investigate 6N^+ /DNA interaction, FRET signal of the mixtures in the presence of SBGII were studied as shown in Figure 3.39. FRET phenomena between 6N^+ /DNA mixtures and SBGII showed similar results as of 3N^+ that the FRET signal was only obtained from the 6N^+ /DNA/SBGII mixture. It is thus indicates that 6N^+ can nicely interact with DNA to give and an effective energy transfer from the fluorophore donor acceptor dye via the association by electrostatic forces of DNA interaction. This result also suggests that the interaction between DNA and 6N^+ may be mainly achieved by coulombic interaction but not affect a whole structure.

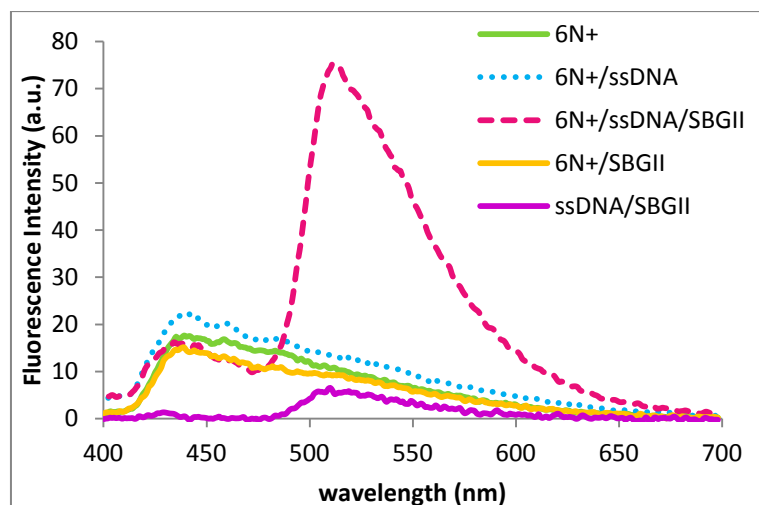


Figure 3.39 Emission spectra of $6N^+$ (1.0 μM) in the presence of ssDNA (5'CCTATATAGGTGATGCCTTCTCCGGCGACG3', $A_{260} = 0.05$) and SyBrGreenII (diluted at 10000X) in sodium phosphate buffer pH 7 (10 mM) and NaCl (150 mM) upon excitation at 376 nm.

To investigate the effect of DNA chain length onto the FRET responses of $6N^+$, we used DNA chain length of random sequences (0 – 30 bases, $A_{260} = 0.05$) in the presence of SBGII. Fluorescence spectra showed that FRET signals (F_{513}/F_{436}) was increased upon the addition of longer DNA chain length but not saturated at even the longest chain length at 30 bases (Figure 3.40). This result implies that DNA chain length with 30 bases has been not sufficiently long to encompass whole six branches of the $6N^+$ arc that is approximately needed at least around 41 bases of DNA chain length.

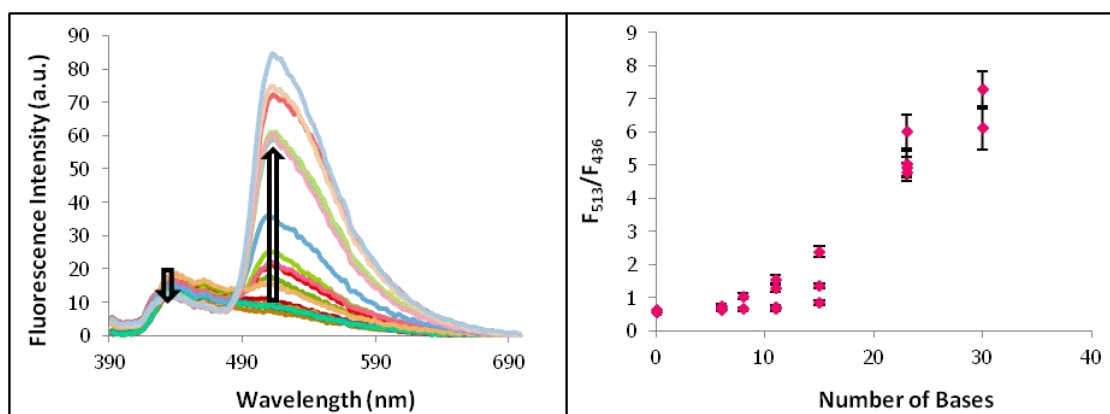


Figure 3.40 Emission spectra of $6N^+$ (1.0 μ M) in the present of various ssDNA chain lengths (0 to 30 bases and $A_{260} = 0.05$ of each ssDNA) in sodium phosphate buffer pH 7 (10 mM) and NaCl (100 mM) upon excitation at 376 nm.

These investigations of FRET phenomena between $6N^+$ and DNA described above bring us up to apply this interaction to be useful for the detection of DNA sequences via the DNA/PNA hybrid and FRET process of $6N^+$ and fluorescein commercial dye as demonstrated in our recent publication. [65]

3.7 Supramolecular interaction of $3N^+$ with BSA protein

Currently, our research group has successfully reported an effective fluorescence sensor array for the protein discrimination base on statistically analysis as principal component analysis that should be valuable for the development of electronic tongue for protein related food analysis and medical diagnosis. [62] It is thus interesting to investigate interactions of fluorophores and proteins. Therefore, $3N^+$ which showed to give sensitively fluorescence responses upon the addition of various proteins is a good probe for the study while bovine serum albumin (BSA, pI = 4.7 at 25°C) which is a useful protein in many applications is also a well-defined protein represent.

To investigate the interaction of $3N^+$ /BSA, absorption change and fluorescence response of $3N^+$ in the presence of BSA were studied. As shown in Figure 3.41, BSA dramatically enhanced the fluorescence signal of $3N^+$ with shorter wavelength while absorption caused a little shift to the longer wavelength. These results indicate that $3N^+$ can possibly interact with BSA relating to non-specific hydrophobic interactions

within higher level of three-dimensional protein structure and may cause slightly change of π -conjugation length of the fluorophore. It is possible involved with the geometrical lock of the fluorophore propeller-like structure or even reducing of solvent relaxation.

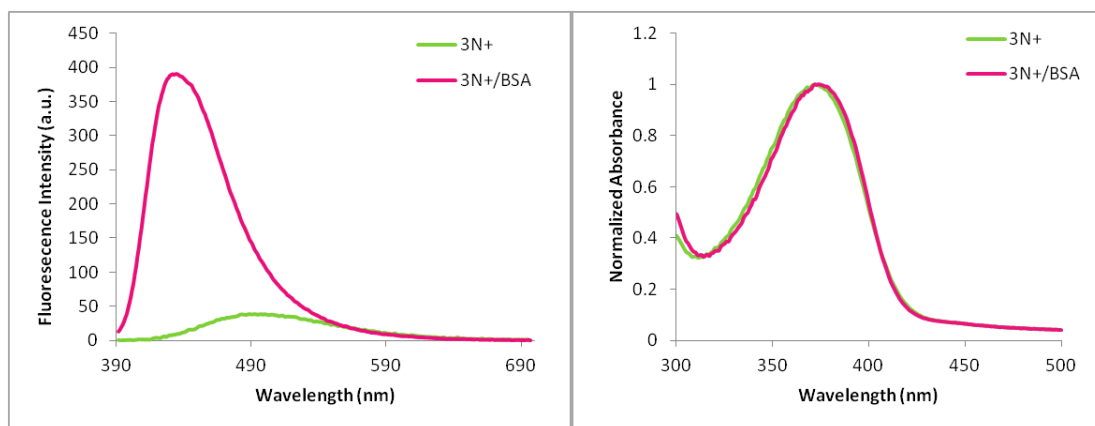


Figure 3.41 Fluorescence spectra (*left*) and Absorption spectra (*right*) of 3N^+ ($5\ \mu\text{M}$) in the present of BSA ($5\ \mu\text{M}$) in sodium phosphate buffer pH 7 (10 mM) and NaCl (100 mM) upon excitation at 370 nm.

To gain insight into the interaction contribution, CD spectroscopy of 3N^+ /BSA mixtures were investigated as shown in Figure 3.42. As an achiral compound, 3N^+ did not give any CD peaks in the range of 200-500 nm; however, BSA showed moderate induced CD negative signal of 3N^+ at around 300-450 nm which was corresponding to the π - π^* absorption of the phenylene-ethynylene conjugated system. The cotton effect of CD signal in this range is a good evidence for the restricted conformation of 3N^+ with an interior environment of protein relating to their hydrophobic parts. Moreover, characteristic peak of protein β -sheet around 240 nm was showed to be a smaller negative value than that of the original one. It is also suggesting that three-dimensional of tertiary protein structure become looser due to the interaction.

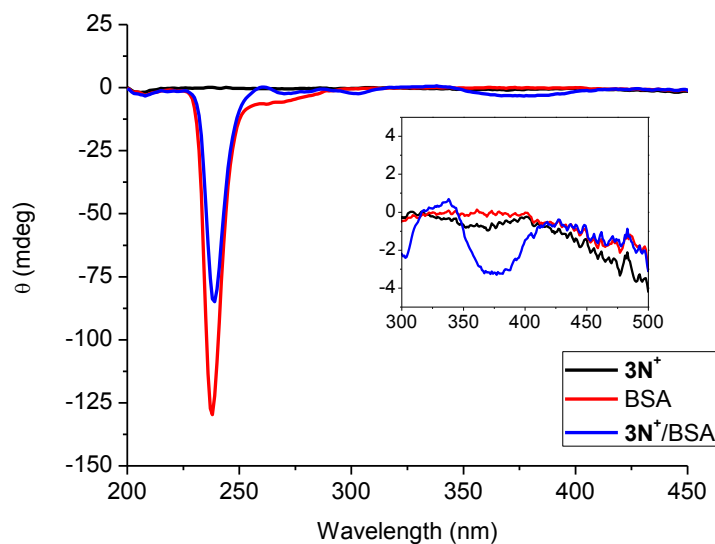


Figure 3.42 CD spectra of $3N^+$ ($10 \mu\text{M}$) in the presence of BSA ($10 \mu\text{M}$) in sodium phosphate buffer pH 7 (10 mM) and NaCl (100 mM) at $20 \text{ }^\circ\text{C}$.

In addition, the stoichiometric ratio of $3N^+$ /BSA binding were studied by varied the concentration of BSA from 0 to $100 \mu\text{M}$. From Figure 3.43, the results showed that fluorescence dramatically enhanced with shift to blue and saturated at 1.0 ratio of $[\text{BSA}]/[3N^+]$. This is indicating that BSA interacts with $3N^+$ with 1:1 stoichiometric complexation ratio.

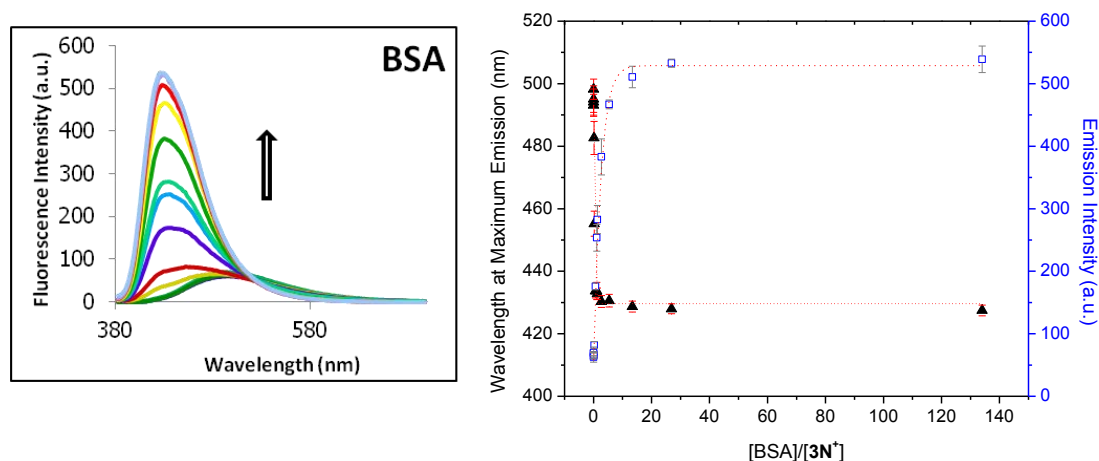


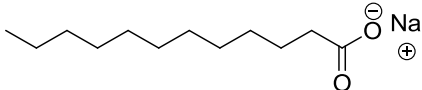
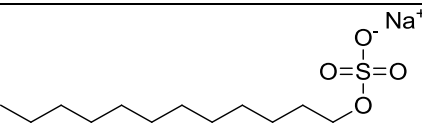
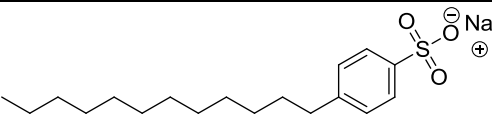
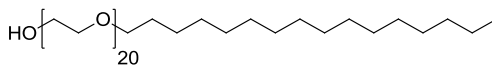
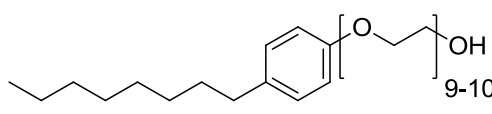
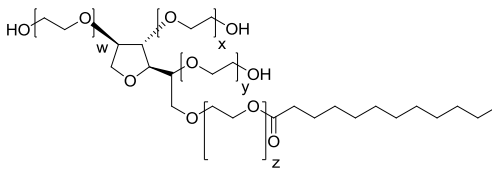
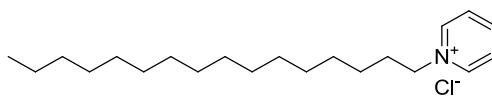
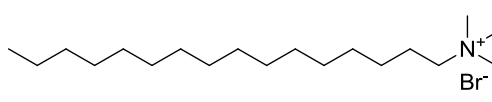
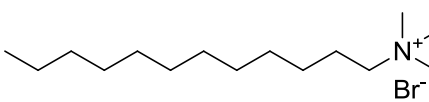
Figure 3.43 (*left*) Fluorescence spectra and (*right*) wavelength shifting at maximum emission (▲) and fluorescence intensity (□) of 3N^+ ($1\ \mu\text{M}$) with various concentrations ($0 - 100\ \mu\text{M}$) of BSA in sodium phosphate buffer pH 7 ($10\ \text{mM}$) and NaCl ($100\ \text{mM}$) upon excitation at $370\ \text{nm}$.

It is also confirm 1:1 complex by the Benesi-Hilderbrand double reciprocal plot to give the binding constant at $6.67 \times 10^5\ \text{M}^{-1}$ (Figure A.44).

3.8 Supramolecular interactions of 3N^+ and 6N^+ with surfactants

Recently, we have been reported the highly selective metal ion sensors such as for Hg^{2+} and Cu^{2+} ions in aqueous media via the quenching mechanism of phenylene-ethynylene fluorophores. These reports were also shown the improvement of the detection in the presence of Triton X-100, a non-ionic surfactant. [60-61] It is thus important to investigate the contribution of the interaction of the fluorophore with various types of surfactants. Therefore, our cationic fluorophores (3N^+ and 6N^+) were suitably represented to study the interaction modes with those surfactants. Various types of 9 surfactants that are represented from anionic, cationic and non-ionic surfactant structures and their CMC were shown in Table 3.2. Sodium dodecanoate (SDC), sodium dodecylsulfate (SDS) and sodium dodecylbenzenesulfonate (SDBS) were selected for anionic surfactant type, hexadecylpyridinium chloride (CPC), hexadecyltrimethylammonium bromide (CTAB) and dodecyltrimethylammonium bromide (DTAB) were selected for the cationic type, and Brij58, Triton X-100 and Tween20 were selected for the non-ionic surfactant representatives.

Table 3.2 Structures and CMC values of various types of surfactants. [179-196]

Surfactants	Structures	CMC (mol/dm ³)
Sodium dodecanoate (SDC)		2.5×10^{-2}
Sodium dodecylsulfate (SDS)		6.9×10^{-3}
Sodium dodecylbenzenesulfonate (SDBS)		1.3×10^{-3}
Brij58		7.7×10^{-6}
Triton X-100		2.5×10^{-4}
Tween20		1.1×10^{-5}
Hexadecylpyridinium chloride (CPC)		9.3×10^{-4}
Hexadecyltrimethylammonium bromide (CTAB)		7.0×10^{-4}
Dodecyltrimethylammonium bromide (DTAB)		1.41×10^{-2}

3.8.1 Fluorogenic responses with anionic surfactants

The concentration of anionic surfactants (SDC, SDS and SDBS) was varied from 0 to 100 mM, 3N^+ solution with the presence of the surfactants revealed the similar fluorescent pattern that fluorescence signal slightly decreased at very low surfactant concentration and then the emission intensity dramatically arose with blue

shift at higher surfactant concentration (Figure 3.44). This is indicating an electrostatic interaction between positive charges of 3N^+ and anionic surfactant head at very low concentration. Fluorescence self-quenching is increased by an aggregation of fluorophore molecules at this point. However, after a micelle assembly spontaneously formed, 3N^+ is disaggregated and be seeded into each micelle resulting to extremely fluorescence enhancement. The shift of emission wavelength is presented since the molecule aggregation through the micellization, these phenomena are possibly caused by a conformation restriction of the fluorophore molecule within the surfactant micelle.

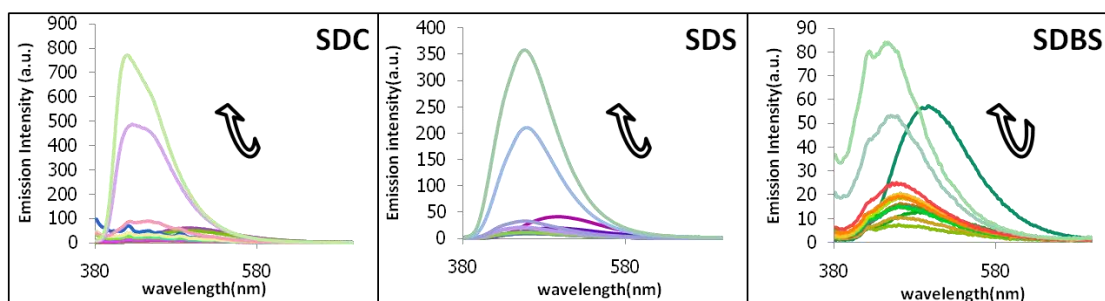
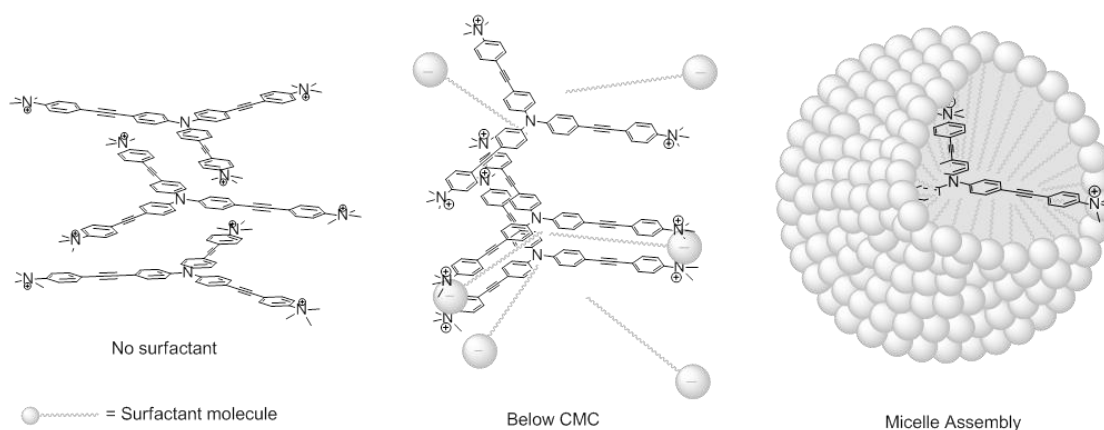


Figure 3.44 Fluorescence spectra of 3N^+ ($1\ \mu\text{M}$) with various concentrations ($0 - 100\ \text{mM}$) of anionic surfactants (SDC, SDS and SDBS) in MilliQ water at room temperature upon excitation at $370\ \text{nm}$.

Therefore, we hypothesize that an initially state without surfactant molecules, some 3N^+ aggregation are possibly formed in the aqueous media due to its hydrophobic part. But at below CMC, electrostatic interactions between anionic surfactant head and 3N^+ cationic peripheries are observed resulting to more aggregation and then at CMC point, surfactant micelles are spontaneously formed with the seeding of 3N^+ molecule inside their assembly as illustrated in Scheme 3.5.



Scheme 3.5 Purposed interactions of 3N^+ with anionic surfactant.

On the other hand, using 6N^+ as a micellization probe with the various concentration of SDS, fluorescence quenching was not observed even at very low surfactant concentration (**Figure 3.45**). This result suggests that more hydrophobicity of 6N^+ comparing to 3N^+ structure present highly aggregation at an initially state as noticed in much lower Φ_F ; therefore, the electrostatic interaction of anionic surfactant cannot relatively effect to the fluorescence quenching. Moreover, less blue shift of emission wavelength with larger fluorescence enhancement was shown at above CMC of surfactant comparing to fluorescence responses of 3N^+ with anionic surfactant. That is to say that the same reason as molecule rotation of 6N^+ are confined in the micelle to cause smaller stoke's shift and molecule disaggregation is then seeded into the micelle formation resulting to increasing of fluorescent signal.

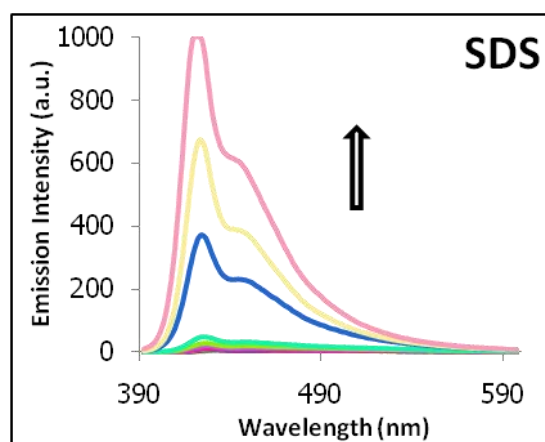


Figure 3.45 Fluorescence spectra of 6N^+ ($0.5 \mu\text{M}$) with various concentrations (0 – 100 mM) of SDS in MilliQ water at room temperature upon excitation 376 nm.

3.8.2 Fluorogenic responses with nonionic surfactants

The concentration of nonionic surfactants (Brij58, Triton X-100 and Tween20) was varied from 0 to 100 mM, 3N^+ mixtures in the presence of the surfactants revealed the similar fluorescent pattern as of anionic types that fluorescence signal were dramatically increased with shorter wavelength shift at higher surfactant concentration (Figure 3.46). Although the fluorescence quenching was not found in this initial state, it is indicating that the electrostatic interaction between fluorophore peripheries and surfactant heads is not found due to its nonionic surfactant head containing the neutral unit that cannot cause more molecule aggregation. However, emission intensity was dramatically enhanced at higher surfactant concentration suggesting the formation of micellization at above CMC.

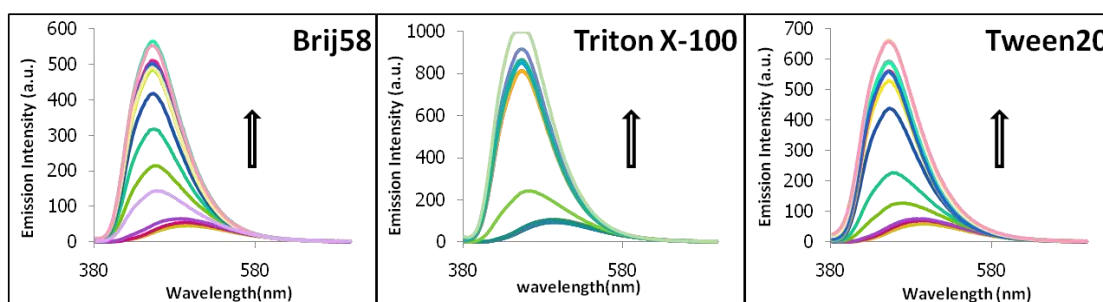


Figure 3.46 Fluorescence spectra of 3N^+ ($1\ \mu\text{M}$) with various concentrations (0 – 100 mM) of nonionic surfactants (Brij58, Triton X-100, Tween20) in MilliQ water at room temperature upon excitation at 370 nm.

In addition, using 6N^+ as a micellization probe with the various concentration of Triton X-100, the similar fluorescence responses were observed while the larger fluorescence enhancement showed less shift of emission wavelength comparing to 3N^+ (Figure 3.47). It is imply that more hydrophobicity of 6N^+ comparing to the 3N^+ structure cause more molecule disaggregation by its seeding into the micelle formation.

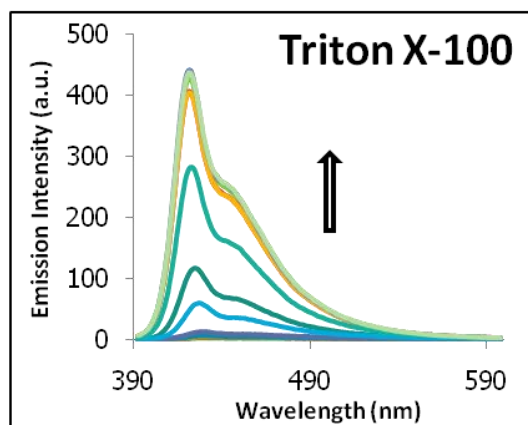


Figure 3.47 Fluorescence spectra of 6N^+ $0.1 \mu\text{M}$ with various concentrations (0 – 100 mM) of Triton X-100 in MilliQ water at room temperature upon excitation at 376 nm.

3.8.3 Fluorogenic responses with cationic surfactants

The concentration of cationic surfactants (CPC, CTAB and DTAB) was varied from 0 to 100 mM, 3N^+ mixtures in the presence of CTAB and DTAB showed the similar fluorescence response pattern as of non-ionic surfactants that fluorescence signals dramatically increased with blue shift at higher surfactant concentration (Figure 3.48). This result indicates that the electrostatic forces between positive charges of 3N^+ peripheries and cationic head of surfactants were not induced to form an aggregation while a little increasing of emission signals at these low surfactant concentrations suggest some ion-ion repulsions of their both positive charges. Also, the signals were extremely enhanced at a higher surfactant concentration indicating the micellization seeding to give the disaggregation of the fluorophore.

However, 3N^+ mixture in the presence of CPC displayed the fluorescent quenching and CPC had also never enhanced the fluorescent signal at even higher surfactant concentration. This indicates that pyridinium group of CPC head probably cause the better fluorescence quenching via an electron transfer from fluorophore unit of 3N^+ to the pyridinium group of CPC structure by the micelle organization.

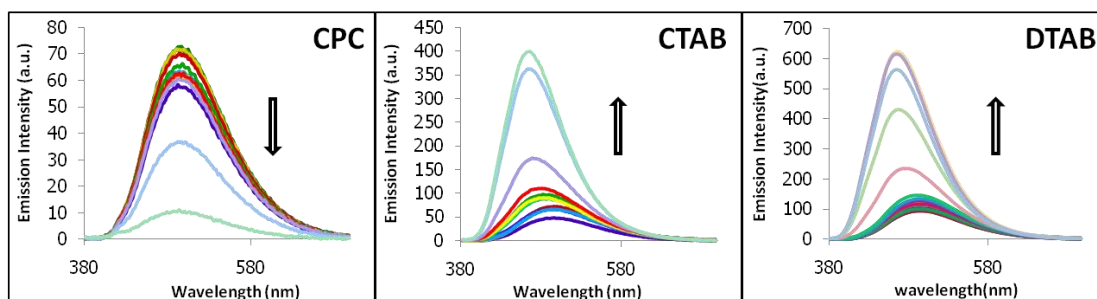


Figure 3.48 Fluorescence spectra of 3N^+ ($1\ \mu\text{M}$) with various concentrations (0 – 100 mM) of cationic surfactants (CPC, CTAB and DTAB) in MilliQ water at room temperature upon excitation at 370 nm.

In addition, using 6N^+ as a micellization probe with the various concentration of DTAB, the similar fluorescence responses were observed while the larger fluorescence enhancement showed less shift of emission wavelength comparing to 3N^+ (Figure 3.49). The results indicate that more hydrophobicity of 6N^+ comparing to the 3N^+ structure cause more molecule disaggregation by its seeding into the micelle formation as similar as other type of surfactants.

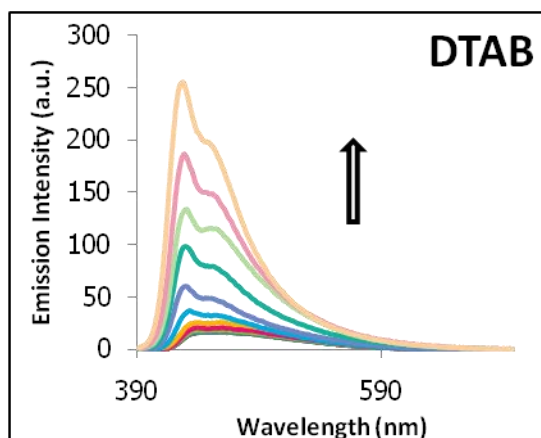


Figure 3.49 Fluorescence spectra of 6N^+ ($1\ \mu\text{M}$) with various concentrations (0 – 100 mM) of DTAB in MilliQ water at room temperature excited at 376 nm.

3.5.4 Determination of critical micelle concentration (CMC)

Since the different fluorescence responses upon the addition of surfactants were observed as previous results, fluorescent changing were rapidly growth at some points of surfactant concentrations. As we know that the critical micelle concentration (CMC) is defined as the concentration of surfactants above

which micelles are spontaneously formed. According to the hypothesis, our fluorophore containing both hydrophobic core and hydrophilic peripheries can induce the surfactant molecule to form micelle at the initially micelle state and after that molecule aggregation of the fluorophore is more discrete into each micelle assemblies; as a consequence, largely fluorescence enhancement can be noticeable at above this surfactant concentration. Therefore, at the point that the fluorescence intensity dramatically change can be applied to determine CMC of the surfactants as in fluorescence probe micellization method.

When the maximum fluorescence signals of $3N^+$ probe were plotted against log of surfactant concentrations following the Boltzman equation as demonstrated in Figure 3.50. From an example of the CMC determination of Triton X-100, sigmoid curve was fitted by using the OriginPro 8 program to get A_1 , A_2 , x_0 and Δx and the reflection point ($x_0 - 2\Delta x$) was derived to obtain CMC value.

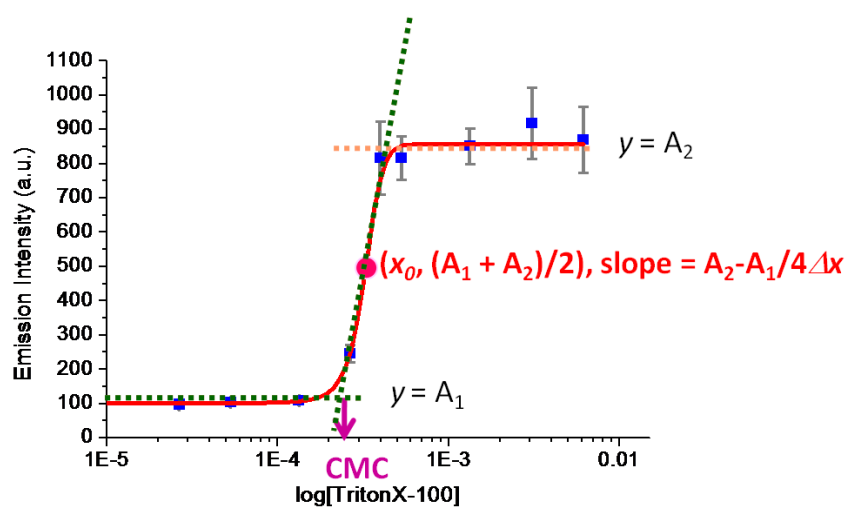


Figure 3.50 The CMC determination of Triton X-100 by fitted sigmoidal traces of graph plot an emission intensity of $3N^+$ against log of Triton X-100 concentration with the Boltzman equation.

Therefore, CMC of the surfactants by using our fluorophores as fluorescence micellization probes were compared with CMC from references as described in Table 3.3. The results showed that CMC of anionic and cationic surfactants were quite not close to that of the references as compared with that of non-ionic surfactants since

there were disturbing interactions between charges of surfactant heads and the fluorophore peripheries during the micelle assembly formation at below their CMC. While nonionic surfactants immediately can form any micelles whenever their concentration reaches the CMC without charge interferes. Besides, CMC of CPC yielded far off the reference values due to the electron transfer process. However, CMC from the 6N^+ probe presented lower value than that from the 3N^+ probe for all surfactant types, this is indicating that a bigger structure size with more both hydrophobicity and hydrophilic peripheries exhibit promptly micelle seeding resulting to less surfactant units requirement for micelle formation.

Table 3.3 The critical micelle concentration (CMC) of surfactants determined by the emission intensity changed of 3N^+ and 6N^+ probes in MilliQ water at room temperature.

Surfactants	CMC, (mol/dm ³)		
	3N^+	6N^+	References
SDC	2.02×10^{-2}	-	2.5×10^{-2} [a]
SDS	2.62×10^{-2}	2.26×10^{-2}	6.9×10^{-3} [b]
SDBS	6.00×10^{-3}	-	1.3×10^{-3} [c]
Brij58	1.95×10^{-5}	-	7.7×10^{-6} [d]
Tween20	2.85×10^{-5}	-	1.1×10^{-5} [c]
Triton-X100	2.42×10^{-4}	1.38×10^{-4}	2.5×10^{-4} [b]
CPC	4.10×10^{-2}	-	9.3×10^{-4} [c]
CTAB	9.63×10^{-3}	-	7.0×10^{-4} [b]
DTAB	9.26×10^{-3}	6.07×10^{-3}	1.4×10^{-2} [c]

Methods: a = Fluorescence probe micellization (ANS), b = Fluorescence probe micellization (3-pyrazolyl-2-pyrazoline derivative), c = surface tension, d = dye micellization (Acridine Orange dye)

In addition, our fluorophores can be useful to determine CMC of surfactants as the fluorescence micellization probes. Also, it is important to explain that Triton X-100, a non-ionic type, can improve the detection of metal ion as reported in our previous researches because the fluorescence signal of the fluorophore at the initial state is enhanced via the pre-micelle assembly process and then it can be easily

interfered by the metal ion that can specific bind stronger with the fluorophore to give the turn-off mode of those detection.

3.9 Comparison of supramolecular interactions of 3N^+ with various analytes

Finally, an absorption changes and fluorescence responses of 3N^+ that differently interacted with various kinds of analytes were shown in Table 3.4. We found that only γ -CyD that formed the stable inclusion complex with 3N^+ gave the absorption blue shift. This is possible imply that stable inclusion complexation of the fluorophore cause the change of electronic ground state of π -conjugation system. While the fluorescence enhancement seem relate with an increasing of the stoke's shift frequency indicating that emission enhancement of the interactions may be influenced by both geometrical restriction in the nano-confined environment and the reduction of solvent relaxation.

Table 3.4 Summary of absorption changes, fluorogenic responses and possible interactions of 3N^+ with various analytes.

Analytes	Interactions (K_b, M^{-1})	Absorption ($\lambda_{\text{max}}, \text{nm}$)	Emission ($\lambda_{\text{max}}, \text{nm}$)	Stoke's shift ($\Delta\lambda, \text{nm}$)	Emission enhancement (F/F_0)
Control (3N^+)	-	372	494	122	1.0
Surfactant (SDS)*	Micelle assembly	370	455	85	8.6
Polyanionic (PVSK)	Aggregation	370	467	97	0.1
β -CyD	Ion-Dipole (1.57×10^4)	370	480	110	3.6
γ -CyD	Stable inclusion complex (3.00×10^4)	364	436	72	8.0

Table 3.4 Summary of absorption changes, fluorogenic responses and possible interactions of **3N⁺** with various analytes (continue).

Analytes	Interactions (K_b , M^{-1})	Absorption (λ_{max} , nm)	Emission (λ_{max} , nm)	Stoke's shift ($\Delta\lambda$, nm)	Emission enhancement (F/F_0)
DNA	Coulombic forces (1.55×10^7)	379	458	79	3.8
BSA protein	Hydrophobic and Hydrophilic (6.67×10^5)	374	427	53	8.6

*Emission has been still increased.

These investigations should be useful for the future applications in designing of guest molecules and sensing of targets in the aqueous media.

CHAPTER IV

CONCLUSION

The fluorescence responses of five amphiphilic fluorophores (N^0N^+ , N^+ , 2N^+ , 3N^+ and 6N^+) with phenylene-ethynylene fluorogenic units in nano-confined environments of DNAs, BSA protein, surfactants and cyclodextrins in aqueous media were investigated. 3N^+ was one of the most responsive probes that showed strong fluorescence enhancement by all analytes. The ^1H NMR study and CD spectroscopy revealed the stable 1:1 inclusion complex of 3N^+ with γ -cyclodextrin. The strong fluorescence enhancement of 3N^+ in the presence of ssDNA chain led to the design of fluorescence aptasensing system for determination of potassium ion. The highest fluorescence enhancement of 3N^+ was observed with BSA protein probably due to effective reduction of self-quenching via both hydrophobic and hydrophilic interaction. It is also used as a fluorescence micellization probe to determine CMC of surfactants. In the case of 6N^+ , the fluorescence enhancements were observed only for BSA protein and surfactants but not for DNA and cyclodextrins. The interaction of 6N^+ with ssDNA was thus proven by FRET experiments which showed strong FRET signals that are used in the DNA sequence detection.

Suggestion for future work: Next study should focus on the discrimination of cyclodextrin in real sample and the investigation of charge effect onto micelle system.

REFERENCES

- [1] Epstein, J. R.; Biran, I. and Walt, D. R. Fluorescence-based nucleic acid detection and microarrays. *Anal. Chim. Acta* 469 (2002): 3-36.
- [2] Ihmels, H. and Otto, D. Intercalation of Organic Dye Molecules into Double-Stranded DNA-General Principles and Recent Developments. *Top. Curr. Chem.* 258 (2005): 161-204.
- [3] Ihmels, H.; Faulhaber, K.; Vedaldi, D.; Dall'Acqua, F. and Viola, G. Intercalation of Organic Dye Molecules into Double-stranded DNA Part 2: The Annealated Quinolizinium Ion as a Structural Motif in DNA Intercalators. *Photochem. Photobiol.* 81 (2005): 1107-1115.
- [4] Armitage, B. A. Cyanine Dye-DNA Interactions: Intercalation, Groove Binding, and Aggregation. *Top. Curr. Chem.* 253 (2005): 55-76.
- [5] Yeung, E. S. High-Throughput Single Molecule Screening of DNA and Proteins. *Chem. Rec.* 1 (2001): 123-139.
- [6] Hawe, A.; Sutter, M. and Jiskoot, W. Extrinsic Fluorescent Dyes as Tools for Protein Characterization. *Pharm. Res.* 25 (2008): 1487-1499.
- [7] Maeztu, R.; Tardajos, G. and Gonzalez-Gaitano, G. Natural cyclodextrins as efficient boosters of the chemiluminescence of luminol and isoluminol: exploration of potential applications. *J. Phys. Chem. B* 114 (2010): 2798-2806.
- [8] Uekama, K.; Hirayama, F. and Irie, T. Cyclodextrin Drug Carrier Systems. *Chem. Rev.* 98 (1998): 2045-2076.
- [9] Dsouza, R.N.; Pischel, U. and Nau, W. M. Fluorescent dyes and their supramolecular host/guest complexes with macrocycles in aqueous solution. *Chem. Rev.* 111 (2011): 7941-7980.

- [10] Horvath, G.; Premkumar, T.; Boztas, A.; Lee, E.; Jon, S. and Geckeler, K.E. Supramolecular Nanoencapsulation as a tool: solubilization of the anticancer drug trans-dichloro(dipyridine)platinum (II) by complexation with β -cyclodextrin. *Mol. Pharmaceutics* 5 (2008): 358-361.
- [11] Xu, D.; Wang, X. and Ding, L. Spectroscopic studies on the interaction of γ -cyclodextrin-daunorubicin inclusion complex with herring sperm DNA. *Carbohydr. Polym.* 83 (2011): 1257-1262.
- [12] Hedges, A. R. Industrial Applications of Cyclodextrins. *Chem. Rev.* 98(1998): 2035-2044.
- [13] Wang, L.; Bian, G.; Wang, L.; Dong, L.; Chen, H. and Xia, T. Fluorescence determination of DNA with 1-pyrenebutyric acid nanoparticles coated with β -cyclodextrin as a fluorescence probe. *Spectrochim. Acta. A* 61(2005): 1201-1205.
- [14] Chaturvedi, K.; Ganguly, K.; Kulkarni, A. R.; Kulkarni, V. H.; Nadagouda, M. N.; Rudzinski, W. E. and Aminabhavi, T. M. Cyclodextrin-based siRNA delivery nanocarriers: a state-of-the-art review. *Expert Opin. Drug Deliv.* 8 (2011): 1455-1468.
- [15] Moya-Ortega, M. D.; Alvarez-Lorenzo, C.; Sigurdsson, H. H. and Concheiro, T. L. Cross-linked hydroxypropyl- β -cyclodextrin and γ -cyclodextrin nanogels for drug delivery: Physicochemical and loading/release properties. *Carbohydr. Polym.* 87 (2012): 2344-2351.
- [16] Chen, Z.; Xue, C.; Shi, W.; Luo, F.T.; Green, S.; Chen, J. and Lui, H. Selective and Sensitive Fluorescent Sensors for Metal Ions Based on Manipulation of Side-Chain Compositions of Poly(p-Phenyleneethynylene)s. *Anal. Chem.* 76 (2004): 6513-6518.
- [17] Chen, Y.G.; Zhao, D.; He, Z.K. and Ai, X.P. Fluorescence quenching of water-soluble conjugated polymer by metal cations and its application in sensor. *Spectrochim. Acta A* 66 (2007): 448-452.

- [18] Lui, Y. and Schanze, K.S. Conjugated polyelectrolyte-Based Real-Time Fluorescence Assay for Alkaline Phosphatase with Pyrophosphate as Substrate. *Anal. Chem.* 80 (2008): 8605-8612.
- [19] Chen, L.; McBranch, D.W.; Wang, H.L.; Helgeson, R.; Wudl, F. and Whitten, D.G. Highly sensitive biological and chemical sensors based on reversible fluorescence quenching in a conjugated polymer. *Proc. Natl. Acad. Sci. USA.* 96 (1999): 12287-12292.
- [20] Wang, D.; Gong, X.; Heeger, P.S.; Rininsland, F.; Bazan, G.C. and Heeger, A.J. Biosensors from conjugated polyelectrolyte complexes. *Proc. Natl. Acad. Sci. USA.* 99 (2002): 49-53.
- [21] Fan, C.; Plaxco, K.W. and Heeger, A.J. High-Efficiency Fluorescence Quenching of Conjugated polymers by Proteins. *J. Am. Chem. Soc.* 124 (2002): 5642-5643.
- [22] Dwight, S.J.; Gaylord, B.S.; Hong, J.W. and Bazan, G.C. Perturbation of Fluorescence by nonspecific Interactions between Anionic Poly(phenylenevinylene)s and proteins: Implications for Biosensors. *J. Am. Chem. Soc.* 126 (2004): 16850-16859.
- [23] Pinto, M.R. and Schanze, K.S. Amplified fluorescence sensing of protease activity with conjugated polyelectrolytes. *Proc. Natl. Acad. Sci. USA.* 101 (2004): 7505-7510.
- [24] An, L.; Tang, Y.; Feng, F.; He, F. and Wang, S. Water-soluble conjugated polymers for continuous and sensitive fluorescence assays for phosphatase and peptidase. *J. Mater. Chem.* 17 (2007): 4147-4152.
- [25] Gaylord, B.S.; Heeger, A.J. and Bazan, G.C. DNA detection using water-soluble conjugated polymers and peptide nucleic acid probes. *Proc. Natl. Acad. Sci. USA.* 99 (2002): 10954-10957.
- [26] Liu, B. and Bazan, G.C. Homogeneous Fluorescence-Based DNA Detection with Water-Soluble Conjugated Polymers. *Chem. Mater.* 16 (2004): 4467-4476.

- [27] Doré, K.; Dubus, S.; Ho, H.A.; Lévesque, I.; Brunette, M.; Corbiel, G.; Boissinot, M.; Boivin, G.; Bergeron, M.G.; Boudreau, D. and Leclerc, M. Fluorescent Polymeric transducer for the Rapid, Simple, and Specific Detection of Nucleic Acids at the Zeptomole Level. *J. Am. Chem. Soc.* 126 (2004): 4240-4244.
- [28] Gaylord, B.S.; Massie, M.R.; Feinstein, S.C. and Bazan, G.C. SNP detection using peptide nucleic acid probes and conjugated polymers: Applications in neurodegenerative disease identification. *Proc. Natl. Acad. Sci. USA.* 102 (2005): 34-39.
- [29] Wang, Y. and Liu, B. Silica nanoparticle assisted DNA assays for optical signal amplification of conjugated polymer based fluorescent sensors. *Chem. Commun.* (2007): 3553-3555.
- [30] Woo, H.Y.; Nag, O.K.; Kim, J.; Kang, M. and Bazan, G.C. Water-Soluble polyelectrolytes for FRET-based DNA Detection. *Mol. Cryst. Liq. Cryst.* 486 (2008): 244-249.
- [31] Lakowicz, J.R. *Principles of Fluorescence Spectroscopy*. LLC, Singapore: Springer Science+Business Media, 2006.
- [32] Zheng, W. and He, L. Label-Free, Real-Time Multiplexed DNA Detection Using Fluorescent Conjugated Polymers. *J. Am. Chem. Soc.* 131 (2009): 3432-3433.
- [33] Lee, K.; Povlich, L.K. and Kim, J. Label-Free and Self-Signal Amplifying Molecular DNA Sensors Based on Bioconjugated Polyelectrolytes. *Adv. Funct. Mater.* 17 (2007): 2580-2587.
- [34] Chi, C.; Mikhailovsky, A. and Bazan, G.C. Design of Cationic Conjugated Polyelectrolytes for DNA Concentration Determination. *J. Am. Chem. Soc.* 129 (2007): 11134-11145.
- [35] Ren, X. and Xu, Q.H. Label-Free DNA Sequence Detection with Enhanced Sensitivity and Selectivity Using Cationic Conjugated Polymers and PicoGreen. *Langmuir* 25 (2009): 43-47.
- [36] Heeger, P.S. and Heeger, A.J. Making sense of polymer-based biosensors. *Proc. Natl. Acad. Sci. USA.* 96 (1999): 12219-12221.

- [37] Tan, C.; Pinto, M.R. and Schanze, K.S. Photophysics, aggregation and amplified quenching of a water-soluble poly(phenylene ethylene). *Chem. Commun.* (2002): 446-447.
- [38] Rininsland, F.; Xia, W.; Wittenburg, S.; Shi, X.; Stankewicz, C.; Achyuthan, K.; McBranch, D. and Whitten, D. Metal ion-mediated polymer superquenching for highly sensitive detection of kinase and phosphatase activities. *Proc. Natl. Acad. Sci. USA.* 101 (2004): 15295-15300.
- [39] Liu, B.; Gaylord, B.S.; Wang, S. and Bazan, G.C. Effect of Chromophore-Charge Distance on the Energy Transfer Properties of Water-Soluble Conjugated Oligomers. *J. Am. Chem. Soc.* 125 (2003): 6705-6714.
- [40] Gaylord, B.S.; Wang, S.; Heeger, A.J. and Bazan, G.C. Water-Soluble Conjugated Oligomers: Effect of Chain Length and Aggregation on Photoluminescence-Quenching Efficiencies. *J. Am. Chem. Soc.* 123 (2001): 6417-6418.
- [41] Vuorimaa, E.; Urtti, A.; Seppänen, R.; Lemmetyinen, H. and Yliperttula, M. Time-Resolved Fluorescence Spectroscopy Reveals Functional Differences of Cationic Polymer-DNA Complexes. *J. Am. Chem. Soc.* 130 (2008): 11695-11700.
- [42] Ghzaoui, A.E.; Gauffre, F.; Caminade, A.M.; Majoral, J.P. and Lannibois-Drean, H. Self-Assembly of Water-Soluble Dendrimers into Thermoreversible Hydrogels and Macroscopic Fibers. *Langmuir* 20 (2004): 9348-9353.
- [43] Kaanumalle, L.S.; Ramesh, R.; Maddipatla, V.S.N., M.; Nithyanandhan, J.; Jayaraman, N. and Ramamurthy, V. Dendrimers as Photochemical Reaction Media. Photochemical Behavior of Unimolecular and Bimolecular Reactions in Water-Soluble Dendrimers. *J. Org. Chem.* 70 (2005): 5062-5069.
- [44] Newkome, G.R.; Moorefield, C.N. and Vögtle, F. *Dendrimers and Dendrons: Concepts, Syntheses, Applications.* Weinheim, Germany: Wiley-VCH, 2001.

- [45] Tang, S.; Martinez, L.J.; Sharma, A. and Chai, M. Synthesis and Characterization of Water-Soluble and Photostable L-DOPA Dendrimers. *Org. Lett.* 8 (2006): 4421-4424.
- [46] Adronov, A.; Gilat, S.L.; Fréchet, J., M.J.; Ohta, K.; Neuwahl, F., V.R. and Fleming, G.R. Light Harvesting and Energy transfer in Laser-Dye-Labeled poly(aryl ether) Dendrimers. *J. Am. Chem. Soc.* 122 (2000): 1175- 1185.
- [47] Wang, S.; Hong, J.W. and Bazan, G.C. Synthesis of Cationic Water-Soluble Light-Harvesting Dendrimers. *Org. Lett.* 7 (2005): 1907-1910.
- [48] Nantalaksakul, A.; Dasari R.R.; Ahn, T.S.; Al-Kaysi, R.; Bardeen, C.J. and Thayumanavan, S. Dendrimer Analogues of Linear Molecules to Evaluate Energy and Charge-transfer properties. *Org. Lett.* 8 (2006): 2981-2984.
- [49] Satoh, N.; Nakashima, T. and Yamamoto, K. Metal-Assembling Dendrimers with a Triarylamine Core and Their Application to a Dye-Sensitized Solar Cell. *J. Am. Chem. Soc.* 127 (2005): 13030-13038.
- [50] Maus, M.; De, R.; Lor, M.; Wiel, T.; Mitra, S.; Wiesler, U.M.; Herrmann, A.; Hofkens, J.; Vosh, T.; Müllen, K. and De Schryver, F.C. Intramolecular Energy hopping and Energy Trapping in polyphenylene dendrimers with Multiple Peryleneimide Donor Chromophores and a Terryeneimide Acceptor Trap Chromophore. *J. Am. Chem. Soc.* 123 (2001): 7668-7676.
- [51] Gabb, K.M.; Thompson, A.L.; Xu, J.; Martinez, T.J. and Bardeen, C.J. Meta-Conjugation and excited-State Coupling in Phenylacetylene Dendrimers. *J. Am. Chem. Soc.* 125 (2003): 9288-9289.
- [52] Stone, D.L.; Smith, D.K. and McGrail, P.T. Ferrocene Encapsulated within Symmetric Dendrimers: A Deeper Understanding of Dendritic Effects on Redox potential. *J. Am. Chem. Soc.* 124 (2002): 856-864.

- [53] Arik, M.; Meral, K. and Onganer, Y. Effect of surfactant on the aggregation of pyronin B and pyronin Y in aqueous solution. *J. Lumin.* 129 (2009): 599-604.
- [54] Tolosa, J. and Bunz, U.H.F. Water Soluble Cruciforms: Effect of Surfactants on Fluorescence. *Chem. Asian. J.* 4 (2009): 270-276.
- [55] Pesak, D.J. and Moore, J.S. Synthesis and Characterization of Water-Soluble Dendritic Macromolecules with a Stiff, Hydrocarbon Interior. *Macromolecules* 30 (1997): 6467-6482.
- [56] McIlroy, S.P.; Cló, E.; Nikolajasen, L.; Frederiksen, P.K.; Nielsen, C.B.; Mikkelsen, K.V.; Gothelf, K.V.; Ogilby, P.R. Two-Photon Photosensitized Production of Singlet Oxygen: Sensitizers with Phenylene-Ethylene-Based Chromophores. *J. Org. Chem.* 70 (2005): 1134-1146.
- [57] Kim, I.; Dunkhorst, A.; Gilbert, J. and Bunz, U.H.F. Sensing of Lead Ions by a Carboxylate-Substituted PPE: Multivalency Effects. *Macromolecules* 38 (2005): 4560-4562.
- [58] Rodriguez, J.G.; Esquivias, J.; Lafuente, A. and Rubio, L. Synthesis of conjugated 2 and 2,5-(ethenyl) and (ethynyl)phenylethynyl thiophenes: fluorescence properties. *Tetrahedron* 62 (2006): 3112-3122.
- [59] Zhang, X.; Ren, X.; Xu, Q.; Ping Loh, K. and Chen, Z. One- and Two-Photon Turn-on Fluorescent Probe for Cysteine and Homocysteine with Large Emission Shift. *Org. Lett.* 11 (2009): 1257-1260.
- [60] Niamnont, N.; Siripornnoppakhun, W.; Rashatasakhon P. and Sukwattanasinitt, M. A polyanionic Dendritic Fluorophore for Selective Detection of Hg^{2+} in Triton X-100 Aqueous Media. *Org. Lett.* 11 (2009): 2768-2771.
- [61] Sirilaksanapong, S.; Sukwattanasinitt, M.; Rashatasakhon, P. 1,3,5-Triphenylbenzene fluorophore as a selective Cu^{2+} sensor in aqueous media. *Chem. Commun.* 48 (2012): 293-295.

- [62] Niamnont, N.; Mungkarndee, R.; Techakriengkrai, I.; Rashatasakhon, P. and Sukwattanasinitt, M. Protein discrimination by fluorescent sensor array constituted of variously charged dendritic phenylene-ethynylene fluoroophores. *Biosens. Bioelectron.* 26 (2010): 863-867.
- [63] Davis, B. W.; Niamnont, N.; Dillon, R.; Bardeen, C. J.; sukwattanasinitt, M. and Cheng, Q. FRET detection of proteins using fluorescently doped electrospun nanofibers and pattern recognition. *Langmuir* 27 (2011): 6401-6408.
- [64] Yuanboonlim, W.; Siripornnoppakhun, W.; Niamnont, N.; Rashatasakhon, P.; Vilaivan, T. and Sukwattanasinitt, M. Phenylene-ethynylene trication as an efficient fluorescent signal transducer in an aptasensor for potassium ion. *Biosens. Bioelectron.* 33 (2012): 17-22.
- [65] Rashatasakhon, P.; Vongnam, K.; Siripornnoppakhun, W.; Vilaivan, T. and Sukwattanasinitt, M. FRET detection of DNA sequence via electrostatic interaction of polycationic phenyleneethynylene dendrimer with DNA/PNA hybrid. *Talanta* 88 (2012): 593-598.
- [66] Moisés de Oliveira, H.P. and Gehlen, M.H. Characterization of Mixed Micelles of Sodium Dodecyl Sulfate and Tetraoxyethylene Dodecyl Ether in Aqueous Solution. *Langmuir* 18 (2002): 3792-3796.
- [67] Rangel-Yagui, C.O.; Pessoa-Jr, A. and Costa Tavares, L. Micellar solubilization of drugs. *J. Pharm. Pharmaceut. Sci.* 8 (2005): 147-163.
- [68] Arumugam, S.; Vutukuri, D.R.; Thayumanavan, V.S. and Ramamurthy, V. Amphiphilic Homopolymer as a Reaction Medium in Water: Product Selectivity within Polymeric Nanopockets. *J. Am. Chem. Soc.* 127 (2005): 13200-13206.
- [69] Mohr, A.; Talbiersky, P.; Korth, H.G.; Boese, R.; Bläser, D. and Rehage, H. A New Pyrene-Based Fluorescent Probe for the Determination of Critical Micelle Concentrations. *J. Phys. Chem. B* 111 (2007): 12985-12992.

- [70] Mehta, S.K.; Chaudhary, S.; Kumar, R. and Bhasin, K.K. Facile Solubilization of Organochalcogen Compounds in Mixed Micelle Formation of Binary and Ternary Cationic-Nonionic Surfactant Mixtures. *J. Phys. Chem. B* 113 (2009): 7188-7193.
- [71] Langevin, D. Complexation of oppositely charged polyelectrolytes and surfactants in aqueous solutions. A review. *Adv. Colloid Interface Sci.* 147-148 (2009): 170-177.
- [72] Piculell, L.; Norrman, J.; Svensson, A. V.; Lynch, I.; Bernardes, J. S. and Loh, W. Ionic surfactants with polymeric counterions. *Adv. Colloid Interface Sci.* 147-148 (2009): 228-236.
- [73] González-Pérez, A.; Dias, R. S.; Nylander, T. and Lindman, B. Cyclodextrin-surfactant complex: A new route in DNA decompaction. *Biomacromol.* 9 (2008): 772-775.
- [74] Al Attar, H.A.; Norden, J.; Ó'Brien, S. and Monkman, A.P. Improved single nucleotide polymorphisms detection using conjugated polymer/surfactant system and peptide nucleic acid. *Biosens. Bioelectron.* 23 (2008): 1466-1472.
- [75] Xiaofang, Z.; Yazhuo, S.; Honglai, L.; Ying, H. and Jainwen, J. Interaction of DNA with Cationic Gemini Surfactant Trimethylene-1,3 bis (dodecyldimethyl-ammonium bromide) and Anionic Surfactant SDS Mixed System. *Chin. J. Chem. Eng.* 126 (2008): 923-928.
- [76] Humpolíčková, J.; Beranová, L.; Štěpánek, M.; Benda, A.; Procházka, K. and Hof, M. Fluorescence Lifetime Correlation Spectroscopy Reveals Compaction Mechanism of 10 and 49 kbp DNA and Differences between Polycationic and Cationic Surfactant. *J. Phys. Chem. B* 112 (2008): 16823-16829.
- [77] Guo, X.; Cui, B.; Li, H.; Gong, Z. and Guo, R. Facilitation Effect of Oligonucleotide on Vesicle Formation from Single-Chained Cationic Surfactant- Dependences of Oligonucleotide Sequence and Size and Surfactant Structure. *J. Polym. Sci. Pol. Chem.* 47 (2009): 434-449.

- [78] Lee, H. and Mijović, J. Bio-nano complexes: DNA/surfactant/single-walled carbon nanotube interactions in electric field. *Polymer* 50 (2009): 881-890.
- [79] Vongsetkul, T.; Taylor, D.J.F.; Zhang, J.; Li, P.X.; Thomas, R.K. and Penfold, J. Interaction of a Cationic Gemini Surfactant with DNA and with Sodium Poly(styrene sulphonate) at the Air/water Interface: A Neutron Reflectometry Study. *Langmuir* 25 (2009): 4027-4035.
- [80] Cheng, X.; Bing, T.; Liu, X. and Shanguan, D. A label-free fluorescence sensor for probing the tineteraction of oligonucleotides with target molecules. *Anal. Chim. Acta* 633 (2009): 97-102.
- [81] Al Attar, H.A. and Monkman, A.P. Effect of Surfactant on FRET and Quenching in DNA sequence Detection Using Conjugated Polymers. *Adv. Funct. Mater.* 18 (2008): 2498-2509.
- [82] Douhal, A. Ultrafast guset dynamics in cyclodextrin nanocativies. *Chem. Rev.* 104 (2004): 1955-1976.
- [83] Sahu, K.; Kumar Mondal, S.; Ghosh S. and Bhattacharyya, K. Ultrafast dynamics in biological systems and in nano-confined environments. *Bull. Chem. Soc. Jpn.* 80 (2007): 1033-1043.
- [84] Das, P.; Chakrabarty, A.; Haldar, B.; Mallick, A. and Chattopadhyay, N. Effect of cyclodextrin nanocavity confinement on the photophysics of a b-carboline analogue: A spectroscopic study. *J. Phy. Chem. B* 111 (2007): 7401-7408.
- [85] Rao, V. G.; Ghatak, C.; Pramanik, R.; Sarkar, S. and Sarkar, N. Solvation and rotaional dynamics of soumarin-153 in ethylammonium nitrate containing g-cyclodextrin. *J. Phys. Chem. B* 115 (2011): 10500-10508.
- [86] Lehn, J. M. Supramolecular chemistry. *Science* 260 (1993): 1762-1763.
- [87] Steed, J. W.; Turner, D. R. and Wallace, K. J. *Core concepts in supramolecular chemistry and nanochemistry*. West Sussex, England: John Wiley & Sons, Ltd, 2007.

- [88] Cram, D. J. Preorganisation – from solvents to spherands. *Angew. Chem., Int. Ed. Engl.* 25 (1986): 1039–1134.
- [89] Steed, J. W. and Atwood, J. L. *Supramolecular chemistry*. West Sussex, England: John Wiley & Sons, Ltd, 2009.
- [90] Lindoy, L. F. and Atkinson, I. M. *Self-assembly in supramolecular systems*. Cambridge, UK: The Royal Society of Chemistry, 2000.
- [91] Lee, Y. S. *Self-assembly and nanotechnology: a force balance approach*. Hoboken, New Jersey: John Wiley & Sons, Inc., 2008.
- [92] Ariga, K. and Kunitake, T. *Supramolecular chemistry-Fundamentals and Applications: Advance textbook*. Leipzig, Germany: Springer-Verlag Berlin Heidelberg, 2006.
- [93] Cragg, P. J. *Supramolecular chemistry: From biological inspiration to biomedical applications*. Houten, Netherlands: Springer Science + Business Media B.V., 2010.
- [94] Leeuwen, P.W.N.M. *Supramolecular catalysis*. Weinheim, Germany: WILEY-VCH Verlag GmbH & Co. KGaA, 2008.
- [95] ChengHe, Z.; LinLing, G.; YiYi, Z.; GuangZhou, W.; Lei, J. and RongXia, G. Review on supermolecules as chemical drugs. *Sci. China. Ser. B-Chem.* 52 (2009): 415-458.
- [96] Connors, K. A. The Stability of Cyclodextrin Complexes in Solution. *Chem. Rev.* 97 (1997): 1325-1357.
- [97] Martin Del Valle, E.M. Cyclodextrins and their uses: a review. *Proc. Biochem.* 39 (2004): 1033-1046.
- [98] Dodziuk, H. *Cyclodextrins and Their Complexes: Chemistry, Analytical Methods, Applications*. Wienheim, Germany: Wiley-VCH Verlag, 2006.
- [99] Szejtli, J. Introduction and General Overview of Cyclodextrin Chemistry. *Chem. Rev.* 98 (1998): 1743-1753.
- [100] Wenz, G.; Han, B.-H. and Müller, A. Cyclodextrin Rotaxanes and Polyrotaxanes. *Chem. Rev.* 106 (2006): 782-817.
- [101] Chernykh, E. V. and Brichkin, S. B. Supramolecular complexes based on cyclodextrins. *High Energy Chem.* 44 (2010): 115-133.

- [102] Hedges, A. R. Industrial Applications of Cyclodextrins. *Chem. Rev.* 98 (1998): 2035-2044.
- [103] Schneider, H.-J.; Hacket, F. and Rüdiger, V. Ikeda, H. NMR Studies of Cyclodextrins and Cyclodextrin Complexes. *Chem. Rev.* 98 (1998): 1755-1785.
- [104] Chen, M.; Diao, G. and Zhang, E. Study of inclusion complex of β -cyclodextrin and nitrobenzene. *Chemosphere* 63 (2006): 522-529.
- [105] Sompornpisut, P.; Deechalao, N. and Vongsvivut, J. An inclusion complex of β -cyclodextrin-L-phenylalanine: ^1H NMR and molecular docking studies. *Science Asia* 28 (2002): 263-270.
- [106] Kato, K.; Sasakawa, H.; Kamiya, Y.; Utsumi, M.; Nakano, M.; Takahashi, N. and Yamaguchi, Y. 920 MHz ultra-high field NMR approaches to structural glycobiology. *Biochim. Biophys. Acta.* 1780 (2008): 619-625.
- [107] Cong, X.; Czerwieniec, G.; McJimpsey, E.; Ahn, S.; Troy, F. A. and Lebrilla, C. B. Structural relationships in small molecule interactions governing gas-phase enantioselectivity and zwitterionic formation. *J. Am. Soc. Mass Spectrom.* 17 (2006): 442-454.
- [108] Verlaysen, K.; Sabah, S.; Scriba, G.; Chen, A. and Sandra, P. Evaluation of the enantioselective possibilities of sulfated cyclodextrins for the separation of aspartyl di- and tripeptides in capillary electrophoresis. *J. Chroma. A* 824 (1998): 91-97.
- [109] Hbaieb, S.; Kalfat, R.; Chevalier, Y.; Amdouni, N. and Parrot-Lopez, H. Influence of the substitution of cyclodextrins by cationic groups on the complexation of organic anions. *Mater. Sci. Eng. C* 28 (2008): 697-704.
- [110] Wang, L.; Bian, G.; Wang, L.; Dong, L.; Chen, H. and Xia, T. Fluorescence determination of DNA with 1-pyrenebutyric acid nanoparticles coated with β -cyclodextrin as a fluorescence probe. *Spectrochim. Acta. A* 61(2005): 1201-1205.

- [111] Al-Hassan, K. A.; Saleh, N.; Abu-Abdoun, I. I. and Yousef, Y. A. Inclusion as a driving force for the intramolecular charge transfer (ICT) fluorescence of p-(N,N-diphenylamino)benzoic acid methylester (DPABME) in α -cyclodextrin (α -CD) aqueous solution. *J. Incl. Phenom. Macrocycl. Chem.* 61 (2008): 361-365.
- [112] Zhang, H.-X.; Huang, X. and Zhang, M. Thermodynamic studies on the interaction of dioxopromethazine to β -cyclodextrin and bovine serum albumin. *J. Fluoresc.* 18 (2008): 753-760.
- [113] Chakraborty, A. and Guchhait, N. Inclusion complex of charge transfer probe 4-amino-3-methylbenzoic acid methyl ester (AMBME) with β -CD in aqueous and non-aqueous medium: medium dependent stoichiometry of the complex and orientation of probe molecule inside β -CD nanocavity. *J. Incl. Phenom. Macrocycl. Chem.* 62 (2008): 91-97.
- [114] Vijayan Enoch, M.; Rajamohan, R. and Swanimathan, M. Fluorimetric and prototropic studies on the inclusion complexation of 3,3'-diaminodiphenylsulphone with β -cyclodextrin and its unusual behavior. *Spectrochim. Acta. A* 77 (2010): 473-477.
- [115] Anibarro, M.; Gabler, K.; Uson, I.; Sheldrick, G.M. and Saenger, W. X-ray structure of β -cyclodextrin-2,7-dihydroxy-naphthalene 4·6 H₂O: and unusually distorted macrocycle. *Carbohydr. Res.* 333 (2001): 251-256.
- [116] Enju, W.; Guangying, C. and Changri, H. Crystal structures of β -cyclodextrin inclusion complexes with 7-hydroxycoumarin and 4-hydroxycoumarin and substituent effects on inclusion geometry. *Chin. J. Chem.* 29 (2011): 617-622.
- [117] Ding, J.; Steiner, T.; Zebel, V.; Hingerty, B. E.; Mason, S. A. and Saenger, W. Neutron diffraction study of the hydrogen bonding in partially deuterated γ -cyclodextrin 15·7D₂O at T = 110K. *J. Am. Chem. Soc.* 113 (1991): 8081-8089.

- [118] Steiner, T.; Mason, S. A. and Saenger, W. Disordered guest and water molecules. Three-center and flip-flop O-H-O Hydrogen bonds in crystalline β -cyclodextrin ethanol octahydrate at T = 295 K: A neutron and x-ray Diffraction study. *J. Am. Chem. Soc.* 113 (1991): 5676-5687.
- [119] Lipkowitz, K. B. Applications of computational chemistry to the study of cyclodextrins. *Chem. Rev.* 98 (1998): 1829-1873.
- [120] Kuntz, I.D.; Gasparro, F.P.; Johnston, M.D. and Taylor, R.P. Molecular Interactions and the Benesi-Hildebrand Equation. *J. Am. Chem. Soc.* 90 (1986): 4778-4781.
- [121] Almansa López E.; Bosque-Sendra, J.M.; Cuadros Rodríguez, L.; García Campanña, A.M. and Aaron, J.J. Applying non-parametric statistical methods to the classical measurements of inclusion complex binding constants. *Anal. Bioanal. Chem.* 375 (2003): 414-423.
- [122] Mukhopadhyay, M.; Banerjee, D.; Koll, A.; Mandal, A.; Filarowshi, A.; Fitzmaurice, D.; Das, R.; Mukherjee, S. Excited state intermolecular proton transfer and caging of salicylidine-3,4,7-methyl amine in cyclodextrins. *J. Photochem. Photobiol. A: Chem.* 175 (2005): 94-99.
- [123] Valeur, B. *Molecular fluorescence: Principles and applications*. Weinheim, Germany: WILEY-VCH Verlag GmbH, 2002.
- [124] Upadhyay, S. P.; Pissurlenkar, R. R. S.; Coutinho, E. C. and Karnik, A. V. Furo-fused BINOL based crown as a fluorescent chiral sensor for enantioselective recognition of phenylethylamine and ethyl ester of valine. *J. Org. Chem.* 72 (2007): 5709-5714.
- [125] Kuntz, I. D.; Gasparro, F. P.; Johnston M. D. and Taylor, R. P. Molecular Interactions and the Benesi-Hildebrand Equation. *J. Am. Chem. Soc.* 90 (1986): 4778-4781.

- [126] Almansa López, E.; Bosque-Sendra, J. M.; Cuadros Rodríguez, L.; García Campanña, A. M. and Aaron, J. Applying non-parametric statistical methods to the classical measurements of inclusion complex binding constants. *J. Anal. Bioanal. Chem.* 375 (2003): 414-423.
- [127] Uekama, K.; Hirayama, F. and Irie, T. Cyclodextrin drug carrier systems. *Chem. Rev.* 98 (1998): 2045-2076.
- [128] Li, X. and Jasti, B. R. *Design of controlled release drug delivery systems*. New Jersey, USA McGraw-Hill Companies, Inc., 2006.
- [129] Arun, R.; Ashok Kumar, C. K. and Sravanthi, V. V. N. S. S. Cyclodextrins as drug carrier molecule: A review. *Sci. Pharm.* 76 (2008): 567-598.
- [130] Xu, M.; Wu, S.; Zeng, F. and Yu, C. Cyclodextrin supramolecular complex as a water-soluble ratiometric sensor for ferric ion sensing. *Langmuir* 26 (2010):4529-2534.
- [131] Bloomfield, V. A.; Crothers, D. M. and Tinoco, I., Jr. *Nucleic acids: Structures, properties, and functions; University Science Books*. California: USA. 2000.
- [132] Watson, J. D. and Crick, F. H. C. Molecular structure of nucleic acids. *Nature* 4356 (1953): 737-738.
- [133] Watson, J. D. and Crick, F. H. C. Genetical implications of the structure of deoxyribonucleic acid. *Nature* 171 (1953): 964-967.
- [134] Blackburn, G. M.; Gait, M. J.; Loakes, D. and Williams, D. M. *Nucleic acids in chemistry and biology*. Cambridge, UK: The Royal Society of Chemistry, 2006.
- [135] Mandelkern, M.; Elias, J. G.; Eden, D. and Crothers, D. M. The dimensions of DNA in solution. *J. Mol. Biol.* 152 (1981): 153-161.
- [136] Neidle, S. *Principles of nucleic acid structure*; Elsevier Inc., USA. 2008.
- [137] Armitage, B. A. Cyanine dye-DNA intereractions: Intercalation, groove binding, and aggregation. *Top. Curr. Chem.* 253 (2005): 55-76.

- [138] Zipper, H.; Brunner, H.; Bernhagen, J. and Vitzthum, F. Investigations on DNA intercalation and surface binding by SYBR Green I, its structure determination and methodological implications. *Nucl. Acids. Res.* 32 (2004): e103.
- [139] Ihmels, H. and Otto, D. Intercalation of organic dye molecules into double-stranded DNA: General principles and recent development. *Top. Curr. Chem.* 258 (2005): 161-204.
- [140] Ihmels, H.; Faulhaber, K.; Vedaldi, D.; Dall'Acqua, F. and Viola, G. Intercalation of organic dye molecules into double-stranded DNA part 2: The annelated quinolizinium ion as a structural motif in DNA intercalators. *Photochem. Photobiol.* 81 (2005): 1107-1115.
- [141] Liu, H.-K. and Saler, P. J. Metal complexes as DNA intercalators. *Acc. Chem. Res.* 44 (2011): 349-359.
- [142] Neto, B. A. D. and Lapis, A. A. M. Recent developments in the chemistry of deoxyribonucleic acid (DNA) intercalators: Principles, design, synthesis, applications and trends. *Molecules* 14 (2009): 1725-1746.
- [143] Beneš, L.; Melánová, K.; Zima, V.; Kalousavá, J. and Votinský, J. Possible Mechanisms of intecalation. *J. Inclus. Phenom. Mole. Recog. Chem.* 31 (1998): 275-286.
- [144] Patel, K. K.; Plummer, E. A.; Darwish, M.; Rodger, A. and Hannon, M. J. Aryl substituted ruthenium bid-terpyridine complexes: intercalation and groove binding with DNA. *J. Inorg. Biochem.* 91 (2002): 220-229.
- [145] Wang, S.; Liu, B.; Gaylord, B. S. and Bazan, G. C. Size-specific interactions between single- and double-stranded oligonucleotides and cationic water-soluble oligofluorenes. *Adv. Funct. Mater.* 13 (2003): 463-467.
- [146] He, F.; Tang, Y.; Wang, S.; Li, Y. and Zhu, D. Fluorescent amplifying recognition for DNA G-quadruplex folding with a cationic conjugated polymer: A platform for homogeneous potassium detection. *J. Am. Chem. Soc.* 127 (2005): 12343-12346.

- [147] Lim, K. W.; Amrane, S.; Bouaziz, S.; Xu, W.; Mu, Y.; Patel, D. J.; Luu, K. N. and Phan, A. T. Structure of the human telomere in K⁺ solution: A stable basket-type G-quadruplex with only two G-tetrad layers. *J. Am. Chem. Soc.* 131 (2009): 4301-4309.
- [148] de-los-Santos-Álvarez, N.; Jesús Lobo-Castañón, M.; Miranda-Ordieres, A. J. and Tuñón-Blanco. Modified-RNA aptamer-based sensor for competitive impedimetric assay of neomycin B. *J. Am. Chem. Soc.* 129 (2007): 3808-3809.
- [149] Xiao, Y.; Pavlov, V.; Niazov, T.; Dishon, A.; Kotler, M. and Willner, I. Catalytic Beacon for the detection of DNA and telomerase activity. *J. Am. Chem. Soc.* 126 (2004): 7430-7431.
- [150] Li, B.; Qin, C.; Li, T.; Wang, L. and Dong, S. Fluorescent switch constructed based on hemin-sensitive anionic conjugated polymer and its applications in DNA-related sensors. *Anal. Chem.* 81 (2009): 3544-3550.
- [151] Nuo, D.; Shi-Jia, W. and Zhou-Ping, W. An aptamer-based fluorescence assay for ochratoxin A. *Chin. J. Ancl. Chem.* 39 (2011): 300-304.
- [152] Pavlov, V.; Shlyahovsky, B. and Willner, I. Fluorescent detection of DNA by the catalytic activation of an aptamer/thrombin complex. *J. Am. Chem. Soc.* 127 (2005): 6522-6523.
- [153] Mok, W. and Li, Y. Recent progress in nucleic acid aptamer-based biosensors and bioassays. *Sensors* 8 (2008): 7050-7084.
- [154] James, W. Aptamers. *Encyclopedia of Analytical Chemistry.* (2000): 4848-4871.
- [156] Xia, F.; Zuo, X.; Yang, R.; Xiao, Y.; Kang, D.; Vallée-Bélisle, A.; Gong, X.; Heeger, A. J. and Plaxco, K. W. On the binding of cationic, water-soluble conjugated polymers to DNA: Electrostatic and hydrophobic interactions. *J. Am. Chem. Soc.* 132 (2010): 1252-1254.

- [157] Nyan Win, M.; Klein, J. S. and Smolke, C. D. Codeine-binding RNA aptamers and rapid determination of their binding constants using a direct coupling surface plasmon resonance assay. *Nucl. Acids Res.* 34 (2006): 5670-5682.
- [158] Kim, M.; Um, H.-J.; Bang, S.; Lee, S.-H.; Oh, S.-J.; Han, J.-H.; Kim, K.-W.; Min, J. and Kim, Y.-H. Arsenic removal from vietnamese groundwater using the arsenic-binding DNA aptamer. *Environ. Sci. Technol.* 43 (2009): 9335-9340.
- [159] Yang, X.; Bing, T.; Mei, H.; Fang, C.; Cao, Z. and Shangguan, D. Characterization and application of a DNA aptamer binding to L-tryptophan. *Analyst* 136 (2011): 57-585.
- [160] Jiang, L. and Patel, D. J. Solution structure of the tobramycin-RNA aptamer complex. *Nature Struct. Biol.* 5 (1998): 769-774.
- [161] Patel, D. J.; Suri, A. K.; Jiang, F.; Jiang, L.; Fan, P; Ajay Kumar, R. and Nonin, S. Structure, recognition and adaptive binding in RNA aptamer complexes. *J. Mol. Biol.* 272 (1997): 645-664.
- [162] Kim, J. N.; Roth, A. and Breaker, R. R. Guanine fiboswitch variants from *Mesoplasma florum* selectively recognize 2'-deoxyguanosine. *Proc. Natl. Acad. Sci. USA.* 104 (2007): 16092-16097.
- [163] Lin, Y.-W.; Ho, H.-T.; Huang, C.-C. and Chang, H.-T. Fluorescence detection of single nucleotide polymorphisms using a universal molecular beacon. *Nucl. Acids Res.* 36 (2008): e123.
- [164] Fersht, A. *Structure and mechanism in protein science: A guide to enzyme catalysis and protein folding.* New York, USA: W.H. Freeman and Company, 1999.
- [165] Bujnicki, J. M. *Prediction of protein structures, functions, and interactions.* West Sussex, UK: John Wiley & Sons, Ltd., 2009.
- [166] Buxbaum, E. *Fundamentals of protein structure and function.* New York, USA: Springer Science+Business Media, LLC, 2007.
- [167] Petsko, G. and Ringe, D. *Protein structure and function.* London, UK: New Science Press, Ltd., 2004.

- [168] Pauling, L.; Corey, R. B. and Brandson, H. R. The Structure of Proteins Two Hydrogen-Bonded Helical Configurations of the Polypeptide Chain. *Proc. Natl. Acad. Sci. USA* 37 (1951): 205–211.
- [169] Chiang, Y.; Gelfand, T. I.; Kister, A. E. and Gelfand, I. M. New classification of supersecondary structures of sandwich-like proteins uncovers strict patterns of strand assemblage. *Proteins* 68 (2007): 915-921.
- [170] Branden, C. and Tooze, J. *Introduction to protein structure*. New York, USA: Garland Publishing, Inc., 1991.
- [171] Rule, G. S. and Hitchems, T. K. *Fundamentals of protein NMR spectroscopy*; Springer. The Netherlands: Dordrecht, 2006.
- [172] Webster, D. M. Methods in Molecular Biology, vol. 143: *Protein structure prediction: Methods and protocols*. Totowa, NJ: Human Press Inc., 2000.
- [173] Creighton, T. E. *Protein structure: A practical approach*. New York, USA: Oxford University Press Inc., 1997.
- [174] Malmsten, M. *Surfactants and polymers in drug delivery*. New York, USA: Marcel Dekker, Inc., 2002.
- [175] Rangel-Yagui, C. O.; Pessoa-Jr, A.; Costa Tavares, L. Micellar solubilization of drugs. *J. Pharm. Pharmaceut. Sci.* 8 (2005): 147-163.
- [176] Tadros, T. F. *Applied surfactants: Principles and applications*. Weinheim, Germany: WILEY-VCH Verlag GmbH & Co. KGaA, 2005.
- [177] Goodwin, J. W. *Colloids and interfaces with surfactants and polymers: An introduction*. West Sussex, England: John Wiley & Sons, Ltd, 2004.
- [178] Myers, D. *Surfactant science and technology*. Hoboken, New Jersey: John Wiley & Sons, Inc., 2006.
- [179] Pérez-Rodríguez, M; Prieto, G.; Rega, C.; Varela, L.M.; Sarmiento, F. and Mosquera, V. A Comparative Study of the Determination of the Critical Micelle Concentration by Conductivity and Dielectric Constant Measurements. *Langmuir* 14 (1998): 4422-4426.

- [180] Modaresi, A.; Sifaoui, H.; Grzesiak, B.; Solimando, R.; Domanska, U. and Rogalski, M. CTAB aggregation in aqueous solutions of ammonium based ionic liquids; conductimetric studies. *Colloids Surfaces A: Physicochem. Eng. Aspects* 296 (2007): 104-108.
- [181] Menger, F.M. and Shi, L. Electrostatic Binding among Equilibrating 2-D and 3-D Self-Assemblies. *J. Am. Chem. Soc.* 131 (2009): 6672-6673.
- [182] Dearden, L.V. and Woolley, E.M. Osmotic coefficients of alkyltrimethylammonium bromides in water and in aqueous sodium bromide solutions at 55°C. *J. Phys. Chem.* 91 (1987): 2404-2408.
- [183] Deshiikan, S.R.; Bush, D.; Eschenazi, E. and Papadopoulos, K.D. SDS, Brij58 and CTAB at the dodecane-water interface. *Colloid. Surface A: Physicochem. Eng. Aspects* 136 (1998): 133-150.
- [184] Patist, A.; Bhagwat, S.S.; Penfield, K.W.; Aikens, P. and Shah, D.O. On the measurement of critical micelle concentrations of pure and technical-grade nonionic surfactants. *J. Surfactants Deterg.* 3 (2000): 53-58.
- [185] Mukherjee, S.; Mitra, D.; Bhattacharya, S. C.; Panda, A. K. and Moulik, S. P. Physicochemical studies on the micellization behavior of cetylpyridinium chloride and triton X-100 binary mixtures in aqueous medium. *Colloid J.* 71 (2009): 662-671.
- [186] Šegota, S.; Heimer, S. and Težak, Đ. New cationic mixtures of dodecyldimethyl ammoniumbromide/sodium dodecylbenzene sulphonate/water I. Surface properties of dispersed particles. *Colloid. Surface A: Physicochem. Eng. Aspects* 274 (2006): 91-99.
- [187] Wydro, P. and Paluch, M. A study of the interaction of dodecyl sulfobetaine with cationic and anionic surfactant in mixed micelles and monolayers at the air/water interface. *J. Colloid Interface Sci.* 286 (2005): 387-391.

- [188] Deng, M.; Huang, X.; Wu, R. and Wang, Y. Micellization-Induced Conformational Change of a Chiral Proline Surfactant. *J. Phys. Chem. B* 112 (2008): 10509-10513.
- [189] Neumann, M.G. and Gehlen, M.H. The Interaction of Cationic Dyes with Anionic Surfactants in the Premicellar Region. *J. Colloid Interface Sci.* 135 (1990): 209-217.
- [190] Qian, J.; Xu, Y.; Qian, X.; Wang, J. and Zhang, S. Effects of anionic surfactant SDS on the photophysical properties of two fluorescent molecular sensors. *J. Photochem. Photobiol. A* 200 (2008): 402-409.
- [191] Monteserín, M.; Burrows, H.D.; Valente, A.J.M.; Lobo, V. M.M.; Mallavia, R.; Tapia, M.J.; García-Zubiri, I.X.; Di Paolo, R.E. and Maçanita, A.L. Modulating the Emission Intensity of Poly-(9,9-bis(6'-*N,N,N*-teimethylammonium)hexyl)-Fluorene Phenylene) Bromide Through Interaction with Sodium Alkylsulfonate Surfactants. *J. Phys. Chem. B* 111 (2007): 13560-13569.
- [192] Banerjee, P.; Pramanik, S.; Sarkar, A. and Chandra Bhattacharya, S. Modulated Photophysics of 3-Pyrazolyl-2-pyrazoline Derivatives Entrapped in Micellar Assembly. *J. Phys. Chem. B* 112 (2008): 7211-7219.
- [193] Romani, A.P.; da Hora Machado, A.E.; Hioka, N.; Severino, D.; Baptista, M.S.; Codognoto, L.; Rodrigues, M.R. and de Olivera, H.P.M. Spectrofluorimetric Determination of Second Critical Micellar Concentration of SDS and SDS/Brij 30 Systems. *J. Fluoresc.* 19 (2009): 327-332.
- [194] Nakahara, Y.; Kida, T.; Nakatsuji, Y. and Akashi, M. New fluorescence method for the determination of the critical micelle concentration by photosensitive monoazacryptand derivatives. *Langmuir* 21 (2005): 6688-6695.
- [195] Diao, X.-L.; Xia, Y.-S.; Zhang, T.-L.; Li, Y. and Zhu, C.-Q. Fluorescence-detecting cationic surfactants using luminescent CdTe quantum dots as probes. *Anal. Bioanal. Chem.* 388 (2007): 1191-1197.

- [196] Chen, X.; Lee, J.; Jou, M.J.; Kim, J.-M. and Yoon, J. Colormetric and fluorometric detection of cationic surfactants based on conjugated polydiacetylene supramolecules. *Chem. Commun.* 23 (2009): 3434-3436.
- [198] Lavigne, J. J.; Broughton, D. L.; Wilson, J. N.; Erdogan, B. and Bunz, U. H. F. "Surfactochromic" conjugated polymers: Surfactant effects on sugar-substituted PPEs. *Macromolecules* 36 (2003): 7409-7412.
- [199] Laurenti, M.; Rubio-Retama, J.; Garcia-Blanco, F. and López-Cabarcos, E. Influence of the surfactant chain length on the fluorescence properties of a water-soluble conjugated polymer. *Langmuir* 24 (2008): 13321-13327.
- [200] Diehl, A. and Kuhn, P. S. Effect of monovalent salt on the conformation of polyelectrolyte-surfactant complexes. *Physical Review E* 79 (2009): 011805.
- [201] González, D. G.; Savariar, E. N. and Thayumanavan, S. Fluorescence patterns from supramolecular polymer assembly and disassembly for sensing metallo- and nonmetalloproteins. *J. Am. Chem. Soc.* 131 (2009): 7708-7716.
- [202] Guo, X.; Cui, B.; Li, H.; Gong, Z.; Zhang, F.; Zheng, S. and Guo, R. Micelle-to-vesicle transition induced by oligonucleotide in SDS/DEAB/mixed system with a net negative charge. *J. Polym. Sci. Pol. Chem.* 46 (2008): 7491-7504.
- [203] Cheng, X.; Bing, T.; Liu, X. and Shangguan, D. A label-free fluorescence sensor for probing the interaction of oligonucleotides with target molecules. *Anal. Chim. Acta.* 633 (2009): 97-102.
- [204] Albani, J. R. *Principles and Applications of Fluorescence Spectroscopy*. Oxford, UK: Blackwell Publishing, 2007.
- [205] Lakowicz, J.R. *Principles of Fluorescence Spectroscopy*. LLC, Singapore: Springer Science+Business Media, 2006.
- [206] Toal, S. J. and Trogler, W. C. Polymer sensors for nitroaromatic explosives detection. *J. Mater. Chem.* 16 (2006): 2871-2883.

- [207] Kim, J. S. and Quang, D.T. Calixaren-derived fluorescent probes. *Chem. Rev.* 107 (2007): 3780-3799.
- [208] Baudin, B.H. *Electron and Energy Transfer in Supramolecular Complexes Designed for Artificial Photosynthesis*. Edsbruk, Sweden: Akademitryck AB, 2001.
- [209] Porres, L.; Mongin, O.; Katan, C.; Charlot, M.; Pons, T.; Mertz, J. and Blanchard-Desce, M. Enhanced two-photon absorption with novel octupolar propeller-shaped fluorophores derived from triphenylamine. *Org. Lett.* 6 (2004): 47-50.
- [210] Kumar Mandal, A.; Kumar Das, D.; Kumar Das, A.; Sen Mojumdar, S. and Bhattachayya, K. Study of γ -cyclodextrin host-guest complex and nanotube aggregate by fluorescence correlation spectroscopy. *J. Phys. Chem. B* 115(2011): 10456-10461.
- [211] Das, P.; Mallick, A.; Sarkar, D. and Chattopadhyay, N. Probe-induced self-aggregation of γ -cyclodextrin: Formation of extended nanotubular suprastructure. *J. Phys. Chem.* 112 (2008): 9600-9603.
- [212] Tanhuanpaa, K.; Hon Cheng, K.; Anttonen, K.; Virtanen, J. A.; Somerharju, P. Characteristics of pyrene phospholipid/ γ -Cyclodextrin complex. *Biophys. J.* 81 (2001): 1501-1510.
- [213] Pumera, M.; Matalova, R.; Jalinec, I.; Jindrich, J. and Juza, J. Comparison of association constants of cyclodextrins and their tert-butyl derivatives with halogenbenzoic acids and acridine derivatives *Molecules* 6 (2001): 221-229.
- [214] Funasaki, N.; Ishikawa, S. and Neya, S. Binding of short-chain lecithin by β -cyclodextrin. *Langmuir* 18 (2002): 1786-1790.
- [215] Dodziuk, H.; Demchuk, O. M.; Bielejewska, A.; Komiski, W. and Dolgonos, G. A study of multiple complexation of α -, β - and γ -cyclodextrins: surprisingly differing stoichiometries of β - and γ -cyclodextrin complexes. *Supramol. Chem.* 16 (2004): 287-292.

- [216] Smith, V. J.; Rougier, N. M.; de Rossi, R. H.; Caira, M. R.; Bujan, E. I.; Fernandez, M. A. and Bourne, S. A. Investigation of the inclusion of the herbicide metobromuron in native cyclodextrins by powder X-ray diffraction and isothermal titration calorimetry. *Carbohydr. Res.* 344 (2009): 2388-2393.
- [217] Green, T. K.; Denoroy, L. and Parrot, S. Fluorescence enhancement of a Meisenheimer complex of adenosine by β -cyclodextrin: A thermodynamic and kinetic investigation. *J. Org. Chem.* 75 (2010): 4048-4055.
- [218] He, Y.; Fu, P.; Shen, X. and Gao, H. Cyclodextrin-based aggregates and characterization by microscopy. *Micron* 39 (2008): 495-516.
- [219] Wu, A.; Shen, X. and He, Y. Micrometer-sized rodlike structure formed by the secondary assembly of cyclodextrin nanotube. *J. Colloid Interf. Sci.* 302 (2006): 87-94.
- [220] Farcas, A.; Ghosh, I.; Jarroux, N.; Harabagiu, V.; Guegan, P. and Nau, W. M. Morphology and properties of a polyrotaxane based on β -cyclodextrin and apolyfluorene copolymer. *Chem. Phys. Lett.* 465 (2008): 96-101.
- [221] Wu, A.; Shen, X. and He, Y. Investigation on β -cyclodextrin nanotube induced by *N,N'*-diphenylbenzidine molecule. *J. Colloid Interf. Sci.* 297 (2006): 525-533.
- [222] Srinivasan, K.; Kayalvizhi, K.; Sivakumar, K. and Stalin, T. Study of inclusion complex of β -cyclodextrin and diphenylamine: Photophysical and electrochemical behaviors. *Spectrochim. Acta A* 79 (2011): 169-178.
- [223] Krois, D. and Brinker, U. H. Induced circular dichroism and UV-Vis absorption spectroscopy of cyclodextrin inclusion complexes: Structural elucidation of supramolecular azi-adamantane (spiro[adamantine-2,3'-diazirine]). *J. Am. Chem. Soc.* 120 (1998): 11627-11632.

APPENDIX

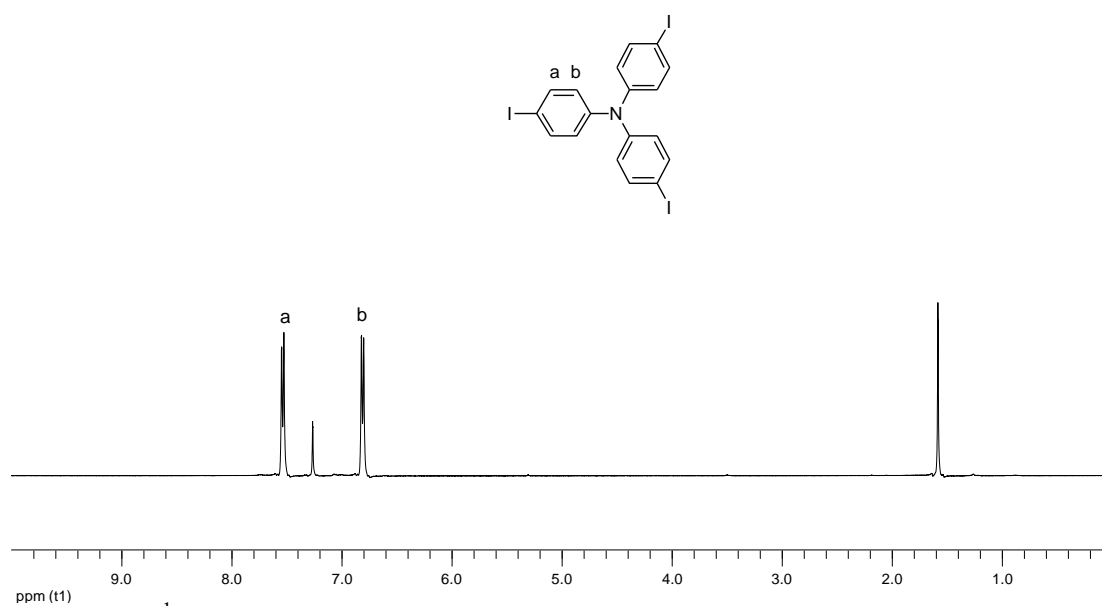


Figure A.1 ^1H NMR of 4,4',4''-triiodotriphenylamine (TI_3) in CDCl_3 .

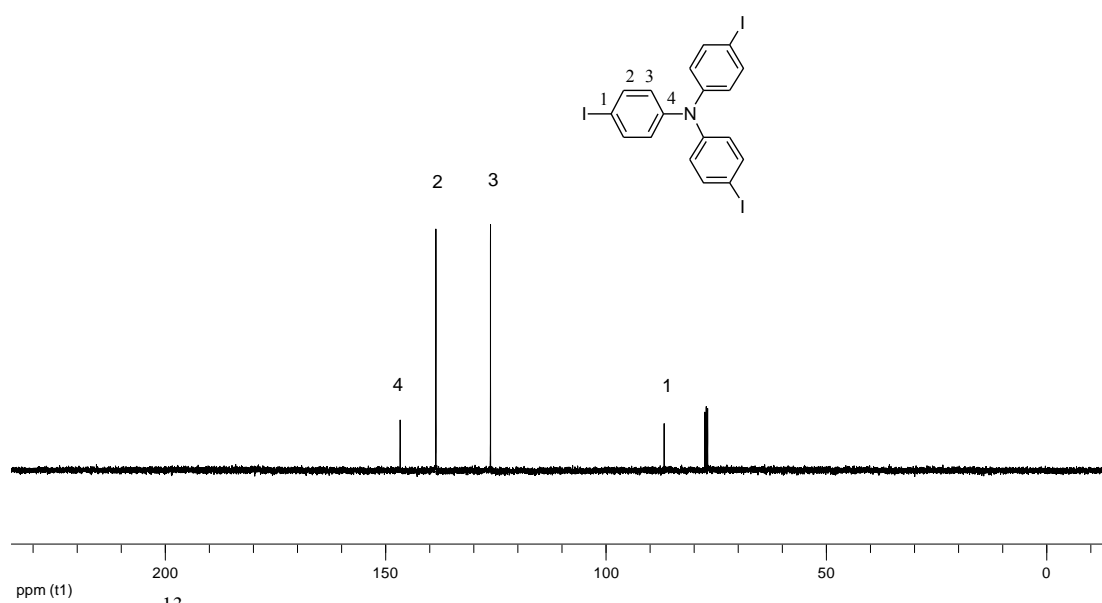


Figure A.2 ^{13}C NMR of 4,4',4''-triiodotriphenylamine (TI_3) in CDCl_3 .

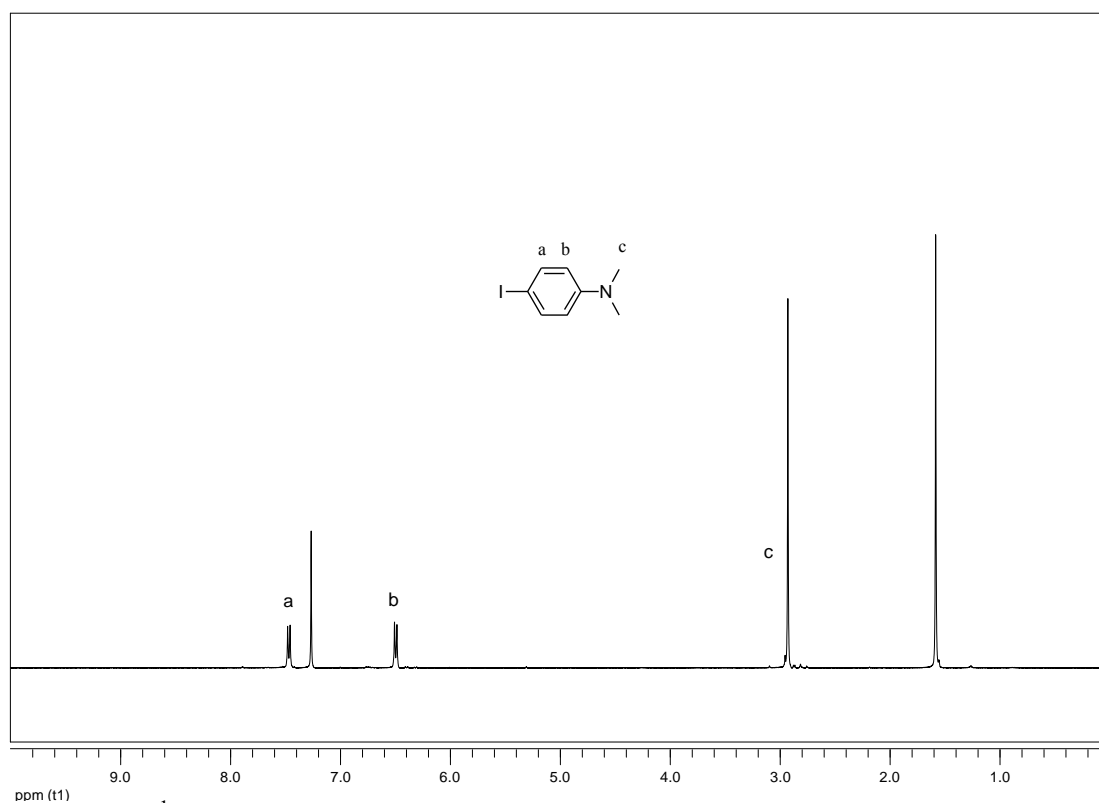


Figure A.3 ¹H NMR of 4-iodo-*N,N*-dimethylaniline (IAME₂) in CDCl₃.

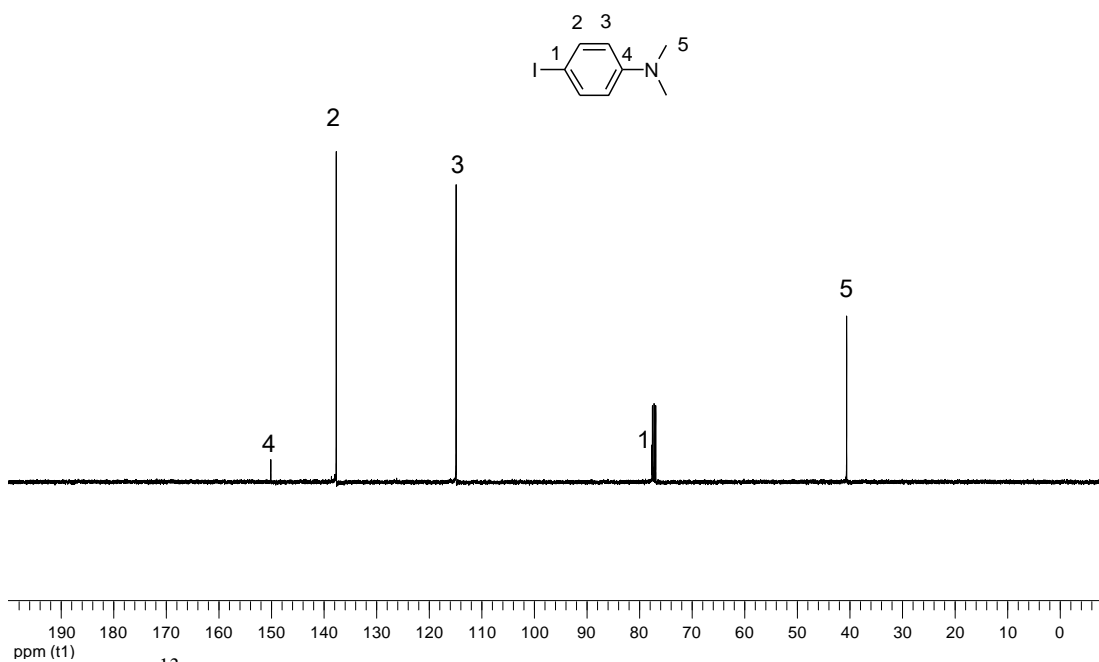


Figure A.4 ¹³C NMR of 4-iodo-*N,N*-dimethylaniline (IAME₂) in CDCl₃.

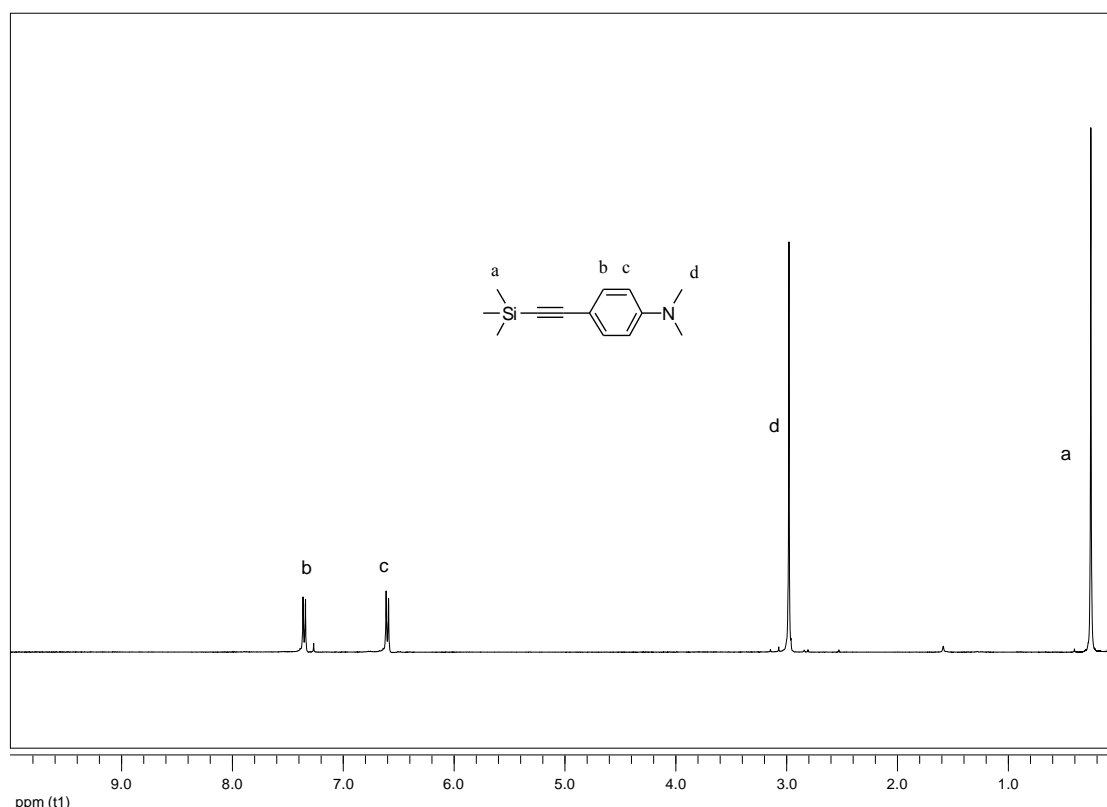


Figure A.5 ^1H NMR of SiEAMe_2 in CDCl_3 .

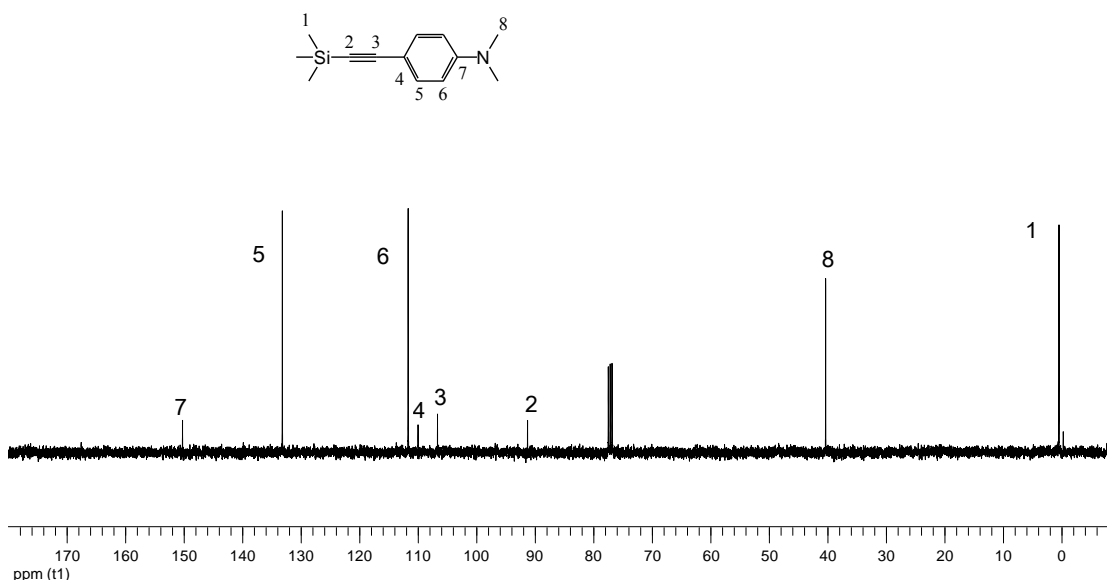


Figure A.6 ^{13}C NMR of SiEAMe_2 in CDCl_3 .

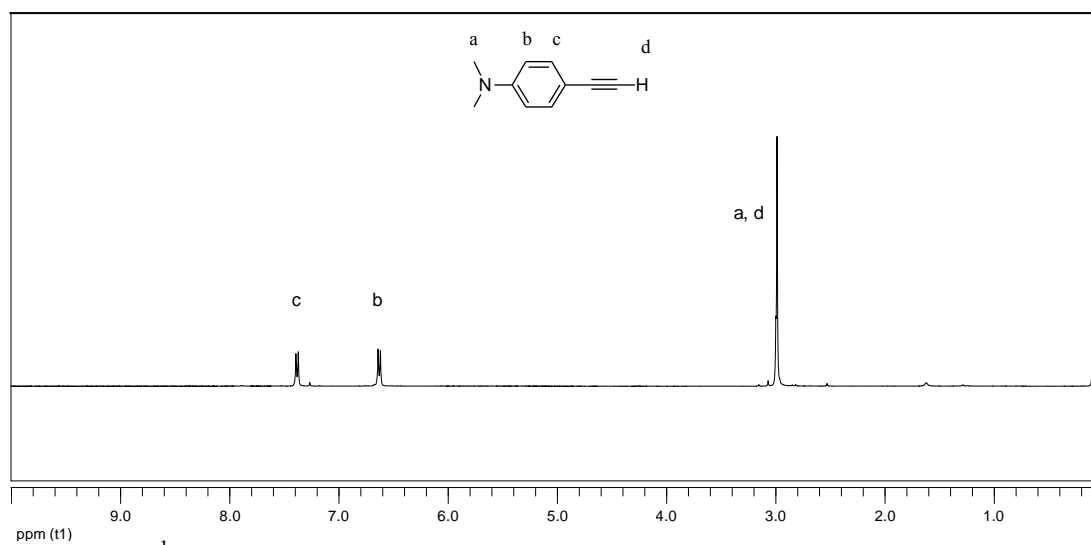


Figure A.7 ^1H NMR of 4-ethynyl *N,N*-dimethylaniline (**EAMe₂**) in CDCl_3 .

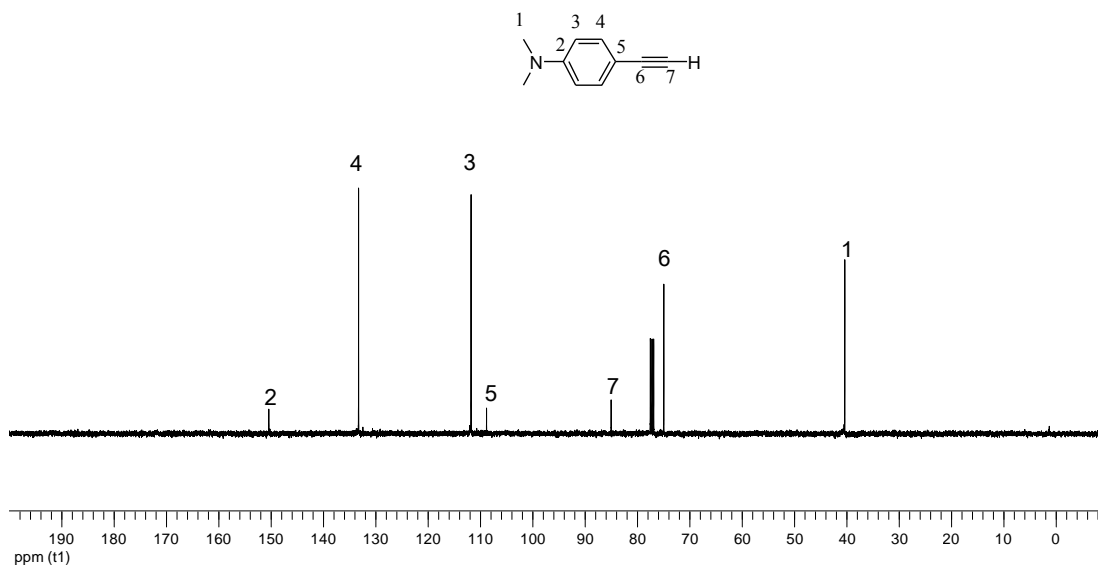


Figure A.8 ^{13}C NMR of 4-ethynyl *N,N*-dimethylaniline (**EAMe₂**) in CDCl_3 .

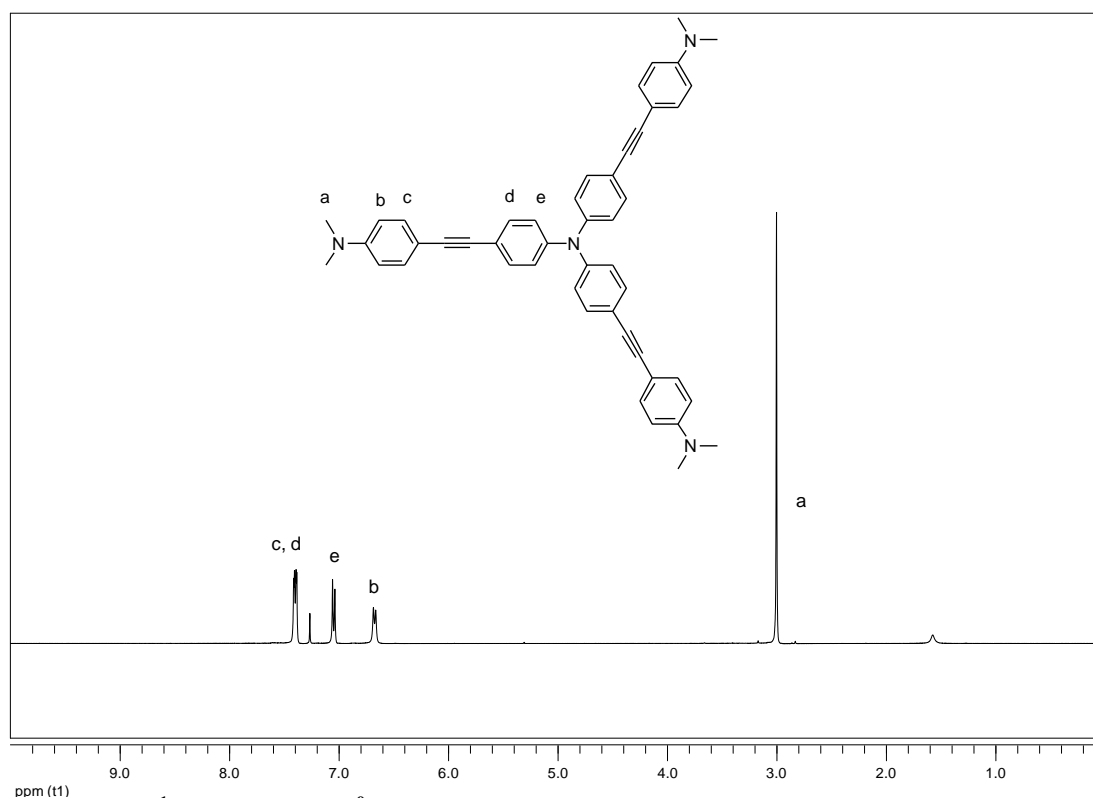


Figure A.9 ^1H NMR of 3N^0 in CDCl_3 .

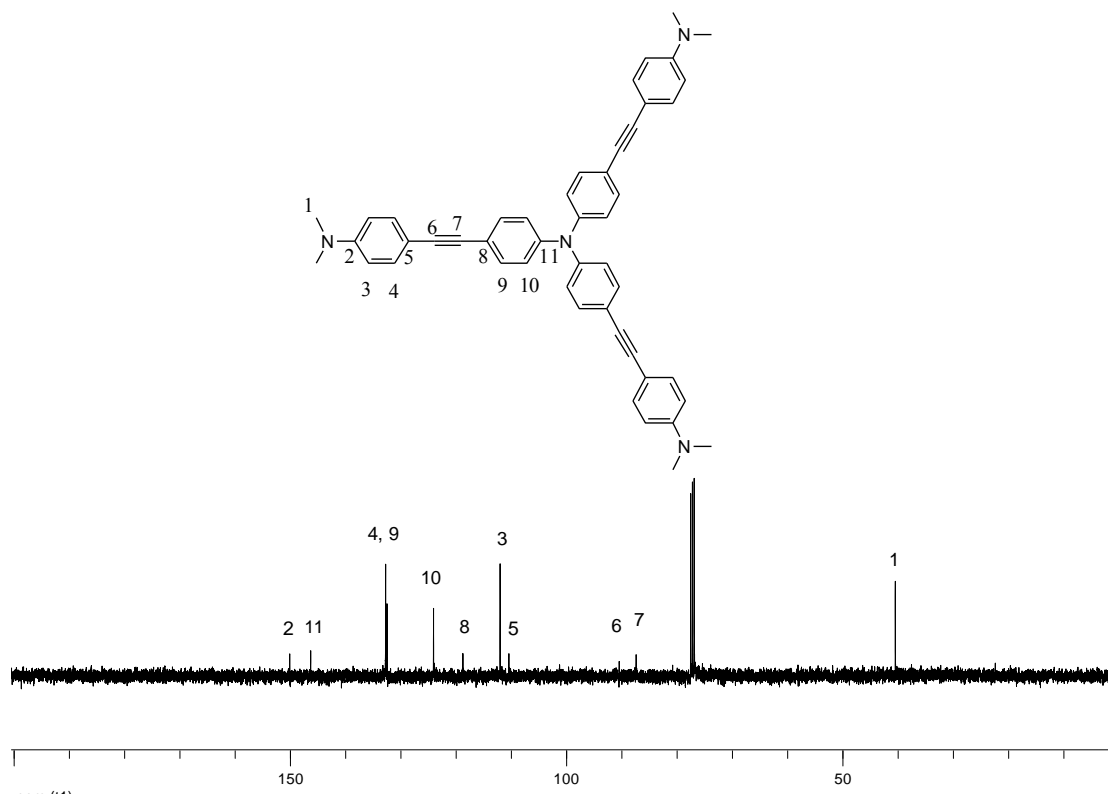


Figure A.10 ¹³C NMR of 3N⁰ in CDCl₃.

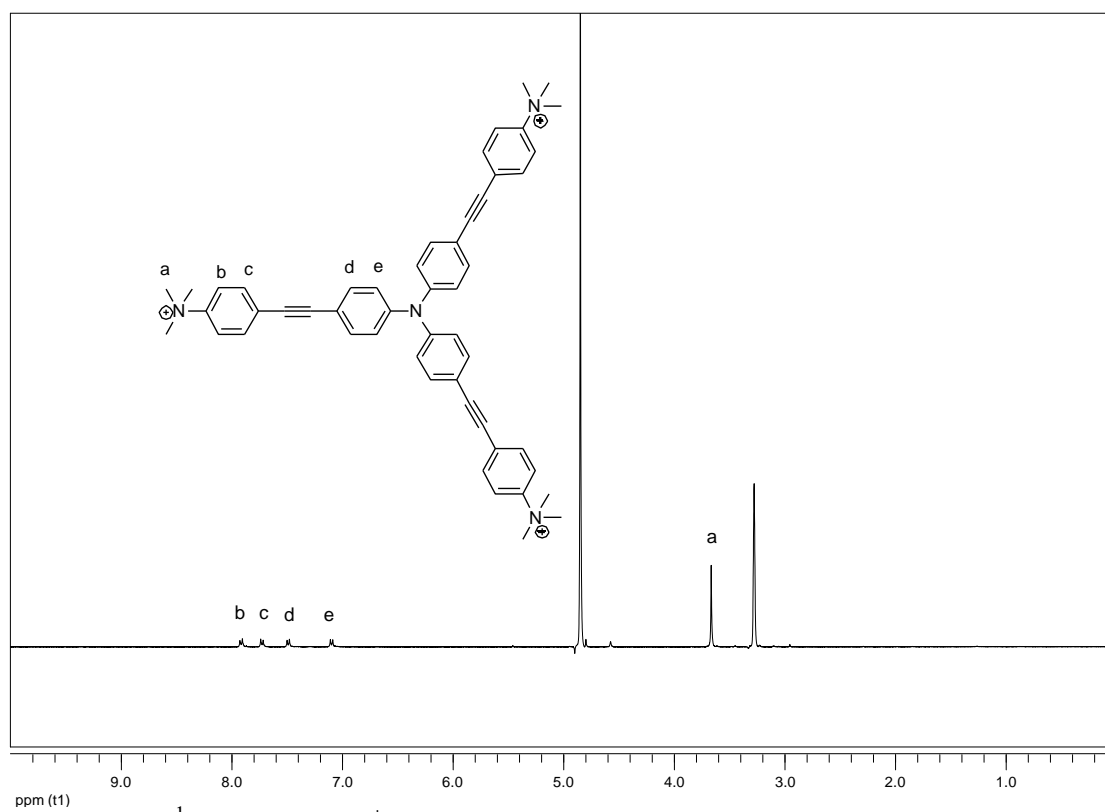


Figure A.11 ^1H NMR of 3N^+ in $\text{MeOH-}d_4$.

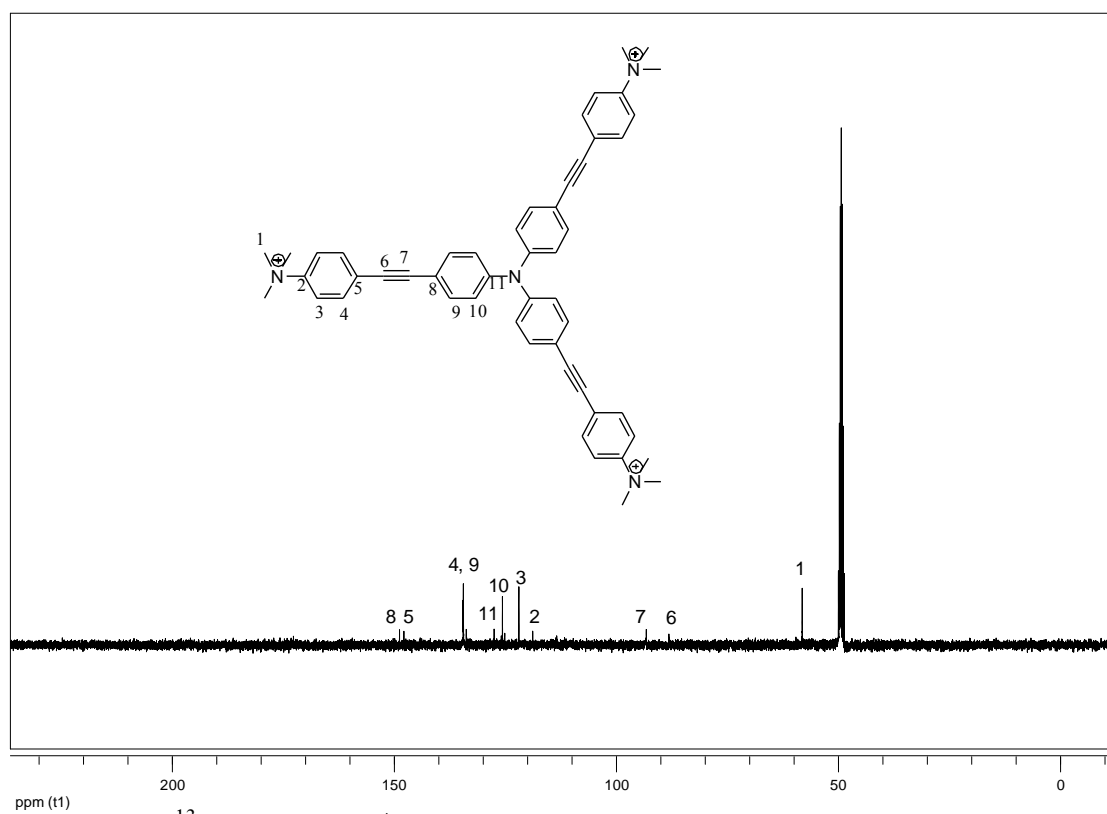


Figure A.12 ^{13}C NMR of $3N^+$ in $MeOH-d_4$.

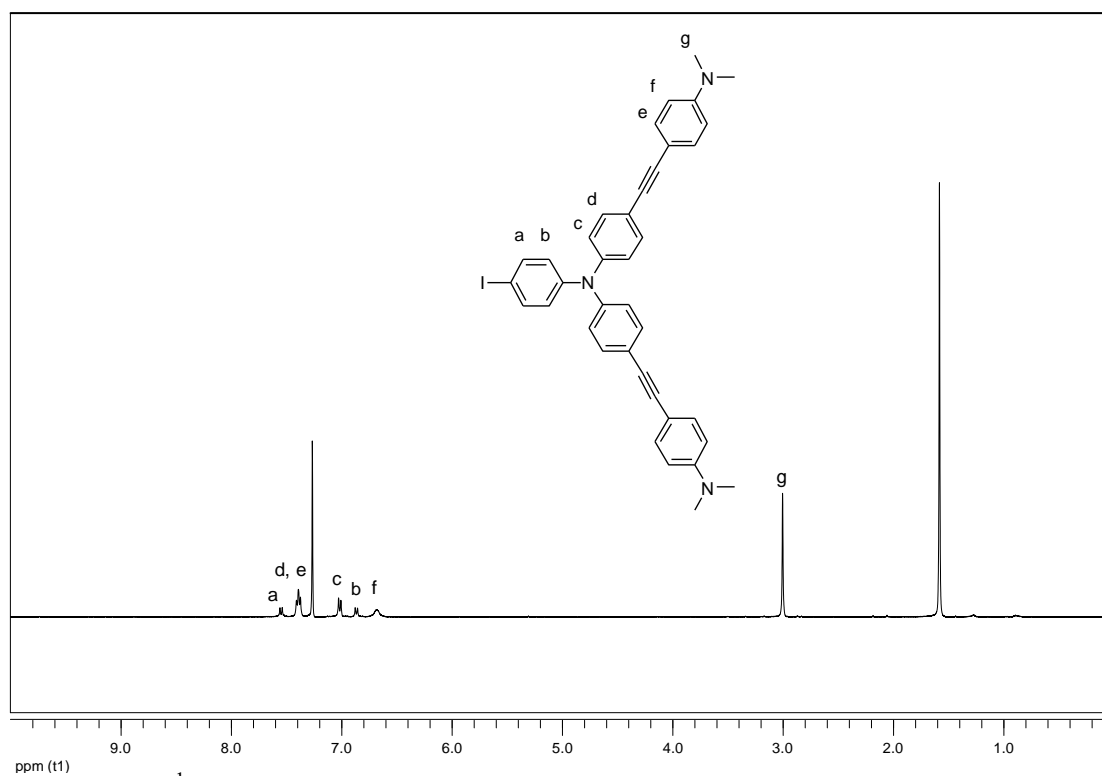


Figure A.13 ^1H NMR of $\text{TI}(\text{EAME}_2)_2$ in CDCl_3 .

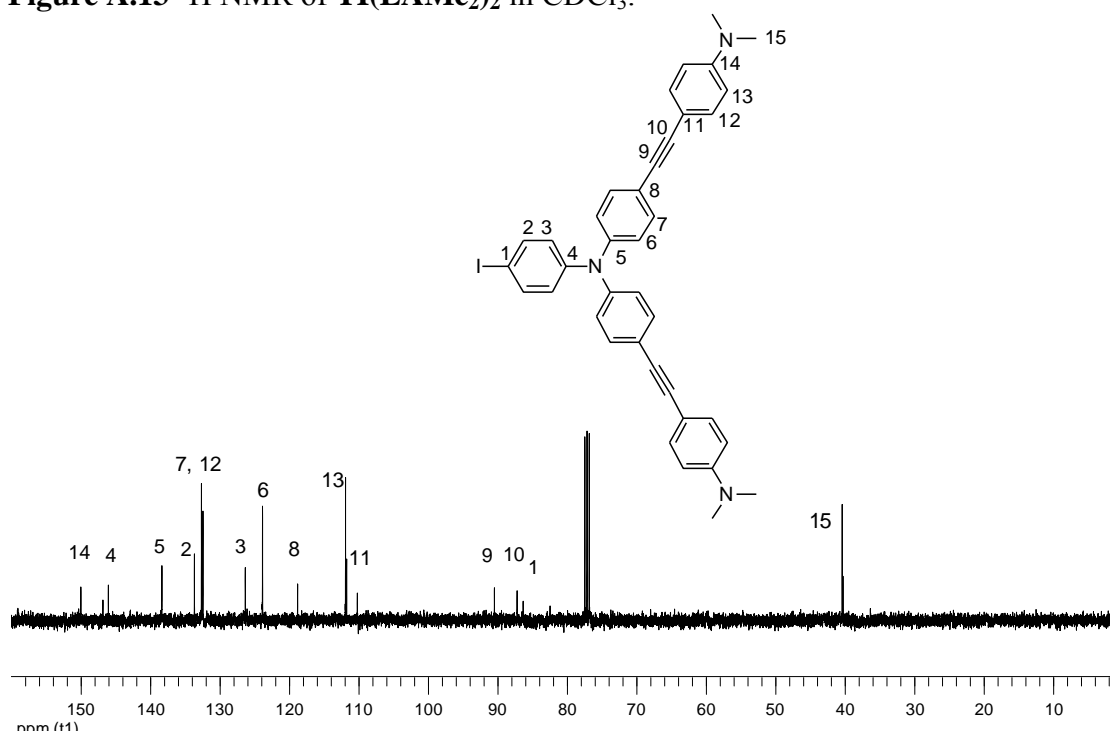


Figure A.14 ^{13}C NMR $\text{TI}(\text{EAME}_2)_2$ in CDCl_3 .

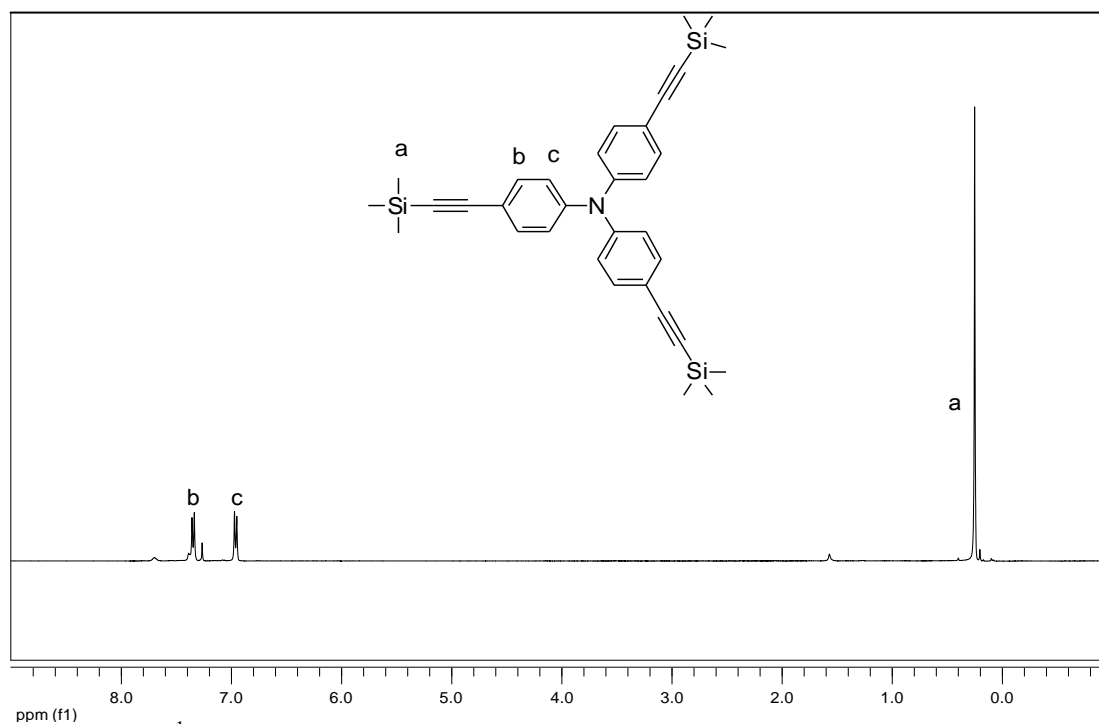


Figure A.15 ^1H NMR of $T(\text{SiET})_3$ in CDCl_3 .

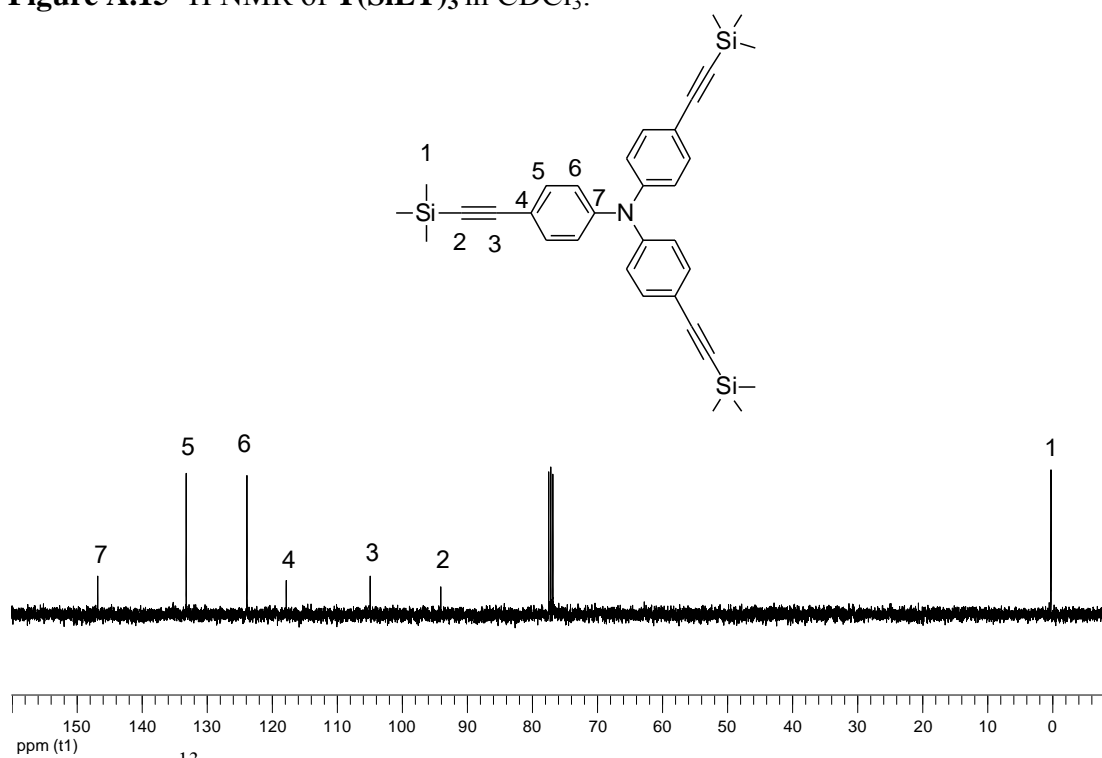


Figure A.16 ^{13}C NMR of $T(\text{SiET})_3$ in CDCl_3 .

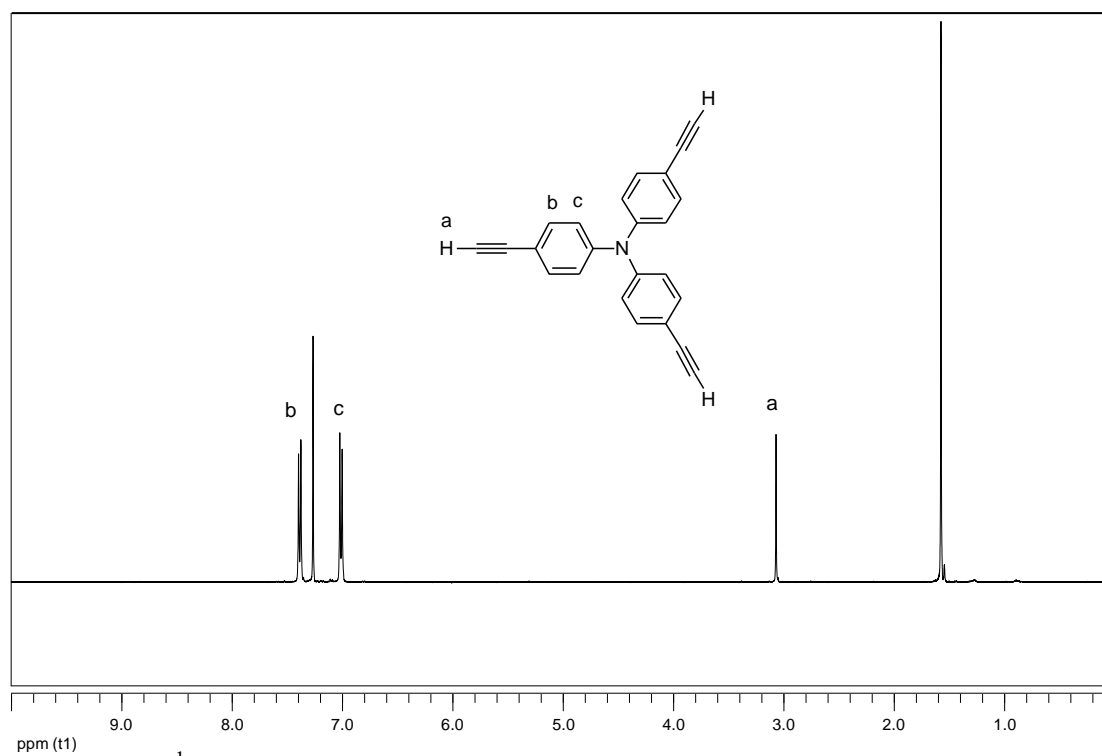


Figure A.17 ^1H NMR of tris(4-ethynylphenyl)amine (T(ET)_3) in CDCl_3 .

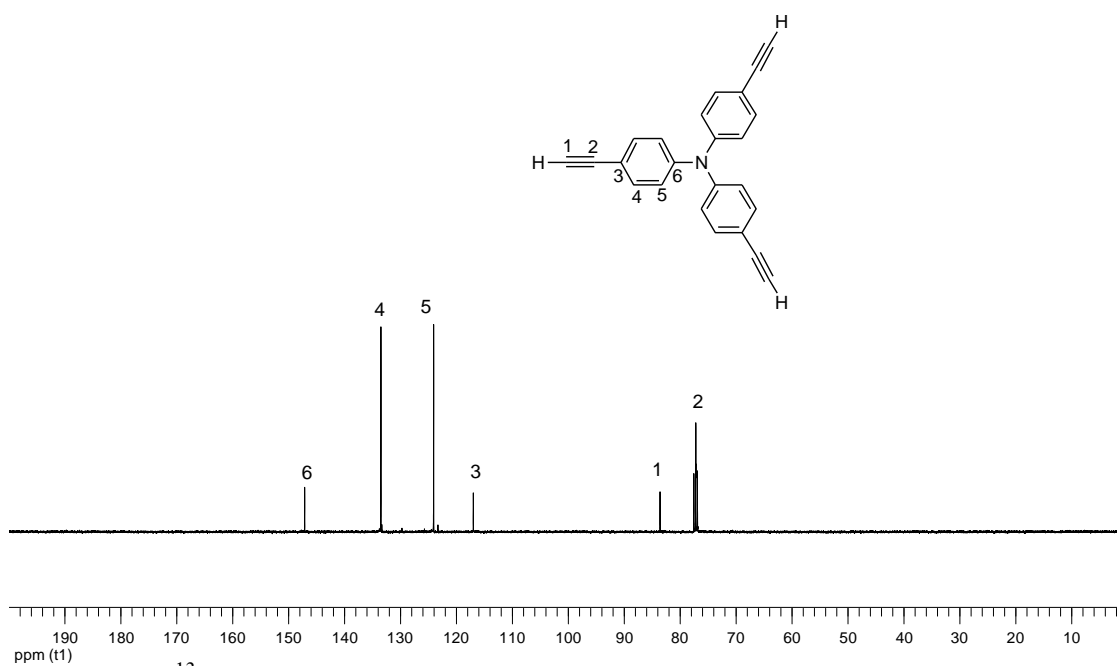


Figure A.18 ^{13}C NMR of tris(4-ethynylphenyl)amine (T(ET)_3) in CDCl_3 .

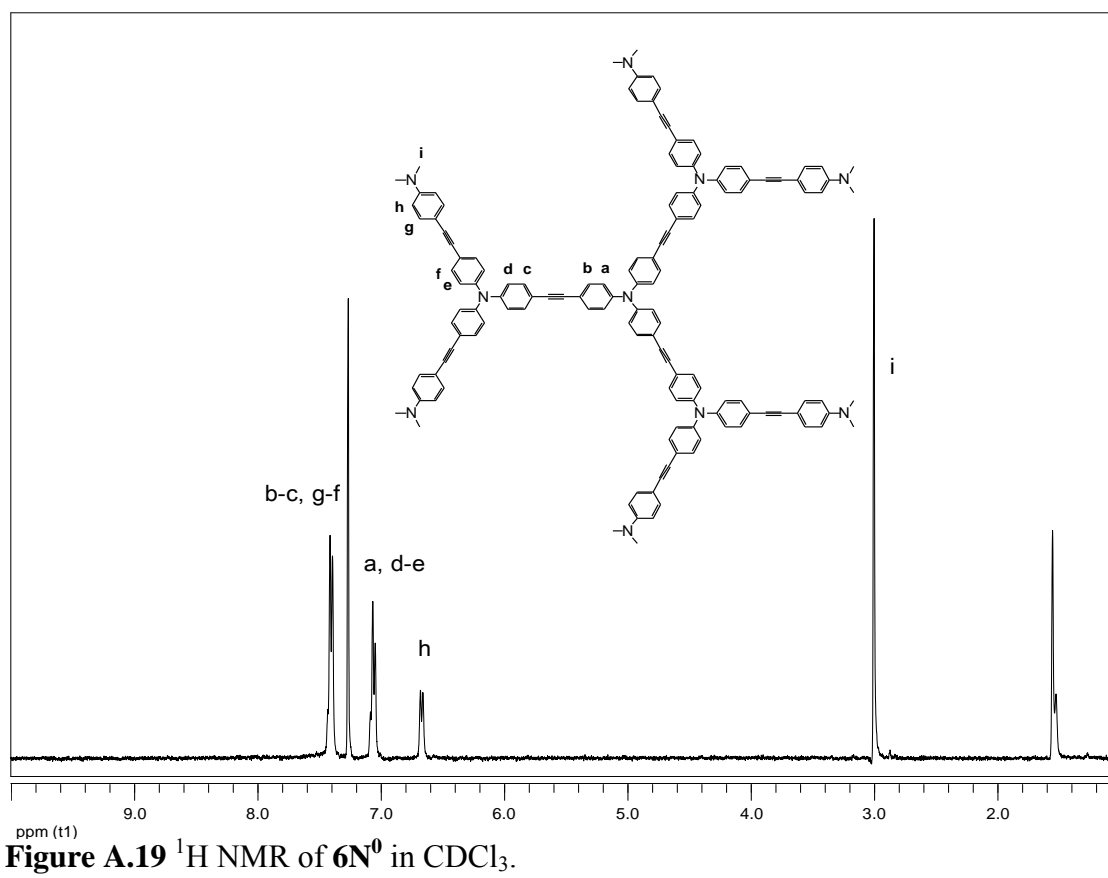


Figure A.19 ^1H NMR of 6N^0 in CDCl_3 .

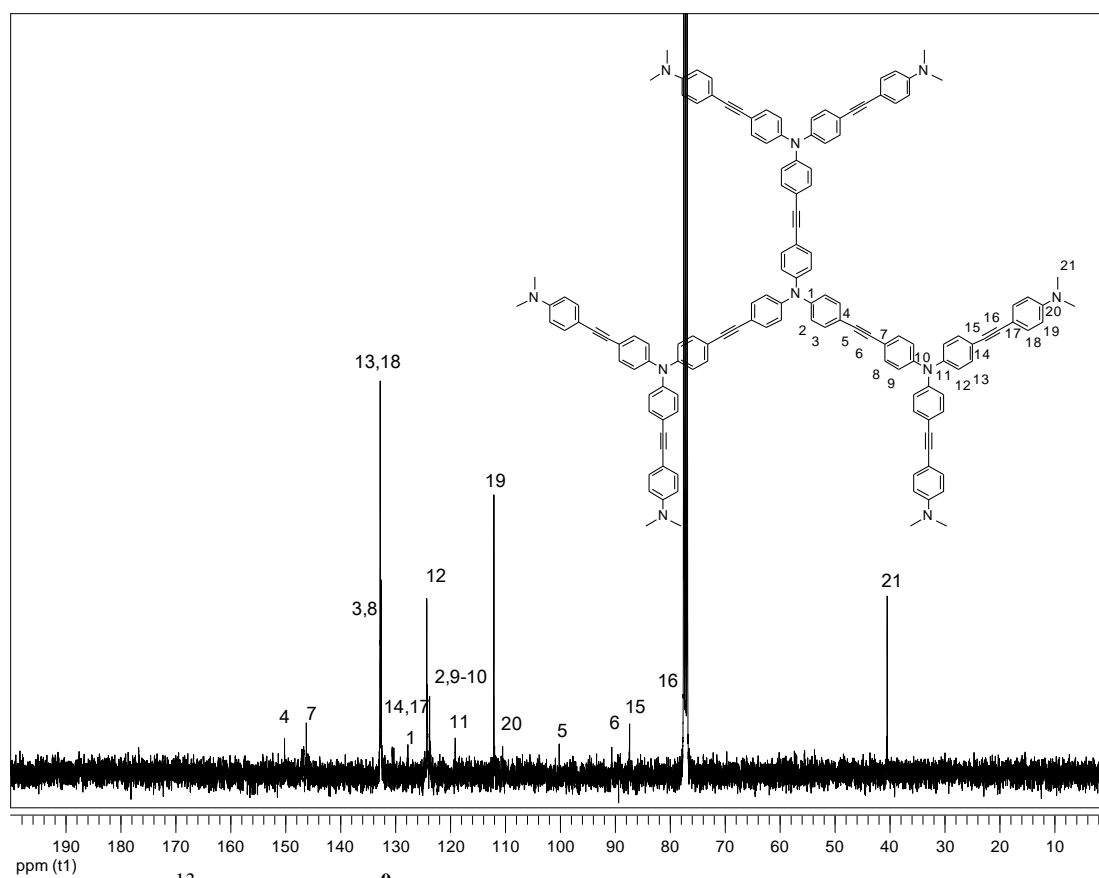


Figure A.20 ^{13}C NMR of 6N^0 in CDCl_3 .

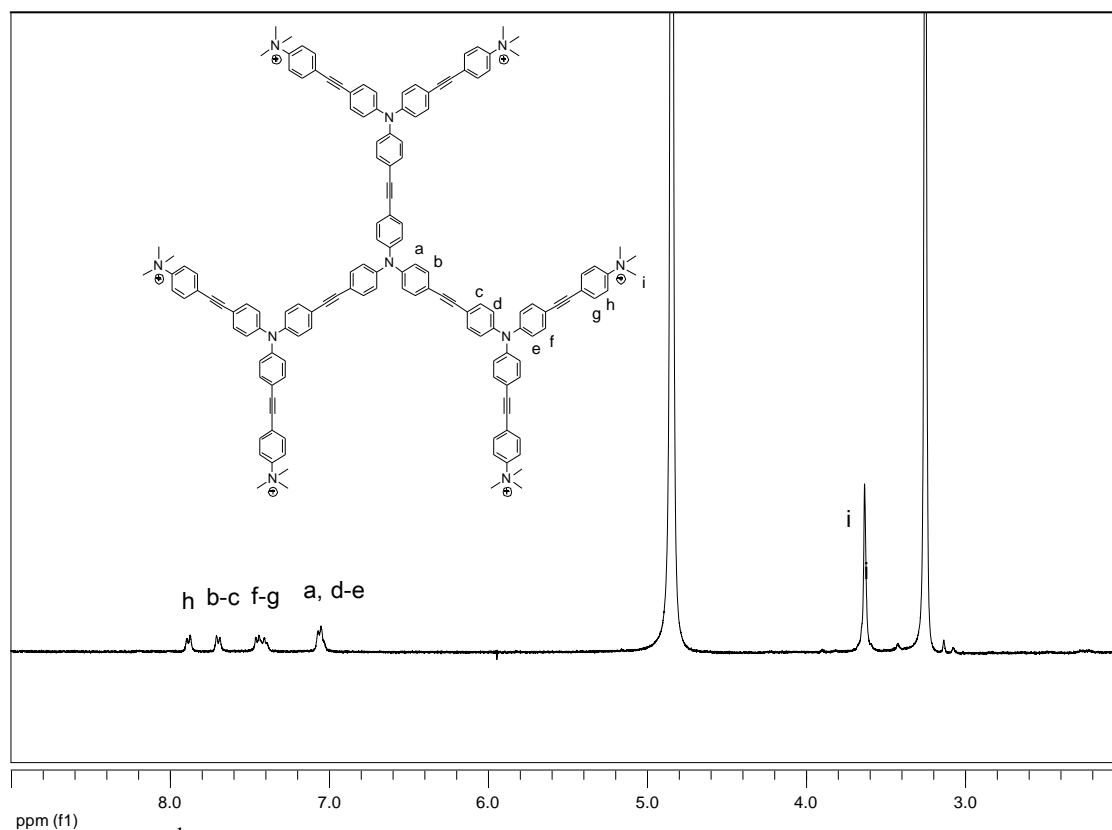


Figure A.21 1H NMR of $6N^+$ in $MeOH-d_4$.

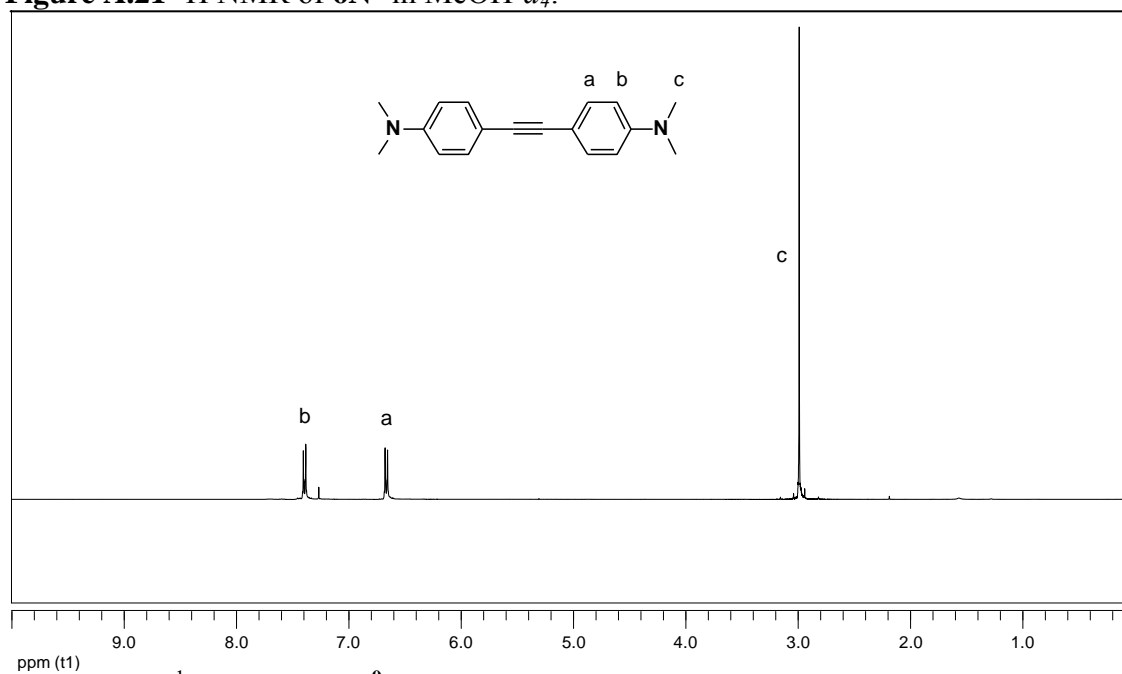


Figure A.22 1H NMR of $2N^0$ in $CDCl_3$.

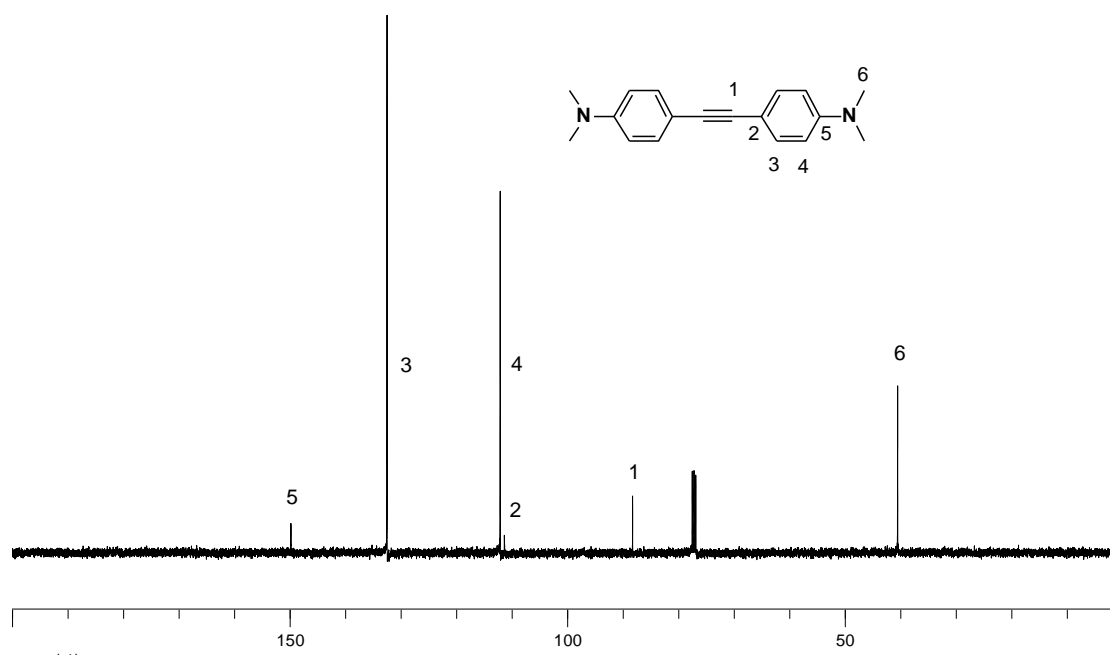


Figure A.23 ^{13}C NMR of 2N^0 in CDCl_3 .

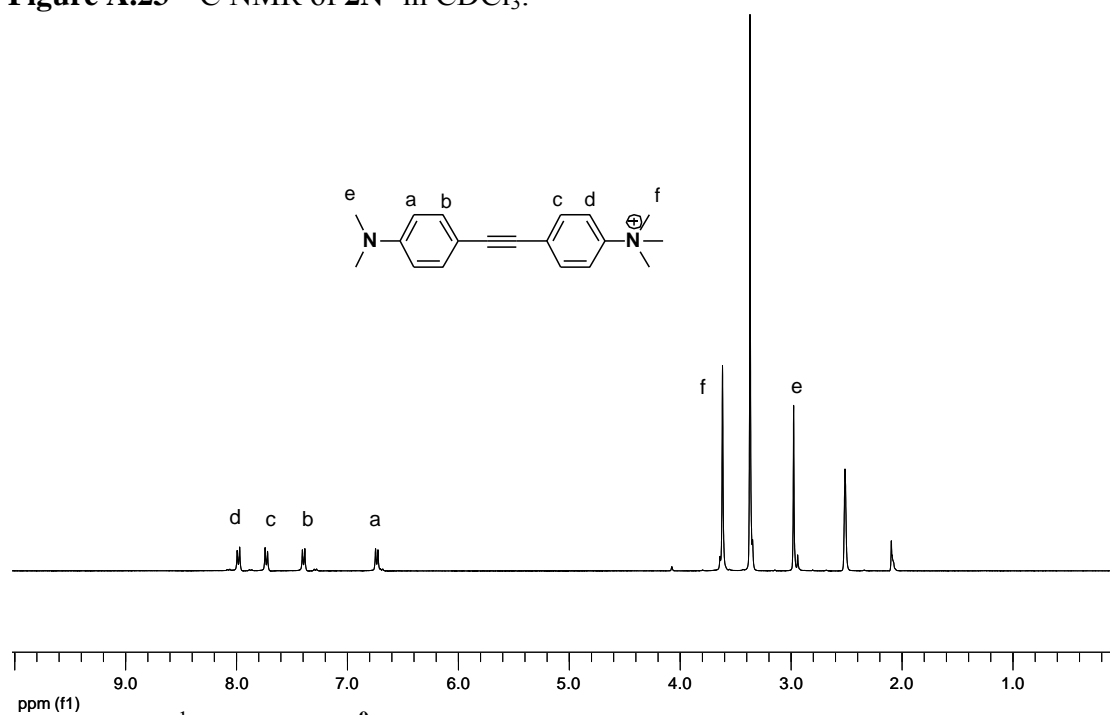
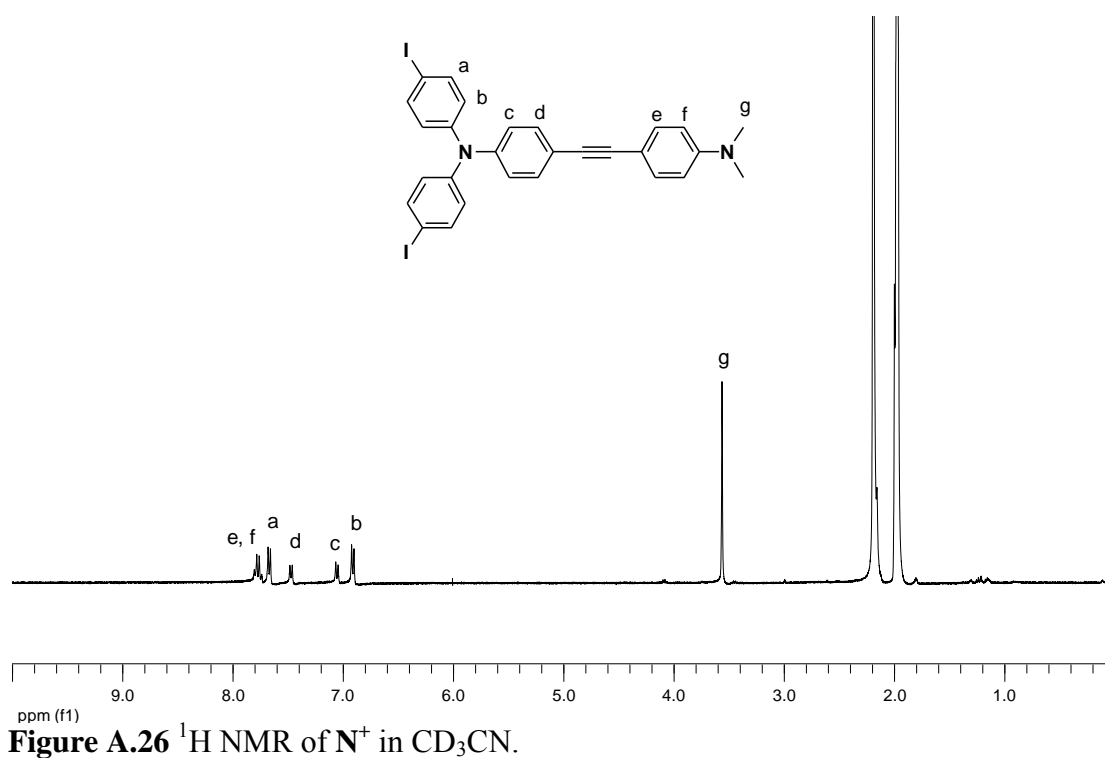
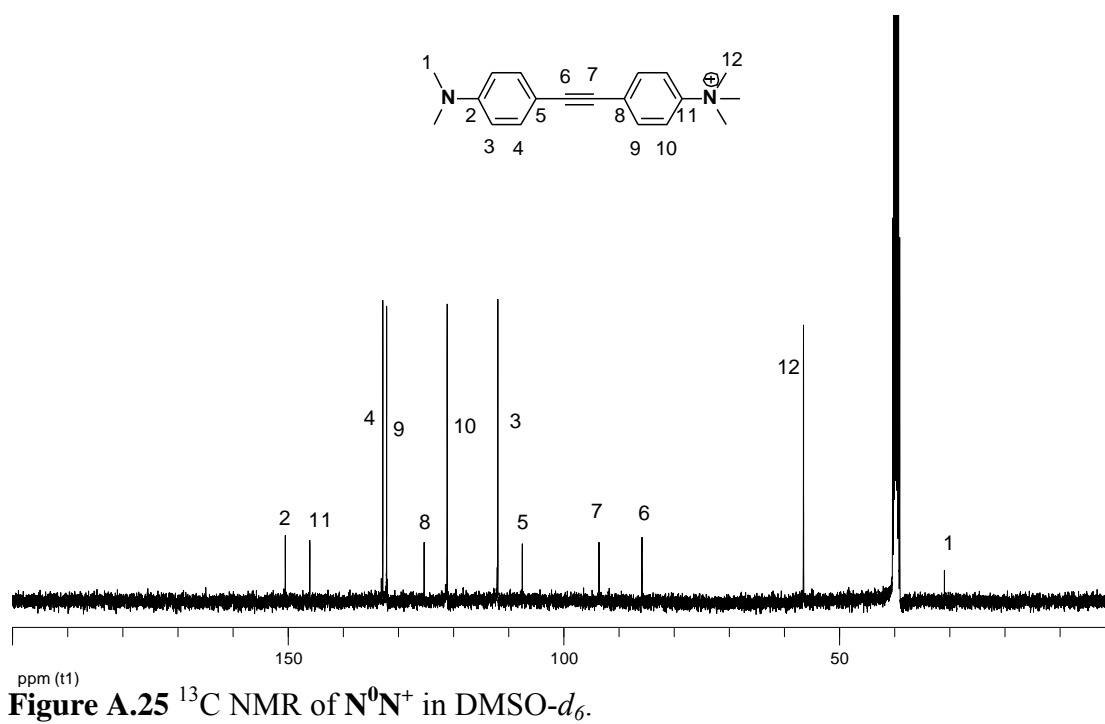


Figure A.24 ^1H NMR of N^0N^+ in $\text{DMSO-}d_6$.



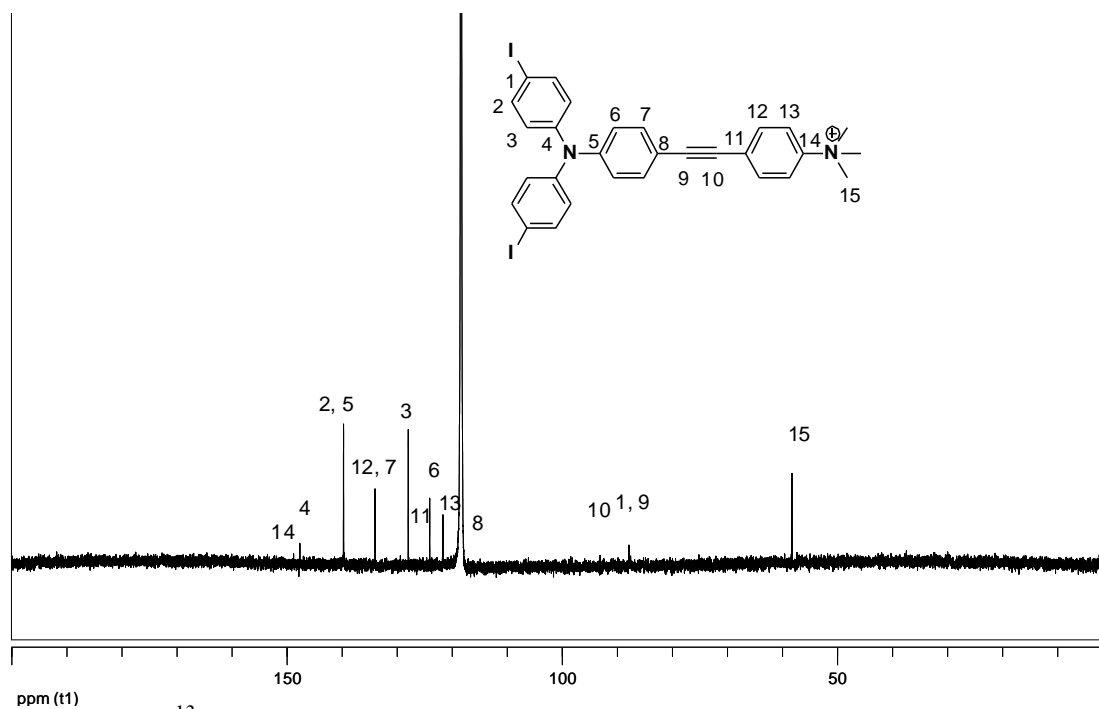


Figure A.27 ^{13}C NMR of N^+ in CD_3CN .

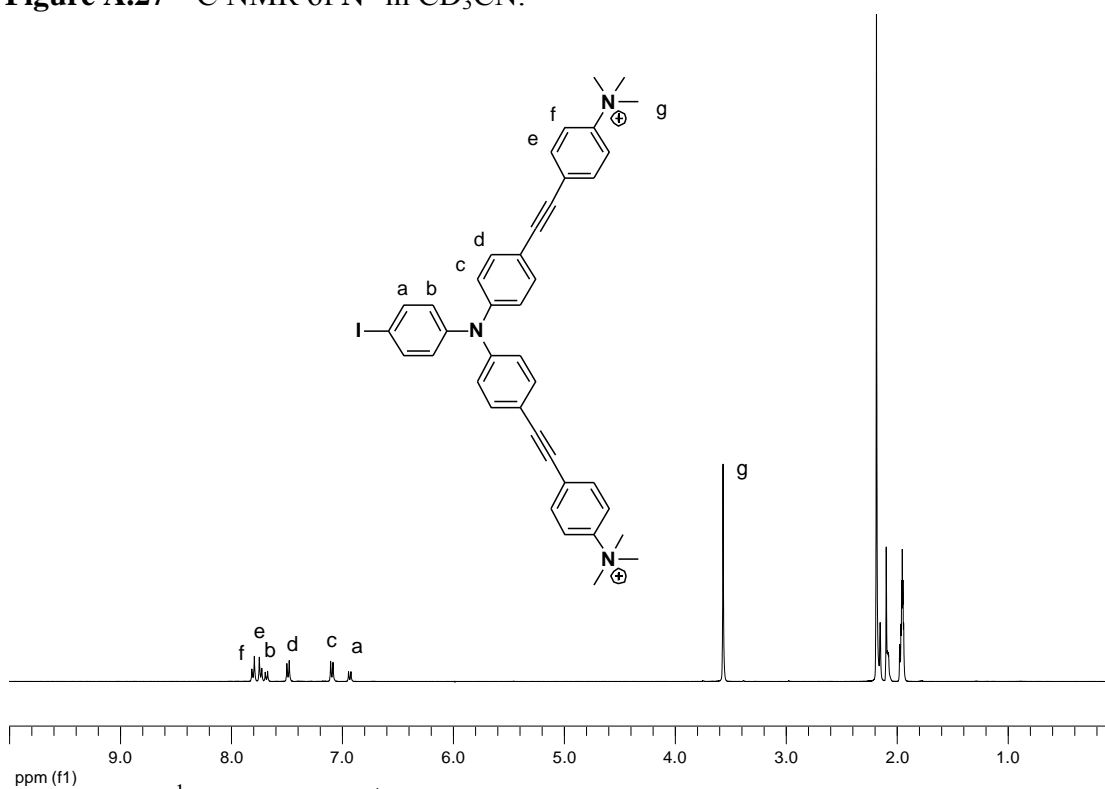


Figure A.28 ^1H NMR of 2N^+ in CD_3CN .

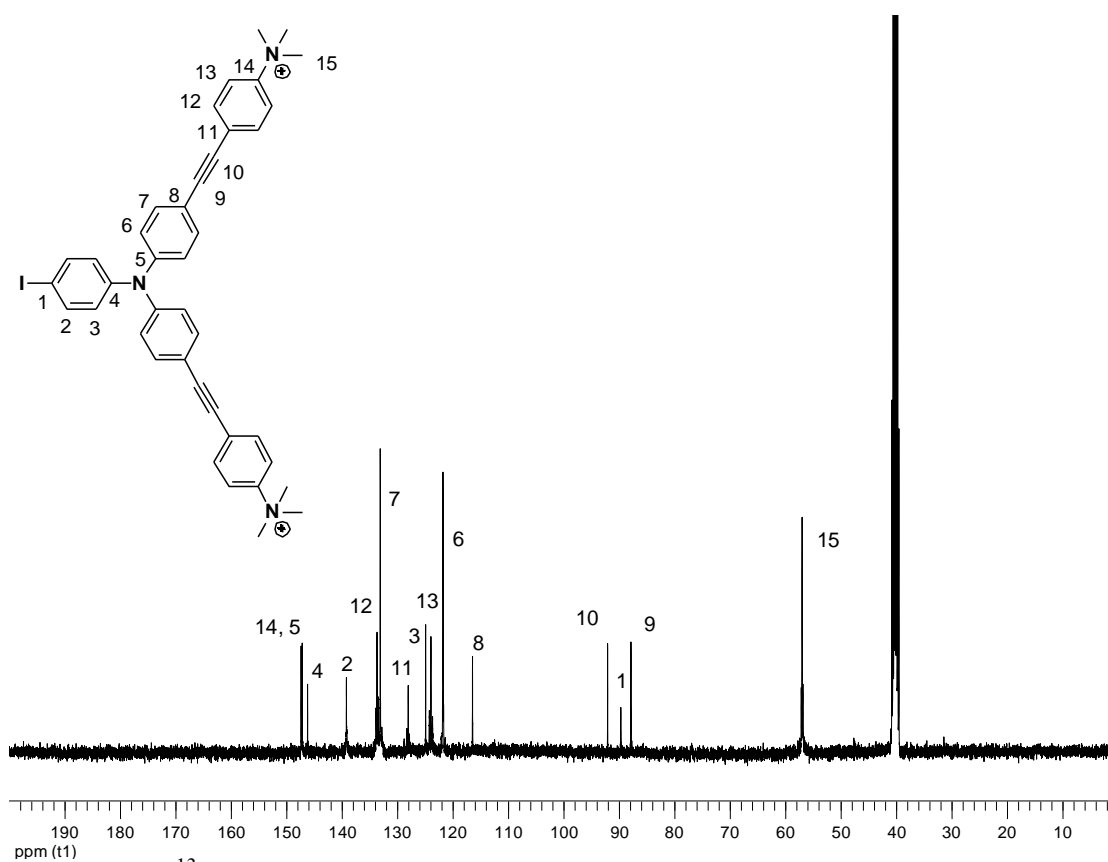


Figure A.29 ^{13}C NMR of 2N^+ in $\text{DMSO-}d_6$.

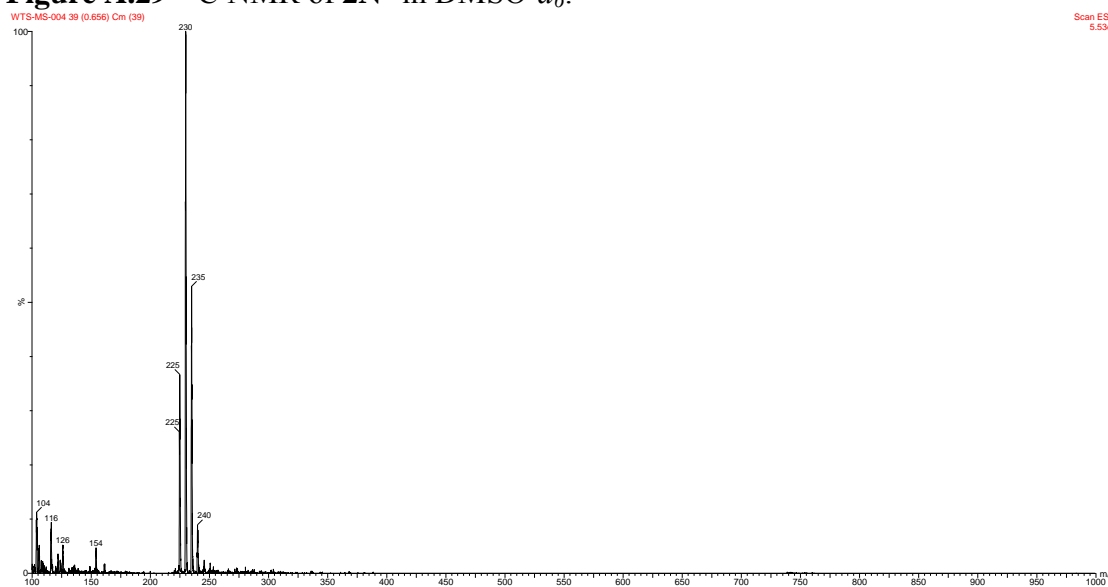


Figure A.30 ESI MS data of 3N^+

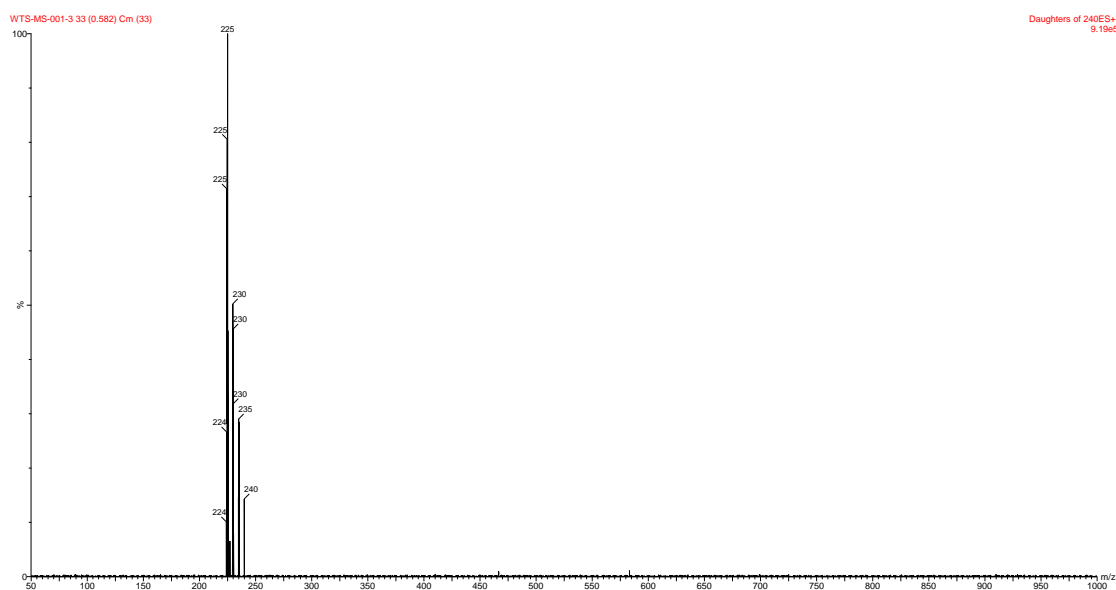


Figure A.31 ESI MS/MS data of $3N^+$

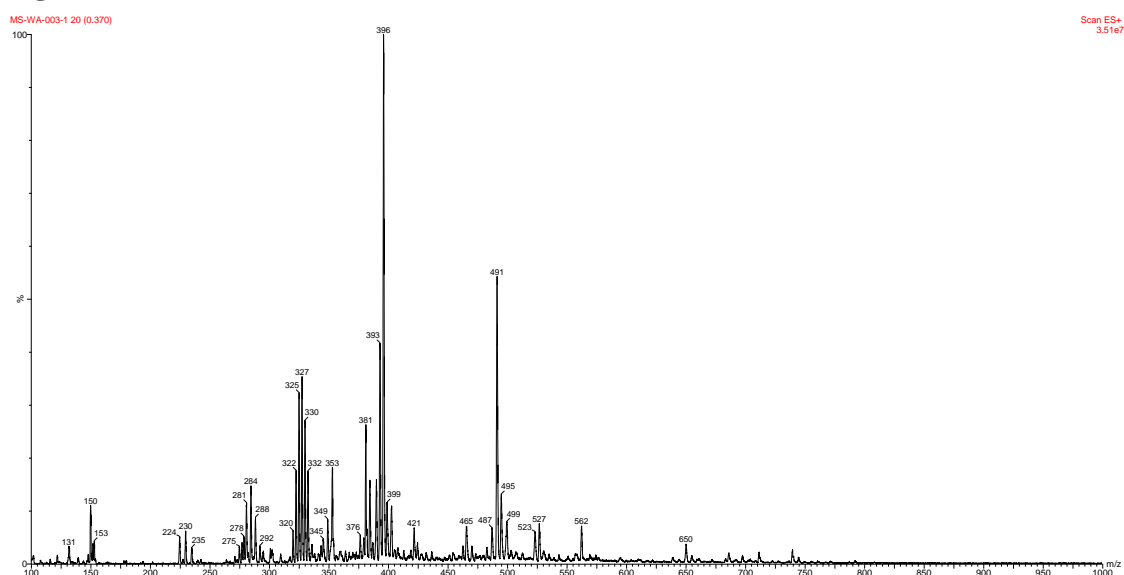


Figure A.32 ESI MS data of $6N^+$

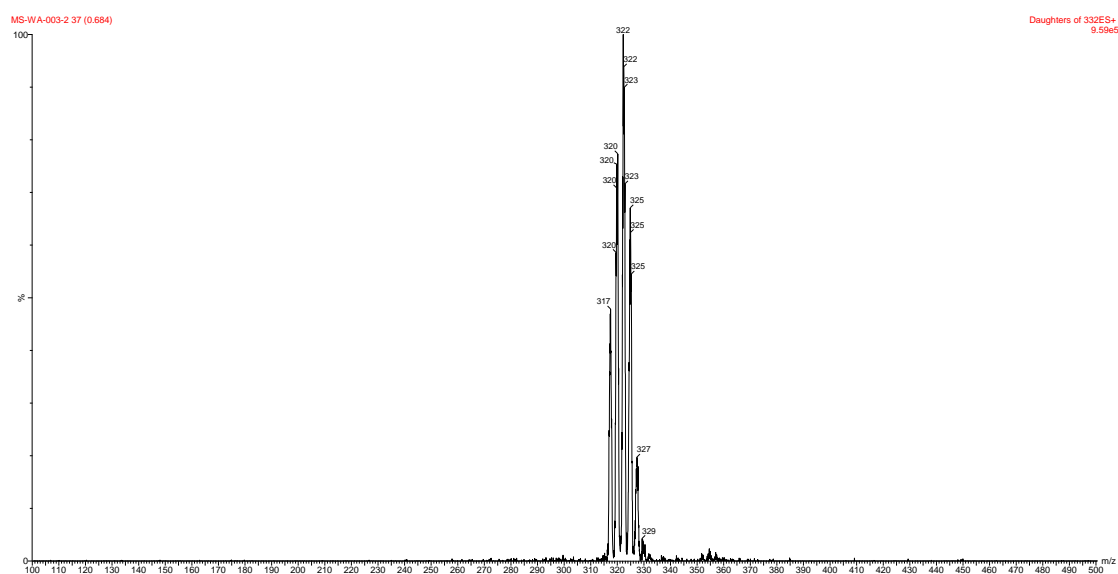


Figure A.33 ESI MS/MS data of $6N^+$

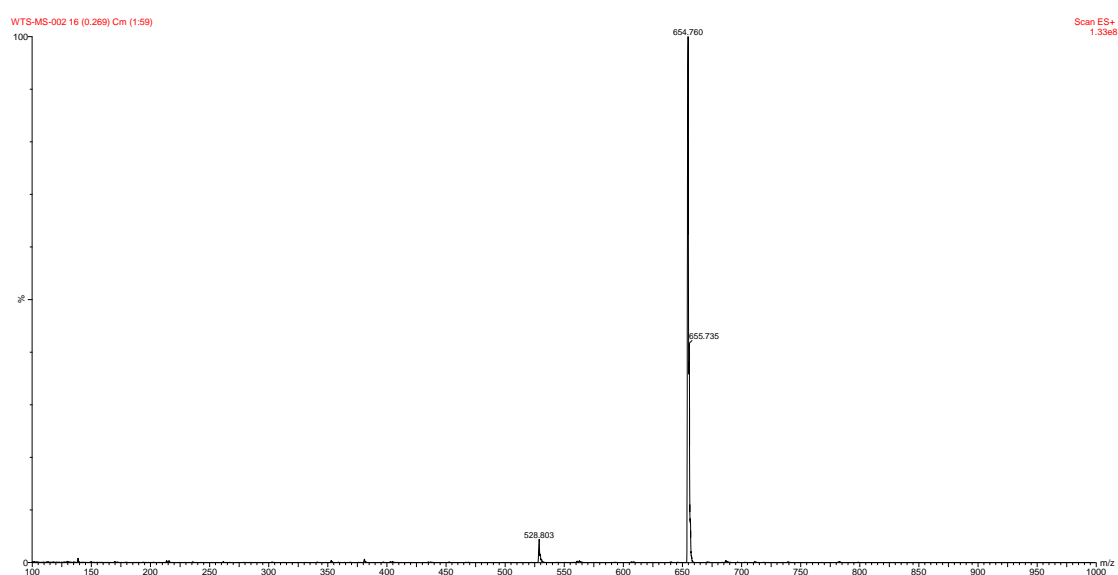
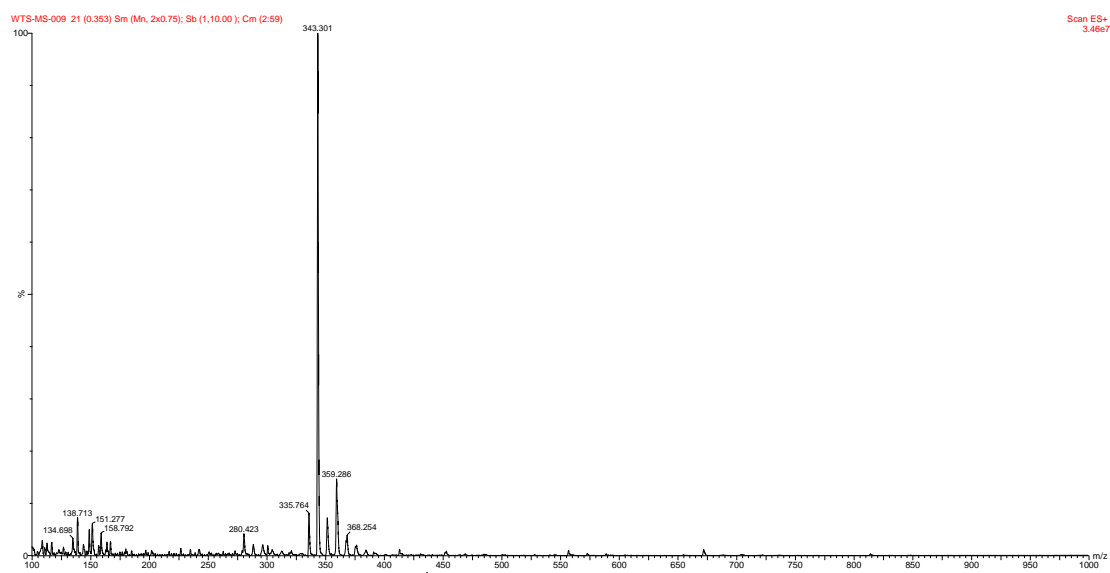


Figure A.34 ESI MS data of N^+

**Figure A.35** ESI MS/MS data of N^+ **Figure A.36** ESI MS data of $2N^+$

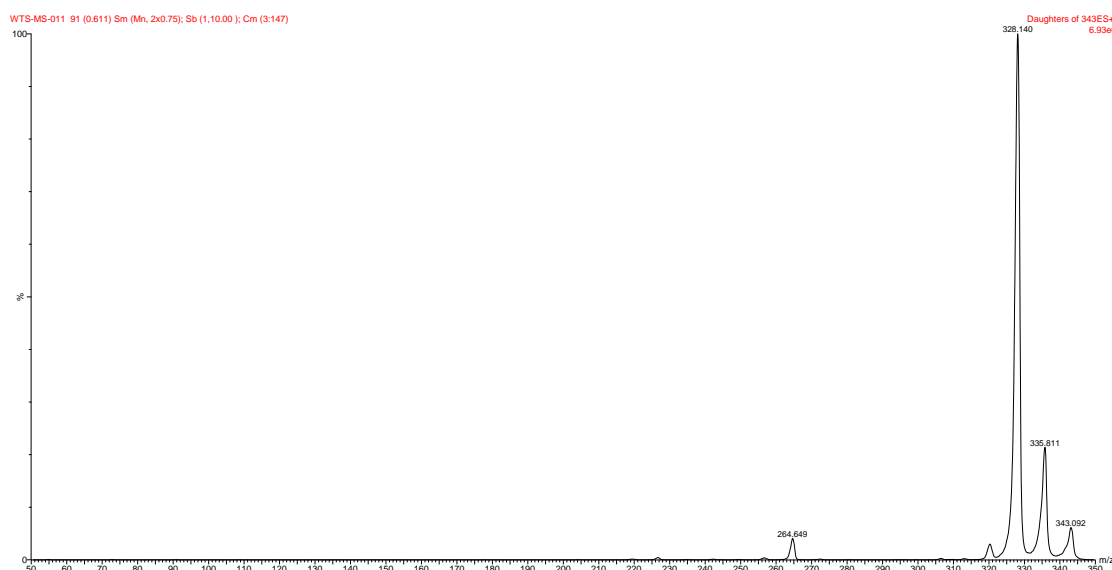


Figure A.37 ESI MS/MS data of $2N^+$

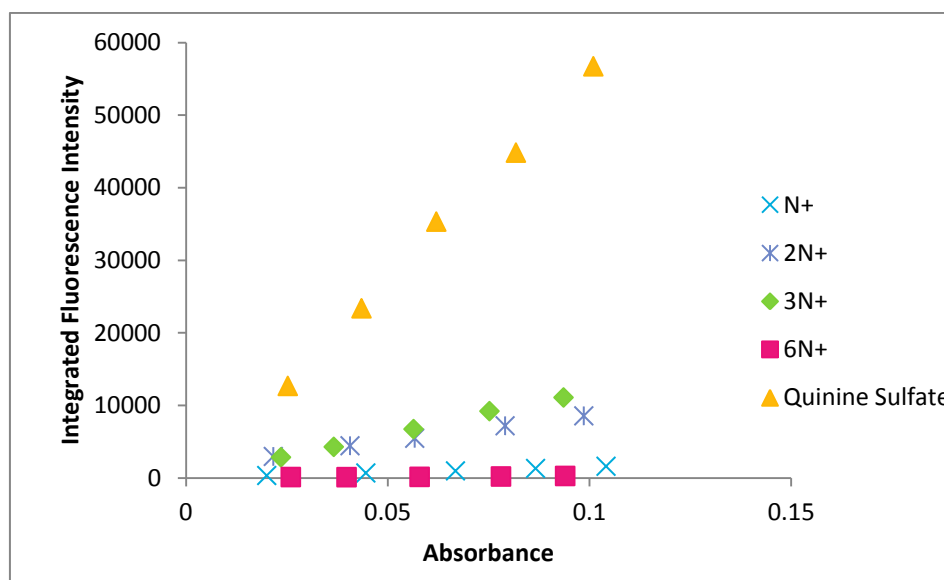


Figure A.38 Linear graph plot between absorbance against absolute integrated fluorescence intensity (390 - 600 nm) of quinine sulfate standard in 0.1 M H_2SO_4 , (400 - 600 nm) of N^+ , $2N^+$, $3N^+$ and $6N^+$ in MilliQ water at room temperature excited at 345, 370, 368, 370 and 376, respectively.

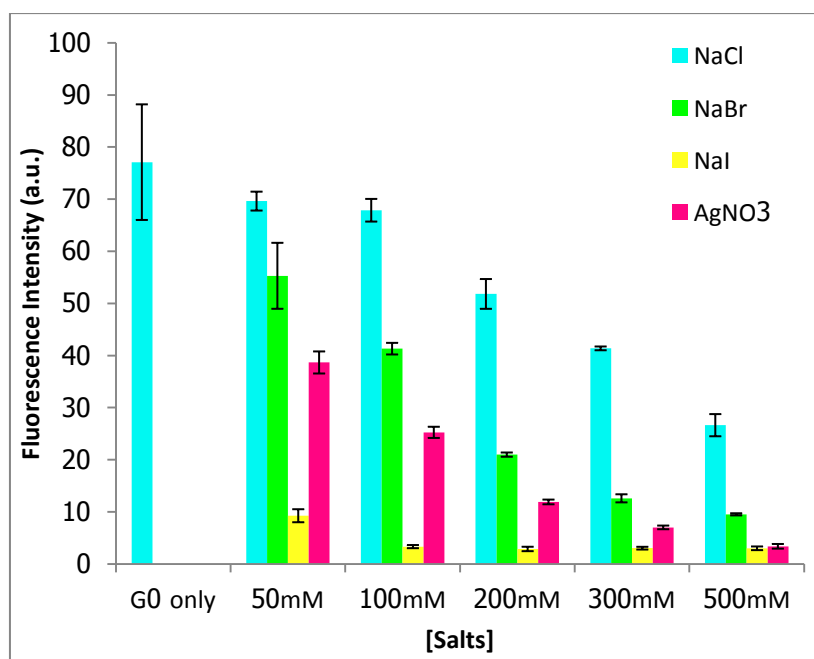


Figure A.39 Histogram showed the emission intensity of $3N^+$ $5 \mu M$ in 10 mM sodium phosphate buffer with various concentration (0 – 500 mM) of NaCl, NaBr, NaI and $AgNO_3$ excited at 370 nm.

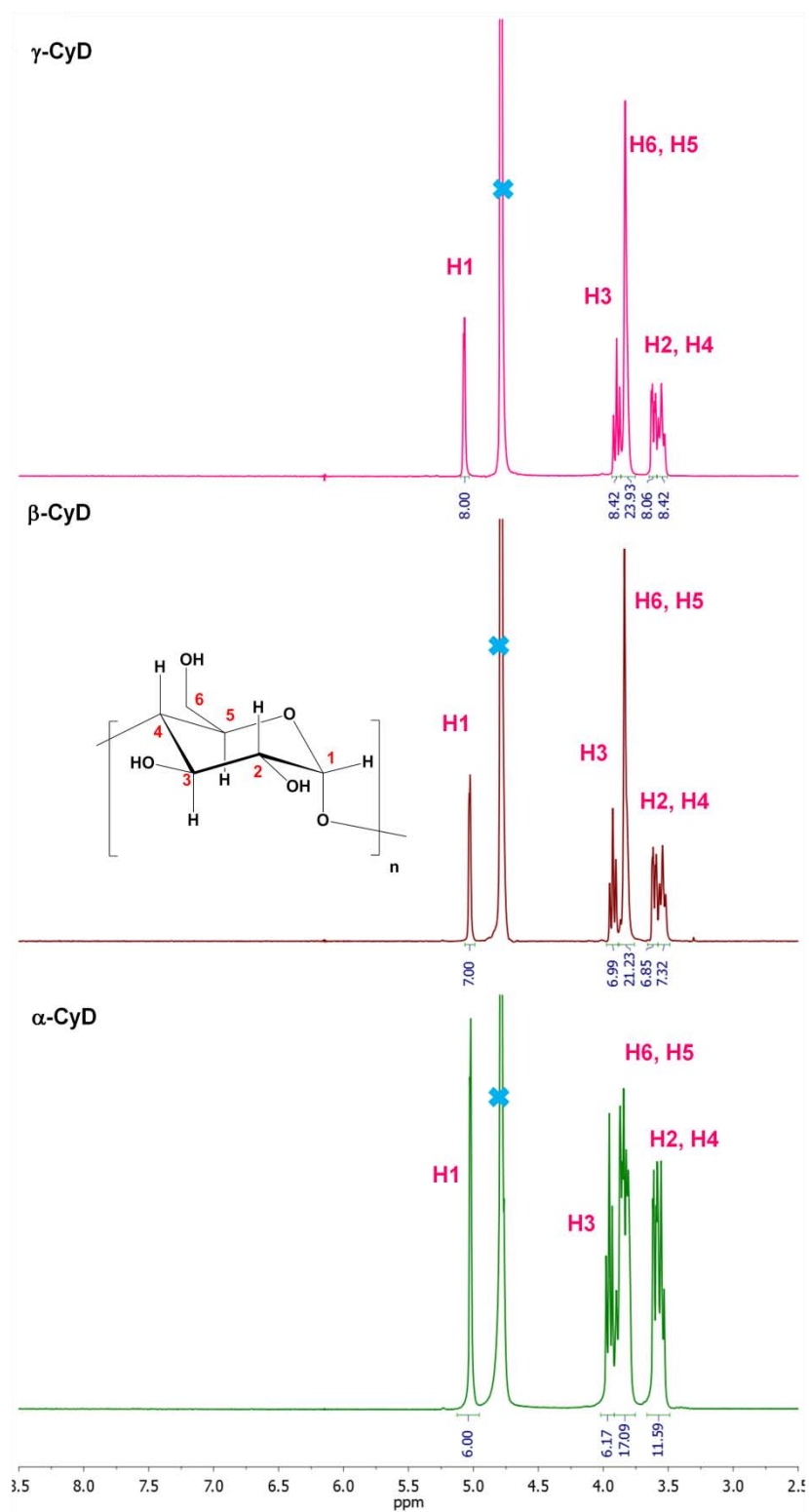


Figure A.40 $^1\text{H-NMR}$ spectra of cyclodextrins in D_2O

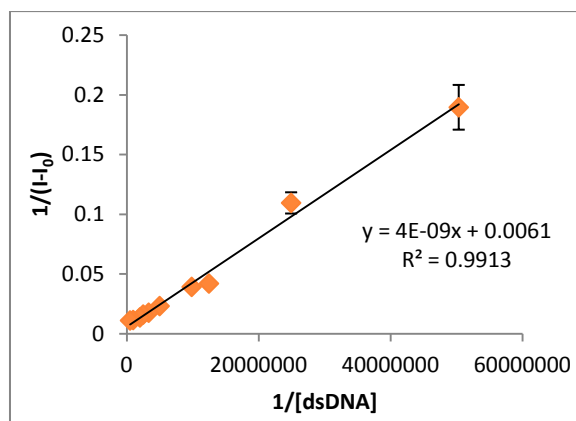


Figure A.41 Benesi-Hilderbrand's plot for 1:1 complexes of $3N^+$ /dsDNA

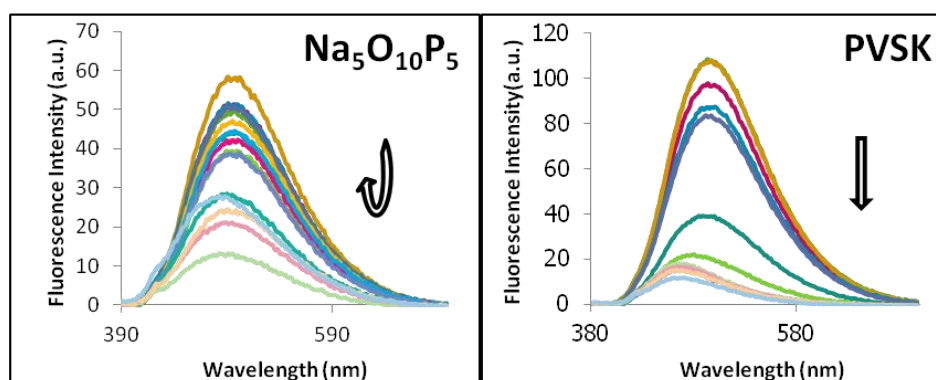


Figure A.42 Fluorescence spectra of $3N^+$ ($1 \mu\text{M}$) with various concentrations ($0 - 300 \text{ mM}$) of sodium triphosphate pentabasic and ($0 - 2 \text{ mM}$) of PVSX in MilliQ water at room temperature upon excitation 370 nm .

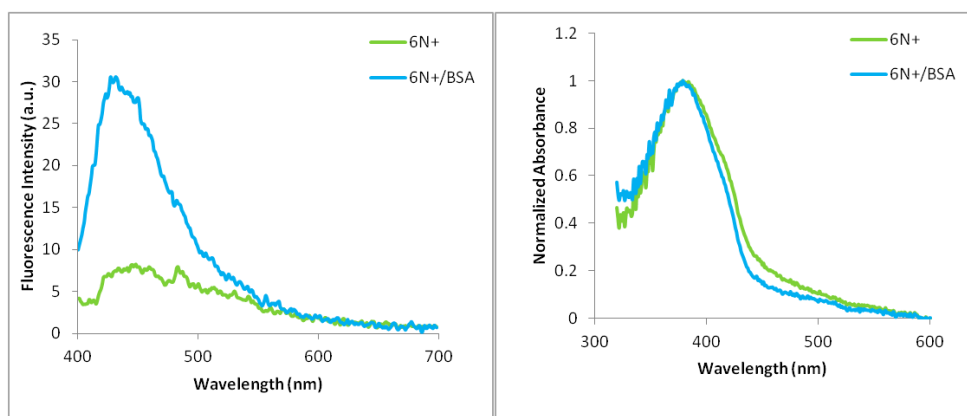


Figure A.43 Fluorescence spectra (*left*) and Absorption spectra (*right*) of $6N^+$ ($5 \mu\text{M}$) in the presence of BSA ($5 \mu\text{M}$) in sodium phosphate buffer pH 7 (10 mM) and NaCl (100 mM) upon excitation at 376 nm .

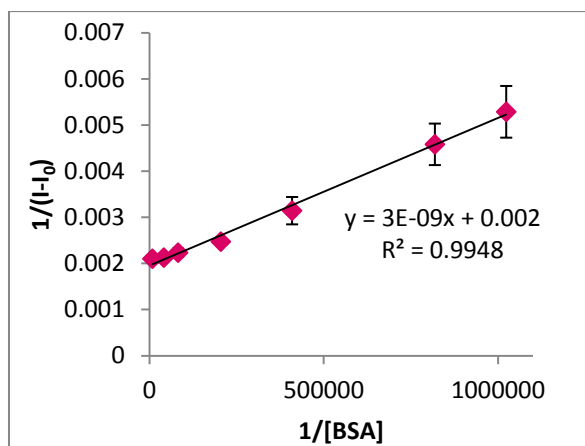


Figure A.44 Benesi-Hilderbrand's plot for 1:1 complexes of $3N^+$ /BSA

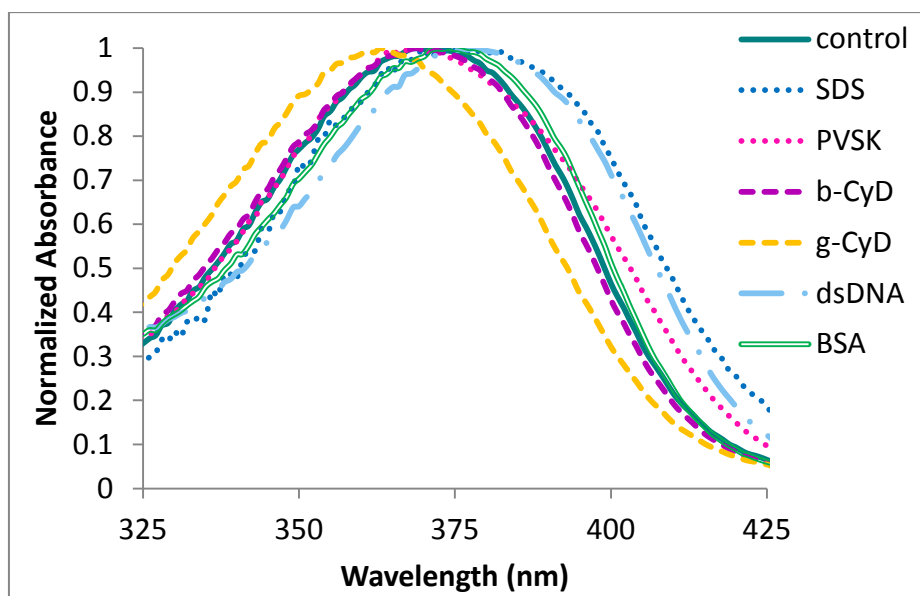


Figure A.45 Normalized absorption spectra of $3N^+$ (5 μ M) in the presence of analytes (SDS, PVSX, β -CyD, γ -CyD, dsDNA (5'GCATATGCCTA3' + 5'TAGGCATATGC 3') and BSA) excited at 370 nm.

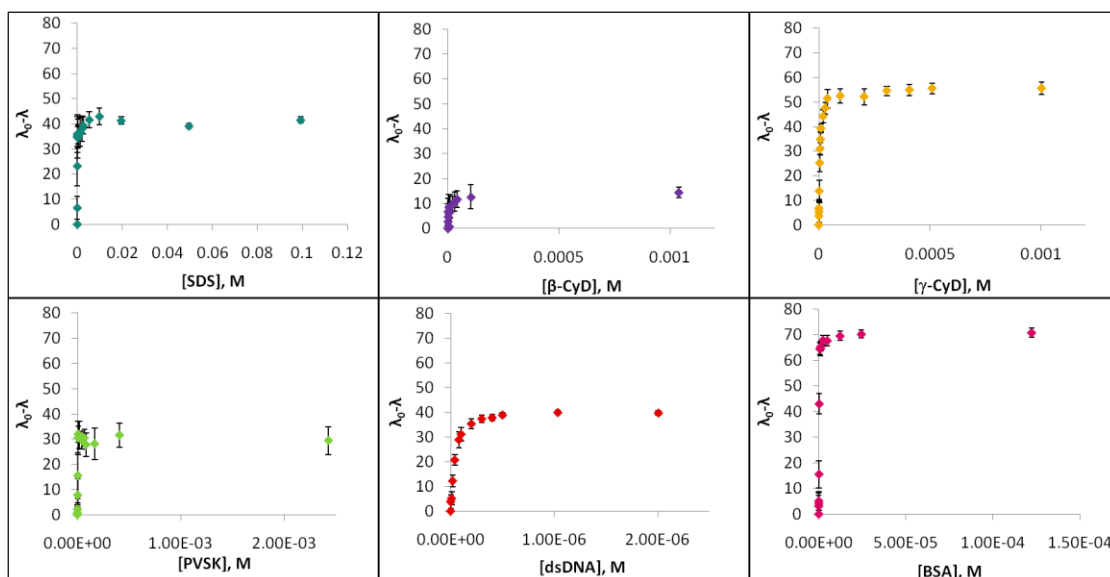


Figure A.46 Wavelength shifting of $3N^+$ ($5 \mu\text{M}$) with various concentrations of analytes (SDS, PVS, β -CyD, γ -CyD, dsDNA (5'GCATATGCCTA3' + 5'TAGGCATATGC 3') and BSA) excited at 370 nm.

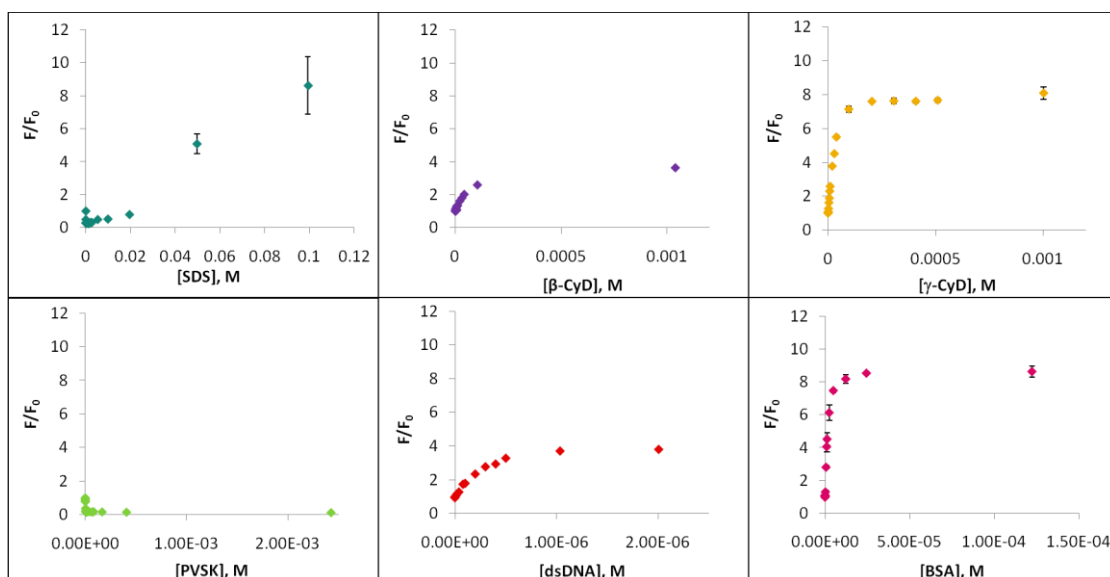


Figure A.47 Fluorescence spectra of $3N^+$ ($5 \mu\text{M}$) with various concentrations of analytes (SDS, PVS, β -CyD, γ -CyD, dsDNA (5'GCATATGCCTA3' + 5'TAGGCATATGC3') and BSA) excited at 370 nm.

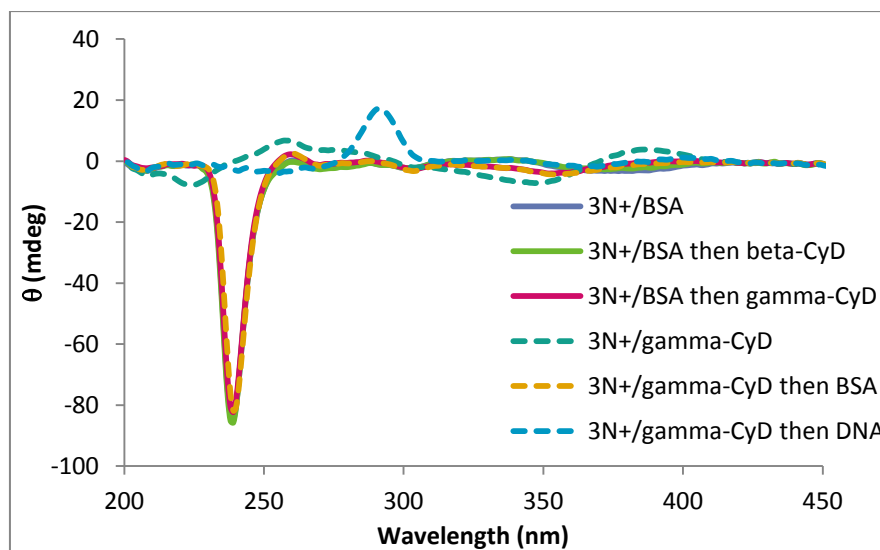


Figure A.48 CD spectra of $3N^+$ ($10 \mu\text{M}$) in the presence of BSA ($10 \mu\text{M}$), γ -CyD ($10 \mu\text{M}$) and DNA ($10 \mu\text{M}$) and $10 \mu\text{M}$ in sodium phosphate buffer pH 7 (10 mM) and NaCl (100 mM) at $20 \text{ }^\circ\text{C}$ excited at 376 nm with alternated mixing steps.

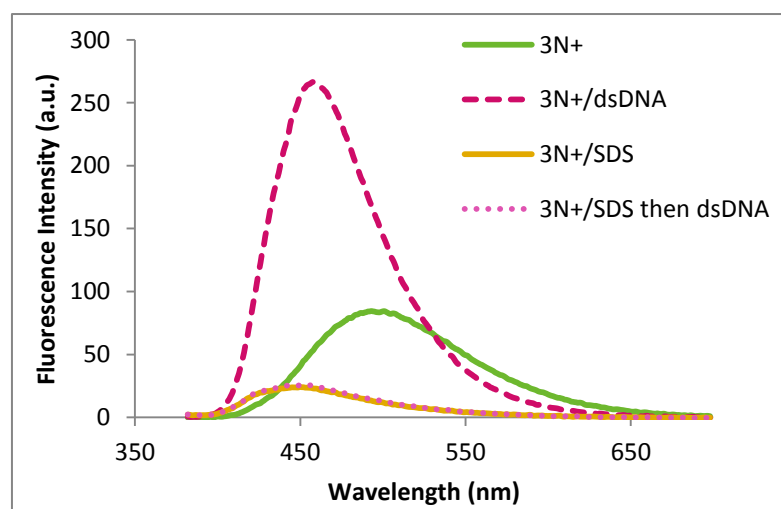


Figure A.49 Fluorescence spectra of $3N^+$ ($1 \mu\text{M}$) and SDS (0.2 mM) mixtures in the presence of dsDNA ($5'\text{GCATATGCCTA}3' + 5'\text{TAGGCATATGC}3'$, $0.25 \mu\text{M}$) excited 370 nm .

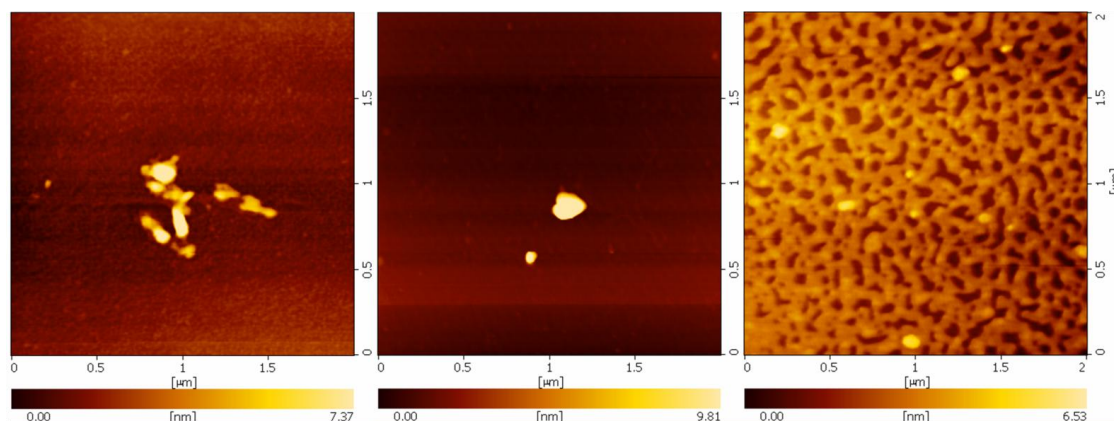


Figure A.50 AFM images on the mica surface of $3N^+$ ($10 \mu\text{M}$), $3N^+/\beta\text{-CyD}$ (1:1), and $3N^+/\gamma\text{-CyD}$ (1:1) in MilliQ water.

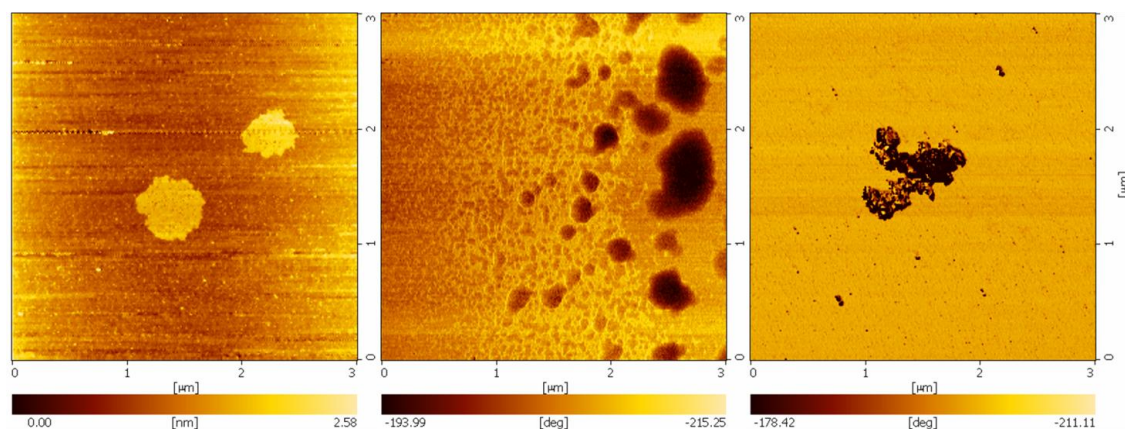


Figure A.51 AFM images on the mica surface of $2N^+$ ($10 \mu\text{M}$), $2N^+/\beta\text{-CyD}$ (1:1), and $2N^+/\gamma\text{-CyD}$ (1:1) in MilliQ water.

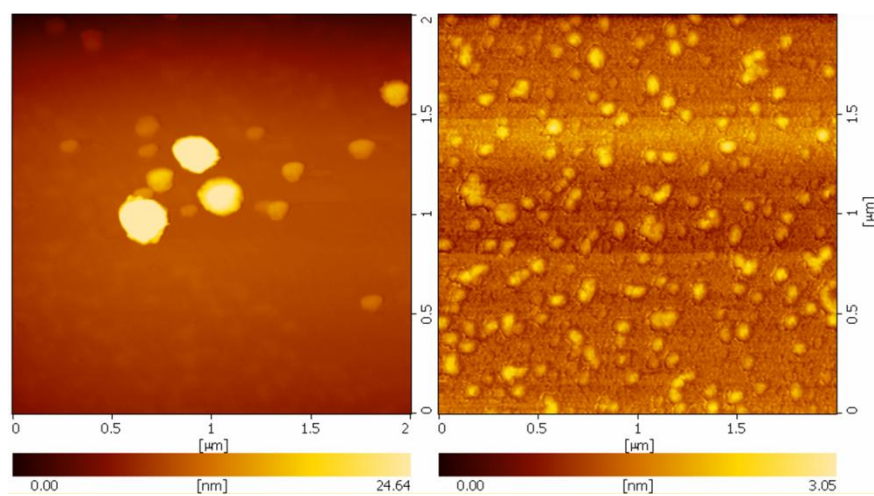


Figure A.52 AFM images on the mica surface of β - and γ -CyD ($10 \mu\text{M}$) in MilliQ water.

VITAE

Ms. Warathip Siripornnoppakhun was born on December 30th, 1982 in Nakhonpathom, Thailand. She was graduated with Bachelor Degree of Science, majoring in Chemistry from Chulalongkorn University in 2004. She has been a graduate student in organic chemistry and become a member of Organic Synthesis Research Unit under supervision of Assoc. Prof. Dr. Mongkol Sukwattanasinitt. She had an opportunity to do the research at the Department of Chemistry at University of Massachusetts Amherst, USA in 2009 (1 year) with Professor Dr. Sankaran Thayumanavan. She has received scholarship from Royal Golden Jubilee Ph.D. program (Grant No financially supported this Work, PHD/0050/2549), the Thailand Research Fund for the financial support. She graduated with a Ph. D. Degree in Chemistry in academic year 2011.

Her present address is 119 Moo 4, Vungyen, Muang, Nakhonpathom, Thailand 73000.